U.S. Department
of Commerce

Volume 118
Number 4
October 2020

Fishery Bulletin

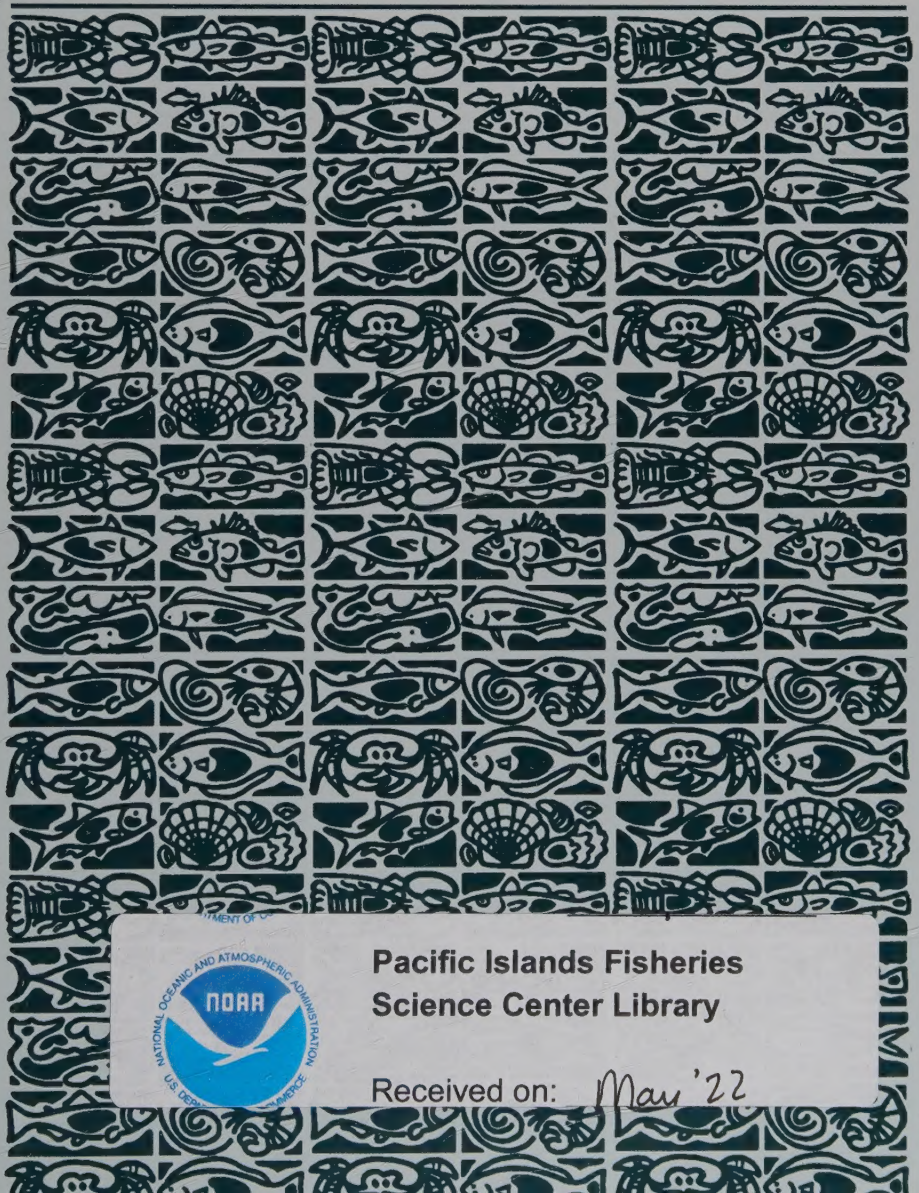

Pacific Islands Fisheries
Science Center Library

Received on: May '22

U.S. Department of Commerce

Wilbur L. Ross Jr.
Secretary

National Oceanic and Atmospheric Administration

Neil A. Jacobs
Acting Administrator

National Marine Fisheries Service

Chris Oliver
Assistant Administrator
for Fisheries

Fishery Bulletin (ISSN 0090-0656) is published quarterly by the Scientific Publications Office, National Marine Fisheries Service, NOAA, 7600 Sand Point Way NE, Seattle, WA 98115-0070.

Although the contents of this publication have not been copyrighted and may be reprinted entirely, reference to source is appreciated.

The Secretary of Commerce has determined that the publication of this periodical is necessary according to law for the transaction of public business of this Department. Use of funds for printing of this periodical has been approved by the Director of the Office of Management and Budget.

For Sale by the Superintendent of Documents, U.S. Government Publishing Office, Washington, DC 20401. Subscription price per year: $32.00 domestic and $44.80 foreign. Cost per single issue: $19.00 domestic and $26.60 foreign. **See back for order form.**

Fishery Bulletin

Scientific Editor
José I. Castro
National Marine Fisheries Service, NOAA
263 13th Avenue South
Saint Petersburg, Florida 33701

Managing Editor
Kathryn Dennis
Scientific Publications Office
National Marine Fisheries Service, NOAA
1845 Wasp Boulevard, Building 176
Honolulu, Hawaii 96818

Associate Editor
Cara Mayo
Scientific Publications Office
National Marine Fisheries Service, NOAA
7600 Sand Point Way NE
Seattle, Washington 98115-0070

Editorial Board

Henry L. Bart Jr.	Tulane University, New Orleans, Louisiana
Matthew D. Campbell	National Marine Fisheries Service, Pascagoula, Mississippi
Shannon L. Cass-Calay	National Marine Fisheries Service, Miami, Florida
William B. Driggers III	National Marine Fisheries Service, Pascagoula, Mississippi
Gretchen L. Grammer	South Australian Research and Development Institute, Adelaide, Australia
Richard Langton	National Marine Fisheries Service, Walpole, Maine (retired)
Richard S. McBride	National Marine Fisheries Service, Woods Hole, Massachusetts
Richard L. Merrick	National Marine Fisheries Service, Falmouth, Massachusetts (retired)
Richard D. Methot	National Marine Fisheries Service, Seattle, Washington
Lisa J. Natanson	National Marine Fisheries Service, Narragansett, Rhode Island
Mark S. Peterson	University of Southern Mississippi, Ocean Springs, Mississippi
Joseph M. Quattro	University of South Carolina, Columbia, South Carolina
John F. Walter III	National Marine Fisheries Service, Miami, Florida
Bruce Wright	Aleutian Pribilof Island Association, Anchorage, Alaska

***Fishery Bulletin* website: https://spo.nmfs.noaa.gov/fb.htm**

Fishery Bulletin carries original research reports on investigations in fishery science, engineering, and economics. It began as the Bulletin of the United States Fish Commission in 1881; it became the Bulletin of the Bureau of Fisheries in 1904 and the *Fishery Bulletin* of the U.S. Fish and Wildlife Service in 1941. Separates were issued as documents through volume 46; the last document was no. 1103. Beginning with volume 47 in 1931 and continuing through volume 62 in 1963, each separate appeared as a numbered bulletin. A new system began in 1963, with volume 63, in which papers are bound together in a single issue. Beginning with volume 70, number 1, January 1972, *Fishery Bulletin* became a periodical, issued quarterly. In this form, it is available by subscription from the Superintendent of Documents, U.S. Government Publishing Office, Washington, DC 20401. It is also available free in limited numbers to libraries, research institutions, and state and federal agencies and in exchange for other scientific publications.

U.S. Department of Commerce
Seattle, Washington

Volume 118
Number 4
October 2020

Fishery Bulletin

Contents

Notes

319–323 **Sergei A. Evseenko and Yana Yu. Bolshakova**

A description of late and transformation stages of larvae of the *Diaphus ostenfeldi* in the western periphery of the South Pacific Gyre

324–328 **Ulianov Jakes-Cota, Arturo Tripp-Valdez, Marisol Arce-Acosta, and Francisco Omar López-Fuerte**

Age and growth of stone scorpionfish (*Scorpaena mystes*) from the Gulf of California in Mexico

Articles

329–345 **Bryan S. Frazier, Dana M. Bethea, Robert E. Hueter, Camilla T. McCandless, John P. Tyminski, and William B. Driggers III**

Growth rates of bonnetheads (*Sphyrna tiburo*) estimated from tag-recapture data

346–358 **Adam A. Kemberling and M. Zachary Darnell**

Distribution, relative abundance, and reproductive output of spawning female blue crab (*Callinectes sapidus*) in offshore waters of the Gulf of Mexico

359–364 **J. Fernando Márquez-Farías**

Length at maturity of the Pacific angel shark (*Squatina californica*) in the artisanal elasmobranch fishery in the Gulf of California in Mexico

365–379 **Oscar G. Zamora-García, J. Fernando Márquez-Farías, Aristóteles Stavrinaky-Suárez, Carlos Díaz-Avalos, Noemí I. Zamora-García, and Raúl E. Lara-Mendoza**

Catch rate, length, and sex ratio of Pacific hake (*Merluccius productus*) in the northern Gulf of California

The National Marine Fisheries Service (NMFS) does not approve, recommend, or endorse any proprietary product or proprietary material mentioned in this publication. No reference shall be made to NMFS, or to this publication furnished by NMFS, in any advertising or sales promotion that would indicate or imply that NMFS approves, recommends, or endorses any proprietary product or proprietary material mentioned herein or that has as its purpose an intent to cause directly or indirectly the advertised product to be used or purchased because of this NMFS publication.

The NMFS Scientific Publications Office is not responsible for the contents of the articles.

380–398 **Shareef M. Siddeek, Benjamin Daly, André E. Punt, Steve Martell, Jie Zheng, and Mark Stichert**

Development of harvest control rules for hard-to-age crab stocks: the example of the golden king crab (*Lithodes aequispinus*) in the eastern Aleutian Islands in Alaska

399–412 **Jeff Kneebone, Heather Bowlby, Joseph J. Mello, Camilla T. McCandless, Lisa J. Natanson, Brian Gervelis, Gregory B. Skomal, Nancy Kohler, and Diego Bernal**

Seasonal distribution and habitat use of the common thresher shark (*Alopias vulpinus*) in the western North Atlantic Ocean inferred from fishery-dependent data

413 **Acknowledgment of reviewers**

414–417 **Guidelines for authors**

National Marine
Fisheries Service
NOAA

Fishery Bulletin
established in 1881

Spencer F. Baird
First U.S. Commissioner
of Fisheries and founder
of *Fishery Bulletin*

Abstract—Postflexion and transformation stages of the *Diaphus ostenfeldi* in the southwestern Pacific Ocean are described for the first time. Identification to the species level was based on tracing characters from fully formed, large metamorphic specimens backward to smaller specimens. It was found that larval *D. ostenfeldi* ≥9.5 mm standard body length (SL) can be characterized by a unique character within the genus *Diaphus*, namely the presence of melanophores at the dorsal fin base and between branchiostegal rays. Metamorphosis in larvae of this species occurs at a much longer body length (~20 mm SL) than in larvae of other species of this genus.

A description of late and transformation stages of larvae of the *Diaphus ostenfeldi* in the western periphery of the South Pacific Gyre

Sergei A. Evseenko (deceased)
Yana Yu. Bolshakova (contact author)

Email address for contact author: yanusrunaa@mail.ru

Shirshov Institute of Oceanology
Russian Academy of Sciences
36 Nakhimovskyi Prospekt
Moscow 117997, Russia

Manuscript submitted 13 April 2020.
Manuscript accepted 5 October 2020.
Fish. Bull. 118:319–323 (2020).
Online publication date: 21 October 2020.
doi: 10.7755/FB.118.4.1

The views and opinions expressed or implied in this article are those of the author (or authors) and do not necessarily reflect the position of the National Marine Fisheries Service, NOAA.

Diaphus is the most speciose genus of the mesopelagic family Myctophidae and plays a key role in oceanic food webs. Larvae of *Diaphus* are poorly known. Of the 80 species in this genus (Fricke et al., 2020), the early stages of development are known for only 10 species. These species are the *D. agassizii* (Pertseva-Ostroumova, 1975), Garman's lanterfish (*D. garmani*) (Sassa et al., 2003), *D. hudsoni* (Olivar, 1987), short-headed lantern fish (*D. brachycephalus* or *D. richardsoni*) (Olivar and Beckley, 1995), *D. diadematus* (Olivar and Beckley, 1995), *D. mollis* (Olivar and Beckley, 1995), *D. metopoclampus* (Sparta, 1952), *D. pacificus* (Moser and Ahlstrom, 1974), California headlightfish (*D. theta*) (Moser and Ahlstrom, 1996), and Malayan lanternfish (*D. malayanus*) (Tsokur, 1975). The early stages of development are known in only 2 species of the 9 species of *Diaphus* that have been observed in the southwestern Pacific Ocean: *D. hudsoni* and *D. mollis* (McGinnis, 1982; Bekker and Evseenko, 1986).

Diaphus ostenfeldi is circumglobal, is distributed in the Subtropical Convergence, a frontal zone between subantarctic and tropical water masses, and is considered to be a convergence (Krefft, 1974), notal or subantarctic (Parin et al., 1974), or transitional (McGinnis, 1982; Bekker and Evseenko, 1986) species. This species has been observed in the central eastern Pacific Ocean (McGinnis, 1982) and in the southwestern Pacific Ocean (Bekker and Evseenko, 1986), and its range is known to extend to about 23–24°S in the region of the Benguela Current (Trunov, 1968; Hulley, 1972). It has been found at depths as great as about 120 m below the sea surface (Bekker, 1983). Juveniles have been taken at depths less than 100 m; larger specimens have been found at depths 160 m below the sea surface (Hulley, 1981; McGinnis, 1982). Little is known of the ecology of this species. Specimens caught in the South Atlantic Ocean were limited between the 10°C and 15°C isotherms at a depth of 200 m; however, it has been assumed that the species can live at shallower depths, in suitable temperatures (Krefft, 1974; Hulley, 1981).

Herein, we present larval descriptions for *D. ostenfeldi* from the southwestern Pacific Ocean based on a developmental series of larvae from the postflexion stage to the transformation stage.

Materials and methods

Larvae of *D. ostenfeldi* were caught at 4 stations (stations [st.] 3049, 3052,

3054, and 3069) during the 34th expedition of the RV *Dmitry Mendeleev* to the southwestern Pacific Ocean in January–February 1985 (Fig. 1). All specimens were caught by using an Isaacs-Kidd mid-water trawl with the Samyshev-Aseev modification in the depth layers of 0–100 m, 0–200 m, and 0–600 m in the area between 35°S and 57°S. This trawl is 25 m long and has a 5-mm mesh net without nodes and with a terminal insertion of 500-µm nylon mesh and a 6-m^2 mouth area. The specimens were preserved and stored in 10% formaldehyde. We captured 62 specimens that were 8.6–20.5 mm standard body length (SL); larvae of smaller sizes were absent in samples of trawl hauls.

Information for the following features are included in the descriptions of larval stages in this paper (Moser, 1996): SL, head length (HL), body depth at pectoral fin base (BD), preanal length (PAL), predorsal length (PDL), snout length (SnL), horizontal diameter of the eye (ED), number of rays in dorsal fin (D), number of rays in anal fin (A), number of rays in pectoral fin (P_1), number of rays in pelvic fin (P_2), number of rays in caudal fin (C), number of gill rakers (GR) on the upper and lower parts of the first gill arch, and number of vertebrae (V). Descriptions include patterns of the following photophores (Bekker, 1983): branchiostegal (Br), opercular (Op), pectolateral (PLO), pectoventral (PVO), pectoral (PO), ventrolateral (VLO), ventral (VO), supraanal (SAO), anterior anal (AOa), posterior anal (AOp), and posterolateral (Pol). Also included in descriptions are the following orbital glands: dorsonasal (Dn), anteorbital (Ant), suborbital (So), and ventronasal (Vn).

Results

Identification

The identification of large specimens (>20 mm SL) as *D. ostenfeldi* was based on the following features: the number of gill rakers on the first gill arch of 25–26, So absent, Ant present, Dn and Vn connected but not extended anteriorly from the olfactory rosette, no enlarged teeth in the lower jaw inner row, head depth approximately equal to its length, VLO about midway between lateral line and base of the ventral fin. The identification of specimens smaller than 20 mm SL was based on tracing characters from fully formed, large metamorphic specimens backward to smaller specimens.

Body proportions

The larvae have a moderately deep body (BD 24–28% SL). The head is relatively small (HL 25–30% SL) but deep with

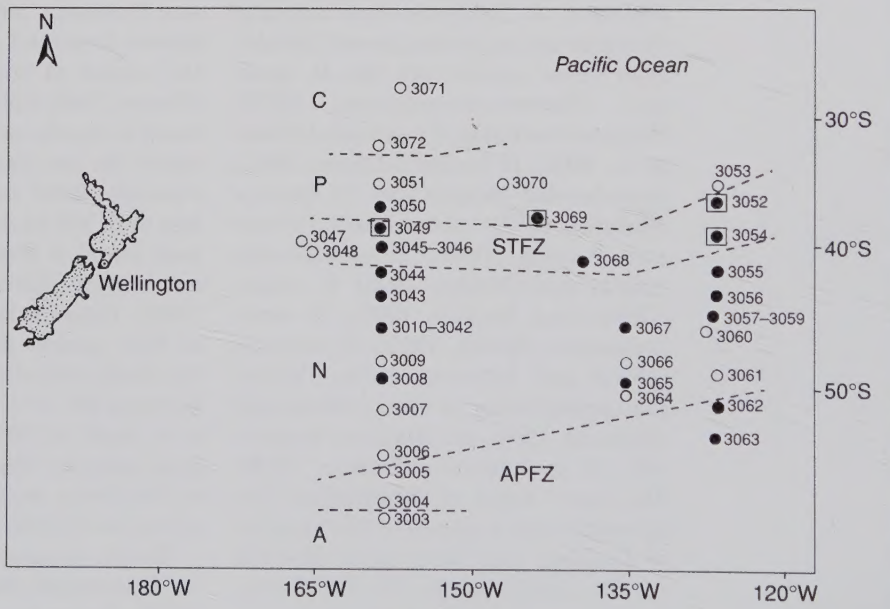

Figure 1

Schematic map of the stations (open circles) where larval (open squares) and adult (black circles) *Diaphus ostenfeldi* were sampled during the 34th cruise of the RV *Dmitry Mendeleev* in the southwestern Pacific Ocean between January and February 1985. Dashed lines indicate the positions of biogeographic borders (Becker and Evseenko, 1986) for the central water mass (C), periphery of the central water mass (P), subtropical frontal zone (STFZ), notal zone (N), Antarctic Polar Frontal Zone (APFZ), and Antarctic (A). Station numbers are given next to station markers.

a steep profile; the depth of the head at the corner of the mouth is almost equal to HL. The jaws are long and continue beyond the vertical of the eye posterior edge; both jaws have small teeth. Jaw length increases with larval size. The snout is short (SnL 19–22% HL), the eye is slightly oval at sizes up to about 16 mm SL (ED 25–30% HL). The anus opens slightly behind the midbody (PAL 57–61% SL). The dorsal fin begins almost at the middle of the body (PDL 44–48% SL). The posterior margin of the pectoral fin rays reaches the vertical of the ventral fin base, and the tips of the ventral fin rays reach the anal fin origin. The proportions are generally retained with increases in larval size.

Meristic characters

D: 16–17, A: 16, P_1: 11, P_2: 8, C: 6–10+9–6(5), GR: (8)9+1+15–17=25–26, V: 37–38. Fin rays are formed in all fins at 8.6 mm SL, and larvae have a definitive number of gill rakers at 12.0 mm SL. Larvae have 37–38 myomeres.

Pigmentation

The 8.6-mm-SL larva (Fig. 2A) has one melanophore dorsally on the peritoneum near the terminus of the gut, one melanophore behind the anal fin base (these melanophores

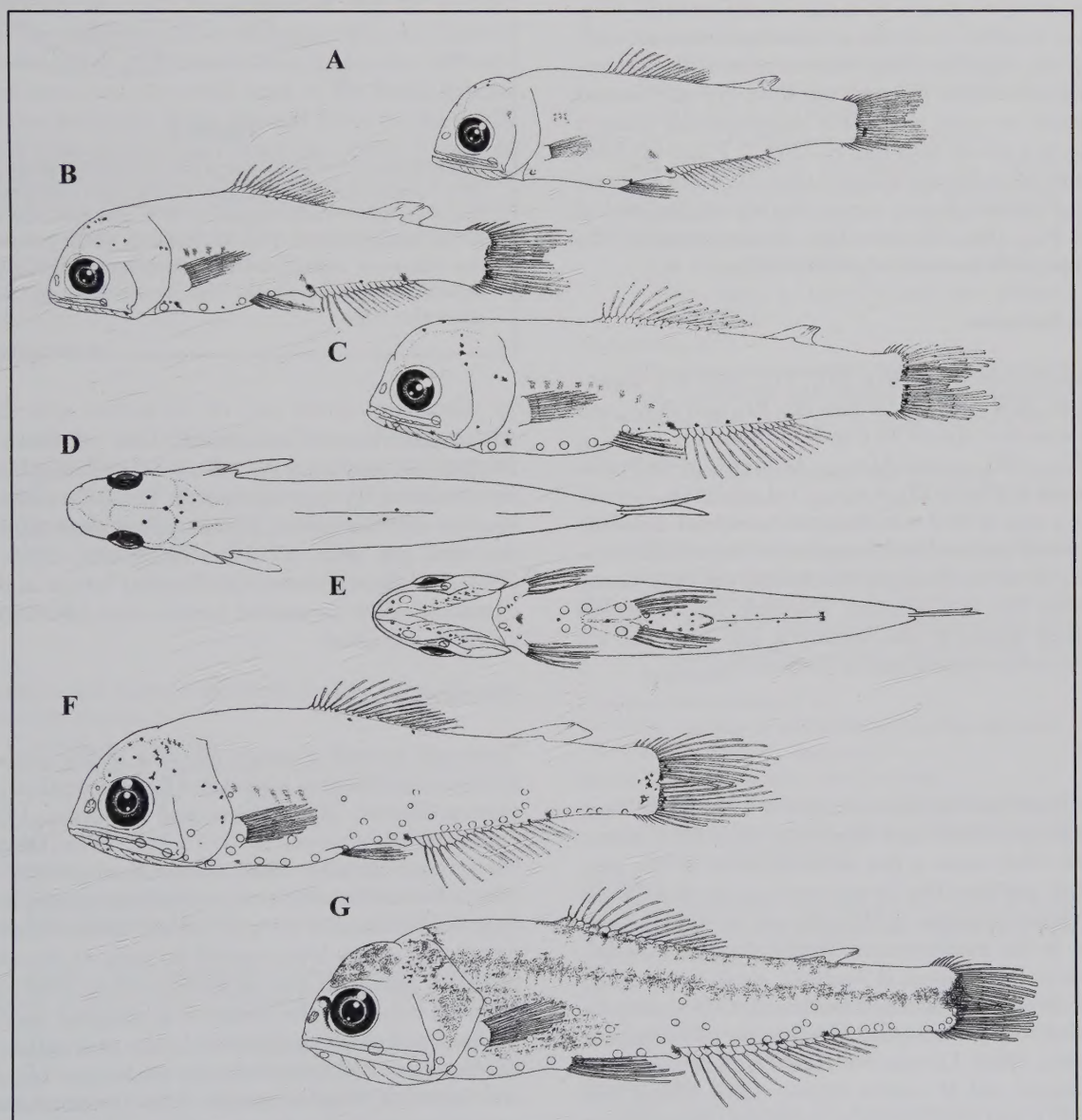

Figure 2

Illustrations of 5 larval and transformation specimens of *Diaphus ostenfeldi* caught in the southwestern Pacific Ocean in 1985: (**A**) 8.6 mm standard body length (SL), (**B**) 9.5 mm SL, (**C**) 10.7 mm SL, (**D**) 10.7 mm SL (dorsal view), (**E**) 10.7 mm SL (ventral view), (**F**) 15.8 mm SL, and (**G**) 20.5 mm SL.

are present in all specimens and noticeable to a size of 20.5 mm SL), and one melanophore above the posterior part of the anal fin base (approximately at the level of the 12th pterygiophore). Several melanophores are present proximally on the lower caudal fin rays. Internal melanophores are visible above the midbrain and above the otic capsules; melanophores are scattered on the dorsolateral part of the peritoneum. In the 9.5-mm-SL larva (Fig. 2B), melanophores are added at the dorsal fin base and at the base of some upper caudal fin rays. An unpaired internal melanophore is visible on the anteroventral part of the liver on the level of the pectoral fin base; melanophores appear above the hindbrain, on the opercle, and on the membrane between the branchiostegal rays. Pigmentation becomes more intense by a size of 10.7 mm SL (Fig. 2, C–E) and is added ventrally at some myosepta on each side along the anal fin base. Melanophores at the dorsal fin base and above the anal fin base are not located symmetrically on each side. This pigmentation pattern persists up to a size of 20.5 mm SL (Fig. 2, F and G). Ventrally, almost all individuals larger than 10.7 mm SL have a row of 2–4 melanophores: approximately at the level of the future PO_2, PO_5, VO_1, and VO_5. Pigmentation of the caudal fin persists to a size of 20.0 mm SL.

Photophore formation

The 8.6-mm-SL larva has Br_2, PO_1, PO_5, and VO_1 beginning to form. At a size of 11.0 mm SL, Br_1 and PO_{2-3} are added. Larvae at a size of 13.0 mm SL have Br_{1-3}, Op_{1-2}, PO_{1-5}, PVO_{1-2}, VO_{1-5}, and AOa_{2-7}. At a size of 16.0 mm SL, formation of PLO, VLO, SAO_{1-3}, Pol, and AOp_{1-5} ends (Fig. 2). By a size of 20.0 mm SL, specimens have a definitive photophore pattern, but formation of the orbital luminous glands is not yet complete: So absent, the dark tissue at the future Ant is triangular, roundish Dn connected with the dark tissue of the future Vn and Ant, and Vn reaches the anteroventral part of the eye (Fig. 3).

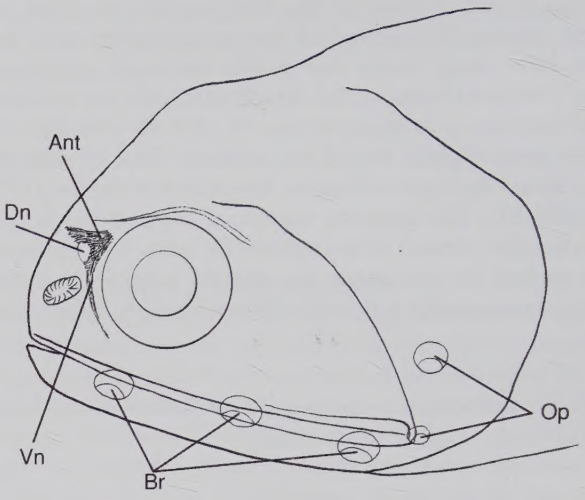

Figure 3

Illustration of the locations of the orbital luminous organs in a transformation specimen of *Diaphus ostenfeldi* that has a standard body length of 20.5 mm and was caught in the southwestern Pacific Ocean in 1985. Locations of the following organs are shown: dorsonasal (Dn), anteorbital (Ant), ventronasal (Vn), branchiostegal (Br), and opercular (Op).

Discussion

The larvae described herein belong to a moderately deep body morphotype (Moser and Ahlstrom, 1972, 1974; Moser et al., 1984). They have a few melanophores on the postanal ventral midline (Fig. 2) and have no So photophore (Fig. 3). In total, 9 species of *Diaphus* can be found in our study area in the southwestern Pacific Ocean: *D. anderseni*, *D. danae*, *D. effulgens*, *D. hudsoni*, small lantern fish (*D. meadi*), *D. mollis*, Taaning's lantern fish (*D. termophilus*), *D. parri*, and *D. ostenfeldi* (McGinnis, 1982; Bekker and Evseenko, 1986). Larvae are known for 2 of these species, *D. hudsoni* and *D. mollis* (Olivar, 1987; Olivar and Beckley, 1995), and they belong to a different morphotype that is moderately slender. In addition, they clearly differ from our larvae by the absence of pigmentation at the dorsal fin base and at the branchiostegal rays. Among the remaining 7 species, only 3 species, *D. effulgens, D. danae*, and *D. ostenfeldi*, have no So photophore as we observed in our transformation specimens. One of these species, *D. effulgens*, has fewer gill rakers on the first gill arch than we observed in our specimens (17–22 versus 24–25); another of those species, *D. danae*, has more gill rakers on the first gill arch (27–30) (Nafpaktitis, 1978; Bekker, 1983). For these reasons, the *Diaphus* larvae in the developmental series presented herein were identified as larvae of *D. ostenfeldi*.

Comparative notes

There are several common features in the pigmentation between our *Diaphus* larvae and those described in earlier reports (Sparta, 1952; Moser and Ahlstrom, 1974, 1996; Pertseva-Ostroumova, 1975; Tsokur, 1975; Olivar, 1987; Olivar and Beckley, 1995; Sassa et al., 2003): melanophores behind the cleithrum symphysis, at the peritoneum near the terminus of the gut, behind the anal fin base, and proximally on the lower caudal fin rays. At the same time, larval *D. ostenfeldi* can be distinguished from all known *Diaphus* larvae by the presence of pigment on the dorsal fin base and the branchiostegal rays at lengths ≥9.5 mm SL. One more difference between the larvae of *D. ostenfeldi* and the other *Diaphus* species is that parietal and peritoneal pigmentation appears earlier in development in the *D. ostenfeldi* than in its congeners. In addition, the transformation of larvae described in this article was still not complete even at a length of 20.5 mm SL; our larvae have a full complex of photophores typical for adults, but the formation of orbital glands was not yet completed. In all

Diaphus larvae described earlier by others (Sparta, 1952; Moser and Ahlstrom, 1974, 1996; Pertseva-Ostroumova, 1975; Tsokur, 1975; Olivar, 1987; Olivar and Beckley, 1995; Sassa et al., 2003), photophores are formed by a size of about 11–15 mm SL. This length may correlate with the size of adults. The *Diaphus ostenfeldi* attains a length of about 120 mm SL (Hulley, 1981), but the sizes of other species whose early stages are known do not exceed 90 mm SL (Hulley, 1981; Bekker, 1983).

Distribution

In the southwestern Pacific Ocean between 35°S and 57°S, adults of this species were encountered at the 18 stations sampled during the 34th expedition of the RV *Dmitry Mendeleev* in different water masses, from the central masses in the north of the study area across the subtropical frontal zone and the notal zone of the South Pacific Ocean to the Antarctic Polar Frontal Zone in the south of the study area (Bekker and Evseenko, 1986). Larvae of *D. ostenfeldi* were found at 4 stations in a narrow range of latitudes between 35°S and 39°S in the subtropical frontal zone. This area was located on the western periphery of the vast anticyclonic South Pacific Gyre.

Acknowledgments

This work was supported by the state assignment of Russian Academy of Sciences Institute of Oceanology no. 0149-2019-0009 and by the Russian Science Foundation (no. 19-14-00026). S. Evseenko submitted and revised this article prior to his death on 15 October 2020.

Literature cited

Bekker, V. E.
1983. Myctophid fishes of the World Ocean, 248 p. Moscow, Russia. [In Russian.]

Bekker, V. E., and S. A. Evseenko.
1986. Distribution of mesopelagic fishes and biogeographic boundaries in the southern part of the Pacific Ocean in January–February 1985. J. Ichthyol. 26:890–901. [In Russian.]

Fricke, R., W. N. Eschmeyer, and R. Van Der Laan (eds.).
2020. Eschmeyer's catalog of fishes: genera, species, references. [Available from website, accessed April 2020.]

Hulley, P. A.
1972. A report on the mesopelagic fishes collected during the deep-sea cruises of R.S. 'Africana II', 1961–1966. Ann. S. Afr. Mus. 60:197–236.
1981. Results of the research cruises of FRV 'Walther Herwig' to South America: 58. Family Myctophidae (Osteichthyes, Myctophiformes). Archiv. Fischereiwiss. 31(1):1–303.

Krefft, G.
1974. Investigations on midwater fish in the Atlantic Ocean. Ber. dt. wiss. Kommn Meeresforsch. 23:226–254.

McGinnis, R. F.
1982. Biogeography of lanternfishes (Myctophidae) south of 30°S. Antarct. Res. Ser. 35, 110 p. Am. Geophys. Union, Washington D.C.

Moser, H. G.
1996. Introduction. *In* The early stages of fishes in the California Current region (H. G. Moser, ed.), p. 1–72. CalCOFI Atlas 33.

Moser, H. G., and E. H. Ahlstrom.
1972. Development of the lanternfish, *Scopelopsis multipunctatus* Brauer 1906, with a discussion of its phylogenetic position in the family Myctophidae and its role in a proposed mechanism for the evolution of photophore patterns in lanternfishes. Fish. Bull. 70:541–564.
1974. The role of larval stages in systematic investigations of marine teleosts: the Myctophidae, a case study. *In* The early life history of fish (J. H. S. Blaxter, ed.), p. 605–607. Springer, Berlin, Germany.
1996. Myctophidae: lanternfishes. *In* The early stages of fishes in the California Current region (H. G. Moser, ed.), p. 387–475. CalCOFI Atlas 33.

Moser, H. G., E. H Ahlstrom, and J. R. Paxton.
1984. Myctophidae: development. *In* Ontogeny and systematics of fishes. Based on an international symposium dedicated to the memory of Elbert Halvor Ahlstrom; La Jolla, CA, 15–18 August 1983 (H. G. Moser, W. J. Richards, D. M. Cohen, M. P. Fahay, A. W. Kendall Jr., and S. L. Richardson, eds.), p. 218–239. Am. Soc. Ichthyol. Herpetol., Spec. Publ. 1.

Nafpaktitis, B. G.
1978. Systematics and distribution of lanternfishes of the genera *Lobianchia* and *Diaphus* (Myctophidae) in the Indian Ocean. Bull. Los Ang. Cty. Mus. Nat. Hist. Sci. 30, 92 p.

Olivar, M. P.
1987. Larval development and spawning of *Diaphus hudsoni* in the Benguela Current region. Mar. Biol. 94:605–611.

Olivar, M.-P., and L. E. Beckley.
1995. Early development of *Diaphus* spp. (Pisces: Myctophidae) of the Agulhas Current. S. Afr. J. Mar. Sci. 16:129–139.

Parin, N. V., A. P. Andriashev, O. D. Borodulina, and V. M. Tchuvasov.
1974. Midwater fishes of the southwestern Atlantic Ocean. Tr. Inst. Okeanol. Akad. Nauk SSSR 98:76–140. [In Russian.]

Pertseva-Ostroumova, T. A.
1975. Larvae of lanternfish *Diaphus agassizii*. J. Ichthyol. 15:677–681. [In Russian.]

Sassa, C., K. Kawaguchi, and V. J. Loeb.
2003. Early development of *Diaphus garmani* (Myctophidae) in the transition region of the western North Pacific. Ichthyol. Res. 50:94–97.

Sparta, A.
1952. Contributo alla conoscenza dello sviluppo larvale di *Myctophum metopoclampum* Cocco. Boll. Pesca Idriobiol. 7:5–10. [In Italian.]

Trunov, I. A.
1968. New data on the distribution of *Electrona rissoi* (Cocco) and *Diaphus ostenfeldi* (Taning) (Myctophidae). J. Ichthyol. 4:745–748. [In Russian.]

Tsokur, A. G.
1975. Materials on the development of the Malayan headlightfish *Diaphus malayanus* Weber, 1913 (Myctophidae, Pisces). J. Ichthyol. 15:682–694. [In Russian.]

National Marine
Fisheries Service
NOAA

Fishery Bulletin
established in 1881

Spencer F. Baird
First U.S. Commissioner
of Fisheries and founder
of *Fishery Bulletin*

Age and growth of stone scorpionfish (*Scorpaena mystes*) from the Gulf of California in Mexico

Ulianov Jakes-Cota (contact author)[1]
Arturo Tripp-Valdez[1]
Marisol Arce-Acosta[1]
Francisco Omar López-Fuerte[2]

Email address for contact author: ujakesc@gmail.com

[1] Departamento de Pesquerías y Biología Marina
Centro Interdisciplinario de Ciencias Marinas
Instituto Politécnico Nacional
Avenida Instituto Politécnico Nacional s/n
Colonia Playa Palo de Santa Rita
Apartado Postal 592
23096 La Paz, Baja California Sur, Mexico

[2] Laboratorio de Sistemas Arrecifales
Departamento Académico de Ciencias
Marinas y Costeras
Universidad Autónoma de Baja California Sur
Carretera al Sur km 5.5
23080 La Paz, Baja California Sur, Mexico

Abstract—The stone scorpionfish (*Scorpaena mystes*) is common throughout the Gulf of California in Mexico. Because little information is available regarding the basic biological characteristics of this species and because commercial demand for it is increasing, the need for studies of population dynamics is urgent. We sampled 233 stone scorpionfish (117 males and 116 females) in the Gulf of California from May 2015 through April 2016 to estimate age and individual growth. Total lengths (TL) ranged between 15.3 and 35.5 cm for males and between 19.0 and 44.5 cm for females. Results from analysis of the edge types of otoliths (opaque and translucent) indicate an annual periodicity in the formation of annuli in sagittae. Ages of stone scorpionfish ranged from 2 to 10 years for males and from 3 to 15 years for females. Estimates for the parameters of the von Bertalanffy growth function were 34.76 and 48.22 cm TL for asymptotic length, 0.202/year and 0.135/year for growth coefficient, and −1.28 and −0.80 years for theoretical age at length zero for males and females, respectively. This study resulted in the first estimates of age and individual growth of stone scorpionfish, information that is essential for evaluation and management of this important fishery resource.

Manuscript submitted 14 May 2020.
Manuscript accepted 15 October 2020.
Fish. Bull. 118:324–328 (2020).
Online publication date: 29 October 2020.
doi: 10.7755/FB.118.4.2

The views and opinions expressed or implied in this article are those of the author (or authors) and do not necessarily reflect the position of the National Marine Fisheries Service, NOAA.

The stone scorpionfish (*Scorpaena mystes*) is commonly found throughout the Gulf of California in Mexico, with a distribution in the eastern Pacific Ocean that extends from southern California to Chile, including offshore islands (Butler et al., 2012). This demersal species occurs in shallow waters and seaweed-covered reefs as well as in open, sandy areas to depths of 85 m. It is considered an opportunistic predator and feeds mainly on crustaceans and small fish (Butler et al., 2012). Adults reach sizes up to 51 cm in total length (TL) (Robertson and Allen, 2015).

The meat of stone scorpionfish is considered to be of excellent quality and has high commercial value; as a result, this species has become an important fishery resource (Jakes-Cota et al., 2017). Historically, however, this species has not been sought after commercially because venom glands located along the spines of the fins can cause painful injuries and severe respiratory disorders (Poss, 1995); it has long been a secondary priority species in the artisanal fishery in the Gulf of California. Since 2012, decreases in the catches of other species of high commercial value, such as the Pacific red snapper (*Lutjanus peru*) and yellowtail jack (*Seriola lalandi*), caused an increase in price and capture volume of the stone scorpionfish, driving this species into the commercial sector as a complementary, high-quality product.

Given the little amount of data available on the basic biological characteristics of this species and its recent commercial exploitation in the region of the Gulf of California, there is an urgent need to document its basic life history (e.g., age, growth, mortality, and reproduction) and its population dynamics and to create a management protocol for this fishery resource. Age and individual growth should be included as key elements in every investigation focused on the rational exploitation of fishing resources (Beamish and Fournier, 1981). Prior to this study, the age and individual growth characteristics of stone scorpionfish were not available; therefore, the aims of our study were 1) to estimate age by using otoliths, 2) to

estimate individual growth parameters, and 3) to test for significant differences in growth trajectories between males and females.

Materials and methods

Stone scorpionfish were collected once a month (21–22 individuals per month) in the artisanal fishery from May 2015 through April 2016. The fish were taken by spearing while using semiautonomous diving equipment (hookah), at depths up to 30 m, at different fishing sites along 20 km of coastline south of the harbor of Santa Rosalia in Baja California Sur, Mexico. The standard length (SL) and TL were measured to the nearest millimeter, and the weight (W) was recorded to the nearest 0.1 g for each individual. Sex was determined by using macroscopic examination of the gonads, and the exact binomial test was used to test differences in sex ratio. Pairs of sagittae were extracted, cleaned, and stored dry in plastic vials in the laboratory, and only the right otoliths were used for the analyses described in the rest of this section.

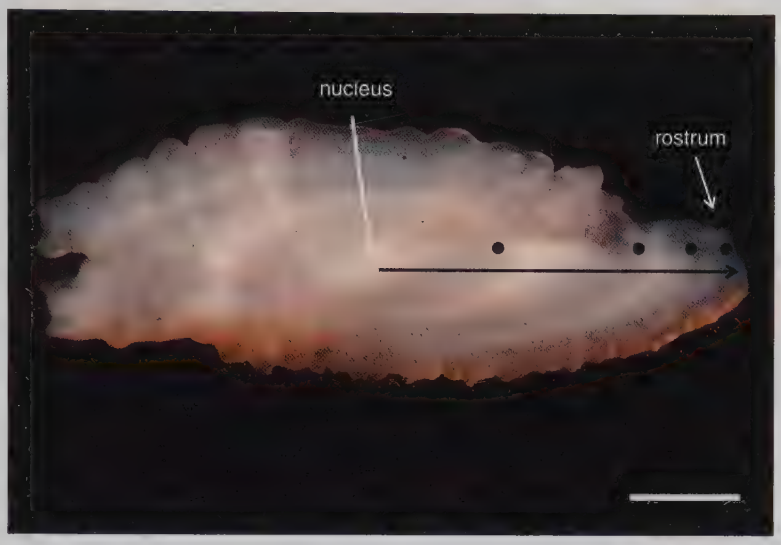

Figure 1

Photograph showing the annular pattern in the sagittae of a 4-year-old male stone scorpionfish (*Scorpaena mystes*) caught in May 2015 in the Gulf of California in Mexico. Black dots indicate annuli. The black arrow indicates the measurement of the otolith radius. The scale bar is equal to 1 mm.

To describe the length–weight relationship, we used this equation:

$$W = aTL^b, \quad (1)$$

where a = the intercept of the regression line; and
b = the allometric coefficient, the slope of the regression line.

To describe the relationship independently for males and females with log-transformed length and weight data, we used this equation:

$$\log W = a + b\log TL. \quad (2)$$

The a and b parameters were estimated by using a simple linear regression analysis. A Student's t-test was performed to evaluate whether the b-value was significantly different from 3, a value that indicates an isometric growth pattern (i.e., all body parts grow at approximately the same rate, and a fish has an unchanging body form throughout development). An analysis of covariance was used to test differences in b-values between males and females.

The otolith radius (OR) (Fig. 1) was measured under a stereoscope (Stemi SV11[1], Carl Zeiss AG, Oberkochen, Germany) at 3.2× magnification by using the imaging software AxioVision, vers. 4.6 (Carl Zeiss AG). The stereoscope was attached to a digital camera (AxioCam MRc 5, Carl Zeiss AG). The relationship between TL and OR was described by using a simple linear regression analysis.

Right otoliths were immersed in ethanol with the concave side down, and 2 independent readers counted the annuli once with a stereoscope, using reflected light against a dark background without prior knowledge of fish length or weight. Under reflected light, the nucleus (the core of the otolith) and the opaque bands appeared as light rings and the translucent bands appeared as dark rings (e.g., La Mesa et al., 2005, 2010; Bilgin and Çelik, 2009). The combination of an opaque band followed by a translucent band was considered to be an annulus, as has been done for other scorpionfish species (e.g., Massutí et al., 2000; La Mesa et al., 2005, 2010; Bilgin and Çelik, 2009). Annuli were counted from the nucleus toward the tip of the rostrum (the anterior projection of the otolith) along the same line (Fig. 1). The precision between readers was evaluated by using the mean coefficient of variation (CV) and average percent error (APE). Values of 5.5% for APE and of 7.6% for CV have been considered adequate in many aging studies (Campana, 2001).

To validate the periodicity of the formation of opaque and translucent bands and to assign a unit of time (e.g., years) to the counted annuli, edge type analysis was used. For this analysis, the edge type of each otolith was recorded as either opaque or translucent, and, for each month, the percentages of opaque edges and of translucent edges in the total number of otoliths analyzed was plotted.

[1] Mention of trade names or commercial companies is for identification purposes only and does not imply endorsement by the National Marine Fisheries Service, NOAA.

The von Bertalanffy growth function was fitted to length-at-age data to estimate individual growth:

$$L_t = L_\infty\left(1 - e^{-k(t-t_0)}\right), \quad (3)$$

where L_t = the length (TL, in centimeters) at age t;
L_∞ = the asymptotic length;
k = the growth coefficient; and
t_0 = the theoretical age at length zero.

Additionally, a likelihood ratio test (Kimura, 1980), also known as the *likelihood ratio chi-square test*, was applied to test for differences between males and females in parameters of individual growth.

Results

During the study period, 233 stone scorpionfish (117 males and 116 females) were sampled. No significant difference was found in the ratio of males to females when applying a 1:1 exact binomial test ($P>0.05$). However, the number of males was lower than the number of females for the large fish (>30 cm TL). Overall, 70% of the sampled individuals ranged in size between 20 and 30 cm TL. The lengths of the males ranged from 15.3 to 35.5 cm TL (12.5–28.9 cm SL), with a mean length of 25.9 cm TL (SE 3.60). Comparatively, the lengths of the females ranged from 19.0 to 44.5 cm TL (15.5–36.5 cm SL), with a mean length of 27.8 cm TL (SE 5.17). Weights ranged from 64 to 1033 g for males, with a mean weight of 406 g (SE 181), and from 119 to 1870 g for females, with a mean weight of 545 g (SE 385). The analysis of variance revealed significant differences in mean length ($F_{(1,231)}=10.67$, $P<0.05$) and mean weight ($F_{(1,231)}=12.57$, $P<0.05$) between males and females. Females were longer and heavier than males.

The length–weight relationship (Table 1) was not significantly different between males and females ($F_{(1,229)}=1.27$, $P>0.05$). The b-value of the length–weight relationship of males and females was not significantly different from 3 ($P>0.05$), indicating an isometric growth pattern.

Otolith radius ranged between 2.5 and 5.6 mm. The linear regression model developed to predict the relationship between OR and TL was as follows:

$$TL = -3.53 + 3.91OR. \quad (4)$$

The linear relationship between both variables was significant (coefficient of determination [r^2]=0.79, $P<0.05$).

The highest percentage of otoliths with opaque edges was recorded in August (81%), followed by the percentage in December (65%), and the highest percentages of otoliths with translucent edges were observed in February (80%) and June (68%). These results indicate that the periodicity of annulus formation is annual and that the formation of a new annulus begins with an opaque band in the months of August–September and ends with a translucent band in the months of May–July.

The detections of annuli were confirmed and annuli could be counted in 98% of the 233 otoliths analyzed. For the remaining 2% of otoliths, the annuli could not be counted because they were not visible. The ages of individual specimens ranged between 2 and 10 years for males and between 3 and 15 years for females. The most frequent ages ranged from 5 to 7 years (63%) for males and from 4 to 6 years (74%) for females. The values of CV and APE were 6.50 and 4.59, respectively.

The parameters of the von Bertalanffy growth function for males and females and the growth curves that were fitted to length-at-age data are shown in Figure 2. Results of the likelihood ratio test indicate significant differences in parameters of the von Bertalanffy growth function between males and females ($\chi^2=1.89$, $P<0.05$); females grew slower (indicated by a lower k value) yet reached a greater maximum average length (indicated by a greater L_∞) than males.

Discussion

In this study, the maximum length recorded for stone scorpionfish was 44.5 cm TL, which is comparable to the maximum length of 51 cm TL previously reported for this species (Robertson and Allen, 2015). In addition, individuals larger

Table 1

Estimates of the parameters from regression analysis of the length–weight relationship for male and female stone scorpionfish (*Scorpaena mystes*) caught in the Gulf of California in Mexico during May 2015–April 2016. The parameters are the intercept (a) and slope (b) of the regression line. r^2=coefficient of determination; CI=confidence interval; SE=standard error of the mean.

	a			b			
Sex	Mean	SE	95% CI	Mean	SE	95% CI	r^2
Males	0.0205	0.29136	0.0115–0.0365	3.01	0.08975	2.84–3.19	0.90
Females	0.0159	0.18687	0.0109–0.0229	3.09	0.05696	2.98–3.21	0.93

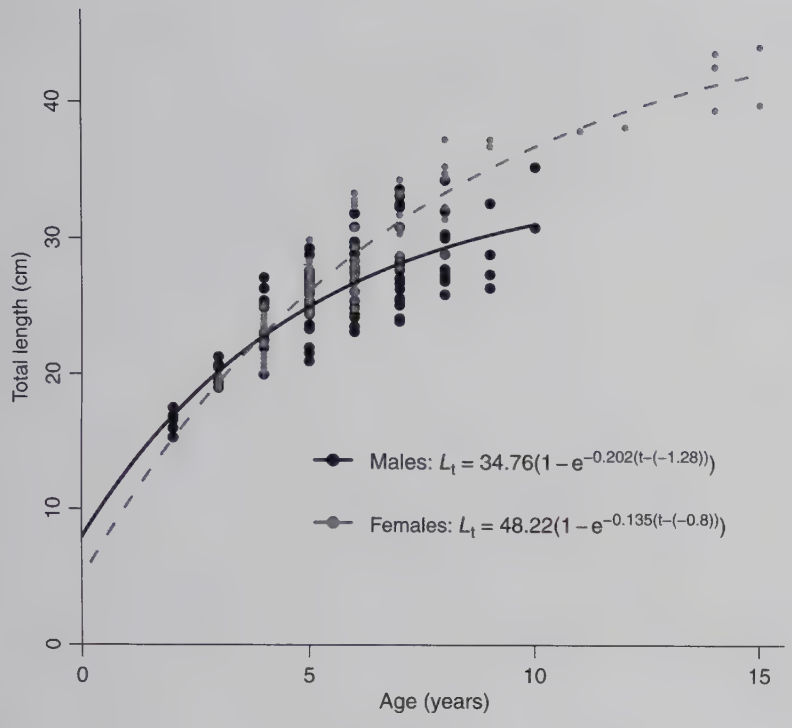

Figure 2

Growth curves from the von Bertalanffy growth function fitted to length-at-age data for male (black dots) and female (gray dots) stone scorpionfish (*Scorpaena mystes*) caught in the Gulf of California in Mexico during May 2015–April 2016. L_t=total length at age t.

than 30 cm TL were scarce in our sampling, possibly a consequence of cumulative mortality in which larger and older individuals are removed by fishing or die naturally (Csirke, 1980).

The characteristics of the length–weight relationship indicate an isometric growth pattern for both males and females. Similar results were reported for this species even when males and females were not analyzed separately (Jakes-Cota et al., 2017). In contrast to these findings, it has been reported that other species of the genus *Scorpaena*, such as the black scorpionfish (*S. porcus*) (Bilgin and Çelik, 2009; Demirhan and Can, 2009), Madeira rockfish (*S. maderensis*) (La Mesa et al., 2005), and small red scorpionfish (*S. notata*) (Neves et al., 2015), commonly have positive allometric growth. However, as in our study of the stone scorpionfish and in studies of other scorpionfish species, such as the blackbelly rosefish (*Helicolenus dactylopterus*) (Massutí et al., 2000), results also indicate isometric growth.

The relationship between OR and TL of stone scorpionfish in our study was linear and statistically significant, indicating that these measurements have a relation of proportionality and that the OR may be a predictor of fish length. This relationship has been reported for other species of *Scorpaena*, such as the Madeira rockfish (La Mesa et al., 2005) and small red scorpionfish (Scarcella et al., 2011).

Results of the edge type analysis indicate that the periodicity of annulus formation in stone scorpionfish has an annual pattern. The highest percentages of opaque edges among all otoliths analyzed coincided with the highest condition factor values reported by Jakes-Cota et al. (2017) for stone scorpionfish for the months of August and September. This finding indicates that conditions for growth (e.g., high temperatures and high food availability) are favorable in our study area (Le Cren, 1951). In contrast, the highest percentages of translucent edges among all otoliths analyzed coincided with the lowest condition factor values reported by Jakes-Cota et al. (2017) for the months of February–June. This finding indicates conditions (e.g., low temperatures and scarce food) are unfavorable in our study area and may limit growth (Le Cren, 1951). The annual periodicity of annulus formation in otoliths has been reported for other scorpionfish species, such as the black scorpionfish (Bilgin and Çelik, 2009; Demirhan and Can, 2009; La Mesa et al., 2010), small red scorpionfish (Scarcella et al., 2011; Neves et al., 2015), Madeira rockfish (La Mesa et al., 2005), and blackbelly rosefish (Massutí et al., 2000).

Annuli were apparent in the otoliths of stone scorpionfish used in this study. In general, translucent bands are slightly wider than the opaque bands, and as the number of annuli increased, the widths of both bands decreased. Both bands were clearly observed and distinguished, and it was relatively simple to count them, as evidenced by the low values of CV and APE; these low values indicate a high concordance between counts performed independently by readers and reflect consistency between observations. In this study, we found a significant relationship between the OR and length of fish, an annual pattern of annulus formation in otoliths, and a high precision in the counting of annuli between technicians. These results indicate that the otolith is a structure that can be used reliably in age estimation of stone scorpionfish.

This study is the first to report age and individual growth characteristics for stone scorpionfish. We found males up to 10 years old and females up to 15 years old, and we determined that individuals 4–7 years old composed the most abundant age class in our sample.

Individual growth characteristics were significantly different between males and females. In addition, our results indicate that females are larger, heavier, and older than males. This pattern of distinctive growth between males and females has been reported previously for the black scorpionfish (Bilgin and Çelik, 2009). However, it is also common that males reach lengths,

ages, and L_∞ that are greater than those of females, as has been observed for other species, such as the Madeira rockfish (La Mesa et al., 2005), small red scorpionfish (Neves et al., 2015), and blackbelly rosefish (Massutí et al., 2000). Results from our study indicate that males and females take approximately 10 years to reach a size of 30 and 35 cm TL, respectively, indicating that the stone scorpionfish is a slow-growing species, like most scorpionfish species.

The estimates of ages and individual growth rates reported from this study improve our knowledge of the stone scorpionfish. Information from this study can be used for stock assessment and management of a species of emerging fishing potential in the artisanal fishery of the Gulf of California.

Acknowledgments

The senior author and A. Tripp-Valdez would like to thank the Instituto Politécnico Nacional for funding through a grant from the Programa de Estímulos al Desempeño de los Investigadores. The senior author, A. Tripp-Valdez, and F. López-Fuerte are grateful for the support of the Sistema Nacional de Investigadores of the Consejo Nacional de Ciencia y Tecnología. D. Whitehead and S. Rousso reviewed the English version of this manuscript.

Literature cited

Beamish, R. J., and D. A. Fournier.
1981. A method for comparing the precision of a set of age determinations. Can. J. Fish. Aquat. Sci. 38:982–983.

Bilgin, S., and E. Ş. Çelik.
2009. Age, growth and reproduction of the black scorpionfish, *Scorpaena porcus* (Pisces, Scorpaenidae), on the Black Sea coast of Turkey. J. Appl. Ichthyol. 25:55–60.

Butler, J. L., M. S. Love, and T. E. Laidig.
2012. A guide to the rockfishes, thornyheads, and scorpionfishes of the Northeast Pacific, 185 p. Univ. Calif. Press, Berkeley, CA.

Campana, S. E.
2001. Accuracy, precision and quality control in age determination, including a review of the use and abuse of age validation methods. J. Fish Biol. 59:197–242.

Csirke, J.
1980. Introducción a la dinámica de poblaciones de peces. FAO Fish. Tech. Pap. 192, 82 p. FAO, Rome. [In Spanish.]

Demirhan, S. A., and M. F. Can.
2009. Age, growth and food composition of *Scorpaena porcus* (Linnaeus, 1758) in the southeastern Black Sea. J. Appl. Ichthyol. 25:215–218.

Jakes-Cota, U., A. Tripp-Valdez, and F. O. López-Fuerte.
2017. Length-weight relationship and relative condition factor of the stone scorpionfish *Scorpaena mystes* in the central area of the Gulf of California, Mexico. Hidrobiológica 27:127–129.

Kimura, D. K.
1980. Likelihood methods for the von Bertalanffy growth curve. Fish. Bull. 77:765–776.

La Mesa, M., G. La Mesa, and M. Micalizzi.
2005. Age and growth of madeira scorpionfish, *Scorpaena maderensis* Valenciennes, 1833, in the central Mediterranean. Fish. Res. 74:265–272.

La Mesa, M., G. Scarcella, F. Grati, and G. Fabi.
2010. Age and growth of the black scorpionfish, *Scorpaena porcus* (Pisces: Scorpaenidae) from artificial structures and natural reefs in the Adriatic Sea. Sci. Mar. 74:677–685.

Le Cren, E. D.
1951. The length-weight relationship and seasonal cycle in gonad weight and condition in the perc (*Perca fluviatilis*). J. Anim. Ecol. 20:201–219.

Massutí, E., B. Morales-Nin, and J. Moranta.
2000. Age and growth of blue-mouth, *Helicolenus dactylopterus* (Osteichthyes: Scorpaenidae), in the western Mediterranean. Fish. Res. 46:165–176.

Neves, A., V. Sequeira, A. R. Vieira, R. B. Paiva, and L. S. Gordo.
2015. Age and growth of small red scorpionfish, *Scorpaena notata* (Actinopterygii: Scorpaeniformes: Scorpaenidae), a common discard species from the Portuguese fishery. Acta Ichthyol. Piscat. 45:13–20.

Poss, S. G.
1995. Scorpaenidae. *In* Guía FAO para la identificación de especies para los fines de la pesca. Pacífico Centro-Oriental. Vol. 3. Vertebrados—parte 2 (W. Fischer, F. Krupp, W. Schneider, C. Sommer, K. E. Carpenter, and V. H. Niem, eds.), p. 1544–1564. FAO, Rome. [In Spanish.]

Robertson, D. R., and G. R. Allen.
2015. Shorefishes of the tropical eastern Pacific: online information system, vers. 2.0. Smithsonian Trop. Res. Inst., Balboa, Panama. [Available from website, accessed November 2019.]

Scarcella, G., M. La Mesa, F. Grati, and P. Polidori.
2011. Age and growth of the small red scorpionfish, *Scorpaena notata* Rafinesque, 1810, based on whole and sectioned otolith readings. Environ. Biol. Fish. 91:369.

National Marine
Fisheries Service
NOAA

Fishery Bulletin
established in 1881

Spencer F. Baird
First U.S. Commissioner
of Fisheries and founder
of *Fishery Bulletin*

Growth rates of bonnetheads (*Sphyrna tiburo*) estimated from tag-recapture data

Bryan S. Frazier (contact author)[1]
Dana M. Bethea[2]
Robert E. Hueter[3]
Camilla T. McCandless[4]
John P. Tyminski[3]
William B. Driggers III[5]

Email address for contact author: frazierb@dnr.sc.gov

[1] Marine Resources Research Institute
South Carolina Department of Natural Resources
217 Fort Johnson Road
Charleston, South Carolina 29412

[2] Southeast Regional Office
National Marine Fisheries Service, NOAA
263 13th Avenue South
Saint Petersburg, Florida 33701

[3] Center for Shark Research
Mote Marine Laboratory
1600 Ken Thompson Parkway
Sarasota, Florida 34236

[4] Northeast Fisheries Science Center
National Marine Fisheries Service, NOAA
28 Tarzwell Drive
Narragansett, Rhode Island 02882

[5] Mississippi Laboratories
Southeast Fisheries Science Center
National Marine Fisheries Service, NOAA
P.O. Drawer 1207
Pascagoula, Mississippi 39567

Abstract—Results from published age and growth models for bonnetheads (*Sphyrna tiburo*) indicate significant differences in life history between populations in the eastern Gulf of Mexico (GOM) and those in estuarine waters of the Atlantic coast of the southeastern United States (hereafter referred to as the *Atlantic region*). An age-independent model, GROTAG, was used with region-specific tag-recapture data to generate estimates of von Bertalanffy growth parameters and growth rates for sharks in each of these regions, and these estimates were compared with age-based life history characteristics. Results from the GROTAG model indicate that female bonnetheads in the GOM initially grew faster and attained a smaller maximum size than females in the Atlantic region. The final GROTAG model for females in the Atlantic region produced estimates of von Bertalanffy parameters and growth rates similar to those produced by the age-based growth model. For the population in the GOM, GROTAG model results indicate that growth rates were slower and average maximum size and longevity were greater than those from age-based models. Although models for males were generated with tag-recapture data, large 95% confidence intervals hindered comparisons. For both sexes and regions, calculated maximum longevity and age at 50% maturity are larger than published estimates, indicating that age underestimation may have occurred in both age and growth studies, with significant differences in estimates of life history characteristics for bonnetheads in the GOM.

Manuscript submitted 1 April 2020.
Manuscript accepted 9 October 2020.
Fish. Bull. 118:329–345 (2020).
Online publication date: 3 November 2020.
doi: 10.7755/FB.118.4.3

The views and opinions expressed or implied in this article are those of the author (or authors) and do not necessarily reflect the position of the National Marine Fisheries Service, NOAA.

Growth of wild fish is primarily estimated by using 3 types of models: age-based models in which length and estimated age are known; length-based models that use modal progressions in length-frequency data; and models that use length at capture, known time at liberty, and length at recapture from tag-recapture data to model growth trajectories. Length-based models are useful; however, they are suitable only for estimating growth in younger age classes because substantial overlap in lengths of fish can occur in older cohorts (Campana, 2001; Natanson et al., 2018a). Methods based on the use of age and tag-recapture data often characterize growth of fish by using the von Bertalanffy growth function (VBGF) (Ricker, 1975; Francis, 1988a). Growth of fish is most commonly estimated by using age-based models; however, models developed with tag-recapture data are often used as alternative models for large, long-lived species that may not be able to tolerate high rates of fishing mortality or for species for which age estimation is difficult or imprecise (Cailliet et al., 1992; Treble et al., 2008).

All methods of modeling growth have limitations and potential biases. Age estimation can be imprecise and is difficult to validate for many species (Beamish and McFarlane, 1983), especially elasmobranchs (Goldman, 2004) and deepwater species (Rigby et al., 2014). Validation of age estimates is recommended for all age and growth studies; however, validation of all age classes is difficult and rarely achieved (Cailliet et al., 2006). Although validation of ages has been completed for several species of elasmobranchs (Campana et al., 2002; Ardizzone et al., 2006; Kneebone et al., 2008), there is a growing body of evidence that indicates that age underestimation commonly occurs for long-lived species, such as sharks (e.g., Francis et al., 2007; Passerotti et al., 2014; Harry, 2018; Natanson et al., 2018b), as well as recent evidence that age underestimation may also occur in sharks with

intermediate longevities (Frazier et al., 2014). For these reasons, modeling of growth with tag-recapture data and newer methods of modeling that combine tag-recapture data with age estimates have been recommended (Eveson et al., 2007; Aires-da-Silva et al., 2015; Francis et al., 2016; Natanson and Deacy, 2019).

Growth models that use tag-recapture data also have limitations and biases. To accurately represent growth in a population, recapture data should include individuals throughout the range of lengths found in the population. However, this goal is rarely achieved with most data sets. Further, growth of fish may be affected by tagging (Kelly and Barker, 1963; Saunders and Allen, 1967), including elasmobranch growth (Gruber, 1982; Parsons, 1987; Davenport and Stevens, 1988; Kalish and Johnston, 2001). Measurement error in body length of tagged and recaptured fish can also bias models; however, some methods of modeling data can incorporate measurement error as a parameter (Francis, 1988b). When sufficient tag-recapture data are available, models can be used to verify or compare growth rates and estimates of longevity (maximum age) and age at maturity with those from traditional age-based models (e.g., Natanson et al., 2002; Welsford and Lyle, 2005; Natanson and Deacy, 2019). One advantage of models based on tag-recapture data is that, if recapture data spans multiple seasons, information about growth variability and seasonal changes in growth can be determined (Francis, 1988b). Such information can be especially useful when comparing region-specific growth rates between or within populations.

The bonnethead (*Sphyrna tiburo*) is a relatively small shark species, with individuals reaching a maximum size of 150 cm total length, that is commonly found in the coastal and estuarine waters of the western North Atlantic Ocean from North Carolina to southern Brazil, including the Gulf of Mexico (GOM) and the Caribbean Sea (Compagno, 1984). Significant differences in life history characteristics exist between bonnetheads captured off the Atlantic coast of the southeastern United States (hereafter referred to as the *Atlantic region*) and those caught in the eastern GOM (Frazier et al., 2014). Regional variation in life history between populations in the Atlantic region and in the GOM has been found for other coastal shark species, including the Atlantic sharpnose shark (*Rhizoprionodon terraenovae*) (Carlson and Loefer[1]), blacknose shark (*Carcharhinus acronotus*) (Driggers et al., 2004), and finetooth shark (*C. isodon*) (Drymon et al., 2006; Vinyard et al., 2019).

The regional differences observed in bonnetheads are greater than those that have been described for any adjoining populations of other elasmobranch species. Significant differences in growth characteristics of bonnetheads have been found between populations in the GOM and the Atlantic region (Frazier et al., 2014). For the population in the Atlantic region, estimated maximum age (males: 12.0 years; females: 17.9 years) and age at 50% maturity (males: 3.9 years; females: 6.7 years) are more than twice the estimates for the population in the GOM (males: 5.5+ years for maximum age, 1.7 years for age at 50% maturity; females: 7.5+ years for maximum age, 2.9 years for age at 50% maturity) (Lombardi-Carlson et al., 2003; Frazier et al., 2014). Previous age and growth studies of bonnetheads in the eastern GOM (Parsons, 1993; Carlson and Parsons, 1997; Lombardi-Carlson et al., 2003) found significant latitudinal variation in life history traits; however, latitudinal variation has not been detected in the population off the Atlantic coast (Frazier et al., 2014). High degrees of site fidelity have been documented for this species (Heupel et al., 2006; Driggers et al., 2014), and tagging data indicate that there is no mixing between populations in the GOM and Atlantic region (Kohler and Turner, 2019).

The population status of bonnetheads in U.S. waters was most recently assessed as a single stock in 2013; however, because of observed differences in life history, tagging data, and genetic population structure, the results of that stock assessment were rejected and it was recommended that regional populations (i.e., those in the GOM and Atlantic region) be assessed as separate stocks (SEDAR, 2013). As such, the population status for both stocks is currently considered to be unknown (SEDAR, 2013).

Recent studies of bonnethead population structure (Escatel-Luna et al., 2015; Portnoy et al., 2015) found that the populations in the GOM and Atlantic region are genetically distinct, with evidence of fine-scale genetic structure within populations. Using a combination of mtDNA and nuclear single nucleotide polymorphisms, Portnoy et al. (2015) found evidence of female philopatry with male-mediated gene flow. Results of further analysis indicate that over half of a small sample of outlier single nucleotide polymorphism loci has signatures of latitudinal selection. Portnoy et al. (2015) proposed that philopatry can lead to adaptive variation on a local scale and that, when combined with sex-biased dispersal, adaptive variation can move among locations and environments. The high degree of site fidelity and latitudinal variation in life history observed for bonnetheads, in addition to localized adaption to environmental conditions, could explain the dissimilarities in life histories between populations in the different regions. However, differences in aging techniques, age estimation, or spatiotemporal biases could also explain observed differences (Campana, 2001; Cailliet and Goldman, 2004).

The objectives of this study were 1) to use 2 long-term mark-and-recapture data sets and an age-independent model, GROTAG, to estimate region-specific growth rates; 2) to generate estimates for age-independent life history parameters and compare results to region-specific estimates based on length-at-age data for verification of current life history information; and 3) to estimate region-specific seasonal growth and growth variability of bonnetheads in the GOM and the Atlantic region.

[1] Carlson, J. K., and J. Loefer. 2007. Life history parameters for Atlantic sharpnose sharks, *Rhizoprionodon terraenovae*, from the United States South Atlantic Ocean and northern Gulf of Mexico. Southeast Data, Assessment, and Review SEDAR13-DW-08, 7 p. [Available from website.]

Materials and methods

Data collection

Data sets from long-term mark-and-recapture studies were available from 2 regions (the northeastern GOM and estuarine waters of the Atlantic coast of the southeastern United States), corresponding to the areas within each region where published, region-specific age and growth studies occurred. Mark-recapture data were provided for 2 surveys conducted in the GOM. Mote Marine Laboratory provided data from fishery-independent gill-net surveys conducted from 1993 through 2006 in the eastern GOM (primarily from Yankeetown to Charlotte Harbor, Florida). Detailed descriptions of the survey methods used by Mote Marine Laboratory can be found in Hueter and Tyminski[2] and in Hueter and Tyminski (2007). Data for the northeastern GOM were obtained for the period from 2003 through 2014 from the National Marine Fisheries Service from its Gulf of Mexico Shark Pupping and Nursery (GULFSPAN) survey. A fishery-independent survey conducted with gill nets made of multiple stretched-mesh panels, the GULFSPAN survey is used to assess populations of juvenile sharks from Cat Island, Mississippi, to Anclote Key, Florida, from April through October each year. Additional details about the GULFSPAN survey can be found in Bethea et al. (2015).

For the population in the Atlantic region, bonnethead mark-recapture data collected from 1998 through 2019 were available from the South Carolina Department of Natural Resources as part of its Cooperative Atlantic States Shark Pupping and Nursery (COASTSPAN) survey. The COASTSPAN survey is conducted in estuarine waters along the coast of South Carolina from Saint Helena Sound to Bulls Bay during April–September each year. Detailed descriptions of COASTSPAN survey methods can be found in Ulrich et al. (2007).

For all surveys, upon capture, the precaudal length, fork length (FL), total length, and stretch total length of each shark were measured in a straight line along the axis of the body to the nearest half centimeter (for sharks from the GOM) or nearest millimeter (for sharks from the Atlantic region). If healthy, sharks were tagged externally either with a nylon dart tag (142-mm tag, Hallprint Fish Tags[3], Hindmarsh Valley, Australia) or a FT-1-94 or T-bar Anchor Tag (Floy Tag Inc., Seattle, WA), at the base of the first dorsal fin (for both populations: GOM and Atlantic region), or with a 3.5-cm rototag (Dalton ID Systems Ltd., Henley-on-Thames, UK), inserted through the cartilage of the leading edge of the first dorsal fin (for the population in the Atlantic region only). A limited number of individuals in the Atlantic region were double tagged with a rototag and a 12-mm, 125-kHz internal passive integrated transponder (Biomark Inc., Boise, ID) at the base of the first dorsal fin prior to release.

Upon recapture during a survey, the date of capture, tag number, capture location (latitude and longitude), and all aforementioned length measurements were recorded before a shark was rereleased. If a bonnethead was recaptured by a commercial or recreational fisherman (not during a survey), lengths, tag number, date of capture, and general capture location were requested. A subset of bonnetheads recaptured in the Atlantic region were sacrificed as part of age validation research (Frazier et al., 2014).

Effects of tagging on growth

Recaptured bonnetheads sacrificed and aged for age-based modeling of growth in a previous study (Frazier et al., 2014) were used in this study to test if there was any effect of tagging and tag type on growth. The residuals at recapture (i.e., at sacrifice, calculated as expected FL at age minus observed length at estimated age) used for analysis were from use of the final VBGF in Frazier et al. (2014). Residuals at initial capture (i.e., at tagging) were determined by using FL at initial tagging and estimated age at initial tagging (calculated as estimated age at sacrifice minus time at liberty) to remodel the data set. The change in residuals at initial capture and in residuals at recapture of sacrificed bonnetheads were plotted against time at liberty. If tagging or tag type had a negative effect on growth, most data points would be less than zero with the slope of the trendline significantly different from zero, indicating slower than predicted growth in tagged sharks.

Modeling growth with tag-recapture data

Growth increment data were modeled by using the Francis (1988b) method (i.e., by using the GROTAG model). In the event that a single individual was recaptured multiple times, only data from the initial capture and final recapture were used in analyses to give equal weight to each fish and to maximize time at liberty (Welsford and Lyle, 2005). Data for all recaptured sharks (excluding data as previously mentioned for sharks recaptured multiple times) were used in the model regardless of time at liberty, negative growth, or potential outliers because the GROTAG model can use these data to inform several calculated parameters. Growth has been found to be significantly different between sexes in previous growth studies (Parsons, 1993; Carlson and Parsons, 1997; Lombardi-Carlson et al., 2003; Frazier et al., 2014); therefore, sex-specific growth was modeled for both regions.

The GROTAG model, which includes an implementation of a maximum likelihood approach, was used to fit the VBGF (von Bertalanffy, 1938) to data for change in FL from initial capture to final recapture (ΔL) and for change in time at liberty (ΔT). The GROTAG model is a reparameterization of the Fabens growth model (Fabens, 1965) that incorporates seasonal growth. Mean annual growth (g),

[2] Hueter, R. E., and J. P. Tyminski. 2002. U.S. shark nursery research overview, Center for Shark Research, Mote Marine Laboratory 1991–2001. Mote Mar. Lab. Tech. Rep. 816, 31 p. [Available from website.]

[3] Mention of trade names or commercial companies is for identification purposes only and does not imply endorsement by the National Marine Fisheries Service, NOAA.

measured in millimeters FL per year, was estimated at 2 user-defined reference lengths, α and β (where α<β). Reference lengths were chosen to ensure that the majority of lengths at initial capture (L_1) fell between the 2 defined reference lengths by taking the mean length of the 3 smallest and 3 largest individuals at initial capture (α and β, respectively; Dureuil and Worm, 2015) in each region-specific data set. These parameters have better statistical properties than the asymptotic length, or the theoretical maximum length (L_∞), and the growth constant (k) because they are not highly correlated. Further, they allow easier interpretation of growth from tagging data (Francis, 1988b). The growth rates relate to the parameters of the von Bertalanffy growth curve as follows:

$$L_\infty = \frac{\beta g_\alpha - \alpha g_\beta}{g_\alpha - g_\beta} \text{ and} \quad (1)$$

$$e^{-k} = 1 + \frac{g_\alpha - g_\beta}{\alpha - \beta}. \quad (2)$$

Seasonal growth is parameterized as w, the time of year when growth is at its maximum, and as u, with a u value of 0.0 indicating no seasonal growth and a u value of 1.0 indicating strong seasonal growth with growth likely ceasing at some point during the year:

$$\Delta L = \left[\frac{\beta g_\alpha - \alpha g_\beta}{g_\alpha - g_\beta} - L_1\right]\left[1 - \left(1 + \frac{g_\alpha - g_\beta}{\alpha - \phi}\right)^{\Delta T + (\phi_2 - \phi_1)}\right], \quad (3)$$

where $\phi_i = u\frac{\sin[2\pi(T_i - w)]}{2\pi}$ for $i = 1, 2$.

The GROTAG model is fit by minimizing the negative log-likelihood function (-λ). Growth variability (v) is incorporated into the model by the parameter u_i, the expected mean growth increment of the ith individual where u_i is normally distributed with a standard deviation (SD) of σ_i. In this study, σ_i was assumed to be a function of the expected growth increment $\sigma_i = v u_i$. An additional parameter p, the probability of outlier contamination, was also fit. For each data set, made up of i=1 to n growth increments where R is the range (largest and smallest) of observed growth increments, the following equation was used:

$$\lambda = \Sigma_i \ln\left[(1 - p)\lambda_i + \frac{p}{R}\right], \quad (4)$$

where $\lambda_i = \exp\frac{-½\,(\Delta L_i - u_i - m)^2 / (\sigma_i^2 + s^2)}{[2\pi(\sigma_i^2 + s^2)]^{½}}$.

The likelihood function estimates the population measurement error in ΔL as being normally distributed with a mean of m and an SD of s. The initial model estimated g_α, g_β, and v with additional parameters (m, s, w, u, and p) added, increasing model complexity (Table 1). Unfitted parameters were held at zero. Optimal model parameterization was determined for each region by using likelihood-ratio chi-square tests to determine if improvement in model fit was significant (P<0.05). Francis (1988b) suggested that the introduction of an additional parameter should increase the log-likelihood value by at least 1.92. Likelihood ratio tests were also conducted to determine significant differences in von Bertalanffy growth curves between regions (Kimura, 1980).

Table 1

Parameters fitted for the GROTAG models used to estimate region-specific growth rates of bonnetheads (*Sphyrna tiburo*) in the Gulf of Mexico during 1993–2006 and in the Atlantic Ocean off the southeastern United States during 1998–2019: growth rate estimates at reference lengths α and β (g_α and g_β), mean (m) and standard deviation (s) of the measurement error, magnitude (u) and timing (w) of seasonal growth, growth variability (v), and outlier contamination probability (p).

GROTAG model	Parameters estimated
1	g_α, g_β, s
2	g_α, g_β, s, v
3	$g_\alpha, g_\beta, s, v, m$
4	$g_\alpha, g_\beta, s, v, m, u, w, p$
5	g_α, g_β, s, p

Age-based growth model

To allow direct comparison of growth estimates based on age data and those based on tag-recapture data, region-specific length-at-age data from Lombardi-Carlson et al. (2003) and Frazier et al. (2014) were remodeled (the authors of both publications used the Beverton and Holt, 1957, method of modeling VBGF parameters) by using an alternative parameterization of the VBGF recommended by Francis (1988a), in which mean length (L) of fish of age t is determined with this equation:

$$L = l_\Phi + \frac{(l_\Psi - l_\Phi)\left(1 - r^{2(t-\Phi)/\Psi-\Phi}\right)}{1 - r^2}, \quad (5)$$

where $r = \frac{l_\Psi - l_X}{l_X - l_\Phi}$,

where X = (Φ + Ψ)/2;
l_Φ = mean length at age Φ;
l_X = mean length at age X; and
l_Ψ = mean length at age Ψ.

Values for Φ and Ψ were chosen to encompass the range of ages represented in the published length-at-age data from both regions (Lombardi-Carlson et al., 2003; Frazier et al., 2014). The Francis (1988a) parameterization yields estimates of VBGF parameters that better represent the growth information modeled from length-at-estimated-age and tagging data. The growth estimates generated from this model allow comparison of the mean growth rate of fish of an estimated age with that of fish of a length equal to the mean length at that age (Francis, 1988a).

Bootstrapping (with 5000 iterations) was used to develop 95% confidence intervals (CIs) for VBGF parameter estimates. Model estimates and CIs were generated by using the FSA package (vers. 0.3.2; Ogle, 2012) in R (vers. 3.6.0; R Core Team, 2019).

Comparisons of tag-recapture and age-based growth

To compare growth rates between models, annual growth rates were estimated by using the parameters of the age and growth models to calculate mean length at estimated age. These values were used to create trend lines of the relationship between mean growth and FL, allowing comparison of the growth rates based on the GROTAG reference lengths. Parameter values from bootstrapping were used to calculate 95% CIs for the age-based growth rates.

To allow statistical and visual comparison of growth rates between the populations in the Atlantic region and GOM, we calculated growth at 2 reference lengths corresponding to the mean of the 3 smallest L_1 of sharks from the Atlantic region and a length less than the smallest age-based bootstrap L_∞ estimate (g_α, g_β). Region-specific bootstrap values (from the use of 5000 iterations) were used to calculate average growth and 95% CIs at the shared reference lengths. To allow comparisons of growth between age-based and length-based models, we calculated mean growth rates for age-based models (g'_α, g'_β) corresponding to growth rates from length-based models (g_α, g_β). These were calculated by using bootstrapped estimates of parameters l_Φ, l_χ, and l_Ψ to solve for age-based growth rates (g'_α, g'_β). The resulting values equate to the expected annual growth rate of fish at the age when mean length is equal to reference length α or β. The length-based (g_α, g_β) and age-based (g'_α, g'_β) growth rates were plotted with 95% CIs to allow comparisons of growth within and between regions and models. All GROTAG models were generated by using the fishmethods package (vers. 1.4-0; Nelson, 2013) in R.

For the GROTAG model, an additional parameter needed to produce von Bertalanffy growth curves, theoretical age at length zero (t_0), was calculated by using model-specific L_∞ and k as well as observed mean size at birth (L_0) with age (t=0):

$$t_0 = t + \left(\frac{1}{k}\right)\ln\left\{\frac{(L_\infty - L_0)}{L_\infty}\right\}. \quad (6)$$

Region-specific mean L_0 was 263 mm FL for sharks from the Atlantic region (Frazier et al., 2014) and 252 mm FL for sharks from the GOM (R. Hueter, unpubl. data).

Longevity and age at 50% maturity

Estimated maximum ages from the region-specific age and growth studies provided initial values of maximum age; however, these values are likely underestimated in a fished population (Bishop et al., 2006). For the age-based and length-based models, longevity was estimated for each region and sex. The recaptured shark with the greatest time at liberty was assigned an age at initial capture by using L_1 and model-specific VBGF parameters reconfigured to solve for age where

$$Age = \left(\frac{\ln\left(1 - \frac{L_1}{L_\infty}\right)}{-k}\right) + t_0. \quad (7)$$

This calculated age at initial capture was then added to time at liberty to estimate longevity.

The GROTAG-derived VBGF parameters were used to solve for sex-specific age at 50% maturity by using equation 7 with L_1 set to estimates of length at 50% maturity of sharks from the Atlantic Ocean (male: 617.8 mm FL; female: 818.5 mm FL; Frazier et al., 2014) and the GOM (male: 630.8 mm FL; female: 716.4 mm FL; Lombardi-Carlson[4]), allowing calculation of age at 50% maturity without introducing bias from age estimation. Confidence intervals for longevity and age at 50% maturity were generated by using the 95% CIs for the VBGF parameters. For the published estimates of age at 50% maturity, 95% CIs are recorded as published for the population in the Atlantic region; however, no measurements of uncertainty were reported for the population in the GOM.

Results

Data collection

A total of 139 and 190 recaptured bonnetheads were available from the GOM and the Atlantic Ocean off the southeastern United States, respectively (Fig. 1). Ranges of lengths at capture and recapture and range and mean of time at liberty, by region and sex, are reported in Table 2. Sex- and region-specific recapture data sets did not encompass the range of lengths that have been reported as present in each region's population (Ulrich et al., 2007; Bethea et al., 2015). Large females were lacking in the GOM data set (n=99, only 2 females greater than 880 mm FL available; Suppl. Table [online only]), and there was no representation of small females in the Atlantic region data set (n=172, no females less than 550 mm FL present; Table 2). Sample sizes for males from the GOM (n=40) and the Atlantic region (n=18) were relatively small, and lengths did not adequately represent the range of individuals found in the population, especially in the Atlantic region (Table 2, Suppl. Table [online only]). In comparison, the smallest and largest bonnetheads in the data used in the age-based models for fish in the Atlantic region are 245 and 825 mm FL (males) and 262 and 1043 mm FL (females) (Frazier et al., 2014), and those in the data used in the GOM

[4] Lombardi-Carlson, L. A. 2007. Life history traits of bonnetheads, *Sphyrna tiburo*, from the eastern Gulf of Mexico. Southeast Data, Assessment, and Review SEDAR13-DW-24, 7 p. [Available from website.]

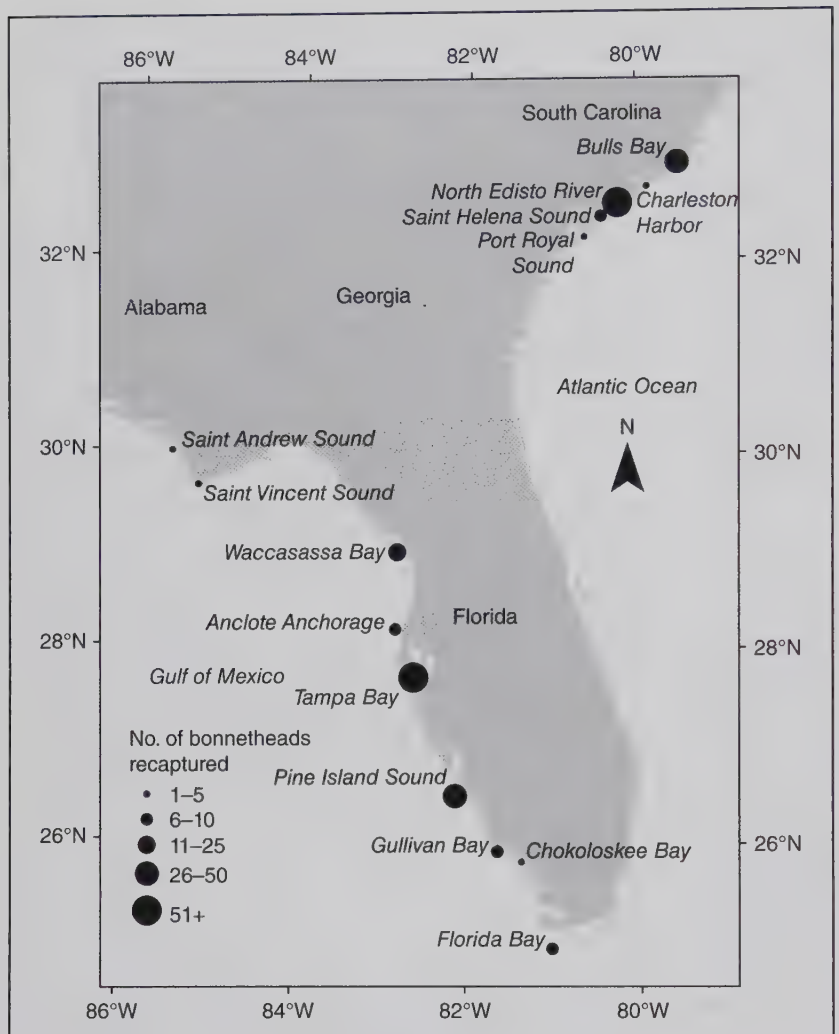

Figure 1

Map showing the locations where bonnetheads (*Sphyrna tiburo*) were recaptured in the northeastern Gulf of Mexico between 1993 and 2006 and in the estuarine waters of the Atlantic coast of the southeastern United States between 1998 and 2019. Circle size indicates the number of bonnetheads recaptured at a location. Data from these tag-recapture efforts were used in an age-independent model, GROTAG, to estimate growth rates of bonnetheads by region.

age-based models are 300 and 760 mm FL (males) and 340 and 960 mm FL (females) (Lombardi-Carlson et al., 2003).

Effects of tagging on growth

A total of 22 recaptured individuals were aged by Frazier et al. (2014), and resulting data were available for analysis of the effect of tag type on growth (8 sharks were tagged with a nylon dart tag, and 14 sharks were tagged with a rototag). The changes in residuals from mean age at initial capture (i.e., tagging) and estimated age at recapture were plotted against time at liberty (Fig. 2). The slope (b) of the line is not significantly different from zero for tag types combined or for individual tag types, and 95% CIs for slopes bound zero (all tags: b=0.005 [95% CI −0.033–0.043], P=0.615, df=20; nylon dart tag: b=0.037 [95% CI −0.109–0.184], P=0.554, df=6; rototag: b=0.005 [95% CI −0.042–0.052], P=0.805, df=12). Therefore, there is no evidence to indicate that tagging or tag type affected growth, and growth increments from tag-recapture data were considered suitable for modeling growth in a population.

Models based on tag-recapture data

The GROTAG model (Francis, 1988b) produced biologically reasonable parameter estimates for males from both regions (Table 3); however, 95% CIs are large, indicating that the sample size was insufficient to produce robust estimates of growth. The best-fit model for males in the GOM (model 3) included parameters for mean growth rates at reference lengths (g_{470}, g_{737}), mean and SD of measurement error, and growth variability; the model failed to converge when the model 1 configuration was used (Table 4). The final model for males in the Atlantic region (model 2) included parameters for mean growth rates at reference lengths (g_{612}, g_{765}), SD of measurement error, and growth variability; model 3 failed to fit the data for this region (Table 4). Estimates of growth variability and seasonal growth for males are uninformative because the low sample size produced large 95% CIs for estimates, with upper and lower limits of 95% CIs above parameter bounds in the GOM model. Although confidence intervals are large and overlap, the SD of measurement error of the GOM model is 3 times that of the Atlantic region model.

Region-specific models for female bonnetheads converged for all models run. The final model for females in the GOM (model 2) included parameters for mean growth rates at reference lengths (g_{465},g_{915}), SD of measurement error, and growth variability (Table 4). The final model for females in the Atlantic region (model 4) is more complex, with the parameters for mean growth rates at reference lengths (g_{555}, g_{1000}), mean and SD of measurement error, growth variability, and seasonal variation included (Table 4). The estimates of growth variability for females are large from both the GOM model (v=0.63) and the Atlantic region model (v=0.56), indicating that individuals in the population could be expected to grow 0.37–1.63 (GOM) or 0.44–1.56 (Atlantic region) times the estimated average growth rate per length class. The model for females in the Atlantic region has a strong seasonal growth component

Table 2

Summary of data collected for bonnetheads (*Sphyrna tiburo*) tagged and recaptured in the northeastern Gulf of Mexico (GOM) during 1993–2006 and in the Atlantic Ocean off the southeastern United States (Atlantic region) during 1998–2019. The number of individuals recaptured (n), the range of fork lengths (FLs) of fish at initial capture and recapture, and the range, mean, and standard deviation (given in parentheses) of times at liberty for recaptured sharks are provided by region and sex.

Region	Sex	n	Initial FL (mm)	Recapture FL (mm)	Time at liberty (d)	Mean time at liberty (d)
GOM	F	99	430–930	450–958	1–2028	308 (366)
	M	40	400–750	520–780	1–1639	259 (319)
Atlantic region	F	172	550–1013	642–1014	10–3263	458 (518)
	M	18	532–767	543–805	13–2659	401 (823)

(u=1.0, w=0.58), indicating that growth likely ceases at some point during the year and that it peaks in June. The SD of the measurement error for the model for females in the GOM (s=11.9 mm FL) is more than double that of the model for females in the Atlantic region (s=4.8 mm FL) with 95% CIs that do not overlap, indicating significant differences in measurement error between the 2 regions. The model for females in the Atlantic region had a negligible mean measurement error of −0.5 mm FL. The contamination probability parameter was not included in 3 of the 4 models and is very low (p<0.001) in the model for females in the Atlantic region; therefore, the occurrence of outliers is scarce in all data sets.

Age-based growth model and regional comparisons

The Francis (1988a) age-based model produced nearly identical estimates of VBGF parameters to those produced by using the Beverton and Holt (1957) modeling method reported in Frazier et al. (2014).

For both regions, the age-based models for males predicted faster mean annual growth at smaller lengths and slower growth than the length-based models as bonnetheads approached estimated L_∞ (Fig. 3). For males in the Atlantic region, 95% CIs for age-based estimates of growth rates overlap at GROTAG-predicted rates for both g_{612} and g_{765} (Fig. 3). For males in the GOM, 95% CIs overlap at GROTAG-predicted rates for g_{470}; however, at g_{737}, 95% CIs do not overlap and rates are significantly different from those from the age-based model, with the age-based model predicting near zero growth by an FL of 708 mm (Fig. 3).

For females from the Atlantic region, the age-based model predicted a faster growth rate at smaller lengths but very similar growth rates at larger lengths compared with predicted rates from the GROTAG model (Fig. 4), and 95% CIs overlap at both g_{555} and g_{1000}. For females in the GOM, the age-based model predicted nearly identical growth rates at the smaller GROTAG reference length (g_{465}); however, the age-based model predicted a much smaller L_∞ than the estimate from the GROTAG model (Fig. 4). The predicted growth rate at the larger reference length (g_{915}) is significantly higher than the estimate from the age-based model, with no overlap in 95% CIs. The significant differences in estimated growth rates for both males and females at g_{737} and g_{915} between the GROTAG and age-based models indicate sampling bias or age underestimation in the GOM age-based model.

Plots of growth rates and 95% CIs estimated for males with the GROTAG model do not indicate significant differences in growth between populations in the Atlantic region and the GOM (Fig. 3); however, results from likelihood-ratio tests (χ^2=40.8, df=3, P<0.001) indicate significant differences in growth between regions.

Plots of growth rates with 95% CIs estimated for females as well as results from likelihood-ratio tests (χ^2=31.2, df=3, P<0.001) for the best-fit GROTAG models indicate that growth was significantly different between regions, with a significant difference in average growth rates occurring in individuals larger than ~850 mm FL (Fig. 4). Plots of von Bertalanffy growth curves by sex, region, and model further illustrate the difference in predicted lengths at age (Fig. 5); however, caution should be used when comparing curves between the GROTAG and age-based models because of different definitions of L_∞ (Francis, 1988a).

To allow comparisons of growth within and between models and regions, growth rates were calculated for 2 reference lengths (g_{555}, g_{830}) by using the GROTAG and age-based models. Plots of bootstrap parameter estimates from the GROTAG model indicate clear differences in g_{830} between regions with no overlap in 95% CIs (Fig. 6). Plots of GROTAG bootstrap parameter estimates indicate less variation in growth with greater length for both regions. Overall, given the estimates from both models, the variation in predicted growth is much higher for the population in the GOM than for the population in the Atlantic region. At the set reference lengths, growth rates do not significantly differ between the age-based and GROTAG models; however, as presented in Figure 3, estimated growth rates

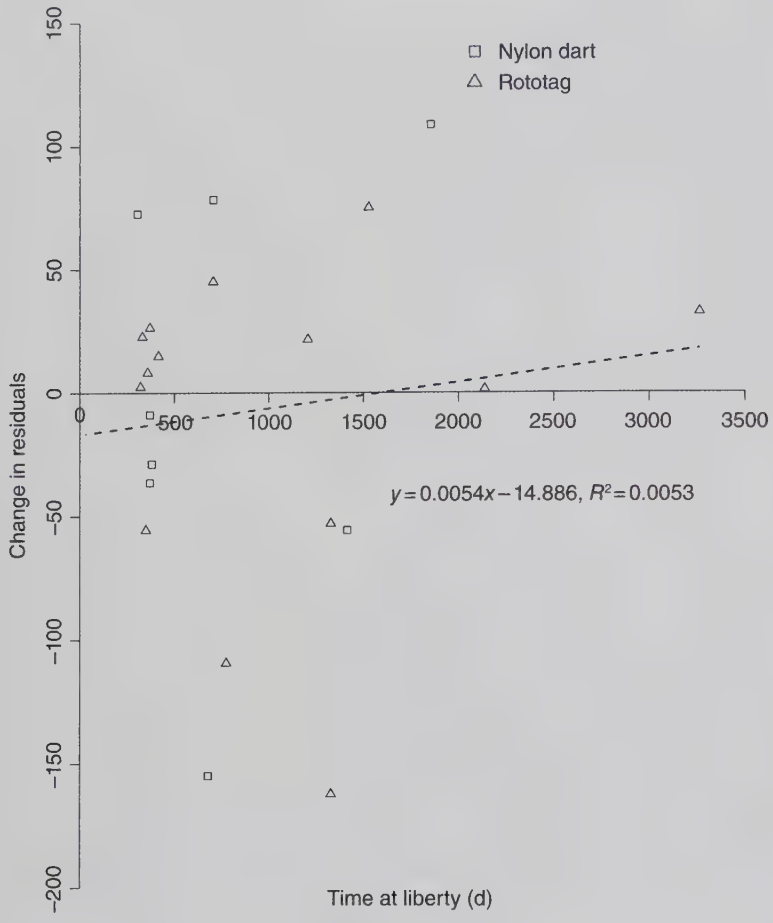

Figure 2

Changes in residuals for ages of recaptured bonnetheads (*Sphyrna tiburo*) in the estuarine waters of the Atlantic coast of the southeastern United States plotted against their times at liberty, by type of tag: nylon dart (squares) and rototag (triangles). If tagging has a negative effect on growth, the majority of data points should be negative and the slope of the dashed line should be significantly different from zero. The equation for the trend line and the coefficient of multiple determination (R^2) are provided. Residuals were calculated by using lengths at initial tagging and at recapture and by using ages and the von Bertalanffy growth curve from Frazier et al. (2014).

deviate between models as individuals grow beyond the upper reference length.

Longevity and age at 50% maturity

For the population in the GOM, data for recaptured bonnetheads from long-term tag-recapture studies, a male and a female with times at liberty of 1639 and 1833 d and initial FLs of 600 and 800 mm, respectively, were used to calculate maximum age in each model. For the population in the Atlantic region, data for a recaptured male and a recaptured female, with times at liberty of 2659 and 3263 d and FLs of 763 and 980 mm, respectively, were used. Calculated ages from the GROTAG model are larger than those from the age-based models for both regions, although 95% CIs overlap (Table 3). For sharks in the GOM, published estimated maximum ages are significantly below calculated maximum ages from models based on age and on tag-recapture data, with published values below 95% CIs for all models with the exception of the GROTAG model used for estimating growth of males; a lower limit of the 95% CI could not be estimated because of the size of the tagged shark used in relation to the lower limit of the 95% CI for the estimate of L_∞. For bonnetheads in the Atlantic region, calculated maximum ages are also significantly larger than published estimates, with the lower limit of the 95% CI falling above maximum estimated age for all models.

Published estimates of age at 50% maturity are lower than those calculated by using the GROTAG models (Table 3). We were unable to calculate the lower limit of the 95% CI for age at 50% maturity of males with either GROTAG model, and 95% CIs based on the GOM data were not published; therefore, we cannot determine if differences are significant for these estimates. Upper and lower confidence intervals for estimates from both length-based and age-based models were available only for females in the Atlantic region. Although the GROTAG model for females in the Atlantic region produced an estimate of age at 50% maturity that is slightly larger than that from the age-based model, 95% CIs for the estimates overlap.

Discussion

This study confirms previously published significant differences in region-specific growth and life history characteristics of bonnetheads between the northeastern GOM and the Atlantic region by using age-independent methods of modeling growth. Growth rates, age at 50% maturity, and longevity all differ for both sexes between these 2 regions. Despite low sample sizes and poor coverage of ranges of lengths for males, we were able to produce reasonable growth estimates for the populations in the northeastern GOM and the Atlantic region by using the GROTAG model; however, we were unable to determine significance of some life history characteristics because of the high uncertainty in estimates of growth and growth parameters. The low sample sizes of males from the Atlantic region available for growth modeling is reflective of the nearshore distribution of male bonnetheads, with tagging effort heavily skewed toward females in estuarine waters where most fishery-independent sampling and tagging

Table 3

Estimates of von Bertalanffy growth function (VBGF) parameters, maximum age, and age at 50% maturity from GROTAG models based on tag-recapture data and from age-based models for male and female bonnetheads (*Sphyrna tiburo*) from the northeastern Gulf of Mexico (GOM) and the Atlantic Ocean off the southeastern United States (Atlantic region). The VBGF parameters, asymptotic length (L_∞), coefficient of growth (k), and theoretical age at length zero (t_0), are provided with 95% confidence intervals, which were generated by using bootstrapping (with 5000 iterations). Also provided are published estimates of maximum age (Lombardi-Carlson et al., 2007; Frazier et al., 2014). Ages at 50% maturity were estimated in GROTAG models by using lengths at 50% maturity published in Lombardi-Carlson et al. (2007) and Frazier et al. (2014). Data used in the models are from sharks tagged and recaptured in the GOM during 1993–2006 and in the Atlantic region during 1998–2019. FL=fork length.

Model	Region	Sex	n	L_∞ (mm FL)	k	t_0 (years)	Age at 50% maturity (years)	Maximum age (years)	Published maximum age (years)
GROTAG	GOM	M	40	769.6	0.254	−1.56	5.2	8.9	
				604.2–823.5	0.470–0.087	−(1.14–4.19)	∞–12.5	∞–15.3	
		F	99	948.3	0.243	−1.27	4.5	11.4	
				921.2–967.9	0.313–0.184	−(1.02–1.64)	3.8–5.7	9.7–14.3	
	Atlantic region	M	18	814.8	0.166	−2.35	6.2	21.5	
				533.4–1135.6	0.386–0.070	−(1.76–3.76)	∞–7.5	19.4–∞	
		F	172	1039.5	0.170	−1.75	7.4	24.0	
				1027.7–1048.5	0.191–0.145	−(1.54–1.99)	6.8–8.5	23.5–25.8	
Age based	GOM	M	245	703.3	0.538	−1.60	2.0+	6.5	5.5+
				663.8–765.2	0.753–0.386	−(1.10–2.25)		6.4–6.6	
		F	254	895.0	0.282	−2.13	3.0+	10.8	7.5+
				842.9–970.3	0.334–0.226	−(1.82–2.55)		10.2–12.1	
	Atlantic region	M	216	779.8	0.296	−1.51	3.9	18.7	16.0
				761.5–799.7	0.320–0.274	−(1.35–1.68)	3.5–4.2	16.8–∞	
		F	329	1032.3	0.188	−1.76	6.7	23.0	17.9
				1011.6–1053.9	0.179–0.198	−(1.59–1.94)	6.4–7.1	21.9–24.9	

occurs (Ulrich et al., 2007). In the GOM, the lower number of male bonnetheads that were recaptured is a result of the primary habitat of male bonnetheads being outside of or on the periphery of the area where sampling occurred and where tags were deployed. Therefore, fewer males than females were tagged and consequently recaptured. Future efforts should focus on sampling and tagging male bonnetheads, especially those in early life stages, to decrease uncertainty in results from length-based models.

Although it is difficult to determine the effects of tagging on growth in wild fish populations, our results do not provide evidence indicating that tagging and tag type affected growth. Growth was variable in the first year after tagging, with a larger number of individuals experiencing slower growth than expected. This slow growth, however, could be due to the short-term effects of the stress from being captured rather than the effect of the tag on the individual (Gruber, 1982; Parsons, 1987; Davenport and Stevens, 1988; Skomal and Bernal, 2010). Over the long term, we found no evidence of effects of tagging on growth of captured bonnetheads, and all individuals at liberty for over 4 years grew older and larger than the age and length predicted by the age-based growth model. These findings contrast with those of studies on lemon sharks (*Negaprion brevirostris*) (Manire and Gruber, 1991; Oliveira, 2001) and northern pike (*Esox lucius*) (Scheirer and Coble, 1991) that indicate that growth could be impaired by up to 50% in tagged individuals when a variety of tag types were used. Results of other growth studies (e.g., Jensen, 1967; Jolivet et al., 2009) indicate that there were no significant effects of tagging on growth; therefore, it is possible that there may be effects specific to species, life stage, or tag type. Caution should be used in interpreting growth data from recaptured individuals to the population level without investigating these effects.

The final GROTAG models for males in both regions included SD of measurement error and growth variability, and the GOM model has the added parameter of mean measurement error. Estimates of growth variability are unreliable because of low sample size, and 95% CIs contain values that are not above and below parameter limits; therefore, no comparisons can be made with these parameters. The final GROTAG models for males and females in the GOM both have large estimates of SD of measurement error compared with those from the models for males and females in the Atlantic region; however, this result was not unexpected. For individuals from the GOM, length was measured to the nearest half centimeter, and several biologists and interns measured fish; whereas, bonnetheads from the Atlantic region were measured to the nearest millimeter by only 2 individuals. The use of fewer individuals to measure all captured specimens and the smaller measurement increment likely led to more precise

Table 4

Results from GROTAG models based on tag-recapture data for bonnetheads (*Sphyrna tiburo*) caught in the northeastern Gulf of Mexico (GOM) and in the Atlantic Ocean off the southeastern United States (Atl.), by sex and region. Reference lengths for each model (α and β), log-likelihood value (λ), estimates of growth rates at reference lengths (g_α and g_β), mean (m) and standard deviation (s) of the measurement error, magnitude (u) and timing (w) of seasonal growth, growth variability (v), outlier contamination probability (p), and von Bertalanffy growth function (VBGF) parameters of asymptotic length (L_∞) and growth coefficient (k) are reported. The 95% confidence intervals are reported for final models, which are indicated with asterisks (*). Data used in the models are from sharks tagged and recaptured in the GOM during 1993–2006 and in the Atlantic Ocean during 1993–2006. FL=fork length.

			Reference length (mm FL)		Log-likelihood	Growth estimates (mm FL/year)		Modeled parameters						VBGF parameters	
Sex	Region	Model	α	β	λ	g_α	g_β	s (mm FL)	v	u	w	m (mm FL)	P	L_∞ (mm FL)	k
Female	GOM	1	465	915	−484.2	105.4	9.7	32.2	–	–	–	–	–	948.0	0.246
		2*	465	915	−454.3	104.3	7.2	11.9	0.63	–	–	–	–	948.3	0.243
			–	–	–	83.5–128.6	3.3–10.4	8.8–15.1	0.46–0.81	–	–	–	–	921.2–967.9	0.184–0.313
		3	465	915	−454.1	99.4	7.2	11.8	0.67	–	–	1.5	–	950.1	0.223
		4	465	915	−453.1	99.0	7.2	11.6	0.64	0.39	0.56	0.3	0.000	951.2	0.228
		5	465	915	−468.9	74.9	7.2	17.2	–	–	–	–	0.168	962.8	0.163
	Atl.	1	555	1000	−793.8	93.9	6.1	24.5	–	–	–	–	–	1030.9	0.220
		2	555	1000	−740.5	76.2	6.1	9.8	0.51	–	–	–	–	1038.7	0.171
		3	555	1000	−738.9	68.3	6.1	8.7	0.60	–	–	2.9	–	1043.6	0.150
		4*	555	1000	−712.0	74.7	6.1	4.8	0.56	1.0	0.58	−0.5	0.000	1039.5	0.167
			–	–	–	66.1–83.7	4.5–7.3	2.9–7.0	0.46–0.65	0.84–1.00	0.46–0.65	−2.4–1.2	0.000	1027.7–1048.5	0.145–0.191
		5	555	1000	−776.4	74.9	6.1	18.1	–	–	–	–	0.055	1039.4	0.169
Male	GOM	1	470	737	–	–	–	–	–	–	–	–	–	–	–
		2	470	737	−189.9	70.7	10.3	15.6	1.00	–	–	–	–	782.6	0.256
		3*	470	737	−189.6	67.3	7.3	15.9	1.00	–	–	3.0	–	769.6	0.254
			–	–	–	14.0–114.8	−4.9–21.5	7.0–24.4	1.00–1.80	–	–	−1.9–8.1	–	604.2–823.5	0.087–0.470
		4	470	737	−185.5	50.7	5.6	14.5	0.41	1.0	0.59	−2.0	0.15	770.2	0.185
		5	470	737	−188.4	50.7	5.6	19.3	–	–	–	–	0.14	770.2	0.185
	Atl.	1	612	765	−63.5	31.9	7.6	8.2	–	–	–	–	–	812.9	0.173
		2*	612	765	−59.8	30.9	7.6	5.7	0.25	–	–	–	–	814.8	0.166
			–	–	–	12.0–48.3	−5.1–9.8	4.2–8.22	−0.06–0.50	–	–	–	–	533.4–1135.6	0.070–0.386
		3	612	765	–	–	–	–	–	–	–	–	–	–	–
		4	612	765	−56.4	25.8	7.6	4.3	0.0	1.0	0.79	−2.8	0.11	829.3	0.126
		5	612	765	−59.4	30.6	8.7	5.0	–	–	–	–	0.15	825.6	0.154

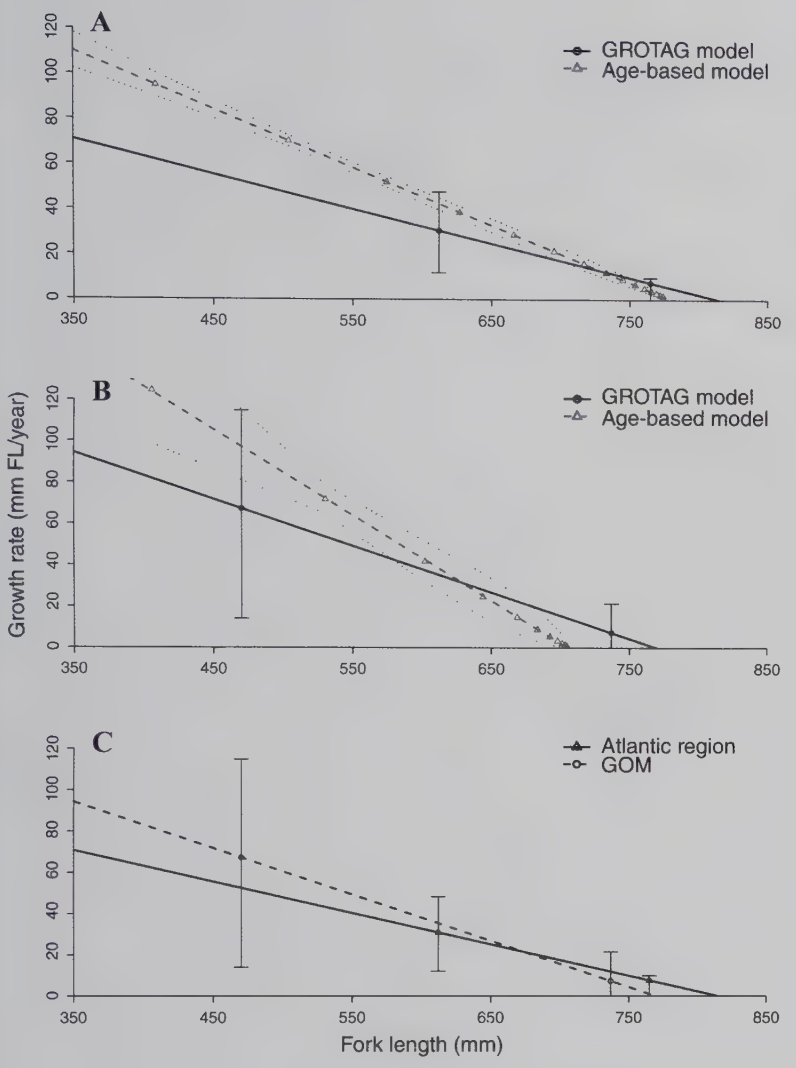

Figure 3

Growth rates of male bonnetheads (*Sphyrna tiburo*) estimated with the optimal GROTAG models, which are based on tag-recapture data, and mean growth rates calculated with the age-based (Francis, 1988a) von Bertalanffy growth function, with associated 95% confidence intervals (dotted lines). Growth rates are shown for bonnetheads tagged (**A**) in the northeastern Gulf of Mexico (GOM) and (**B**) in the estuarine waters of the Atlantic coast of the southeastern United States (Atlantic region). Also provided are (**C**) estimates of growth rates from the optimal GROTAG model for each of the 2 regions. Age-based models were generated by using original length-at-age data from Lombardi et al. (2007) for sharks in the GOM and from Frazier et al. (2014) for sharks in the Atlantic region. Data used in the GROTAG models are from bonnetheads tagged and recaptured in the GOM during 1993–2006 and in the Atlantic region during 1998–2019. Error bars indicate 95% confidence intervals generated by bootstrapping (with 5000 iterations). FL=fork length.

measurements at tagging and recapture and consequently lower chances of errors in measurement.

Results from the final GROTAG models for females indicate that growth is more variable for bonnetheads from the GOM (v=0.63) than for those from the Atlantic region (v=0.56); however, these differences are not significant and differences in these growth rates may be an artifact of sample size given the observed 95% CIs. Regardless, these variability estimates are among the highest published values for elasmobranchs with values ranging from 0.06 for the tope (*Galeorhinus galeus*) (Francis and Mulligan, 1998) to 0.58 for the spotted estuary smooth-hound (*Mustelus lenticulatus*) (Francis and Francis, 1992), with most falling in a range of 0.15–0.40 (e.g., Simpfendorfer, 2000; Meyer et al., 2014; Natanson and Deacy, 2019).

Results from the final GROTAG models indicate a strong seasonal growth pattern in the population in the Atlantic region (u=1) but not in the population in the GOM (the seasonal growth parameter was not included in the final GOM model). Latitudinal variation in growth has been previously detected for bonnetheads in the GOM but not for those in the Atlantic region (Parsons, 1993; Carlson and Parsons, 1997; Lombardi-Carlson et al., 2003; Frazier et al., 2014).

The more variable growth for sharks in the GOM and lack of a seasonal signal may indicate that there are differences within the population in growth along the western coast of Florida, where sampling for this study occurred. Site fidelity has been established for bonnetheads in both the Atlantic region and the GOM (Heupel et al., 2006; Driggers et al., 2014), and bonnetheads are known to make predictable temperature-driven migrations in response to declining water temperatures (Ulrich et al., 2007; Driggers et al., 2014). In the Atlantic region, all bonnetheads were tagged and recaptured within their established summer range. In the GOM, bonnetheads were also predominantly captured and recaptured during summer months; however, capture and recapture of sharks took place at multiple locations along the coast. Because these sampled subpopulations likely have site fidelity to their area of capture, they likely experience differential growth due to differences in water temperatures (Carlson and Parsons, 1999; Pistevos et al., 2015), in food availability or energetic value of food (Bethea et al., 2007; Vucic-Pestic et al., 2011), and in energetic needs during winter migrations necessary to find optimum water temperatures for overwintering (Carlson and Parsons, 1999; Hoffmayer et al., 2006). However, the lack of a detection of seasonal growth patterns and greater growth

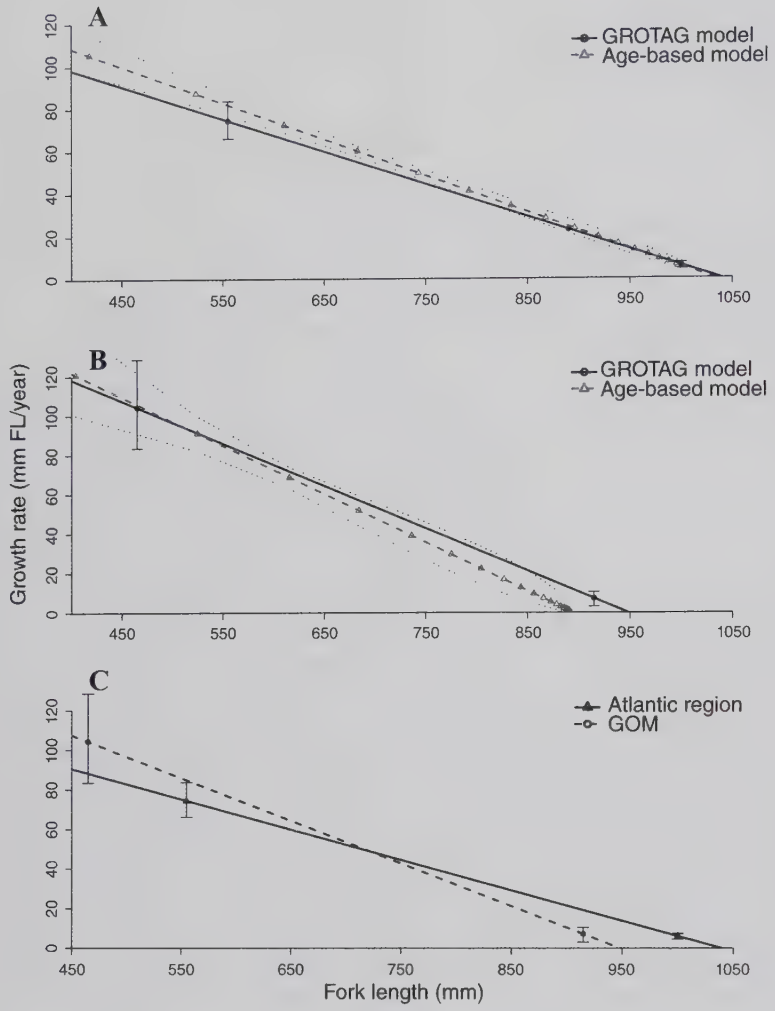

Figure 4

Growth rates of female bonnetheads (*Sphyrna tiburo*) estimated with the optimal GROTAG models, which are based on tag-recapture data, and mean growth rates calculated with the age-based (Francis, 1988a) von Bertalanffy growth function, with associated 95% confidence intervals (dotted lines). Growth rates are shown for bonnetheads tagged (**A**) in the northeastern Gulf of Mexico (GOM) and (**B**) in the estuarine waters of the Atlantic coast of the southeastern United States (Atlantic region). Also provided are (**C**) estimates of growth rates from the optimal GROTAG model for each of the 2 regions. Age-based models were generated by using original length-at-age data from Lombardi et al. (2007) for sharks in the GOM and from Frazier et al. (2014) for sharks in the Atlantic region. Data used in the GROTAG models are from bonnetheads tagged and recaptured in the GOM during 1993–2006 and in the Atlantic region during 1998–2019. Error bars indicate 95% confidence intervals generated by bootstrapping (with 5000 iterations). FL=fork length.

variation may also be artifacts of sample size. Future efforts should focus on continued tagging of bonnetheads in these regions because a more robust data set would allow age-independent comparisons of growth and, therefore, determination of latitudinal differences in growth within the GOM.

Results from GROTAG models confirm previously published differences in growth between the 2 regions. Both males and females in the GOM had faster average growth at smaller lengths and slower growth with a smaller L_∞ than bonnetheads from the Atlantic region. Visual inspection of 95% CIs does not reveal significant differences between regions because of large uncertainty caused by low sample sizes, but results of likelihood-ratio tests confirm differences in growth. Significant differences in growth have been detected for other coastal migratory sharks (Carlson and Baremore, 2003; Driggers et al., 2004; Vinyard et al., 2019); however, the reasons for these regional growth differences are unknown.

Growth curves derived from GROTAG and age-based models are not directly comparable; instead, Francis (1988a) suggested that comparisons of growth rates between data types are more appropriate. All GROTAG models predicted slower initial growth and faster growth at longer lengths compared with estimates from age-based models. The slower estimated initial growth rates likely result from a lack of tagged young-of-the-year bonnetheads in all 4 data sets, likely a combination of gear bias and variation in spatial distribution of young-of-the-year bonnetheads (Driggers et al., 2014). The GROTAG model for females in the GOM is based on the largest sample size of tagged and recaptured juvenile bonnetheads (including individuals tagged as small as 400 mm FL) and, consequently, the best agreement between model growth rates at small lengths. However, growth rates are significantly different at long lengths. Estimates from the GROTAG model for females in the Atlantic region have excellent agreement with those from the age-based model, especially as lengths reach predicted L_∞. Parameters of the VBGF are not significantly different between models, confirming estimated growth from the age-based model for females in the Atlantic region. Although the VBGF parameters are defined differently for the length-at-age data and tag-recapture data, the results of other studies indicate that models based on tag-recapture data can produce growth curves that are similar to those from age-based models (Natanson et al., 2002).

The GROTAG models for males and females predicted significantly faster growth at longer lengths, larger L_∞,

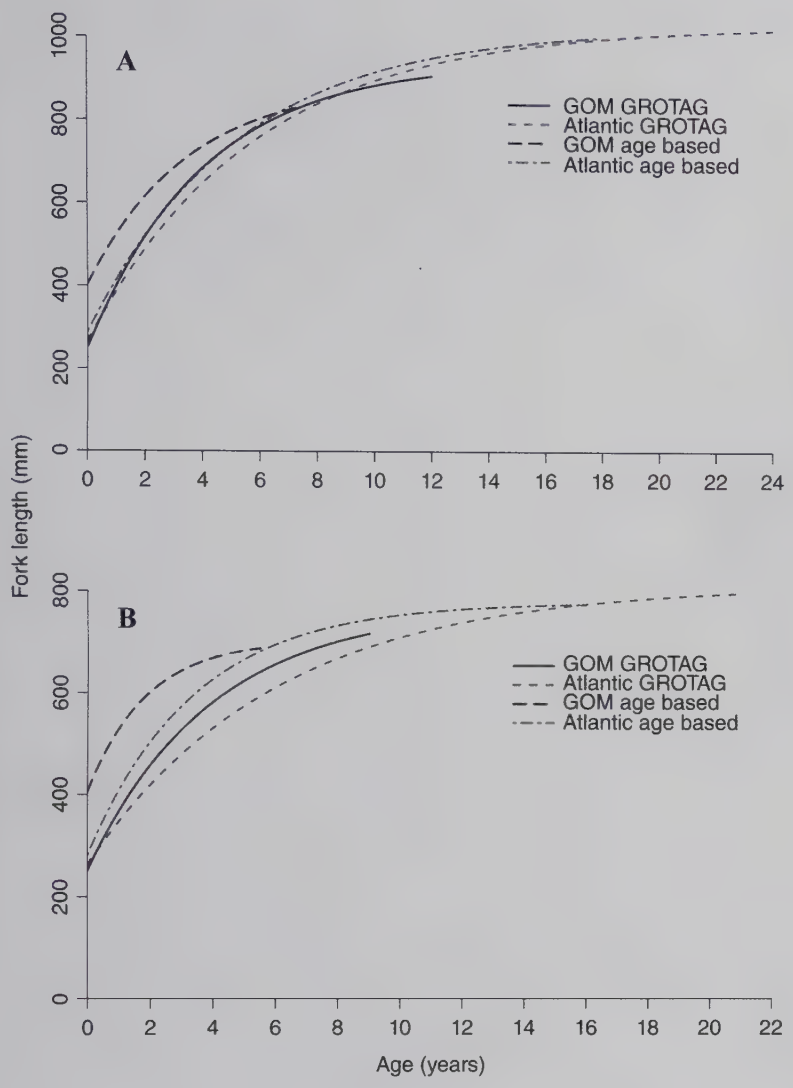

Figure 5

Comparison of growth curves from GROTAG models, which are based on tag-recapture data, and from age-based von Bertalanffy growth functions based on data from Lombardi et al. (2007) and Frazier et al. (2014) for (**A**) female and (**B**) male bonnetheads (*Sphyrna tiburo*) tagged in the northeastern Gulf of Mexico (GOM) during 1993–2006 and off the Atlantic coast of the southeastern United States (Atlantic) during 1998–2019. Age-based models were generated by using original length-at-age data from Lombardi et al. (2007) for sharks in the GOM because published models used total length and band count.

and faster rates at which k is reached compared with estimates from age-based models. Plots of bootstrapped growth estimates for females from the GOM age-based model indicate large uncertainty in growth estimates at the upper reference length. Comparatively, results from GROTAG models for bonnetheads in the Atlantic region and in the GOM and from the age-based model for bonnetheads in the Atlantic region indicate less uncertainty at the upper reference length compared with the lower reference length at which growth is expected to be more variable (Erzini, 1994). The large uncertainty in the age-based model for females in the GOM may be an artifact of sample size, although the model produced much greater variation in growth estimates at g_{830}, contrary to the estimates from other models indicating a source of variation other than sample size. These results indicate that there may be significant underestimation of ages of bonnetheads in the GOM with the age-based models.

Sampling, fishing pressure, or gear bias could have affected results of the age-based models; however, estimates of age at 50% maturity calculated by using age-independent, length-based growth estimates also point to significant differences in maturity. These estimates of age at 50% maturity indicate that female bonnetheads mature at an average of 1.5 years and males mature at an average of 3.2 years later than females and males do according to age-based estimates, providing further evidence of age underestimation in the GOM data set. The GROTAG model does not produce comparable estimates of average age at length; however, data from long-term tag-recapture studies were available. When these data were combined with results from growth models, calculated longevity for female and male bonnetheads in the GOM are 8.9 and 11.4 years from the GROTAG models and 6.5 and 10.8 years from the age-based models; these ages are considerably older than the maximum age estimates of 5.5+ and 7.5+ reported by Lombardi-Carlson et al. (2003).

Data from long-term tag-recapture efforts and longevity estimates calculated from GROTAG models confirm the report of age underestimation for bonnetheads in the Atlantic region by Frazier et al. (2014). However, for females, length-based estimates of age at 50% maturity are not significantly different from age-based estimates. If age underestimation was common in the age-based study for sharks in the Atlantic region, it may be rare or only in individuals at or near L_∞ given the agreement between growth models and life history parameters for females.

Although age and growth studies are not necessarily expected to encounter the oldest individuals in a population because of their relative scarcity (Bishop et al., 2006), there is increasing evidence that age is frequently underestimated in many studies of age and growth of elasmobranch species, especially in those of long-lived species (e.g., Kalish and Johnston, 2001; Francis et al., 2007; Frazier et al., 2015; Harry, 2018; Natanson et al., 2018b).

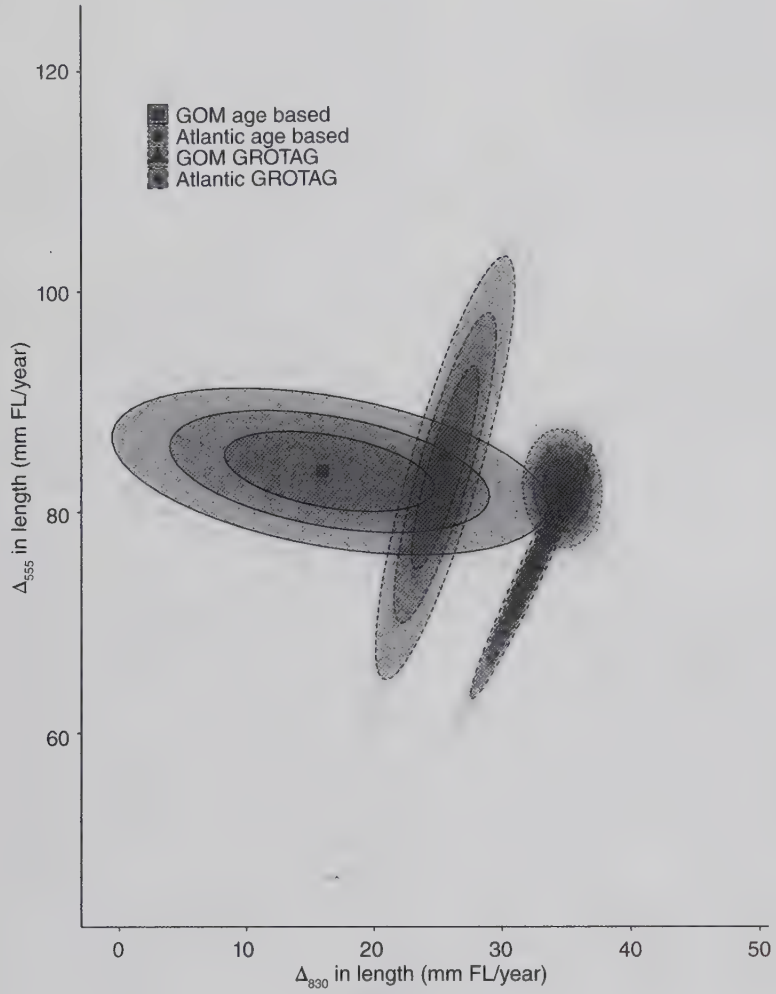

Figure 6

Plot of bootstrap estimates of growth rates (g) at the 2 reference lengths of 555 and 830 mm fork length (FL), parameters g_{555} and g_{830}, from GROTAG models based on tag-recapture data for female bonnetheads (*Sphyrna tiburo*) tagged in the northeastern Gulf of Mexico (GOM) during 1993–2006 and off the Atlantic coast of the southeastern United States (Atlantic region) during 1998–2019 and from region-specific, age-based von Bertalanffy growth functions generated by using original length-at-age data from Lombardi et al. (2007) for sharks in the GOM and from Frazier et al. (2014) for sharks in the Atlantic region. Mean growth rates for age-based models were calculated from bootstrapped estimates of lengths at ages Φ, X, and Ψ (parameters l_{Φ}, l_{X}, l_{Ψ}). Estimates are shown with 50%, 80%, and 95% polygon ellipsoid confidence intervals. Bootstrapping was done with 5000 iterations.

Results of recent studies indicate that in some species of sharks, band-pair formation may be a function of growth and body girth, not age (Natanson et al., 2018b). The results of our study indicate that the use of tag-recapture methods can produce estimates of growth that are similar to those produced with age-based methods.

When sufficient tag-recapture data are available, models should be used to verify growth estimates from age-based models and provide independent, and perhaps more reliable, estimates of longevity and age-independent estimates of maturity. Although methods of modeling growth with tag-recapture data have historically been considered inferior to age-based methods (Harry, 2018), given recent doubts about the suitability of vertebrae for aging, methods based on tag-recapture data may be more reliable than age-based methods (Harry, 2018; Natanson and Deacy, 2019). When possible, more computationally advanced methods, such as those of Aires-da-Silva et al. (2015) and Francis et al. (2016), which incorporate all available growth data (length based, tag and recapture, and age based) that can be integrated directly into stock assessment models, should be considered because they can combine all available data sources to estimate growth characteristics of a population. Additionally, methods that involve tag-recapture data may be useful in providing growth information for species that are difficult to age and for populations for which sacrifice of specimens is not preferred or fishery-dependent catch are not available for sampling (e.g., for protected species).

Given the large discrepancies between the age-based model and the model based on tag-recapture data for bonnetheads in the GOM, the length-based tag-recapture estimates generated in our study (especially age at 50% maturity and longevity) likely more accurately describe growth of bonnetheads in the GOM than age-based estimates. Parameters of the VBGF are commonly used in modeling estimates of mortality, maturity, and longevity and in modeling for stock assessments. Use of current age-based parameters for the population in the GOM should be carefully considered until growth in the population can be reexamined. Using parameters that underestimate age and maturity can lead to overly optimistic estimates of growth and mortality rates, increasing the potential for overexploitation of stocks. Results of this study indicate that bonnetheads in the GOM may be more susceptible to overexploitation than previously believed. The status of the stocks of bonnetheads in the northeastern GOM and off the Atlantic coast of the southeastern United States are currently considered to be unknown, and no stock assessments are pending. Given these results, we recommend that region-specific assessments be conducted and that they incorporate these new age-independent estimates of life history characteristics.

Acknowledgments

We thank G. Ulrich, J. Morris, C. Manire, A. Galloway, and the numerous interns whose countless hours of sampling made this study possible. We also thank L. Natanson, R. Francis, J. Sulikowski, C. Simpfendorfer, J. Ballenger, and L. Lombardi-Carlson for sharing data and providing guidance and input. This research was enabled by NOAA funding to Mote Marine Laboratory, the NOAA COASTSPAN and GULFSPAN surveys, the U.S. Environmental Protection Agency, and the Florida Department of Environmental Protection. This paper is contribution 830 of the South Carolina Marine Resources Center.

Literature cited

Aires-da-Silva, A. M., M. N. Maunder, K. M. Schaefer, and D. W. Fuller.
2015. Improved growth estimates from integrated analysis of direct ageing and tag–recapture data: an illustration with bigeye tuna (*Thunnus obesus*) of the eastern Pacific Ocean with implications for management. Fish. Res. 163:119–126.

Ardizzone, D., G. M. Cailliet, L. J. Natanson, A. H. Andrews, L. A. Kerr, and T. A. Brown.
2006. Application of bomb radiocarbon chronologies to shortfin mako (*Isurus oxyrinchus*) age validation. Environ. Biol. Fish. 77:355–366.

Beamish, R. J., and G. A. McFarlane.
1983. The forgotten requirement for age validation in fisheries biology. Trans. Am. Fish. Soc. 112:735–743.

Bethea, D. M., L. Hale, J. K. Carlson, E. Cortés, C. A. Manire, and J. Gelsleichter.
2007. Geographic and ontogenetic variation in the diet and daily ration of the bonnethead shark, *Sphyrna tiburo*, from the eastern Gulf of Mexico. Mar. Biol. 152:1009–1020.

Bethea, D. M., M. J. Ajemian, J. K. Carlson, E. R. Hoffmayer, J. L. Imhoff, R. D. Grubbs, C. T. Peterson, and G. H. Burgess.
2015. Distribution and community structure of coastal sharks in the northeastern Gulf of Mexico. Environ. Biol. Fish. 98:1233–1254.

Beverton, R. J. H., and S. J. Holt.
1957. On the dynamics of exploited fish populations. Fish. Invest. Ser. 2, vol. 19, 533 p. HMSO, London.

Bishop, S. D. H., M. P. Francis, C. Duffy, and J. C. Montgomery.
2006. Age, growth, maturity, longevity and natural mortality of the shortfin mako shark (*Isurus oxyrinchus*) in New Zealand waters. Mar. Freshw. Res. 57:143–154.

Cailliet, G. M., and K. J. Goldman.
2004. Age determination and validation in chondrichthyan fishes. *In* Biology of sharks and their relatives (J. C. Carrier, J. A. Musick, and M. R. Heithaus, eds.), p. 399–447. CRC Press, Boca Raton, FL.

Cailliet, G. M., H. F. Mollet, G. G. Pittenger, D. Bedford, and L. J. Natanson.
1992. Growth and demography of the Pacific angel shark (*Squatina californica*), based upon tag returns off California. Mar. Freshw. Res. 43:1313–1330.

Cailliet, G. M., W. D. Smith, H. F. Mollet, and K. J. Goldman.
2006. Age and growth of chondrichthyan fishes: the need for consistency in terminology, verification, validation, and growth function fitting. Environ. Biol. Fish. 77:211–228.

Campana, S. E.
2001. Accuracy, precision and quality control in age determination, including a review of the use and abuse of age validation methods. J. Fish Biol. 59:197–242.

Campana, S. E., L. J. Natanson, and S. Myklevoll.
2002. Bomb dating and age determination of large pelagic sharks. Can. J. Fish. Aquat. Sci. 59:450–455.

Carlson, J. K., and G. R. Parsons.
1997. Age and growth of the bonnethead shark, *Sphyrna tiburo*, from northwest Florida with comments on clinal variation. Environ. Biol. Fish. 50:331–341.
1999. Seasonal differences in routine oxygen consumption rates of the bonnethead shark. J. Fish Biol. 55:876–879.

Carlson, J. K., and I. E. Baremore.
2003. Changes in biological parameters of Atlantic sharpnose shark *Rhizoprionodon terraenovae* in the Gulf of Mexico: evidence for density-dependent growth and maturity? Mar. Freshw. Res. 54:227–234.

Compagno, L. G. V.
1984. FAO species catalogue. Vol. 4. Sharks of the world. An annotated and illustrated catalogue of shark species known to date. Part 2. Carcharhiniformes. FAO Fish. Synop. 125, p. 251–655. FAO, Rome.

Davenport, S., and J. D. Stevens.
1988. Age and growth of two commercially important sharks (*Carcharhinus tilstoni* and *C. sorrah*) from northern Australia. Aust. J. Mar. Freshw. Res. 39:417–433.

Driggers, W., J. Carlson, B. Cullum, J. Dean, and D. Oakley.
2004. Age and growth of the blacknose shark, *Carcharhinus acronotus*, in the western North Atlantic Ocean with comments on regional variation in growth rates. Environ. Biol. Fish. 71:171.

Driggers, W. B., III, B. S. Frazier, D. H. Adams, G. F. Ulrich, C. M. Jones, E. R. Hoffmayer, and M. D. Campbell.
2014. Site fidelity of migratory bonnethead sharks *Sphyrna tiburo* (L. 1758) to specific estuaries in South Carolina, USA. J. Exp. Mar. Biol. Ecol. 459:61–69.

Drymon, J. M., W. B. Driggers III, D. Oakley, and G. F. Ulrich.
2006. Investigating life history differences between finetooth sharks, *Carcharhinus isodon*, in the northern Gulf of Mexico and the western North Atlantic Ocean. Gulf Mex. Sci. 24:2–10.

Dureuil, M., and B. Worm.
2015. Estimating growth from tagging data: an application to north-east Atlantic tope shark *Galeorhinus galeus*. J. Fish Biol. 87:1389–1410.

Erzini, K.
1994. An empirical study of variability in length-at-age of marine fishes. J. Appl. Ichthyol. 10:17–41.

Escatel-Luna, E., D. H. Adams, M. Uribe-Alcocer, V. Islas-Villanueva, and P. Díaz-Jaimes.
2015. Population genetic structure of the bonnethead shark, *Sphyrna tiburo*, from the western North Atlantic Ocean based on mtDNA sequences. J. Hered. 106:355–365.

Eveson, J. P., T. Polacheck, and G. M. Laslett.
2007. Consequences of assuming an incorrect error structure in von Bertalanffy growth models: a simulation study. Can. J. Fish. Aquat. Sci. 64:602–617.

Fabens, A. J.
1965. Properties and fitting of the von Bertalanffy growth curve. Growth 29:265–289.

Francis, M. P., and R. I. C. C. Francis.
1992. Growth rate estimates of New Zealand rig (*Mustelus lenticulatus*). Aust. J. Mar. Freshw. Res. 43:1157–1176.

Francis, M. P., and K. P. Mulligan.
1998. Age and growth of the New Zealand school shark, *Galeorhinus galeus*. N. Z. J. Mar. Freshw. Res. 32:427–440.
Francis, M. P., S. E. Campana, and C. M. Jones.
2007. Age under-estimation in New Zealand porbeagle sharks (*Lamna nasus*): is there an upper limit to ages that can be determined from shark vertebrae? Mar. Freshw. Res. 58:10–23.
Francis, R. I. C. C.
1988a. Are growth parameters estimated from tagging and age–length data comparable? Can. J. Fish. Aquat. Sci. 45:936–942.
1988b. Maximum likelihood estimation of growth and growth variability from tagging data. N. Z. J. Mar. Freshw. Res. 22:43–51.
Francis, R. I. C. C., A. M. Aires-da-Silva, M. N. Maunder, K. M. Schaefer, and D. W. Fuller.
2016. Estimating fish growth for stock assessments using both age–length and tagging-increment data. Fish. Res. 180:113–118.
Frazier, B. S., W. B. Driggers III, D. H. Adams, C. M. Jones, and J. K. Loefer.
2014. Validated age, growth and maturity of the bonnethead *Sphyrna tiburo* in the western North Atlantic Ocean. J. Fish Biol. 85:688–712.
Frazier, B. S., W. B. Driggers III, and G. F. Ulrich.
2015. Longevity of Atlantic sharpnose sharks *Rhizoprionodon terraenovae* and blacknose sharks *Carcharhinus acronotus* in the western North Atlantic Ocean based on tag-recapture data and direct age estimates [version 2; peer review: 2 approved]. F1000Research 3:190.
Goldman, K. J.
2004. Age and growth of elasmobranch fishes. *In* Elasmobranch fisheries management techniques (J. A. Musick and R. Bonfil, eds.), p. 97–132. Asia Pacific Economic Cooperation, Singapore.
Gruber, S. H.
1982. Role of the lemon shark, *Negaprion brevirostris* (Poey) as a predator in the tropical marine environment: a multidisciplinary study. Fla. Sci. 45:46–75.
Harry, A. V.
2018. Evidence for systemic age underestimation in shark and ray ageing studies. Fish Fish. 19:185–200.
Heupel, M. R., C. A. Simpfendorfer, A. B. Collins, and J. P. Tyminski.
2006. Residency and movement patterns of bonnethead sharks, *Sphyrna tiburo*, in a large Florida estuary. Environ. Biol. Fish. 76:47–67.
Hoffmayer E. R., G. R. Parsons, and J. Horton.
2006. Seasonal and interannual variation in the energetic condition of adult male Atlantic sharpnose shark *Rhizoprionodon terraenovae* in the northern Gulf of Mexico. J. Fish Biol. 68:645–653.
Hueter, R. E., and J. P. Tyminski.
2007. Species-specific distribution and habitat characteristics of shark nurseries in Gulf of Mexico waters off peninsular Florida and Texas. Am. Fish. Soc. Symp. 50:193–223.
Kalish, J., and J. Johnston.
2001. Determination of school shark age based on analysis of radiocarbon in vertebral collagen. *In* Use of the bomb radiocarbon chronometer to validate fish age (J. M. Kalish, ed.), p. 116–129. Fish. Res. Dev. Corp., Canberra, Australia.
Kelly, G. F., and A. M. Barker.
1963. Estimation of population size and mortality rates from tagged redfish, *Sebastes marinus* L., at Eastport, Maine. ICNAF Spec. Publ. 4:204–209.
Kimura, D. K.
1980. Likelihood methods for the von Bertalanffy growth curve. Fish. Bull. 77:765–776.
Kneebone, J., L. J. Natanson, A. H. Andrews, and W. H. Howell.
2008. Using bomb radiocarbon analyses to validate age and growth estimates for the tiger shark, *Galeocerdo cuvier*, in the western North Atlantic. Mar. Biol. 154:423–434.
Jensen, A. C.
1967. Effects of tagging on the growth of cod. Trans. Am. Fish. Soc. 96:37–41.
Jolivet, A., H. de Pontual, F. Garren, and M. L. Bégout.
2009. Effects of T-bar and DST tagging on survival and growth of European hake. *In* Tagging and tracking of marine animals with electronic devices (J. L. Nielsen, H. Arrizabalaga, N. Fragoso, A. Hobday, M. Lutcavage, and J. Sibert, eds.) p. 181–193. Springer, Dordrecht, Netherlands.
Kohler, N. E., and P. A. Turner.
2019. Distributions and movements of Atlantic shark species: a 52-year retrospective atlas of mark and recapture data. Mar. Fish. Rev. 81(2):1–93.
Lombardi-Carlson, L. A., E. Cortés, G. R. Parsons, and C. A. Manire.
2003. Latitudinal variation in life-history traits of bonnethead sharks, *Sphyrna tiburo*, (Carcharhiniformes, Sphyrnidae), from the eastern Gulf of Mexico. Mar. Freshw. Res. 54:875–883.
Manire, C. A., and S. H. Gruber.
1991. Effect of M-type dart tags on field growth of juvenile lemon sharks. Trans. Am. Fish. Soc. 120:776–780.
Meyer, C. G., J. M. O'Malley, Y. P. Papastamatiou, J. J. Dale, M. R. Hutchinson, J. M. Anderson, M. A. Royer, and K. N. Holland.
2014. Growth and maximum size of tiger sharks (*Galeocerdo cuvier*) in Hawaii. PLoS ONE 9(1):e84799.
Natanson, L. J., and B. M. Deacy.
2019. Using oxytetracycline validation for confirmation of changes in vertebral band-pair deposition rates with ontogeny in sandbar sharks (*Carcharhinus plumbeus*) in the western North Atlantic Ocean. Fish. Bull. 117:50–58.
Natanson, L. J., J. J. Mello, and S. E. Campana.
2002. Validated age and growth of the porbeagle shark (*Lamna nasus*) in the western North Atlantic Ocean. Fish. Bull. 100:266–278.
Natanson, L. J., A. H. Andrews, M. S. Passerotti, and S. P. Wintner.
2018a. History and mystery of age and growth studies in elasmobranchs: common methods and room for improvement. *In* Shark research: emerging technologies and applications for the field and laboratory (J. C. Carrier, M. R. Heithaus, and C. A. Simpfendorfer, eds.), p. 177–199. CRC Press, Boca Raton, FL.
Natanson, L. J., G. B. Skomal, S. L. Hoffman, M. E. Porter, K. J. Goldman, and S. David.
2018b. Age and growth of sharks: do vertebral band pairs record age? Mar. Freshw. Res. 69:1440–1452.
Nelson, G. A.
2013. fishmethods: fisheries methods and models in R. R package, vers. 1.4-0. [Available from website, accessed November 2019.]
Ogle, D. H.
2012. FSA: fisheries stock analysis. R package, vers. 0.3.2. [Available from website, accessed November 2019.]
Oliveira, P. G. V.
2001. Levantamento da fauna de elasmobranquios e estudo da biologia comportamental do tubarao limao, *Negaprion brevirostris* (Poey, 1868), tubarao lixa, *Ginglymostoma cirratum* (Bonnaterre, 1788) na Reserva Biologica do Atol das Rocas, RN-Brasil. M.S. thesis, 114 p. Univ. Fed. Pernambuco, Recife, Brasil. [In Portuguese.]

Parsons, G. R.
1987. Life history and bioenergetics of the bonnethead shark, *Sphyrna tiburo* (Linnaeus): a comparison of two populations. Ph.D. diss., 167 p. Univ. S. Fla., Tampa, FL.
1993. Age determination and growth of the bonnethead shark *Sphyrna tiburo*: a comparison of two populations. Mar. Biol. 117:23–31.

Passerotti, M. S., A. H. Andrews, J. K. Carlson, S. P. Wintner, K. J. Goldman, and L. J. Natanson.
2014. Maximum age and missing time in the vertebrae of sand tiger shark (*Carcharhinus taurus*): validated lifespan from bomb radiocarbon dating in the western North Atlantic and southwestern Indian Oceans. Mar. Freshw. Res. 65:674–687.

Pistevos, J. C. A., I. Nagelkerken, T. Rossi, M. Olmos, and S. D. Connell.
2015. Ocean acidification and global warming impair shark hunting behaviour and growth. Sci. Rep. 5:16293.

Portnoy, D. S., J. B. Puritz, C. M. Hollenbeck, J. Gelsleichter, D. Chapman, and J. R. Gold.
2015. Selection and sex-biased dispersal in a coastal shark: the influence of philopatry on adaptive variation. Mol. Ecol. 24:5877–5885.

R Core Team.
2019. R: a language and environment for statistical computing. R Foundation for Statistical Computing, Vienna, Austria. [Available from website, accessed November 2019.]

Ricker, W. E.
1975. Computation and interpretation of biological statistics of fish populations. Bull. Fish. Res. Board Can. 191, 333 p.

Rigby, C. L., B. B. Wedding, S. Grauf, and C. A. Simpfendorfer.
2014. The utility of near infrared spectroscopy for age estimation of deepwater sharks. Deep-Sea Res. Oceanogr., 1 94:184–194.

Saunders, R. L., and K. R. Allen.
1967. Effects of tagging and fin-clipping on the survival and growth of Atlantic salmon between smolt and adult stages. J. Fish. Res. Board Can. 24:2595–2611.

Scheirer, J. W., and D. W. Coble.
1991. Effects of Floy FD-67 anchor tags on growth and condition of northern pike. North Am. J. Fish. Manage. 11:369–373.

SEDAR (Southeast Data Assessment and Review).
2013. SEDAR 34 stock assessment report: HMS bonnethead shark, 217 p. SEDAR, North Charleston, SC. [Available from website.]

Simpfendorfer, C. A.
2000. Growth rates of juvenile dusky sharks, *Carcharhinus obscurus* (Lesueur, 1818), from southwestern Australia estimated from tag-recapture data. Fish. Bull. 98:811–822.

Skomal, G., and D. Bernal.
2010. Physiological responses to stress in sharks. *In* Sharks and their relatives II: biodiversity, adaptive physiology, and conservation (J. C. Carrier, J. A. Musick, and M. R. Heithaus, eds.), p. 459–490. CRC Press, Boca Raton, FL.

Treble, M. A., S. E. Campana, R. J. Wastle, C. M. Jones, and J. Boje.
2008. Growth analysis and age validation of a deepwater Arctic fish, the Greenland halibut (*Reinhardtius hippoglossoides*). Can. J. Fish. Aquat. Sci. 65:1047–1059.

Ulrich, G. F., C. M. Jones, W. B. Driggers III, J. M. Drymon, D. Oakley, and C. Riley.
2007. Habitat utilization, relative abundance, and seasonality of sharks in the estuarine and nearshore waters of South Carolina. Am. Fish. Soc. Symp. 50:125–139.

Vinyard, E. A., B. S. Frazier, J. M. Drymon, J. J. Gelsleichter, and W. J. Bubley.
2019. Age, growth, and maturation of the finetooth shark, *Carcharhinus isodon*, in the Western North Atlantic Ocean. Environ. Biol. Fish. 102:1499–1517.

von Bertalanffy, L.
1938. A quantitative theory of organic growth (inquiries on growth laws. II). Hum. Biol. 10:181–213.

Vucic-Pestic, O., R. B. Ehnes, B. C. Rall, and U. Brose.
2011. Warming up the system: higher predator feeding rates but lower energetic efficiencies. Global Chang. Biol. 17:1301–1310.

Welsford, D. C., and J. M. Lyle.
2005. Estimates of growth and comparisons of growth rates determined from length- and age-based models for populations of purple wrasse (*Notolabrus fucicola*). Fish. Bull. 103:697–711.

National Marine
Fisheries Service
NOAA

Fishery Bulletin
established in 1881

Spencer F. Baird
First U.S. Commissioner
of Fisheries and founder
of *Fishery Bulletin*

Distribution, relative abundance, and reproductive output of spawning female blue crab (*Callinectes sapidus*) in offshore waters of the Gulf of Mexico

Adam A. Kemberling
M. Zachary Darnell (contact author)

Email address for contact author: zachary.darnell@usm.edu

Division of Coastal Sciences
School of Ocean Science and Engineering
The University of Southern Mississippi
703 E. Beach Drive
Ocean Springs, Mississippi 39564

Abstract—Effective assessment and management of migratory species require an understanding of stock boundaries and habitat use during critical life history periods. The blue crab (*Callinectes sapidus*) is considered a primarily estuarine species and has traditionally been assessed and managed on a state basis, relying on abundance estimates derived from estuarine sampling. Females undertake a seaward spawning migration, and recent evidence indicates that coastal and offshore waters may provide important spawning habitat. We investigated occurrence and reproductive output of spawning blue crab in offshore waters of the northwestern Gulf of Mexico, and results indicate that these waters may be an important spawning area for this species. Densities of blue crab were low offshore compared with those in estuaries, but given the large extent of available offshore habitat, the total abundance of adult females is likely similar in offshore and estuarine waters. Analyses of the reproductive output of females collected offshore indicate that they continue to spawn after leaving the estuaries. Fecundity and measures of egg quality were assessed and were similar to previous estimates for estuarine regions. Future management and assessment efforts should account for this previously understudied portion of the blue crab spawning stock.

Manuscript submitted 6 March 2020.
Manuscript accepted 14 October 2020.
Fish. Bull. 118:346–358 (2020).
Online publication date: 11 December 2020.
doi: 10.7755/FB.118.4.4

The views and opinions expressed or implied in this article are those of the author (or authors) and do not necessarily reflect the position of the National Marine Fisheries Service, NOAA.

Fisheries management is most effective when the scale of management matches the scale of the stock (Begg et al., 1999; Al-Humaidhi et al., 2013). The modern stock concept describes units of a population that can be considered homogeneous (in terms of life history, responses to environmental fluctuations, genetic diversity, etc.) and can inform the scale of assessments and management decisions (Begg and Waldman, 1999). The failure to correctly identify spatial complexity within a stock has been identified as one of the main factors contributing to the collapse of some high-profile fisheries in the recent past (Hutchinson, 2008), and studies examining genetic stock structure have identified cases with clear mismatches between the genetic stock structure and the management of the stock as a singular unit (Bonanomi et al., 2015; Kerr et al., 2017).

Migratory stages are common in marine and estuarine species (e.g., Forward and Tankersley, 2001; Potter et al., 2015; Secor, 2015). Large-scale seasonal or annual movements can complicate fisheries management because different life stages may occupy different habitats. For these species, understanding habitat use during critical life history stages (e.g., spawning) is particularly important in the context of temporal or spatial management actions (e.g., season and area closures, spawning sanctuaries, migratory corridors, and ecosystem-based management).

Blue crab (*Callinectes sapidus*) support highly valuable fisheries along the Atlantic and Gulf coasts of the United States, with landings in 2018 totaling over 62,000 metric tons and having a wholesale value of over $193 million (NMFS[1]). Following their terminal molt, female blue crab mate and store the sperm necessary for their life-long reproductive output (Millikin and Williams, 1984). After mating, female blue crab forage for several weeks (Turner et al., 2003) before beginning a seaward spawning migration (Aguilar et al., 2005). This migration ensures that females reach spawning grounds of sufficiently high salinity (>20.1; Costlow and Bookhout, 1959)

[1] NMFS (National Marine Fisheries Service). 2020. Fisheries of the United States, 2018. NOAA, Natl. Mar. Fish. Serv., Curr. Fish. Stat. 2018, 140 p. [Available from website.]

for larval survival. Spawning female blue crab are often found in large numbers at or near the mouths of estuaries (e.g., Rittschof et al., 2010; Anderson et al., 2017); these areas are typically assumed to be the primary spawning grounds. The blue crab is a highly fecund species, with females producing multiple clutches of several million larvae at a time (Hines et al., 2003). Each brood of larvae is released into the water column as zoeae that disperse through currents for 30–50 d (Costlow and Bookhout, 1959) before their return and recruitment to coastal habitat as megalopae soon after (Rabalais et al., 1995; Ogburn et al., 2009).

Mature females can travel great distances (>200 km; Aguilar et al., 2005) during their spawning migration, and migration rates can exceed 8 km/d (Carr et al., 2004). Female blue crab continue migrating throughout their reproductive period (Hench et al., 2004) and are, therefore, likely moving out of estuaries and continuing their migration in offshore waters. Adults of this species typically are considered estuarine, but large numbers of spawning female blue crab have been found in waters off both the Atlantic coast (Rittschof et al., 2010; Ogburn and Habegger, 2015) and Gulf coast (Gelpi et al., 2009, 2013) of the United States. Although observed densities of blue crab are typically lower offshore than in estuaries, evidence from the Atlantic coast of the southeastern United States indicates that this often-overlooked offshore population may represent a substantial fraction of the regional spawning stock (Ogburn and Habegger, 2015). In the Gulf of Mexico, Gelpi et al. (2009, 2013) found large numbers of spawning females residing on Ship, Trinity, and Tiger Shoals and surrounding waters, 20–40 km off the coast of Louisiana. All developmental stages of eggs were observed, and 81% of females had full ovaries at the time of capture, indicating that they would continue to spawn at least one additional clutch of eggs during the season (Gelpi et al., 2009). Furthermore, spawning female blue crab are regularly captured in trawl surveys conducted by the Southeast Area Monitoring and Assessment Program (SEAMAP) in the Gulf of Mexico, as far as 200 km offshore.

Given the large extent of relatively shallow offshore habitat in the Gulf of Mexico and with offshore habitat proving to be of larger importance to the spawning stock of blue crab in the Atlantic Ocean than previously thought (Ogburn and Habegger, 2015), we sought to identify the contribution of this offshore habitat to the spawning stock of blue crab in the northwestern Gulf of Mexico. The goal of this study was to conduct an investigation of spawning female blue crab in offshore waters of the northwestern Gulf of Mexico. We examined temporal and spatial variation in catch of blue crab in fishery-independent SEAMAP groundfish trawl surveys over a 20-year period (2000–2019) and examined the reproductive output and overall condition of females collected in offshore waters during the SEAMAP groundfish trawl surveys in 2017. We also compared results for spawning females found offshore in our study with previous findings for blue crab found spawning in inshore areas.

Materials and methods

Survey design and methods

The SEAMAP involves the cooperation of state, federal, and university partners for the collection of fishery-independent data. The SEAMAP-Gulf of Mexico groundfish trawl survey is conducted twice each year during summer and fall at distances from shore up to 370 km (200 nautical miles) and at depths up to 109.7 m (60 fathoms). The summer survey typically occurs in June and July but can start as early as May and end as late as August. The fall survey typically occurs during October and November but can start as early as September and end as late as December. Sampling is done by using a stratified random design and a 12.2-m (40-ft) trawl net with stretched mesh of 40.3–41.9 mm. Environmental conditions, including salinity and temperature, were measured either at 3 positions in the water column, the surface, mid-water, and bottom, or through a profile of the full water column at each sampling location.

Prior to fall 2008, sampling was stratified by depth (with 23 depth strata, including 1-fathom strata for 5–20 fathoms, a 2-fathom stratum of 20–22 fathoms, a 3-fathom stratum of 22–25 fathoms, 5-fathom strata for 25–50 fathoms, and a single stratum of 25–50 fathoms), by geographic area (based on groupings of 2–3 shrimp statistical zones [SSZ], which are defined by the National Marine Fisheries Service), and by time of day (day or night) (Nichols[2]). Trawl tows were conducted perpendicular to the depth contours and covered the entire depth stratum at each sampling location. Tow time ranged from 10 to 55 min; if sufficient depth coverage was not possible in a single 55-min tow, multiple consecutive tows were conducted. Sampling was limited to SSZ 11–21. A survey design change occurred between summer and fall 2008. Under the new survey design, selection of sampling locations was stratified by individual SSZ (Fig. 1), and sampling extended into the eastern Gulf of Mexico. The stratifications for time of day and for depth were dropped. In 2014, depth stratification resumed with 2 depth strata: 5–20 fathoms and 20–60 fathoms (Pollack et al.[3]). The number of randomly selected sampling locations (stations) within each stratum that combined geographic area and depth was proportional to the geographic area of that stratum. The trawl was towed for 30 min at each sampling location.

For all tows, abundance of each species in the catch was recorded. In the case of an extremely large catch (typically >22.7 kg), the catch was subsampled and total abundance of each species was extrapolated. For blue crab, carapace widths (CWs), measured as the distance between the tips of the lateral spines, of up to 20 individuals

[2] Nichols, S. 2004. Derivation of red snapper time series from SEAMAP and groundfish trawl surveys. Southeast Data Assess. Rev. SEDAR7-DW-01, 26 p. [Available from website.]

[3] Pollack, A. G., D. S. Hanisko, and G. W. Ingram Jr. 2016. Wenchman abundance indices from SEAMAP groundfish surveys in the northern Gulf of Mexico. Southeast Data Assess. Rev. SEDAR49-DW-19, 27 p. [Available from website.]

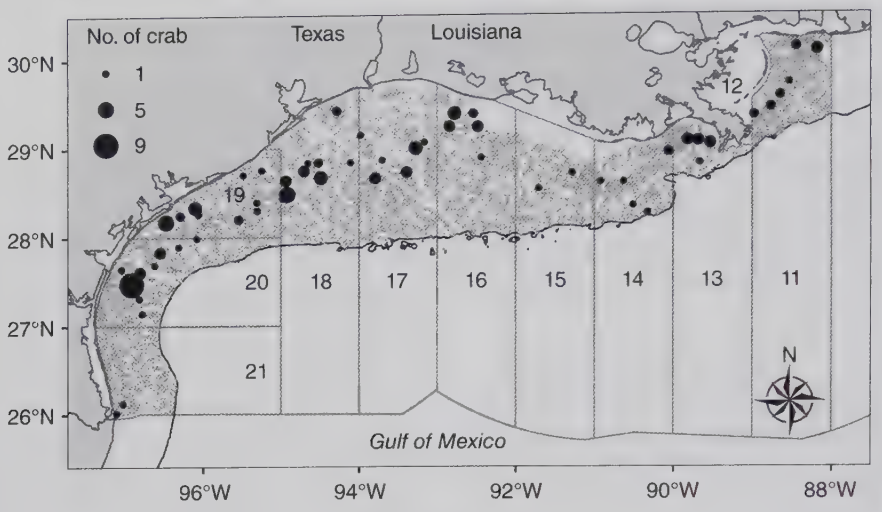

Figure 1

A map of the study area in the northwestern Gulf of Mexico showing the locations where blue crab (*Callinectes sapidus*) were collected in groundfish trawl surveys as part of the Southeast Area Monitoring and Assessment Program (SEAMAP). Small gray dots indicate locations of trawl tows for the study period 2000–2019. Black circles indicate locations where adult female blue crab were caught, for reproductive analyses, during the SEAMAP groundfish surveys conducted in 2017, with circle size proportional to the number of blue crab collected from that location. The boxes outlined in gray and the numerals inside them indicate shrimp statistical zones (defined by the National Marine Fisheries Service), which were used in the stratified random sampling design. The black line indicates the 109.7-m (60-fathom) depth contour, which is used as the outer limit for SEAMAP groundfish surveys.

(chosen haphazardly from the total catch) and the sex of every fifth measured crab were recorded for each station (GSMFC[4]).

Long-term patterns of distribution and relative abundance

Our analyses focused on the period 2000–2019 and included only offshore areas that were sampled before and after the change in survey design in 2008 (SSZ 11 and SSZ 13–21). Chandeleur Sound in Louisiana (SSZ 12) was excluded because this inshore area was not consistently sampled. Over this 20-year period, 7–119 trawl tows were conducted in each SSZ per year (Suppl. Tables 1 and 2) (online only). Data collected prior to 2000 were not included because of uncertainty surrounding species identification. Data were filtered to include only tows of 12.2-m trawl nets with stretched mesh sizes ranging from 40.3 to 41.9 mm and conducted at depths >9.1 m (>5 fathoms). Any sampling events with incomplete data for geographic location or vessel speed or with operation codes indicating a bad tow (e.g., if the doors came up crossed, if the codend came untied, or if the net was fouled or torn) were excluded from analysis.

Maturity stage is not recorded for blue crab; therefore, it was necessary to classify crab as adult or juvenile on the basis of CW. We classified blue crab ≥125 mm CW as adults, following the cutoff used in recent Gulf-wide (VanderKooy, 2013) and state-level (West et al.[5]) blue crab stock assessments. Because not all blue crab are measured and only a small proportion are assigned a sex, it was necessary to estimate the catch of adult female blue crab from each trawl tow by using the total catch multiplied by the proportion of measured blue crab from the tow that were ≥125 mm CW and by the proportion of blue crab from the tow that had their sex determined and that were classified as female:

$$\textit{adult female catch} = \textit{total catch} \times \textit{proportion adult} \times \textit{proportion female}.$$

For a small number of trawl tows (n=385 tows, 4.3% of the tows in the data set used in analysis), sex was not recorded, even though adult blue crab were caught during the tow. For these tows, the mean proportion of

[4] GSMFC (Gulf States Marine Fisheries Commission). 2016. SEAMAP operations manual for trawl and plankton surveys, 61 p. GSMFC, Ocean Springs, MS. [Available from website.]

[5] West, J., H. Blanchet, and P. Cagle. 2019. Update assessment of blue crab in Louisiana waters: 2019 report, 32 p. Louisiana Dep. Wildl. Fish., Baton Rouge, LA. [Available from website.]

crab that were female for that year was used. Sex was not determined for blue crab in 2004; therefore, the overall mean proportion that was female (0.930) was used. Catch per unit of effort (CPUE) of adult female blue crab was calculated by dividing the adult female catch (measured as number of individuals) by the area swept by the trawl (calculated by using the recorded speed and duration of a tow and by assuming a 12.2-m net spread). Values of CPUE are given as number of individuals per hectare.

To examine overall temporal and spatial patterns in CPUE of blue crab in the SEAMAP survey area, adult female catch was modeled by using a 2D generalized additive model (Potts and Rose, 2018) with a negative binomial error distribution and log link function. Multiple candidate models were fit and compared by using Akaike information criteria (AIC) to determine the most appropriate model. Adult female catch was the response variable. Year was included in all models as a categorical variable. Geographic location was included as a 2D smooth function with thin-plate spline bases. Season (summer or fall) was included as an additional temporal covariate. All models also included an offset term for the area swept by the trawl to account for differences in sampling effort among trawl tows. Following model selection, a Wald chi-square test was used to test for significance of predictor variables.

An index of abundance for the spawning stock in the northwestern Gulf of Mexico was estimated to allow examination of population trends, accounting for spatial and temporal variation in sampling effort. Estimated marginal means for each year were extracted from the model output, reflecting the main effect of year averaged over the full study area and across both seasons. Estimated marginal means were then standardized relative to the average annual estimated marginal mean across the study period by using a Z-transformation, providing an index of abundance in units of standard deviations above or below the mean for the 20-year period for which we analyzed survey data.

Relative importance of offshore and estuarine waters

To assess the importance of offshore spawning areas relative to estuarine spawning areas for the spawning stock of blue crab in the Gulf of Mexico, total abundance of adult female blue crab was estimated and compared between offshore and estuarine waters of the study area. Abundance estimates were limited to the areas west of the Mississippi River (SSZ 13–21), because of the lack of consistent and spatially widespread fishery-independent trawl sampling for blue crab in estuarine waters of the state of Mississippi. Temporal coverage of abundance estimates was limited to the period 2006–2018 because of limitations on availability of data for sampling in estuarine areas in other years. Observed CPUE was used as a proxy for density of blue crab. Because gear efficiencies are unknown for the trawl surveys examined in our study, we were unable to correct for gear efficiency; actual densities of blue crab, and therefore abundances, are likely substantially higher than estimates calculated in our study.

Offshore abundance of blue crab was estimated by using the annual mean observed CPUE of adult female blue crab from the summer SEAMAP groundfish trawl survey and the total area of potential offshore spawning habitat, defined as all waters in the Gulf of Mexico west of the Mississippi River (SSZ 13–21) from the estuarine mouth or barrier islands to the 109.7-m (60-fathom) depth contour (depth contours were derived from gridded bathymetry data from the General Bathymetric Chart of the Oceans (GEBCO_2020 Grid, available from website). Annual mean CPUE values, meaning numbers of individuals per hectare, were multiplied by the total area of potential offshore spawning habitat to estimate total abundance of blue crab in offshore waters for each year. These estimates of offshore abundance were compared with similar estimates of abundance in estuarine waters of Texas and Louisiana, by using CPUE from fishery-independent trawl surveys conducted in estuarine areas by the Texas Parks and Wildlife Department (TPWD) and Louisiana Department of Wildlife and Fisheries (LDWF). Only data collected during June and July were included in these analyses because these summer months represent the time of peak adult female abundance in estuarine waters of Louisiana and Texas and also correspond with the timing of the summer SEAMAP trawl survey.

The TPWD conducts fishery-independent sampling by using 6.1-m trawl nets with 38.1-mm stretched mesh, towed for 10 min at a speed of 4.8 km/h. Sampling is based on a stratified random design, with each of the 8 major bay systems in Texas (Sabine, Galveston, Matagorda, San Antonio, Aransas, Corpus Christi, Upper Laguna Madre, and Lower Laguna Madre) divided into grid cells that were 1.85 by 1.85 km. Each month, 10–20 grid cells in each major bay system are randomly selected for trawl sampling, with the number of cells depending on the bay system. Statewide annual mean CPUE of adult (≥125 mm CW) females was calculated for the period June–July and then was multiplied by the total available habitat area to estimate the total abundance of mature females in estuarine waters of Texas for each year. Habitat area was defined as the total area of the Texas coastal bay systems extracted from geographic information systems data obtained from TPWD (available from website).

The LDWF conducts fishery-independent sampling by using 4.9-m flat trawl nets with a 38.1-mm stretched mesh body and a 12.7-mm stretched mesh bag, towed for 10 min. Sampling occurs at fixed stations, semimonthly during November–February and weekly during March–October. Vessel speed is not recorded but typically ranges from 2.6 to 4.8 km/h (Cagle[6]). For CPUE calculations, an average vessel speed of 3.7 km/h was assumed because it is the midpoint of the typical range. Because stations were added and deleted during the period of interest, we used only data from stations that were sampled in 2018 and had

[6] Cagle, P. 2020. Personal commun. Louisiana Dep. Wildl. Fish., P.O. Box 98000, Baton Rouge, LA 70898.

been sampled for at least 8 years during the period 2006–2018. Additionally, only stations west of the Mississippi River were included, to correspond with the spatial extent of the SEAMAP data used for offshore abundance estimates. Annual mean CPUE of adult (≥125 mm CW) female blue crab was then multiplied by the total available habitat area to estimate the total abundance of mature females in estuarine waters of Louisiana west of the Mississippi River for each year. Total available estuarine habitat area in Louisiana was calculated by using the NOS80K shoreline data set from the NOAA Office of Ocean Resources Conservation and Assessment (NOAA[7]). This shoreline layer was created in 1994, however, and substantial land loss has occurred in Louisiana since that time (Couvillion et al.[8]). The total available estuarine habitat in the Louisiana portion of their study area was, therefore, corrected on the basis of observed rates of coastal land loss in our study area (Couvillion et al.[8]).

Condition and reproductive output of spawning females

Mature female blue crab were collected offshore during the summer and fall SEAMAP groundfish trawl surveys in 2017 for analyses of overall condition and reproductive output. Mature females were haphazardly selected from the haul of each trawl tow, individually bagged and frozen, and sent to the Gulf Coast Research Laboratory in Ocean Springs, Mississippi, for analysis. During the summer survey (30 May–2 July 2017), 109 blue crab were collected from 48 stations, and during the fall survey (13 October–8 November 2017), 11 females were collected from 10 stations (Fig. 1).

Following thawing, CW and total mass were recorded for each crab. Gills were inspected for the presence of the parasitic gooseneck barnacle *Octolasmis muelleri* and for the parasitic nemertean worm *Carcinonemertes carcinophila*. Spermathecae, the paired sperm storage organs, were located to determine if the female had recently mated. A female was determined to have recently mated (within the past 3–5 weeks; Wolcott et al., 2005) if her spermathecae had a large size, firm texture, and pink color (Wolcott et al., 2005; Ogburn and Habegger, 2015). Because females mate only once in their lifetime, following their terminal molt, large, firm, pink spermathecae serve as an indication that a female moved offshore soon after her mating or that a female mated while offshore. Each female was determined to be spawning capable if she had developed, full ovaries or carried an egg mass.

For ovigerous females, the egg mass was carefully separated from the pleopods and weighed. A subsample <1 g (typically 500–1000 eggs) was then removed and weighed, and the total number of eggs in the subsample was counted by using a stereoscopic microscope. Total fecundity was estimated for each ovigerous female by dividing the number of eggs in the subsample by the mass of the subsample and multiplying by the mass of the entire egg mass. Relationships between fecundity and body size were examined by using generalized linear models (GLMs) with a Gaussian distribution and log link function and with fecundity as the response variable. Separate GLMs were fit to model fecundity as a function of CW and body mass (excluding the mass of the egg mass). Because of missing data for body mass of 16 of the 73 ovigerous blue crab, it was not possible to directly compare the model fits by using AIC or the AIC corrected for bias of small sample sizes (AICc) because the 2 models used slightly different data sets. For comparisons, the GLM with CW as the predictor was refit by using only individuals with data for both CW and body mass, and then the models were compared by using AICc.

The embryonic developmental stage for each egg sample was determined by visual examination under a compound microscope and classified as early (stages 1–3 of DeVries et al., 1983), middle (stages 4–6 of DeVries et al., 1983), and late (stages 7–9 of DeVries et al., 1983). The percentage of embryos that were developing normally (Darnell et al., 2009) was visually assessed for each egg mass on the basis of 20 eggs chosen at random from the subsample. Egg size for 20 normally developing embryos was determined by measuring along the long axis and the perpendicular axis with a compound microscope. Egg volume was calculated for each measured egg as the volume of a prolate spheroid by using the short and long axis measurements. Egg volume measurements were averaged for each egg mass, and this mean volume for each egg mass was then used in subsequent analyses. Egg volume was analyzed by using a GLM with a gaussian distribution and a log link function and with egg volume as the response variable. Egg volume was modeled as a function of CW and embyronic developmental stage (early, middle, and late).

Results

Long-term patterns of distribution and relative abundance

A total of 8996 trawl tows were conducted in offshore waters across the study area in 2000–2019. During that time, 97.7% of summer sampling occurred in June and July, with 1.3% occurring in May and 1.0% occurring in August. Fall sampling was primarily (97.7%) conducted during October and November, with 2.2% occurring in September and 0.1% occurring in December. Depths sampled were 9.2–109.5 m. Salinities measured at the bottom of the water column at sampling locations were 10.9–39.5, with 97.3% of trawl tows conducted in waters with salinities ≥30.0. Bottom temperatures were 16.0–30.5°C.

Blue crab were caught in 19.4% of all trawl tows, with 11,021 caught during 2000–2019 across the full study

[7] NOAA. 1994. NOS80K: medium resolution digital vector U.S. shoreline shapefile. Strategic Environ. Assess. Div., Off. Ocean Resour. Conserv., Natl. Ocean Serv., NOAA, Silver Spring, MD. [Available from website, accessed May 2020.]

[8] Couvillion, B. R., H. Beck, D. Schoolmaster, and M. Fischer. 2017. Land area change in coastal Louisiana 1932 to 2016: U.S. Geological Survey scientific investigations map 3381, 16 p. [Pamphlet.] [Available from website, accessed May 2020.]

area. Recorded CWs were 3–281 mm (median: 136 mm), with 99.5% of blue crab having CWs of 20–200 mm. Although sex was not recorded for all blue crab, 93.0% of the 1597 blue crab for which sex was determined were female. Adult female blue crab were caught in 17.1% of all trawl tows, with a total of 6355 caught. The overall mean CPUE of adult females was 0.25 individuals/ha (standard error of the mean [SE] 0.01) over the full study period, with annual mean CPUE ranging from 0.06 individuals/ha (SE 0.02) in 2013 to 0.53 individuals/ha (SE 0.09) in 2010. Annual frequencies of occurrence for adult female blue crab ranged from 8.5% in 2000 to 25.7% in 2011 (Table 1). The maximum annual mean CPUE of adult females observed during the summer surveys was 0.87 individuals/ha (SE 0.31) in 2006, and the maximum annual mean CPUE of adult females observed during the fall surveys was 0.29 individuals/ha (SE 0.09) in 2011.

Following comparisons of candidate models, the selected model included year, season, an interaction of year and season, and separate smooth terms for geographic location in each season (Table 2), with the selected model explaining 47.9% of the deviance in catch. Results of the Wald chi-square test indicate that all predictors had a significant effect on catch (Table 3). Averaged over the full study period, CPUE of adult female blue crab was higher during the summer surveys (0.39 individuals/ha [SE 0.03]) than during the fall surveys (0.11 individuals/ha [SE 0.01]), although this pattern was not consistent across all years (Fig. 2). The spatial distribution of adult female blue crab also differed between the 2 seasons (Table 3). In summer surveys, CPUE was generally highest in nearshore regions off Louisiana and along the central and upper coasts of Texas, primarily at depths <36.6 m (<20 fathoms). The CPUE from fall surveys was generally highest off southeastern Louisiana and at intermediate distances from shore (Fig. 3).

Estimated marginal mean CPUE for each year, standardized relative to the 20-year average, provides a standardized index of abundance for the offshore spawning stock of blue crab in the northwestern Gulf of Mexico (Fig. 4). With the exception of 2010 and 2011, the index of abundance for each year was within 1.5 standard deviations of the mean value. The index indicates a trend of slight increases in abundance from 2000 to 2009, followed by a large increase in 2010, a sustained high level of abundance in 2011, and a marked decrease after 2011. After a low in 2012, the index has steadily increased back to average levels of abundance.

Table 1

Summary information by year for adult female blue crab (*Callinectes sapidus*) collected in the northwestern Gulf of Mexico during groundfish trawl surveys conducted in 2000–2019 as part of the Southeast Area Monitoring and Assessment Program. The number of trawl tows; total catch (number of individuals); mean catch per unit of effort (CPUE), calculated by dividing catch by the area swept by the trawl (number of individuals per hectare) and given with standard error of the mean (SE) in parentheses; and percent occurrence of female adult blue crab are provided.

Year	No. of trawl tows	Total catch	Mean CPUE (SE)	Percent occurrence
2000	585	159	0.14 (0.06)	8.55
2001	525	179	0.14 (0.03)	10.86
2002	575	292	0.19 (0.03)	17.39
2003	528	454	0.26 (0.05)	16.48
2004	533	319	0.26 (0.05)	14.63
2005	517	457	0.31 (0.04)	22.63
2006	529	673	0.48 (0.16)	18.34
2007	510	327	0.26 (0.05)	16.86
2008	642	557	0.23 (0.05)	13.86
2009	689	575	0.33 (0.05)	20.90
2010	431	692	0.53 (0.09)	23.43
2011	381	520	0.49 (0.08)	25.72
2012	336	161	0.16 (0.04)	15.18
2013	261	55	0.06 (0.02)	9.58
2014	342	111	0.11 (0.02)	15.79
2015	346	126	0.12 (0.02)	18.21
2016	309	147	0.16 (0.03)	20.71
2017	333	259	0.26 (0.05)	19.82
2018	308	122	0.13 (0.02)	17.86
2019	316	170	0.17 (0.03)	18.35

Table 2

Candidate models used to estimate catch of adult female blue crab (*Callinectes sapidus*) collected from the northwest Gulf of Mexico between 2000 and 2019. Model selection criteria also are given for each model: the difference in Akaike information criterion (AIC) between each model and the model with the lowest AIC (ΔAIC), AIC weight (w_{AIC}), and the proportion of deviance explained. The characters "s()" indicate that a continuous variable was included as a smooth term. All models included an offset term for the area swept by the trawl to account for differences in sampling effort among trawl tows.

Model formulation	AIC	ΔAIC	w_{AIC}	D^2
Year + season + (year × season) + s(geographic location) × season	12,947.7	0.00	1	0.479
Year + season + s(geographic location) × season	13,072.6	124.93	0	0.454
Year + season + (year × season) + s(geographic location)	13,302.3	354.60	0	0.402
Year + season + s(geographic location)	13,410.7	462.99	0	0.376
Year + s(geographic location)	13,636.8	689.07	0	0.334
Year + season	14,560.2	1612.55	0	0.104
Year	14,797.0	1849.35	0	0.043

Table 3

Results from the Wald chi-square (χ^2) test for significance of predictor variables in the 2D generalized additive model used to examine overall temporal and spatial patterns in catch of adult female blue crab (*Callinectes sapidus*) collected during trawl surveys in the northwestern Gulf of Mexico between 2000 and 2019. The characters "s()" indicate that a continuous variable was included as a smooth term. Degrees of freedom (df) and estimated degrees of freedom (edf) are shown for parametric factor terms and smooth terms, respectively.

Source	df or edf	χ^2	*P*
Year	19	240.40	<0.0001
Season	1	21.54	<0.0001
Year × season	19	174.71	<0.0001
s(geographic location): summer	66.16	745.00	<0.0001
s(geographic location): fall	69.20	530.10	<0.0001

Relative importance of offshore and estuarine waters

During 2006–2018, considering only SSZ 13–21, CPUE of adult females from summer surveys in offshore waters of the Gulf of Mexico averaged 0.38 individuals/ha (SE 0.03), compared with the CPUE values of 0.46 individuals/ha (SE 0.03) in estuaries of Texas and of 3.92 individuals/ha (SE 0.17) in estuaries of Louisiana. Total available habitat area was estimated to be 11,473,937.0 ha for the offshore SSZ 13–21 in the SEAMAP study area, 578,310.7 ha for estuaries of Texas, and 853,436.2 ha for estuaries of Louisiana west of the Mississippi River. Rough calculations made by using CPUE of adult females (as a proxy for density) and total habitat area indicate that estuarine areas during June–July supported a minimum abundance of 1,248,675 adult female blue crab in 2017 and a maximum abundance of 8,631,449 adult female blue crab in 2006 and that the offshore SEAMAP survey area during June–July supported a minimum abundance of 664,203 adult female blue crab in 2013 and a maximum abundance of 9,509,020 adult female blue crab in 2010 (Fig. 5). On average, across the 13-year period of 2006–2018, the offshore SEAMAP survey area supported 48.8% of the total spawning stock in the northwestern Gulf of Mexico, although this percentage ranged from 26.5% in 2014 to 79.7% in 2017.

Condition and reproductive output of spawning females

Collection of blue crab for reproductive analyses occurred on each state and federal leg of the SEAMAP groundfish trawl surveys during summer and fall 2017. In total, 120 mature female blue crab were collected, with CWs ranging from 110 to 209 mm. The vast majority of blue crab (109 of 120) were collected during the summer survey (30 May–2 July 2017), and the rest of the individuals (11 of 120) were caught during the fall survey (13 October–8 November 2017).

Of the 109 mature females collected during summer, 95 individuals (87.2%) were spawning capable, as evidenced by an external egg mass (65 individuals) or mature ovaries (30 individuals). All embryonic developmental stages were observed in ovigerous blue crab collected during the summer survey, with 56.9% (37 individuals) in the early developmental stage, 10.8% (7 individuals) in the middle developmental stage, and 32.3% (21 individuals) in the late developmental stage. Additionally, 26.2% (17 individuals) of the ovigerous females collected during the summer survey also possessed developed, full ovaries, indicating the capacity to produce at least one additional clutch of eggs following the clutch carried at the time of collection. Only 1 female (0.9%) collected during the summer survey had mated recently.

Of the 11 mature females collected during the fall survey, 6 individuals (54.4%) were spawning capable, as evidenced by an external egg mass (5 individuals) or developed, full ovaries (1 individual). Of these 5 ovigerous individuals, 4 crab carried eggs in the early

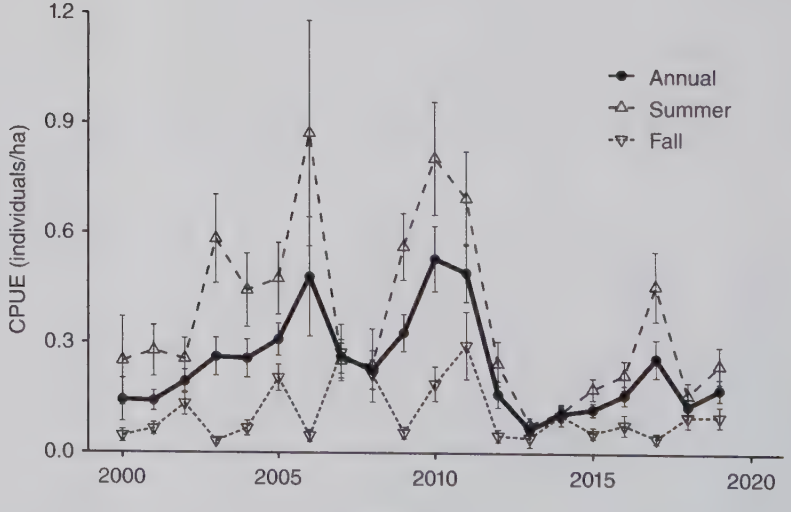

Figure 2

Observed mean annual (solid line) and seasonal (broken lines) catch per unit of effort (CPUE) for adult female blue crab (*Callinectes sapidus*) collected during groundfish surveys conducted in the northwestern Gulf of Mexico from 2000 through 2019 as part of the Southeast Area Monitoring and Assessment Program. Values of CPUE were calculated by dividing catch by the area swept by the trawl. Error bars indicate standard errors of the mean.

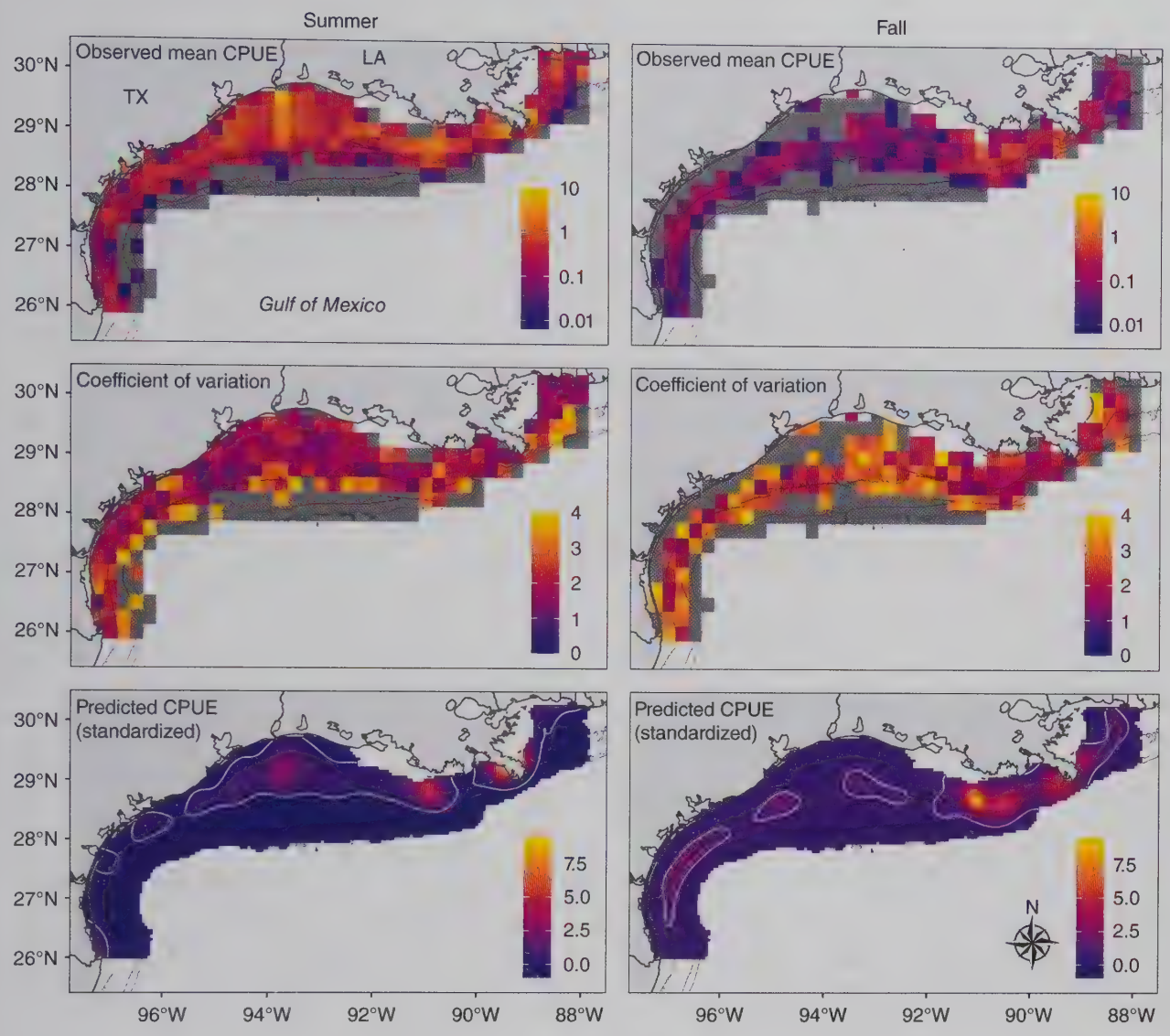

Figure 3

Spatial patterns of catch per unit of effort (CPUE) for adult female blue crab (*Callinectes sapidus*) collected during groundfish trawl surveys conducted in the northwestern Gulf of Mexico in summer (left panels) and fall (right panels) across the study period 2000–2019. The top panels show observed CPUE (number of individuals per hectare), binned into 0.25° grid cells and averaged across all years on a log scale. White areas represent areas that were not sampled, and gray grid cells represent areas with no catch of adult female blue crab over the full study period. The middle panels show interannual variability in catch rates, calculated as the coefficient of variation of observed annual mean CPUE. The bottom panels show predicted CPUE of adult female blue crab for each season from the generalized additive model, averaged across all years and standardized by using a Z-transformation based on the mean and standard deviation for that particular season. Values are depicted in units of standard deviations above (positive values) or below (negative values) the mean. White contours delineate a standardized value of zero, representing the mean for that season. Black lines represent the 36.6-, 73.2-, and 109.7-m (20-, 40-, and 60-fathom) depth contours.

developmental stage and 1 crab carried eggs in the late stage. None of the females collected during the fall survey had mated recently.

Fecundity was 1.07–8.93 million eggs (mean: 3.27 million eggs [SE 0.15 million]) and was strongly related to size of female crab, with larger females having higher fecundity. This relationship was evident when both CW ($P<0.0001$, deviance explained [D^2]=0.539) and body mass ($P<0.0001$, $D^2=0.712$) were considered (Fig. 6). Results of the comparison of model fits based on AICc indicate that body mass was a better predictor of fecundity than CW, with an AICc weight >0.98.

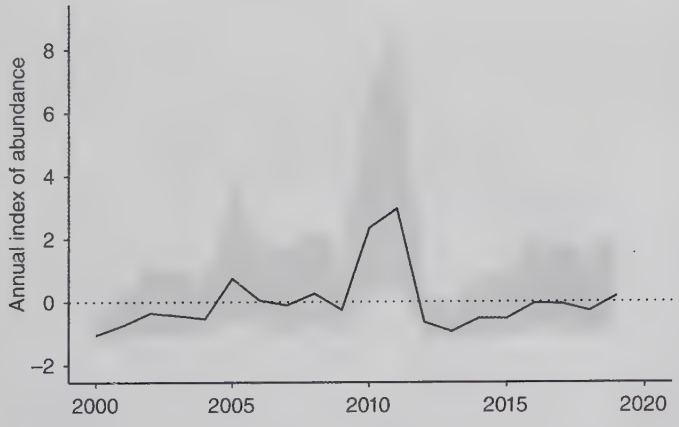

Figure 4

Standardized index of abundance for adult female blue crab (*Callinectes sapidus*) in the northwestern Gulf of Mexico during the study period 2000–2019. The gray shaded area indicates the 95% confidence interval. The horizontal dotted line indicates a value of zero, representing the average annual predicted catch per unit of effort across the full study period.

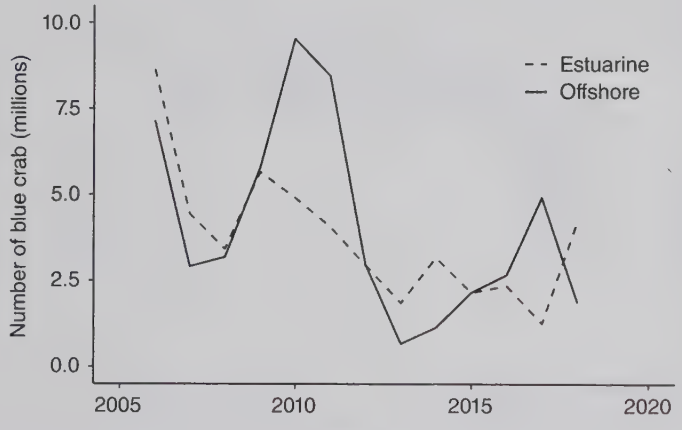

Figure 5

Estimated total abundance (in millions) of adult female blue crab (*Callinectes sapidus*) in offshore (solid line) and estuarine (dashed line) areas of the northwestern Gulf of Mexico west of the Mississippi River during June and July in 2006–2018.

On average across both seasons, 91.7% (SE 0.01) of eggs were fertilized and embryos were developing normally, with 91.6% (SE 0.01) of embryos developing normally in the summer and 93.0% (SE 0.05) of embryos developing normally in the fall. Eggs that were not developing normally were either unfertilized or fertilized but had ceased development in an earlier developmental stage than the majority of the egg mass. Average egg size was 243.6 µm (SE 0.5) along the long axis and 236.1 µm (SE 0.5) along the perpendicular axis. Average egg volume was 0.0073 mm^3 (SE 0.0001). There was a significant relationship between egg volume and embryonic developmental stage (F=29.76, P<0.0001), with a general increasing trend as the embryos develop further (Fig. 7). There was no significant relationship between egg volume and maternal CW (F=2.371, P=0.1286) and no significant interaction between maternal CW and embryonic developmental stage (F=2.363, P=0.1023).

The parasitic barnacle *O. muelleri* was commonly found on the gills of blue crab, with prevalence of 66.1% in summer and prevalence of 100.0% in fall. The nemertean worm *C. carcinophila* that is a predator of crab eggs was less common, with prevalence of 6.4% in summer and prevalence of 0.0% in fall.

Discussion

Results of this study indicate that the offshore waters of the northwestern Gulf of Mexico are an important spawning habitat for blue crab. Mature female blue crab are routinely caught in offshore waters of the northwestern Gulf of Mexico each year in the SEAMAP groundfish trawl survey, as far as 200 km from shore (Fig. 3). Our results support the substantial numbers of spawning blue crab in offshore areas of the Gulf of Mexico documented in previous studies (Gelpi et al., 2009, 2013).

The CPUE of adult female blue crab in offshore waters was greater in the summer than in the fall during most years (Fig. 3). This difference in CPUE between summer and fall may be indicative of a postspawning return to inshore habitats, as proposed by Tankersley et al. (1998). Given that findings from more recent studies indicate that migration back to estuaries is unlikely (Hench et al., 2004; Darnell et al., 2012), this pattern more likely is indicative of an offshore population decline from natural mortality due to predation and the high energy expenditures of migration and reproduction. It is important to note that the SEAMAP-Gulf of Mexico groundfish surveys are limited to summer (primarily June–July) and fall (primarily October–November). Blue crab recruitment in the northwestern Gulf of Mexico generally peaks from August to October (Rabalais et al., 1995; Perry et al. 2003), which corresponds with the observed peak in adult female densities during the summer SEAMAP trawl survey. Given that earlier recruitment peaks are observed in some areas (Rabalais et al., 1995; Sullivan and Neigel, 2017), late spring may also be an important time for offshore spawning in this region (data are not available to test this hypothesis).

Throughout the study period, the highest densities of adult female blue crab were present in the waters off

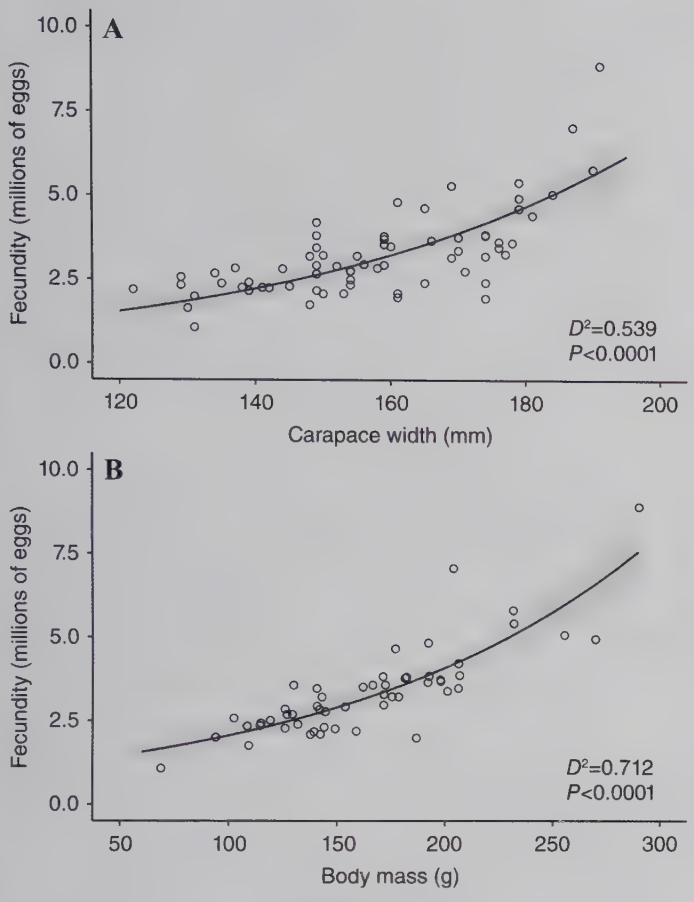

Figure 6

Relationships between fecundity and (**A**) carapace width and (**B**) body mass for ovigerous female blue crab (*Callinectes sapidus*) collected during the groundfish trawl survey conducted in 2017 in the northwestern Gulf of Mexico as part of the Southeast Area Monitoring and Assessment Program. Lines indicate relationships from generalized linear models. Shaded regions represent the 95% confidence interval. D^2=deviance explained.

Louisiana, and this pattern was consistent for both summer and fall surveys (Fig. 4). This spatial pattern reflects reported inshore fishery landings, with areas off Louisiana accounting for 88% of the blue crab landings in the Gulf of Mexico in 2018 (NMFS[9]). The large numbers of blue crab caught offshore of Louisiana relative to catch in other regions likely reflect the low salinities present in estuaries of Louisiana. Egg hatching and larval survivorship is negatively affected by salinities <20.1 (Costlow and Bookhout, 1959); during the spawning migration, therefore, females move to spawning grounds suitable for offspring survival. It is possible that the low salinities in estuaries of Louisiana result in greater numbers of females migrating out of the estuaries and continuing to migrate into the offshore environment, compared with the numbers of females that migrate out of estuaries in other regions. Although CPUE was highest off Louisiana in both seasons, the spatial distribution of the CPUE differed between summer and fall (Fig. 4). During summer, adult females were primarily caught in nearshore regions, at depths <36.6 m (<20 fathoms). During fall, adult females were primarily caught at depths of 36.6–73.2 m (20–40 fathoms) off both Texas and Louisiana.

Ogburn and Habegger (2015) conducted a similar examination of blue crab spawning in offshore waters of North Carolina, South Carolina, Georgia, and Florida, by using data from the SEAMAP-South Atlantic trawl surveys, with similar results. The highest CPUE of mature female blue crab occurred during the summer, females were actively spawning offshore, and a substantial portion of the spawning stock in Georgia occurred in offshore waters. Using only data from summer surveys, we observed a maximum annual mean CPUE of 0.87 individuals/ha (SE 0.31) (in 2006), a level substantially lower than the maximum of 1.58 individuals/ha observed (in 1991) by Ogburn and Habegger (2015). When interpreting this difference in CPUE, however, it is important to consider the differences in survey design between the SEAMAP trawl surveys conducted along the Atlantic coast of the southeastern United States and in the Gulf of Mexico. The SEAMAP-South Atlantic survey samples at depths of 4.0–10.0 m (2–5 fathoms), and the SEAMAP-Gulf of Mexico survey samples at depths of 9.1–109.7 m (5–60 fathoms). If the SEAMAP-Gulf of Mexico data set examined in this study is limited to depths <15 m, mean adult female CPUE was 1.96 individuals/ha (SE 0.97) in summer 2006, 1.58 individuals/ha (SE 1.13) in summer 2010, and 1.53 individuals/ha (SE 1.09) in summer 2000.

Although densities of adult female blue crab observed in the SEAMAP study area were relatively low, the offshore areas sampled in our study support a substantial portion (up to 79.7%, depending on the year) of the spawning stock in the northwestern Gulf of Mexico. We acknowledge that our estimates of total abundance of the spawning stock are rough, with multiple potential sources of error. A size-based cutoff was used to classify blue crab as adults or juveniles, rather than a visual morphological examination. Although the fishery-independent trawl surveys conducted by the LDWF and TPWD record maturity stage for blue crab, this information is not recorded in the SEAMAP trawl surveys. For consistency, we therefore classified all blue crab ≥125 mm CW as adults for data from all 3 survey programs. Additionally, these estimates do not account for differences in gear or gear efficiencies in the 3 survey programs. Actual abundances, therefore, are likely to be substantially

[9] NMFS (National Marine Fisheries Service). 2018. Commercial landings query, release 3.1.0.2. Off. Sci. Technol., Natl. Mar. Fish. Serv, Silver Spring, MD. [Available from website, accessed March 2020.]

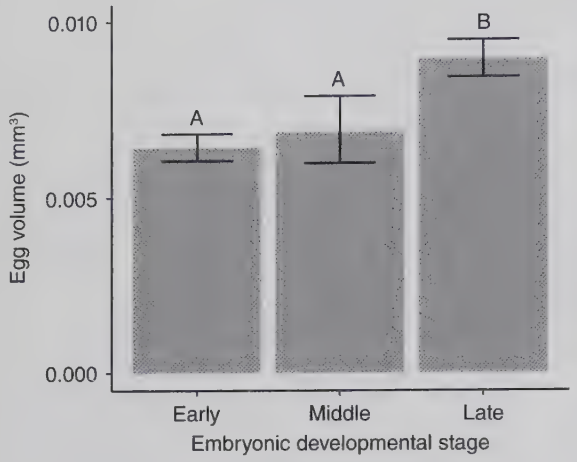

Figure 7

Mean egg volume for each embryonic developmental stage for ovigerous female blue crab (*Callinectes sapidus*) collected during the groundfish trawl survey conducted in 2017 in the northwestern Gulf of Mexico as part of the Southeast Area Monitoring and Assessment Program. Mean egg volumes are estimated marginal means from the generalized linear model. Error bars indicate the back-transformed 95% confidence intervals. The different letters above the bars indicate statistically significant differences between developmental stages.

higher than the estimates presented here. It is also important to consider the fate of larvae spawned offshore. There may be some distance offshore beyond which it is highly unlikely that a blue crab larva could successfully make it back to an estuary. To date, most larval transport modeling efforts for blue crab in the Gulf of Mexico have focused on spawning occurring at or near the estuarine mouth (e.g., Johnson and Perry, 1999; Jones et al., 2015; Criales et al., 2019). Further work is needed to better understand the fate of larval blue crab that have been spawned offshore.

Our analyses of the reproductive health of female blue crab collected in offshore habitats gave no indication that these females are of poor health or that they are of any lesser value to the spawning stock than females spawning in estuarine waters. Estimated fecundity was 1.07–8.93 million eggs, with an average of 3.27 million eggs (SE 0.15 million). In comparison, Graham et al. (2012) reported fecundity estimates of ~0.9–7.0 million eggs for ovigerous blue crab collected from estuarine waters of Mississippi Sound, and Prager et al. (1990) reported fecundity estimates of ~0.5–8.0 million eggs (mean: 3.2 million eggs) for ovigerous blue crab collected from Chesapeake Bay. Egg size in our study was also similar to that found in previous studies of ovigerous females collected in estuarine waters. We observed egg measurements of 243.6 µm (SE 0.5) along the long axis and of 236.1 µm (SE 0.5) along the perpendicular axis. In comparison, Graham et al. (2012) reported egg diameters of ~215–310 µm (~215–275 µm during the summer and fall only) for blue crab from Mississippi Sound, and Darnell et al. (2009) reported an average egg diameter of 267.5 µm (SE 1.9) for blue crab from North Carolina.

Fecundity of blue crab declines with age, with the greatest fecundity in the first clutch of eggs produced by a female (Darnell et al., 2009). That females collected in offshore and estuarine waters produce similar quantities of eggs indicates that offshore females are at a similar stage of their reproductive period as females spawning in estuarine areas. This notion is supported by our observation of a high percentage of eggs that were fertilized with embryos developing normally (91.7% [SE 0.01]). Darnell et al. (2009) observed a decrease in the percentage of embryos developing normally in later clutches, from 96.7% (SE 0.9) in a female's first clutch to 55.0% (SE 20.1) in its fourth clutch. Assuming a similar pattern in blue crab from the Gulf of Mexico, this finding indicates that the females assessed in our study were producing their first or second clutch of eggs. We observed full, developed ovaries in >50% of females collected offshore during the summer, indicating that these blue crab would spawn at least once more in their lifetime. Our results also indicate that oviposition and continued spawning is occurring in offshore waters, and we observed all stages of embryonic development.

The results of this study indicate that the coastal and offshore waters of the northwestern Gulf of Mexico are an important spawning habitat for blue crab. Although densities of blue crab offshore were low, these crab were primarily adult females and were actively spawning. Given the large amount of available shelf habitat, our results indicate that offshore areas support a substantial portion of the spawning stock in the northwestern Gulf of Mexico. Fecundity of females caught offshore was similar to that reported for estuarine spawning crab, and these females are continuing to spawn multiple clutches of eggs in offshore waters. Additional research is needed to understand the causes of temporal and spatial variation in densities of spawning female blue crab in the Gulf of Mexico. Furthermore, it is critical that this previously understudied portion of the spawning stock of blue crab in the Gulf of Mexico be considered and accounted for in future management and assessment efforts in the Gulf of Mexico.

Acknowledgments

We thank the Pascagoula Laboratory of the NOAA Southeast Fisheries Science Center, the LDWF, The University of Southern Mississippi Center for Fisheries Research and Development, H. Olmi, and C. Hayes for assisting with crab collection during the SEAMAP trawl surveys conducted in 2017. P. Cagle (LDWF) and M. Fisher (TPWD) provided assistance with access to inshore fishery-independent survey data for Louisiana and Texas, respectively. This study

was funded by the National Marine Fisheries Service under award NA15NMF4270328.

Literature cited

Aguilar, R., A. H. Hines, T. G. Wolcott, D. L. Wolcott, M. A. Kramer, and R. N. Lipcius.
2005. The timing and route of movement and migration of post-copulatory female blue crabs, *Callinectes sapidus* Rathbun, from the upper Chesapeake Bay. J. Exp. Mar. Biol. Ecol. 319:117–128.

Al-Humaidhi, A. W., J. A. Wilson, and T. H. Young.
2013. The local management of migratory stocks: implications for sustainable fisheries management. Fish. Res. 141:13–23.

Anderson, J., Z. Olsen, T. W. G. Sutton, C. Gelpi, and D. Topping.
2017. Environmental drivers of the spatial and temporal distribution of spawning blue crabs *Callinectes sapidus* in the western Gulf of Mexico. North Am. J. Fish. Manage. 37:920–934.

Begg, G. A., and J. R. Waldman.
1999. An holistic approach to fish stock identification. Fish. Res. 43:35–44.

Begg, G. A., K. D. Friedland, and J. B. Pearce.
1999. Stock identification and its role in stock assessment and fisheries management: an overview. Fish. Res. 43:1–8.

Bonanomi, S., L. Pellissier, N. O. Therkildsen, R. B. Hedeholm, A. Retzel, D. Meldrup, S. M. Olsen, A. Nielsen, C. Pampoulie, J. Hemmer-Hansen, et al.
2015. Archived DNA reveals fisheries and climate induced collapse of a major fishery. Sci. Rep. 5:15395.

Carr, S. D., R. A. Tankersley, J. L. Hench, R. B. Forward Jr., and R. A. Luettich Jr.
2004. Movement patterns and trajectories of ovigerous blue crabs *Callinectes sapidus* during the spawning migration. Estuar. Coast. Shelf Sci. 60:567–579.

Costlow, J. D., Jr., and C. G. Bookhout.
1959. The larval development of *Callinectes sapidus* Rathbun reared in the laboratory. Biol. Bull. 116:373–396.

Criales, M. M., L. Chérubin, R. Gandy, L. Garavelli, M. A. Ghannami, and C. Crowley.
2019. Blue crab larval dispersal highlights population connectivity and implications for fishery management. Mar. Ecol. Prog. Ser. 625:53–70.

Darnell, M. Z., D. Rittschof, K. M. Darnell, and R. E. McDowell.
2009. Lifetime reproductive potential of female blue crabs *Callinectes sapidus* in North Carolina, USA. Mar. Ecol. Prog. Ser. 394:153–163.

Darnell, M. Z., T. G. Wolcott, and D. Rittschof.
2012. Environmental and endogenous control of selective tidal-stream transport behavior during blue crab *Callinectes sapidus* spawning migrations. Mar. Biol. 159:621–631.

DeVries, M. C., C. E. Epifanio, and A. I. Dittel.
1983. Lunar rhythms in the egg hatching of the subtidal crustacean: *Callinectes arcuatus* Ordway (Decapoda: Brachyura). Estuar. Coast. Shelf Sci. 17:717–724.

Forward, R. B., Jr., and R. A. Tankersley.
2001. Selective tidal-stream transport of marine animals. Oceanogr. Mar. Biol., Annu. Rev. 39:305–353.

Gelpi, C. G., Jr., R. E. Condrey, J. W. Fleeger, and S. F. Dubois.
2009. Discovery, evaluation, and implications of blue crab, *Callinectes sapidus*, spawning, hatching, and foraging grounds in federal (US) waters offshore of Louisiana. Bull. Mar. Sci. 85:203–222.

Gelpi, C. G., Jr., B. Fry, R. E. Condrey, J. W. Fleeger, and S. F. Dubois.
2013. Using $\delta^{13}C$ and $\delta^{15}N$ to determine the migratory history of offshore Louisiana blue crab spawning stocks. Mar. Ecol. Prog. Ser. 494:205–218.

Graham, D. J., H. Perry, P. Biesiot, and R. Fulford.
2012. Fecundity and egg diameter of primiparous and multiparous blue crabs *Callinectes sapidus* (Brachyura: Portunidae) in Mississippi waters. J. Crustac. Biol. 32:49–56.

Hench, J. L., R. B. Forward Jr., S. D. Carr, D. Rittschof, and R. A. Luettich Jr.
2004. Testing a selective tidal-stream transport model: observations of female blue crab (*Callinectes sapidus*) vertical migration during the spawning season. Limnol. Oceanogr. 49:1857–1870.

Hines, A. H., P. R. Jivoff, P. J. Bushmann, J. van Montfrans, S. A. Reed, D. L. Wolcott, and T. G. Wolcott.
2003. Evidence for sperm limitation in the blue crab, *Callinectes sapidus*. Bull. Mar. Sci. 72:287–310.

Hutchinson, W. F.
2008. The dangers of ignoring stock complexity in fishery management: the case of the North Sea cod. Biol. Lett. 4:693–695.

Johnson, D. R., and H. M. Perry.
1999. Blue crab larval dispersion and retention in the Mississippi Bight. Bull. Mar. Sci. 65:129–149.

Jones, B. T., J. Gyory, E. K. Grey, M. Bartlein, D. S. Ko, R. W. Nero, and C. M. Taylor.
2015. Transport of blue crab larvae in the northern Gulf of Mexico during the Deepwater Horizon oil spill. Mar. Ecol. Prog. Ser. 527:143–156.

Kerr, L. A., N. T. Hintzen, S. X. Cadrin, L. W. Clausen, M. Dickey-Collas, D. R. Goethel, E. M. C. Hatfield, J. P. Kritzer, and R. D. M. Nash.
2017. Lessons learned from practical approaches to reconcile mismatches between biological population structure and stock units of marine fish. ICES J. Mar. Sci. 74:1708–1722.

Millikin, M. R., and A. B. Williams.
1984. Synopsis of biological data on the blue crab, *Callinectes sapidus* Rathbun. NOAA Tech. Rep. NMFS 1, 39 p.

Ogburn, M. B., and L. C. Habegger.
2015. Reproductive status of *Callinectes sapidus* as an indicator of spawning habitat in the South Atlantic Bight, USA. Estuar. Coasts 38:2059–2069.

Ogburn, M. B., H. Diaz, and R. B. Forward Jr.
2009. Mechanisms regulating estuarine ingress of blue crab *Callinectes sapidus* megalopae. Mar. Ecol. Prog. Ser. 389:181–192.

Perry, H., D. R. Johnson, K. Larsen, C. Trigg, and F. Vukovich.
2003. Blue crab larval dispersion and retention in the Mississippi Bight: testing the hypothesis. Bull. Mar. Sci. 72:331–346.

Potter, I. C., J. R. Tweedley, M. Elliott, and A. K. Whitfield.
2015. The ways in which fish use estuaries: a refinement and expansion of the guild approach. Fish Fish. 16:230–239.

Potts, S. E, and K. A. Rose.
2018. Evaluation of GLM and GAM for estimating population indices from fishery independent surveys. Fish. Res. 208:167–178.

Prager, M. H., J. R. McConaugha, C. M. Jones, and P. J. Geer.
1990. Fecundity of blue crab, *Callinectes sapidus*, in Chesapeake Bay: biological, statistical and management considerations. Bull. Mar. Sci. 46:170–179.

Rabalais, N. N., F. R. Burditt, L. D. Coen, B. E. Cole, C. Eleuterius, K. L. Heck, T. A. McTigue, S. G. Morgan, H. M. Perry, F. M. Truesdale, et al.
1995. Settlement of *Callinectes sapidus* megalopae on artificial collectors in four Gulf of Mexico estuaries. Bull. Mar. Sci. 57:855–876.

Rittschof, D., M. Z. Darnell, K. M. Darnell, M. Goldman, M. B. Ogburn, and R. E. McDowell.
2010. Estimating relative abundance of the female blue crab spawning stock in North Carolina. *In* Biology and management of exploited crab populations under climate change (G. H. Kruse, G. L. Eckert, R. J. Foy, R. N. Lipcius, B. Sainte-Marie, D. L. Stram, and D. Woodby, eds.), p. 91–108. Alaska Sea Grant College Prog. Rep. AK-SG-10-01. Univ. Alaska Fairbanks, Fairbanks, AK.

Secor, D. H.
2015. Migration ecology of marine fishes, 304 p. Johns Hopkins Univ. Press, Baltimore, MD.

Sullivan, T. J., and J. E. Neigel.
2017. Misidentification of megalopae as a potential source of error in studies of population genetics and ecology of the blue crab *Callinectes sapidus*. Mar. Ecol. Prog. Ser. 565:95–111.

Tankersley, R. A., M. G. Wieber, M. A. Sigala, and K. A. Kachurak.
1998. Migratory behavior of ovigerous blue crabs *Callinectes sapidus*: evidence for selective tidal-stream transport. Biol. Bull. 195:168–173.

Turner, H. V., D. L. Wolcott, T. G. Wolcott, and A. H. Hines.
2003. Post-mating behavior, intramolt growth, and onset of migration to Chesapeake Bay spawning grounds by adult female blue crabs, *Callinectes sapidus* Rathbun. J. Exp. Mar. Biol. Ecol. 295:107–130.

Wolcott, D. L., C. W. B. Hopkins, and T. G. Wolcott.
2005. Early events in seminal fluid and sperm storage in the female blue crab *Callinectes sapidus* Rathbun: effects of male mating history, male size, and season. J. Exp. Mar. Biol. Ecol. 319:43–55.

VanderKooy, S (ed.).
2013. GDAR 01 stock assessment report: Gulf of Mexico blue crab, 231 p. Gulf States Mar. Fish. Comm., Ocean Springs, MS. [Available from website.]

National Marine
Fisheries Service
NOAA

Fishery Bulletin
established in 1881

Spencer F. Baird
First U.S. Commissioner
of Fisheries and founder
of *Fishery Bulletin*

Length at maturity of the Pacific angel shark (*Squatina californica*) in the artisanal elasmobranch fishery in the Gulf of California in Mexico

J. Fernando Márquez-Farías

Email address for contact author: fmarquez@uas.edu.mx

Facultad de Ciencias del Mar
Universidad Autónoma de Sinaloa
Paseo Claussen s/n
Col. Los Pinos
82000 Mazatlán, Sinaloa, Mexico

Abstract—Median length at maturity was determined for Pacific angel sharks (*Squatina californica*) captured incidentally in the artisanal elasmobranch fishery in the Gulf of California in Mexico. A total of 306 Pacific angel sharks (192 females and 114 males) were analyzed. The size of the females ranged between 23 and 100 cm total length (TL), whereas males ranged between 25 and 99 cm TL. The maturity stages of both females and males were determined by using the development of internal and external organs. The results of analysis of covariance reveal a significant effect of sex ($P<0.001$) on length at maturity. A binary logistic regression was applied for each sex to estimate the length at which half of the individuals were considered mature (L_{50}). For females, L_{50} was 74.41 cm TL (95% confidence interval [CI]: 72.81–76.00 cm TL), and the steepness coefficient (Φ) was 1.43 (95% CI: 0.84–2.42). For males, L_{50} was 77.82 cm TL (95% CI: 75.66–79.97 cm TL), and the Φ was 3.08 (95% CI: 1.98–4.77). The maturity ogive produced by using a logistic function is suitable to represent the development pattern of this species because it describes maturity as a gradual process.

Manuscript submitted 28 October 2019.
Manuscript accepted 30 October 2020.
Fish. Bull. 118:359–364 (2020).
Online publication date: 11 December 2020.
doi: 10.7755/FB.118.4.5

The views and opinions expressed or implied in this article are those of the author (or authors) and do not necessarily reflect the position of the National Marine Fisheries Service, NOAA.

The Pacific angel shark (*Squatina californica*) belongs to the family Squatinidae and inhabits the eastern Pacific Ocean. Its geographical distribution is discontinuous: from southern Alaska to the Gulf of California (GOC) in Mexico and from Ecuador to Chile (Compagno et al., 2005). This species is a nocturnal opportunistic predator of demersal fish species (Pittenger, 1984; Fouts and Nelson, 1999). In California, this species has been found in shallow waters at depths of 3–46 m, whereas in the GOC it has been observed at a depth of 183 m. This species has been found buried in muddy and sandy bottoms. It also has been observed around rocks and in kelp forests (Compagno, 1984). The demography of the northern population off California has been studied, and the low productivity of this population has been modeled (Cailliet et al., 1992). The low productivity of this species is consistent with the characteristics of elasmobranchs that make them susceptible to overfishing: late maturity, low fecundity, and long life (Walker, 1998).

The capture of Pacific angel sharks is mostly incidental in the artisanal elasmobranch fishery and the finfish trawl fishery both in the GOC and on the Pacific coast of the Baja California Peninsula (BCP) in Mexico. Biological information about the Pacific angel shark in Mexico is fragmented and limited to a few studies on trophic ecology and reproduction (Escobar-Sánchez et al., 2006, 2011; Romero-Caicedo et al., 2016). Using mitochondrial DNA, Ramírez-Amaro et al. (2017) reported genetic differences between specimens from the GOC and Pacific coast of the BCP, validating previous observations of life history differences between specimens from these areas (Villavicencio-Garayzar, 1996). Similarly, Márquez-Farías (2007) found maximum lengths and lengths at maturity for the population of shovelnose guitarfish (*Pseudobatus productus*) in the GOC that are different from those reported for the population along the Pacific coast of the BCP (Villavicencio-Garayzar, 1995).

Because of its historical exploitation rates and vulnerability, the Pacific angel shark is classified as near threatened on the IUCN Red List of Threatened Species (Cailliet et al., 2016). The significant fishing effort in the elasmobranch fishery of the GOC (Bizzarro et al., 2007) makes understanding the life history and population dynamics of this species essential to identification of strategies for its future management.

The objective of this study was to estimate median length at maturity (L_{50}) of the Pacific angel shark in the eastern GOC. Differences in life history characteristics have important management implications if they result in different population responses to fishing pressure.

Materials and methods

The artisanal elasmobranch fisheries of Sonora and Sinaloa, Mexico (Fig. 1), operate open-hulled fiberglass boats that are 5.5–7.6 m long and have outboard motors with 55–115 hp. Pacific angel sharks were collected at fishery landings during 1998–2005 (for details, see Bizzarro et al., 2009). Length, sex, and maturity stage of specimens were recorded. Total length (TL) was measured in centimeters from the tip of the rostrum to the end of the stretched caudal fin. Length-frequency distributions were constructed to examine the structure of the sample. Normality of length distributions was verified by using the Kolmogorov–Smirnov (K–S) test. If normality data were rejected, the nonparametric Mann–Whitney test was used to compare mean lengths of each sex. A chi-square test was used to compare the observed sex ratio of the entire sample and the ratio of maturity stages (immature to mature) against the expected value of 1:1. Reproductive status was assessed through macroscopic examination following Clark and von Schmidt (1965) and Castro (2000). Mature males had hardened claspers that could rotate from the base by directing the claspers anteriorly on the inner side of the shark. The inner clasper length was measured from the point of insertion of the clasper to the clasper tip. The clasper length was plotted against TL to show how the clasper grew as an individual approached maturity. Females were considered mature when they had ripe oocytes (>20 mm in diameter) and a thickened uterus or when they were pregnant. Histograms and box plots of lengths by maturity stage were constructed to identify outliers.

For statistical treatment, the classification of maturity stages used 0 for immature individuals and 1 for mature individuals. Binary logistic regression between TL and maturity data was applied to estimate the regression coefficients a and b. The significance of the difference in maturity stage between sexes was tested with an analysis of covariance by applying a general linear model with a significance level of 0.01. With the coefficients a and b, the proportion of mature sharks by length was determined by using the following logistic function (maturity ogive):

$$Pm_{TL} = \frac{1}{1 + \exp\left[-\frac{TL - L_{50}}{\Phi}\right]},$$

where Pm = the proportion of mature fish given the length (TL);

L_{50} = the median length of the sample when half of the individuals had reached maturity ($L_{50}=a/b$); and

Φ = the steepness of the model ($\Phi=L_{50}/a$).

All the parameters and their 95% confidence intervals (CIs) were estimated with Minitab[1], vers. 19.0 (Minitab, State College, PA).

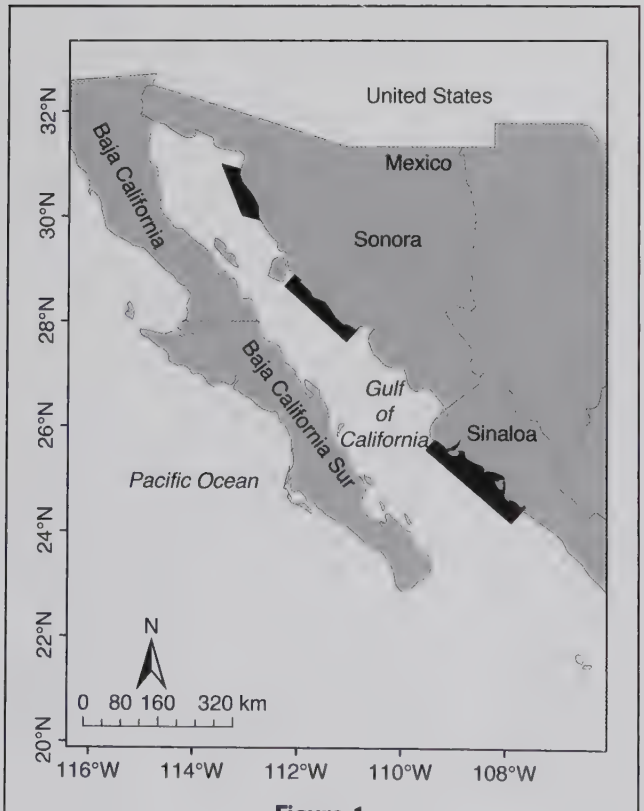

Figure 1

A map of the study area, showing the fishing grounds (black areas) in the Gulf of California off Sonora and Sinaloa, Mexico, where Pacific angel sharks (*Squatina californica*) were captured between 1998 and 2005.

Results

A total of 306 Pacific angel sharks (192 females and 114 males) were measured (χ^2=19.9, P<0.05). The mean length for females was 72.91 cm TL (standard deviation [SD] 16.88) with a range of 23–100 cm TL; the mean length for males was 80.32 cm TL (SD 13.32) with a range of 25–99 cm TL (Fig. 2A). For both sexes, the length distributions had maximum frequencies in the length class of 85–90 cm TL, a class that mostly corresponds with mature individuals (Fig. 2, B and C). Results of analysis of the normality of length distributions with the K–S test indicate non-normal distributions of length for males (K–S test: D=0.209, P<0.01) and females (K–S test: D=0.174, P<0.01). The nonparametric test revealed significant

[1] Mention of trade names or commercial companies is for identification purposes only and does not imply endorsement by the National Marine Fisheries Service, NOAA.

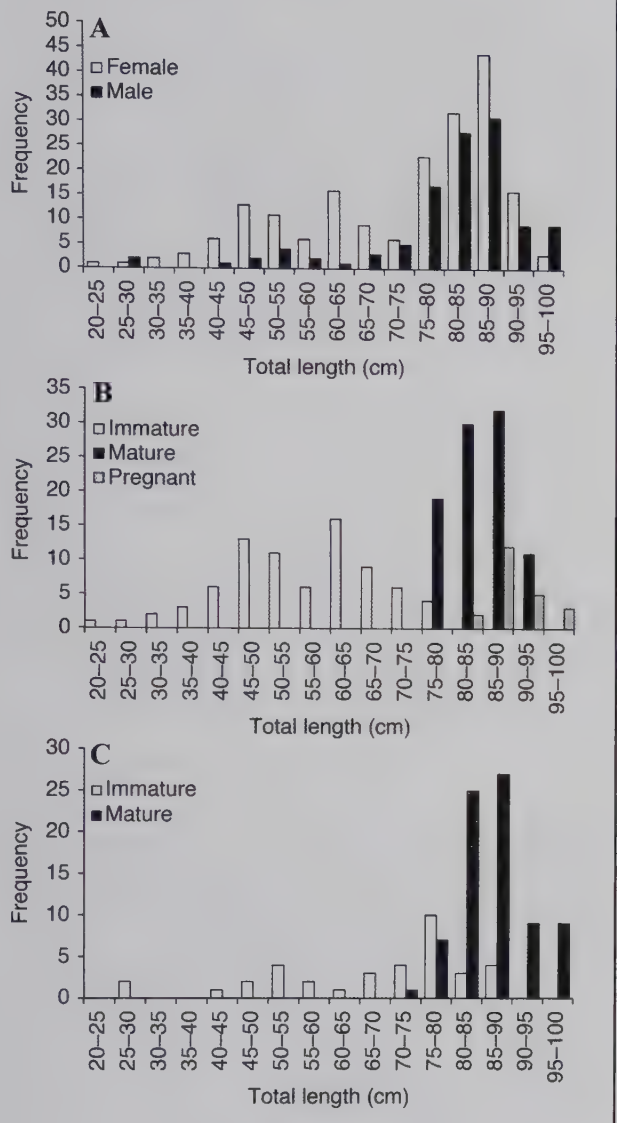

Figure 2

Length-frequency distributions (**A**) by sex and by maturity stage for (**B**) female and (**C**) male Pacific angel sharks (*Squatina californica*) captured from the eastern Gulf of California in Mexico between 1998 and 2005.

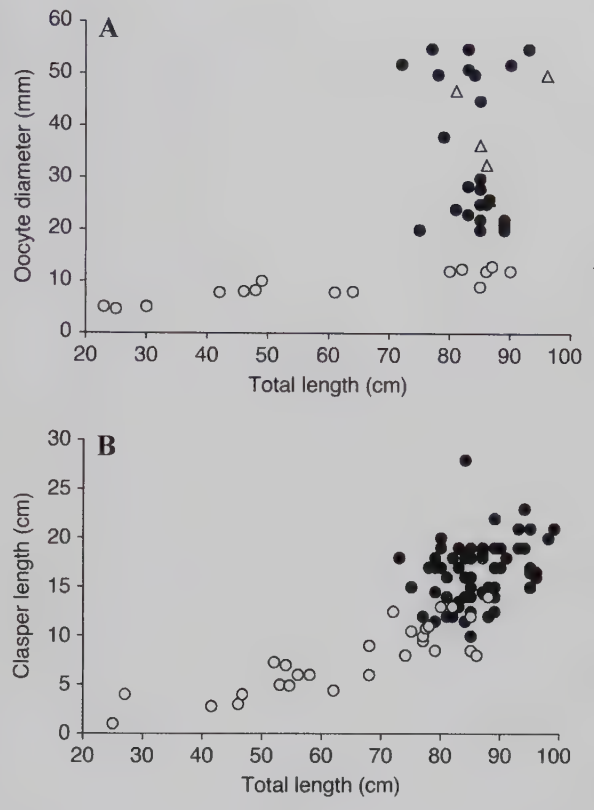

Figure 3

The relationship between total length and (**A**) maximum oocyte diameter and (**B**) clasper length for female and male Pacific angel sharks (*Squatina californica*), respectively, captured from the eastern Gulf of California in Mexico during 1998–2005. Open circles indicate immature individuals, black circles represent mature individuals, and open triangles indicate pregnant females.

differences in mean length by sex for the Pacific angel sharks captured in the GOC (Mann–Whitney test: U=26,818, P=0.001). The mean length for mature females was 84.83 cm TL (SD 4.83) with a range of 75–100 cm TL (number of specimens [n]=114). The diameters of the largest oocytes were 20–60 mm and, in pregnant females, ranged between 26 and 50 mm (Fig. 3A). The mean length of mature males was 86.18 cm TL (SD 5.54) with a range of 73–99 cm TL (n=78); clasper lengths ranged from 10 to 30 mm (Fig. 3B). Length ranges and maturity condition by sex are presented in Table 1 and Figure 4.

The analysis of covariance from the binary logistic regression revealed a significant effect of sex (χ^2=14.9, df=1, P<0.001). The model explained 75.0% of the variance. The contribution of TL to variance was 71.5%, and sex explained 3.7% of the variance. The coefficients of the binary logistic regression for females (a=–51.95, b=0.698) were used in the logistic function to describe the estimated proportion of mature fish by length. For females, the L_{50} was 74.41 cm TL (95% CI: 72.81–76.00 cm TL), and the Φ was 1.43 (95% CI: 0.84–2.42) (Fig. 5A). For males, the regression coefficients (a=–25.27, b=0.3247) yielded a L_{50} of 77.82 cm TL (95% CI: 75.66–79.97 cm TL) and a Φ of 3.08 (95% CI: 1.98–4.77) (Fig. 5B).

Discussion

The results of this study, conducted on the coasts of Sonora and Sinaloa, indicate differences between the lengths of Pacific angel sharks in the GOC and those of individuals along the Pacific coast of the BCP. In general, individuals from the Pacific coast of the BCP grow larger than those

Table 1

Length-frequency distributions, by sex and maturity stage, for Pacific angel sharks (*Squatina californica*) captured in the eastern Gulf of California in Mexico between 1998 and 2005.

Total length (cm)	Female			Male			Both sexes		
	Immature	Mature	Total	Immature	Mature	Total	Immature	Mature	Total
20–25	1	0	1	0	0	0	1	0	1
25–30	1	0	1	2	0	2	3	0	3
30–35	2	0	2	0	0	0	2	0	2
35–40	3	0	3	0	0	0	3	0	3
40–45	6	0	6	1	0	1	7	0	7
45–50	13	0	13	2	0	2	15	0	15
50–55	11	0	11	4	0	4	15	0	15
55–60	6	0	6	2	0	2	8	0	8
60–65	16	0	16	1	0	1	17	0	17
65–70	9	0	9	3	0	3	12	0	12
70–75	6	0	6	4	1	5	10	1	11
75–80	4	19	23	10	7	17	14	26	40
80–85	0	32	32	3	25	28	3	57	60
85–90	0	44	44	4	27	31	4	71	75
90–95	0	16	16	0	9	9	0	25	25
95–100	0	3	3	0	9	9	0	12	12
Total	78	114	192	36	78	114	114	192	306

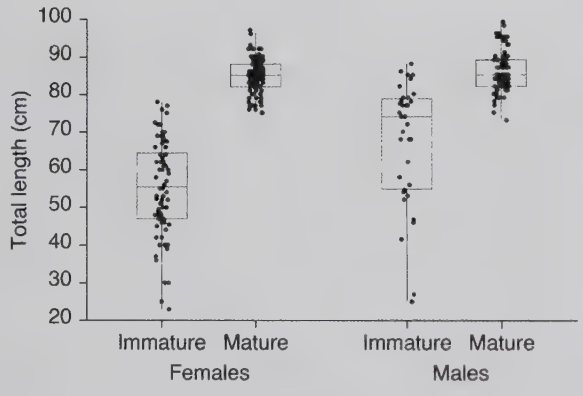

Figure 4

Box plot of the relationship between total length and maturity stage for Pacific angel sharks (*Squatina californica*) captured from the eastern Gulf of California in Mexico during 1998–2005. The black dots indicate observed lengths by sex and maturity stage. The upper and lower parts of each box represent the first and third quartiles (the 25th and 75th percentiles), and the horizontal line is the median. The vertical lines that extend above and below each box indicate minimum and maximum values.

from the GOC. In addition, a latitudinal gradient in the maximum reported sizes of Pacific angel sharks has been observed, with sharks being larger on the coast of California and decreasing in length toward the southern part of the BCP on the Pacific coast. For instance, Miller and Lea (1972) reported a maximum length of 152.4 cm TL for individuals from the coast of California, and Natanson and Cailliet (1986) reported an L_{50} of 107 cm TL for the same area (~70% of the maximum length). For individuals on the northern part of the BCP, Cartamil et al. (2011) reported lengths of 120–130 cm TL; whereas, Villavicencio-Garayzar (1996) reported a maximum length of 117 cm TL for individuals on the southern part of the BCP. Ramírez-Amaro et al. (2017) reported an unusually large size of 180 cm TL for individuals in this same area. For Pacific angel sharks in the Bay of La Paz, part of the GOC, Romero-Caicedo et al. (2016) reported that the largest sizes were 90–100 cm TL and estimated that the L_{50} for males and females was 75.6 and 77.7 cm TL, respectively (~77% of the maximum length). In contrast, in the study described here and conducted in Sonora and Sinaloa, the observed maximum length of Pacific angel sharks was 100 cm TL, and the estimated L_{50} was 74.41 cm TL for females and 77.82 cm TL for males, values that correspond to 74% and 77% of the maximum length, respectively.

The frequency distribution of lengths at a given time can vary because of different factors, including selectivity of fishing gear and the seasonal availability of the species in the area. Differences in the length-frequency distributions of Pacific angel sharks in the GOC have been reported. In this study, a peak of abundance was found for the length class of 85–90 cm TL for both sexes. However, for both sexes, Romero-Caicedo et al. (2016) reported a peak of abundance for individuals that were 60–90 cm TL.

Female sharks often reach larger sizes than males (Castro, 2011), including sharks of the species smoothback angelshark (*S. oculata*) (Capapé et al., 2002), sawback

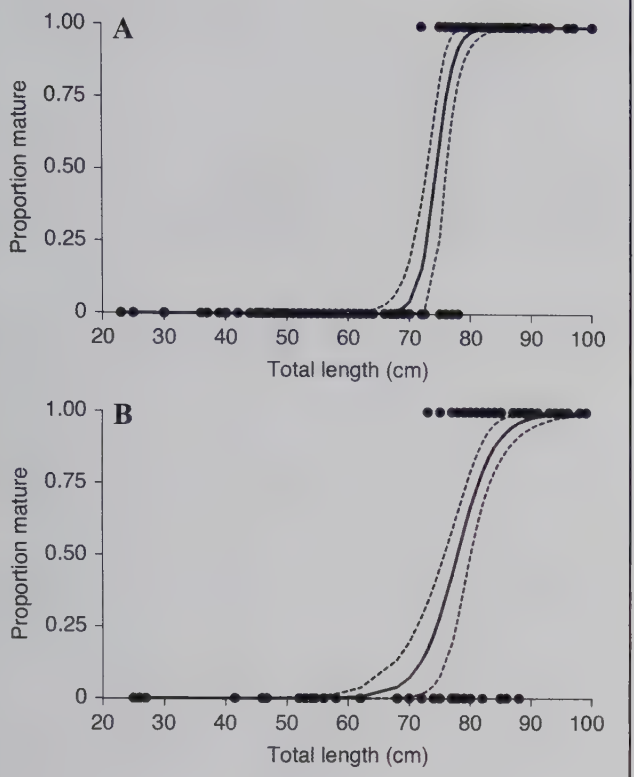

Figure 5

The proportion of (**A**) female and (**B**) male Pacific angel sharks (*Squatina californica*) that were mature, by total length, among those captured from the eastern Gulf of California in Mexico between 1998 and 2005. The dashed lines indicate the 95% confidence intervals of the estimated proportions from the logistic function.

angelshark (*S. aculeata*) (Capapé et al., 2005), and angular angel shark (*S. guggenheim*) (Colonello et al., 2007). However, at some point, the length structure of a stock can be altered by the level of historical exploitation (Stevens et al., 2000). Different factors, such as migration and gear selectivity, can influence the observed lengths in a sample. In particular, the effect of gear selectivity may be significant when interpreting life history characteristics and could distort growth curves and maturity ogives (Walker et al., 1998; Walker, 2005).

The artisanal elasmobranch fishery in the GOC is intense and has been developing for several decades (Bizzarro et al., 2009). It is likely that the maximum sizes between sexes are similar in this study because Pacific angel sharks no longer reach the sizes they had reached before exploitation became extreme. The level of exploitation in the GOC does not allow individuals to reach maximum size and affects the L_{50}.

Walker (2005) suggested that reported differences in length at maturity may also be a result of the criteria adopted to define maturity. In early studies of the biology of sharks, length at first maturity was based mostly on the smallest mature individuals in the sample (Branstetter, 1987). Such an approach fundamentally differs from the way L_{50} is estimated by using a binary logistic regression (Walker, 2005, 2007). Technically, having insufficient data for the lengths of individuals that are in the transition in maturity from immature to mature hampers maximum likelihood estimation and makes estimation of the coefficients and 95% CIs of the logistic function challenging (Christmann and Rousseeuw, 2001). The reproductive strategy of the Pacific angel shark, including vitellogenesis and the gestation period, can be understood only with systematic monitoring over time (Castro, 2009). Such monitoring can be challenging because some shark species are not available in fishing grounds year-round.

The incidental catch of Pacific angel sharks in artisanal and trawl fisheries in the GOC is concerning because of the low resilience of this species to fishing mortality (Cailliet et al., 1992). There are still gaps in our knowledge of the natural history of this species in the GOC; research needs include examination of seasonal migratory patterns and studies of age and growth. The estimate of L_{50} from this study provides an important input to estimation of demographic characteristics. The maturity ogive produced by using a logistic function suitably represents the development pattern of this species because it describes maturity as a gradual process.

Acknowledgments

The Lucile and Packard Foundation and Instituto Nacional de Pesca y Acuacultura partially supported data collection. I thank L. González-Ania for review and advice on the results of the general linear model. I am grateful to C. Lozano-Alberú and M. Weber for their language editing. The comments and suggestions of 2 anonymous reviewers are much appreciated.

Literature cited

Bizzarro, J. J., W. D. Smith, R. E. Hueter, J. Tyminski, J. F. Márquez-Farías, J. L. Castillo-Géniz, G. M. Cailliet, and C. J. Villavicencio-Garayzar.
2007. The status of shark and ray fishery resources in the Gulf of California: applied research to improve management and conservation. Moss Landing Mar. Lab. Tech. Publ. 2009-01, 211 p.

Bizzarro, J. J., W. D. Smith, J. F. Márquez-Farías, J. Tyminski, and R. E. Hueter.
2009. Temporal variation in the artisanal elasmobranch fishery of Sonora, Mexico. Fish. Res. 97:103–117.

Branstetter, S.
1987. Age, growth and reproductive biology of the silky shark, *Carcharhinus falciformis*, and the scalloped hammerhead, *Sphyrna lewini*, from the northwestern Gulf of Mexico. Environ. Biol. Fish. 19:161–173.

Cailliet, G. M., H. F. Mollet, G. G. Pittenger, D. Bedford, and L. J. Natanson.
1992. Growth and demography of the Pacific angel shark (*Squatina californica*), based upon tag returns off California. Mar. Freshw. Res. 43:1313–1330.

Cailliet, G. M., C. L. Chabot, M. C. Nehmens, and A. B. Carlisle.
2016. *Squatina californica*. The IUCN Red List of Threatened Species 2016: e.T39328A80671059. [Available from website.]
Capapé, C., A. A. Seck, A. Gueye-Ndiaye, Y. Diatta, and M. Diop.
2002. Reproductive biology of the smoothback angel shark, *Squatina oculata* (Elasmobranchii: Squatinidae), from the coast of Senegal (eastern tropical Atlantic). J. Mar. Biol. Assoc. U.K. 82:635–640.
Capapé, C., Y. Diatta, A. A. Seck, O. Guélorget, J. Ben Souissi, and J. Zaouali.
2005. Reproduction of the sawback angel shark *Squatina aculeata* (Chondrichthyes: Squatinidae) off Senegal and Tunisia. Cybium 29:147–157.
Cartamil, D., O. Santana-Morales, M. Escobedo-Olvera, D. Kacev, L. Castillo-Geniz, J. B. Graham, and O. Sosa-Nishizaki.
2011. The artisanal elasmobranch fishery of the Pacific coast of Baja California, Mexico. Fish. Res. 108:393–403.
Castro, J. I.
2000. The biology of the nurse shark, *Ginglymostoma cirratum*, off the Florida east coast and the Bahama Islands. Environ. Biol. Fish. 58:1–22.
2009. Observations on the reproductive cycles of some viviparous North American sharks. Aqua 15:205–222.
2011. The sharks of North America, 640 p. Oxford Univ. Press, New York.
Christmann, A., and P. J. Rousseeuw.
2001. Measuring overlap in binary regression. Comput. Stat. Data Anal. 37:65–75.
Clark, E., and K. von Schmidt.
1965. Sharks of the central Gulf coast of Florida. Bull. Mar. Sci. 15:13–83.
Colonello, J. H., L. O. Lucifora, and A. M. Massa.
2007. Reproduction of the angular angel shark (*Squatina guggenheim*): geographic differences, reproductive cycle and sexual dimorphism. ICES J. Mar. Sci. 64:131–140.
Compagno, L. J. V.
1984. FAO species catalogue. Vol. 4. Sharks of the world. An annotated and illustrated catalogue of shark species known to date. Part 1. FAO Fish. Synop. 125, 249 p. FAO, Rome.
2005. Checklist of living chondrichtyes. *In* Reproductive biology and phylogeny of chondrichthyes: sharks, batoids and chimaeras (W. C. Hamlett, ed.), p. 503–548. Science Publishers Inc., Enfield, NH.
Escobar-Sánchez, O., L. A. Abitia-Cárdenas, and F. Galván-Magaña.
2006. Food habits of the Pacific angel shark *Squatina californica* in the southern Gulf of California, Mexico. Cybium 30:91–97.
Escobar-Sánchez, O., F. Galván-Magaña, and L. A. Abitia-Cárdenas.
2011. Trophic level and isotopic composition of $\delta^{13}C$ and $\delta^{15}N$ of Pacific angel shark, *Squatina californica* (Ayres, 1859), in the southern Gulf of California, Mexico. J. Fish. Aquat. Sci. 6:141–150.
Fouts, W. R., and D. R. Nelson.
1999. Prey capture by the Pacific angel shark, *Squatina californica*: visually mediated strikes and ambush-site characteristics. Copeia 1999:304–312.
Márquez-Farías, J. F.
2007. Reproductive biology of shovelnose guitarfish *Rhinobatos productus* from the eastern Gulf of California México. Mar. Biol. 151:1445–1454.
Miller, D. J., and R. N. Lea.
1972. Guide to the coastal marine fishes of California. Calif. Dep. Fish Game, Fish Bull. 157, 235 p.
Natanson, L. J., and G. M. Cailliet.
1986. Reproduction and development of the Pacific angel shark, *Squatina californica*, off Santa Barbara, California. Copeia 1986:987–994.
Pittenger, G. G.
1984. Movements, distributions, feeding, and growth of the Pacific angel shark, *Squatina californica*, at Catalina Island, California. M.S. thesis, 83 p. Calif. State Univ., Long Beach, CA.
Ramírez-Amaro, S., D. Ramírez-Macías, R. Vázquez-Juárez, S. Flores-Ramírez, F. Galván-Magaña, and J. N. Gutiérrez-Rivera.
2017. Population structure of the Pacific angel shark (*Squatina californica*) along the northwestern coast of Mexico based on the mitochondrial DNA control region. Cienc. Mar. 43:69–80.
Romero-Caicedo, A. F., F. Galván-Magaña, A. Hernández-Herrera, and M. Carrera-Fernández.
2016. Reproductive parameters of the Pacific angel shark *Squatina californica* (Selachii: Squatinidae). J. Fish Biol. 88:1430–1440.
Stevens, J. D., R. Bonfil, N. K. Dulvy, and P. A. Walker.
2000. The effects of fishing on sharks, rays, and chimaeras (chondrichthyans), and the implications for marine ecosystems. ICES J. Mar. Sci. 57:476–494.
Villavicencio-Garayzar, C. J.
1995. Distribución temporal y condición reproductiva de las rayas (Pisces: Batoidei), capturadas comercialmente en Bahía Almejas, Baja California Sur, México. Rev. Invest. Cient. Univ. Auton. Baja Calif. Sur (Ser. Cienc. Mar.) 6(1–2):1–12. [In Spanish.]
1996. Aspectos poblacionales del angelito, *Squatina californica*, en Baja California, México. Rev. Invest. Cient. Univ. Auton. Baja Calif. Sur (Ser. Cienc. Mar.) 7(12):15–21. [In Spanish.]
Walker, T. I.
1998. Can shark resources be harvested sustainably? A question revisited with a review of shark fisheries. Mar. Freshw. Res. 49:553–572.
2005. Reproduction in fisheries science. *In* Reproductive biology and phylogeny of chondrichthyes: sharks, rays and chimaeras (W. C. Hamlett, ed.), p. 81–127. Science Publishers Inc., Enfield, NH.
2007. Spatial and temporal variation in the reproductive biology of gummy shark *Mustelus antarcticus* (Chondrichthyes: Triakidae) harvested off southern Australia. Mar. Freshw. Res. 58:67–97.
Walker, T. I., B. L. Taylor, R. J. Hudson, and J. P. Cottier.
1998. The phenomenon of apparent change of growth rate in gummy shark (*Mustelus antarcticus*) harvested off southern Australia. Fish. Res. 39:139–163.

National Marine Fisheries Service
NOAA

Fishery Bulletin
established in 1881

Spencer F. Baird
First U.S. Commissioner
of Fisheries and founder
of *Fishery Bulletin*

Catch rate, length, and sex ratio of Pacific hake (*Merluccius productus*) in the northern Gulf of California

Oscar G. Zamora-García[1]
J. Fernando Márquez-Farías (contact author)[2]
Aristóteles Stavrinaky-Suárez[3]
Carlos Díaz-Avalos[4]
Noemí I. Zamora-García[5]
Raúl E. Lara-Mendoza[6]

Email address for contact author: fmarquez@uas.edu.mx

[1] Posgrado en Ciencias del Mar y Limnología
Universidad Nacional Autónoma de Mexico
Avenida Ciudad Universitaria 3000
04510 Coyoacán, Mexico City, Mexico

[2] Facultad de Ciencias del Mar
Universidad Autónoma de Sinaloa
Paseo Claussen s/n
Colonia Los Pinos
82000 Mazatlán, Sinaloa, Mexico

[3] Environmental Defense Fund de Mexico
Surfrider Way 5701
Goleta, California 93117

[4] Departamento de Probabilidad y Estadística
Instituto de Investigaciones en Matemáticas Aplicadas y en Sistemas
Universidad Nacional Autónoma de Mexico
Circuito Escolar s/n, Ciudad Universitaria
04510 Coyoacán, Mexico City, Mexico

[5] Comisión Nacional de Acuacultura y Pesca
Secretaria de Agricultura y Desarrollo Rural
Avenida Camarón Sábalo 1210
82100 Mazatlán, Sinaloa, Mexico

[6] Dirección General Adjunta de Investigación Pesquera en el Atlántico
Instituto Nacional de Pesca y Acuacultura
Secretaría de Agricultura y Desarrollo Rural,
Avenida Mexico 190
Colonia del Carmen
04100 Coyoacán, Mexico City, Mexico.

Abstract—The fishery for Pacific hake (*Merluccius productus*) was established in the northern Gulf of California (NGC) in Mexico in 2000. To describe relevant features of the fishery and biology of Pacific hake, we analyzed 5 years of data from an on board observers program. Using generalized additive models, we standardized catch per unit of effort (CPUE), mean standard length (SL), and sex ratio. Also, we investigated by year the joint effect of maturity stage and sex on size distribution, biometric relationships, and the effect of maturity stage (juvenile or adult) on sex ratio. For all characteristics, significant interannual variability was observed. An average decrease was observed both in CPUE (52%) and mean SL (7%) during January–March. Adult males were more abundant in catch, with a male-to-female ratio of 1.12:1.00 (P<0.05), and adult females were larger than males (F=807.09, P<0.05). Our results support the previously suggested hypothesis that the NGC is the winter spawning ground for Pacific hake in the region. Further research is needed to determine the status of the stock in the NGC and to outline specific potential management strategies.

Manuscript submitted 31 January 2020.
Manuscript accepted 17 November 2020.
Fish. Bull. 118:365–379 (2020).
Online publication date: 17 December 2020.
doi: 10.7755/FB.118.4.6

The views and opinions expressed or implied in this article are those of the author (or authors) and do not necessarily reflect the position of the National Marine Fisheries Service, NOAA.

The Pacific hake (*Merluccius productus*) is the most productive and economically important fish species on the west coasts of the United States and Canada (Hamel et al., 2015), with landings exceeding 400,000 metric tons (t) in recent years (Grandin et al., 2020). This species is distributed from the Gulf of Alaska to Costa Rica, including the Gulf of California (Lloris et al., 2003). In Mexico, early estimates of biomass of Pacific hake in the northern Gulf of California (NGC) ranged from 30,000 to 65,000 t (Mathews et al., 1974; Padilla-García, 1981), and the maximum sustainable yield was 2288–11,453 t. Despite the known abundance of Pacific hake, trawlers licensed to catch shrimp and finfish species were not interested in commercial use of Pacific hake until the late 1990s (Ramírez-Rodríguez, 2017). Total landings of Pacific hake have ranged from 197 t (in 2000) to a peak of 6628 t (in 2014), with a mean of approximately 2225 t for 2000–2019 in the NGC (Fig. 1).

The Pacific hake, one of the most abundant fish species in the California Current Large Marine Ecosystem, plays a significant ecological role as a link between species of low (euphausiids) and high (sharks and seals) trophic levels (Ressler et al., 2007). Because of the commercial importance of this demersal species, its biological, ecological, migratory, and fishery traits have been widely

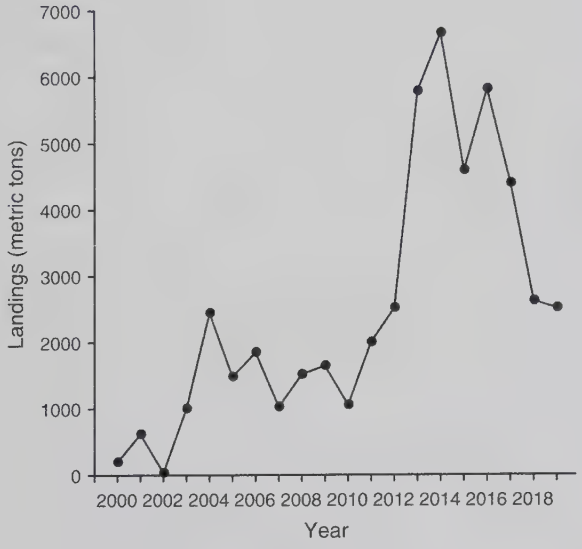

Figure 1

Annual landings of Pacific hake (*Merluccius productus*) from the northern Gulf of California in Mexico during 2000–2019, in metric tons, from the Mexico National Aquaculture and Fishing Commission database of landing notifications. Data for 2019 include landings only up to 4 September.

studied in the United States and Canada (McFarlane and Beamish, 1985; Smith et al., 1992; Saunders and McFarlane, 1997; Benson et al., 2002; King et al., 2012). However, studies of Pacific hake in Mexico are few and scattered.

The government of Mexico began issuing permits for the commercial catch of Pacific hake in 2018 to states around the Gulf of California (Sonora, Baja California, and Sinaloa). Currently, the only rule to control fishing effort is a limit of the number of permits to 80 (DOF, 2018). The fishing season for this species occurs, on average, during winter and spring (January–March) each year, and the largest portion of landings come from Sonora.

Little is known about the biology and population dynamics of Pacific hake in the NGC. It has been hypothesized that this population belongs to a different species, the Cortez hake (*M. hernandezi*) (Mathews, 1985), mainly because of its maximum size of 107 cm total length (TL), much larger than that of the unfished population of what had been considered Panama hake (*M. angustimanus*), a species that was also called the *dwarf hake*, from the southern Gulf of California and Baja California Sur (33.5 cm TL) (Mathews, 1975; Balart-Páez, 2005). Nevertheless, results from molecular and meristic studies indicate the presence of a single species, *M. productus*, in North America with different population units (Silva-Segundo et al., 2011; García-De León et al., 2018).

This study aimed to describe relevant features of the fishery and biology of the Pacific hake caught in the NGC. We report for the first time the variability of catch rates and population structure, by length and sex, of this species in this region, as well as the morphometric relationships (length–weight and length–length). This information can be used as a baseline for future stock assessments and fisheries management.

Materials and methods

Data and sample collection

The fishery was monitored by an on board observer program from 2015 through 2019 during the January–March fishing season with a percentage of coverage of total trips ranging from 5% (in 2016) to 12% (in 2019). The fleet that targeted Pacific hake was based in Puerto Peñasco (76%) and Guaymas (12%), Sonora; Mazatlán, Sinaloa (8%); and San Felipe, Baja California (4%). During 77 trips on board 25 commercial ships, 817 trawl tows were completed.

The fishery used diurnal bottom trawling, and vessels deployed trawl net sets from 0600 to 1800. The width of the net mouth was 30 m on average and opened vertically (to about 4 m) as a result of a floating line in the top rope and a ballast chain in the lower rope of about 450 kg. The mesh size in the codend of nets ranged from 6.35 to 12.70 cm (2.5–5.0 in), and the most common (89%) mesh sizes were 10.16 cm (58%), 7.62 cm (18%), and 8.89 cm (13%). The average speed and duration of trawl tows were 4.37 km/h (standard deviation [SD] 0.55) (2.36 kt [SD 0.30]) and 3.53 h (SD 1.27), respectively. The depth of trawl tows varied, with a range of 111–335 m and a mean of 253.2 m (SD 28.75). Trawl tows followed the slope of the Delfín Basin, always south of the Upper Gulf of California and Colorado River Delta Biosphere Reserve and a refuge for vaquitas (*Phocoena sinus*) in a fishing zone called *the horseshoe* by fishermen because of its shape (Fig. 2).

On board fishing vessels, fishermen head and gut Pacific hake. A total of 2853 Pacific hake were weighed before and after processing. We estimated that an average of 38.74% (SD 7.30) of total weight was lost during processing. Then, to account for the percentage of loss, the processed weight was multiplied by a conversion factor (FAO[1]) of 1.65 (SD 0.19).

After processing, fish are arranged in plastic boxes that weigh ~70 kg, washed with seawater, and stored between ice layers in the cargo hold. During this process, small (<40 cm TL) and damaged Pacific hake are discarded. Nominal catch (NC) of Pacific hake per tow was estimated with the following equation:

$$NC = CF\,(B \times W) + D, \quad (1)$$

where CF = the conversion factor needed to estimate live weight from Pacific hake gutted and headed;
B = the number of boxes stored;
W = the weight of each box (~70 kg); and
D = an observer's estimate of the weight of Pacific hake discarded.

[1] FAO. 2000. Conversion factors: landed weight to live weight. FAO Fish. Circ. 847, 176 p. FAO, Rome. [Available from website.]

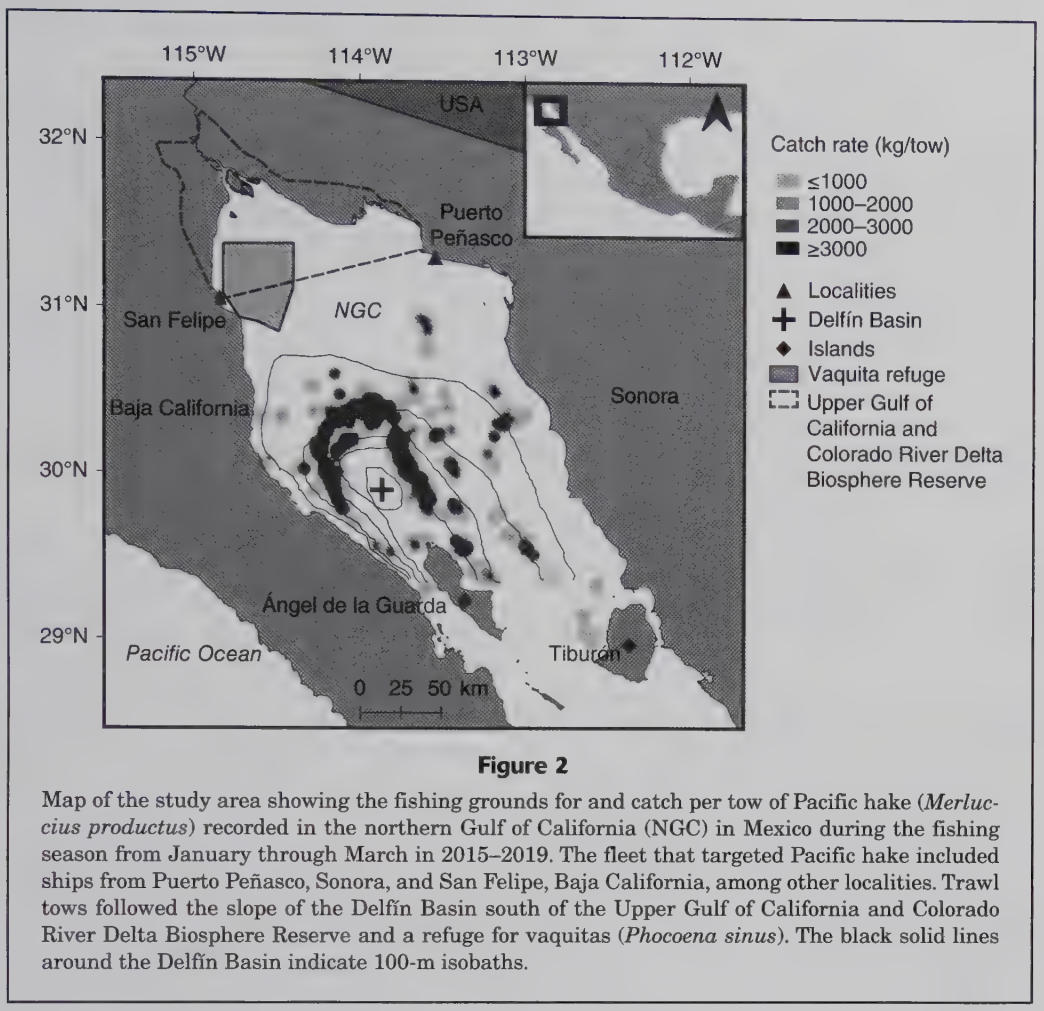

Figure 2

Map of the study area showing the fishing grounds for and catch per tow of Pacific hake (*Merluccius productus*) recorded in the northern Gulf of California (NGC) in Mexico during the fishing season from January through March in 2015–2019. The fleet that targeted Pacific hake included ships from Puerto Peñasco, Sonora, and San Felipe, Baja California, among other localities. Trawl tows followed the slope of the Delfín Basin south of the Upper Gulf of California and Colorado River Delta Biosphere Reserve and a refuge for vaquitas (*Phocoena sinus*). The black solid lines around the Delfín Basin indicate 100-m isobaths.

The NC was divided by the duration of the trawl tow (from the end of net launch until the start of net collection), to obtain the catch rate, or catch per unit of effort (CPUE), in kilograms per hour.

Observers recorded biometrics, including standard length (SL) and total fresh weight, from ~60% of tows per trip: 98 of 131 trips in 2015, 69 of 118 trips in 2016, 93 of 181 trips in 2017, 105 of 170 trips in 2018, and 108 of 217 trips in 2019. They selected random samples of fish (maximum of 100 fish per set) and identified them to species following Lloris et al. (2003). Standard length of fish was measured from the tip of the mouth to the caudal peduncle to the nearest 0.1 cm. Total fresh weight was measured by using a digital balance with an accuracy of 1 g. The specimens were dissected to determine sex and maturity stages. We used a 5-stage morpho-chromatic key to determine the maturity of Pacific hake, according to Holden and Raitt (1975): immature (stage 1), developing (stage 2), mature (stage 3), spawning (stage 4), and postspawning or spent (stage 5). To ease comparisons, we considered fish that had signs of recent, current, or imminent spawning (stages 3–5) to be adults. Fish assigned to stages 1 and 2 were considered juveniles.

Data analysis

Catch rate standardization From all the trawl tows completed (number of tows [*n*]=817), we excluded 3 tows because of gear malfunction, according to Maunder and Punt (2004), and 9 tows completed in April 2019 because of incomparability. A log-transformed index of catch per unit of effort (logCPUE) of the positive values (number of values=805) was used for hypothesis testing because these values followed a log-normal-like frequency distribution. The geometric mean was used as the index for mean CPUE.

First, we developed generalized linear models (GLMs) to test the effect of the selected explanatory variables. However, we found several nonlinear effects, a result that violates the main assumption of GLMs. Then, we used generalized additive models (GAMs), which are semiparametric extensions of GLMs with an additive predictor (Guisan et al., 2002), to identify significant explanatory variables (speed of trawl, mesh size in the codend, depth, and the hour of the day, month, and year) and the nature of the relationships with the logCPUE. We considered a normal probability distribution of

logCPUE and used its canonical link function (*identity*), meaning that a proportional rate of change between the set of explanatory variables and logCPUE was expected, and we evaluated each model's residuals to verify compliance with assumptions. To avoid confounding effects, we tested multicollinearity in explanatory variables through tests of correlation and analysis of variance inflating factors. We used only variables with variance inflating factors <3 (Zuur et al., 2009). Model formulations were tested according to our previous knowledge of the system. Stepwise addition of terms was conducted, and we kept only variables that reduced the Akaike information criterion (AIC) by at least 2 units and that had a significant increase of explained deviance (Marín-Enríquez et al., 2020). Also, variables with effective degrees of freedom greater than 8 were excluded because they are considered highly nonlinear and difficult to interpret (Zuur et al., 2009). The model with the lowest AIC was considered the best (Burnham and Anderson, 2004). Equal fishing power for the entire fleet was assumed.

Variability of length and sex composition The length and sex composition of the catch of Pacific hake were assessed by using a 2-step approach. First, using GAMs, we repeated the analysis previously described to identify significant explanatory variables and the nature of the relationship. For this purpose, we used only tows for which biometrics were recorded (n=469) and estimated the mean SL and sex ratio for each one. An index of the natural logarithms of sex ratios (logSR) and mean SL were used as response variables of the GAMs.

The second step involved a detailed analysis of the distribution of SL in catch related to the factors of sex and maturity stage (juvenile or adult) by using a 2-way analysis of variance with interaction. For significant effects, we included the year factor to evaluate temporal consistency. A Tukey's honestly significant difference test was carried out to identify level-specific differences.

Also, we performed a set of chi-square tests to examine significant departures from the null hypothesis of an equal sex ratio (ratio of the number of males to the number of females: 1:1) according to Zar (1999).

Biometric relationships The length–weight relationship (LWR) was estimated by fitting a power model:

$$TW = a(SL)^b, \tag{2}$$

where TW = the total weight (in grams);
a = the intercept; and
b = the slope (allometric coefficient).

Models were fit hierarchically to each data set for Pacific hake caught in this study, starting with the full data set and continuing with data sets for each sex, maturity stage, and year. Parameter optimization for each model was conducted by minimizing the residual sum of squares (RSS). Statistical differences in the LWR by sex, maturity stage, and year were assessed by a series of "extra sum of squares" tests (Ritz and Streibig, 2008) defined by the following equation:

$$F = \frac{(RSS_0(\beta_0) - RSS_1(\beta_1)) / (df_0 - df_1)}{RSS_1 / df_1}, \tag{3}$$

where F = the Fisher's parameter;
df = the degrees of freedom;
β_0 = the nested model; and
β_1 = subset of each model.

To describe the relationships of TL and fork length (FL) to SL, we used linear regression models:

$$y = a + b(SL), \tag{4}$$

where y = TL or FL.

Pearson's correlation coefficient (r) was used to evaluate the level of association of each pair of variables. The existence of differences between males and females for each relationship was determined by using analysis of covariance.

All data and statistical analyses were carried out by using a significance level of 0.05, Microsoft Excel[2] 2016 (Microsoft Corp., Redmond, WA), and statistical software R, vers. 3.6.1 (R Core Team, 2019).

Results

Catch rate standardization

Year and the interaction of month and year were the most important variables (explained 10.69% of total deviance). Also, nonlinear effects (explained by smoothers) were found between tow speed, mesh size of trawl net, depth of tow, and hour of the day of tow in logCPUE (Table 1). The final model explained 19.9% of the total deviance. Levels of CPUE were higher during tows with speeds of 3.50–4.70 km/h (1.89–2.54 kt) and declined inversely with speed (Fig. 3A). Tows of trawl nets with mesh sizes of 7.62–8.16 cm (3.00–3.25 in) had the highest CPUE values, followed by tows of nets with mesh sizes of 9.80–10.00 cm (Fig. 3B). Values of CPUE remained mostly stable with depth. However, lower CPUE levels were observed for tows at depths >280 m, with a consequent increase in the uncertainty (Fig. 3C). The highest CPUE values were recorded during the morning from 0800 to 1000 with a significant decrease beginning after 1400 (Fig. 3D).

Estimated mean CPUE was the highest in 2015 with 633 kg/h (95% confidence interval [CI]: 484–830 kg/h) and the lowest in 2016 with 199 kg/h (95% CI: 158–250 kg/h), and estimates indicate less variability for 2017 (529 kg/h [95% CI: 368–773 kg/h]), 2018 (379 kg/h [95% CI: 310–464 kg/h]),

[2] Mention of trade names or commercial companies is for identification purposes only and does not imply endorsement by the National Marine Fisheries Service, NOAA.

Table 1

Summary of variables in the generalized additive models used to standardize the natural logarithm of catch per unit of effort (logCPUE), the mean standard length (SL), and the natural logarithm of the sex ratio (logSR) for Pacific hake (*Merluccius productus*) in the northern Gulf of California. The model with the lowest Akaike information criterion (AIC) was considered the best. Also provided are the differences in AIC values between the best model and each of the other models (ΔAICs). The explanatory variables used in the models include tow speed (in kilometers per hour), mesh size in the codend (in centimeters), average depth of trawl tow (in meters), hour of the beginning of the tow (with hours expressed as numerals between 1 and 24), month, year, and the interaction of month and year. Models were fit to data for Pacific hake caught in 2015–2019 during the fishing season from January through March. Asterisks (*) indicate variables that were excluded from the final models because their inclusion did not reduce AIC in at least 2 units along with a significant increase in the explained variance. The variable hour in the model for mean SL was excluded because it had high nonlinearity (effective degrees of freedom=8.59), considered difficult to interpret.

Response variable	Explanatory variable	Explained deviance (%)	Cummulative deviance explained (%)	AIC	ΔAIC
logCPUE	Null	0.00	0.00	2603.70	
	Covariates				
	+s(Speed)	2.43	2.43	2598.48	−5.22
	+s(Mesh)	3.69	6.12	2580.93	−17.55
	+s(Depth)	2.04	8.16	2571.97	−8.96
	+s(Hour)	1.05	9.21	2454.34	−117.63
	Factors				
	+Month	1.09	10.30	2449.98	−4.36
	+Year	2.10	12.40	2439.75	−10.23
	Interactions				
	+Month × Year	7.50	19.90	2380.46	−59.29
Mean SL	Null	0.00	0.00	3505.75	
	Covariates				
	+s(Mesh)*	0.17		3505.59	−0.15
	+s(Hour)*	4.35		3391.07	−114.68
	+s(Speed)	8.68	8.68	3473.78	−32.97
	+s(Depth)*	1.32		3472.30	−1.47
	Factors				
	+Month	4.40	11.70	3460.61	−13.71
	+Year	4.60	15.00	3448.03	−12.53
	Interactions				
	+ Month × year*	1.90		3449.56	+1.41
logSR	Null	0.00	0.00	1042.23	
	Covariates				
	+s(Mesh)*	2.40		1042.15	−0.08
	+s(Depth)	4.90	4.90	1026.90	−15.25
	+s(Speed)*	2.43		1026.00	−0.90
	+s(Hour)*	0.40		985.29	−40.71
	Factors				
	+Month*	−0.29		1030.00	−44.71
	+Year	7.14	7.14	1024.37	−2.53
	Interactions				
	+ Month × year	5.76	12.90	1013.30	11.08

and 2019 (433 kg/h [95% CI: 321–590 kg/h]) (Fig. 4A). In addition, a negative trend in CPUE was observed on a monthly basis (Fig. 4B). On average, January had the highest mean CPUE (719 kg/h [95% CI: 493–1057 kg/h]), followed by significant decreases of 43% and 52% in February (376 kg/h [95% CI: 305–454 kg/h]) and March (312 kg/h [95% CI: 253–385 kg/h]), respectively. However, this pattern was not consistent across years, as indicated by the relevance of the month and year interaction term (Table 1).

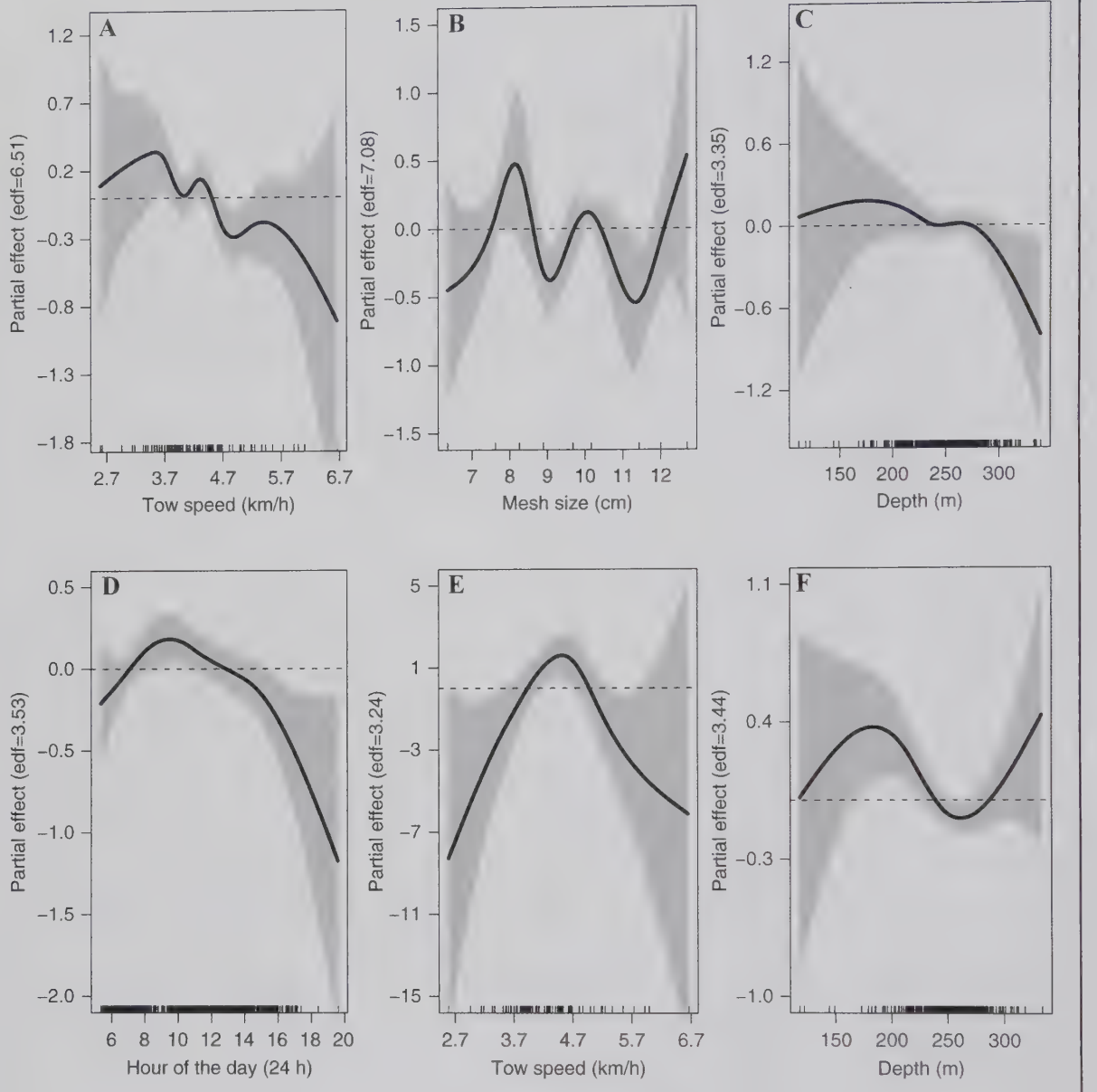

Figure 3

Partial effect plots of generalized additive models fit to the (**A-D**) natural logarithm of catch per unit of effort, (**E**) mean standard length, and (**F**) natural logarithm of sex ratio of Pacific hake (*Merluccius productus*) in the northern Gulf of California in Mexico. Explanatory variables in the models include speed of trawl tow, mesh size of trawl net, depth of trawl tow, and hour of the day of trawl tow (with hours expressed as numerals between 1 and 24). Data used in models are from Pacific hake caught in 2015–2019 during the fishing season from January through March. The gray shaded area in each plot represents the 95% confidence interval, and black lines just above the x-axis represent the density of observations for each covariate. edf=effective degrees of freedom.

Variability of mean length

The final model for mean SL did not include mesh size, the hour of the day, or depth (Table 1). This model explained 15% of deviance and used just a smoother for tow speed as well as the factors of month and year without interaction. The smoother for speed indicates that tows made slower and faster than the interval of 4.00–5.00 km/h (2.16–2.66 kt) caught Pacific hake with sizes under the mean SL of fish caught in this study (Fig. 3E).

The minimum annual mean SL occurred in 2015 (45.7 cm [95% CI: 44.2–47.1 cm]), and the maximum was observed in 2018 (51.8 cm [95% CI: 50.5–53.2 cm]). Although yearly differences in mean SL were significant

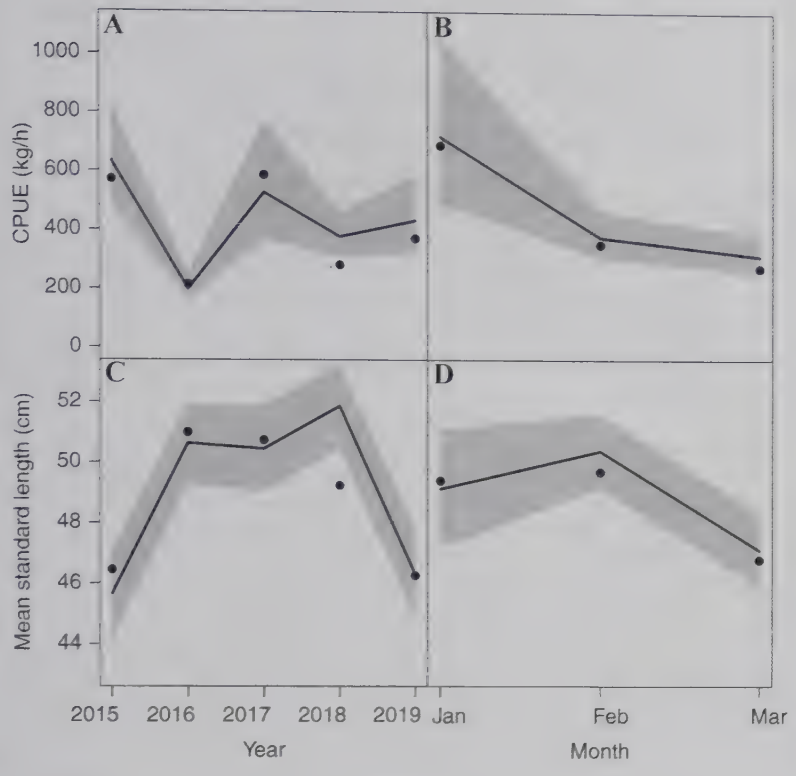

Figure 4

Observed (black dots) and predicted (black lines) geometric means for (**A** and **B**) catch per unit of effort (CPUE) and (**C** and **D**) mean standard length of Pacific hake (*Merluccius productus*) caught in the northern Gulf of California in Mexico during 2015–2019, by year and month. The gray shaded area in each plot represents the 95% confidence interval of the predicted mean from the generalized additive model.

(P<0.05), a specific trend in mean SL was not observed (Fig. 4C). The monthly variability of mean SL indicates that the highest mean SLs occurred during January (49.1 cm [95% CI: 47.2–51.1 cm]) and February (50.3 cm [95% CI: 49.2–51.6 cm]) and that CPUE decreased 7% by March (47.1 cm [95% CI: 45.9–48.3 cm]), as shown in Figure 4D.

Variability of sex ratio

The final model of logSR explained 12.9% of the total deviance. The GAM used only a smoother for depth and the parametric effect of year as well as the interaction of month and year (Table 1). Results from the use of a smoother of depth indicate that tows with male-biased catch were conducted at depths <225 m and >275 m and that, at depths of 225–275 m, logSR tended to be zero (1:1 male-to-female ratio) or below (Fig. 3F).

No difference was found between months in logSR, but a difference was observed between years. However, the relevance of the month and year interaction means that there is no consistent trend of change of logSR during the fishing season.

Size distribution, sex ratio, and maturity

The sizes of Pacific hake sampled ranged from 11.8 to 89.2 cm SL (15.2–108.8 cm TL) with a mean of 47.4 9 cm SL (SD 13.7) (58.2 cm TL [SD 17.6]). During 2015–2017, the length-frequency distribution was bimodal. Pacific hake in the size class of 15–25 cm SL were most common, and fish in the size classes of 30–45 cm SL and 45–65-cm SL were caught in low numbers. In 2018 and 2019, a more normal distribution of SLs was observed with no clear size classes or flattened intervals. The dominant sex of Pacific hake at SLs >70 cm was female, and females had significantly larger sizes (F=807.09, P<0.05) than males (Table 2, Fig. 5). As expected, adults had significantly higher SL than juveniles (F=5174.49, P<0.05), and there was a trend across years (F=135.91, P<0.05).

Adults accounted for 72% of all sampled Pacific hake, 70% of females, and 73% of males. Results of the Tukey's honest significant difference test indicate that all mature females were significantly larger than mature males, and the difference was consistent across years. In 2015 (adjusted P=0.99) and 2019 (adjusted P=0.99), no difference was detected in SL between sexes in juveniles (Fig. 6).

Results from the series of chi-square tests indicate a male-skewed sex ratio for all sampled Pacific hake (male-to-female ratio of 1.12:1.00, P<0.05), but particularly for adult specimens (male-to-female ratio of 1.16:1.00, P<0.05). For juveniles, the sex ratio was 1.00:1.00 (P=0.70). There was no specific annual trend in the sex ratio for juveniles, but for adults, there were significantly more males in 4 out of 5 years. In 2018, we observed a female-biased sex ratio for all sampled Pacific hake (male-to-female ratio of 0.91:1.00). However, data split by maturity stage indicate that the sex ratio of adults favored males (male-to-female ratio of 1.09:1.00) and that females were dominate among juveniles (male-to-female ratio of 0.36:1.00). Although there was no significant bias in the sex ratio in 2019 (P=0.09), males were still more abundant (Table 3).

Biometric relationships

We found differences in the LWR between years (F=216.55, P<0.05). The highest allometric coefficient (b) was estimated for 2015, followed by the lowest estimate for 2016; no differences were observed between 2016 and 2017 (F=1.96, P=0.34). For 2018 and 2019, an increasing tendency was observed, but differences remained present (F=86.81, P<0.05). Differences in the LWR by sex were found in the

Table 2

Standard lengths and total weights of Pacific hake (*Merluccius productus*) caught in the northern Gulf of California during the fishing season from 2015 through 2019, by year and sex. Lengths and weights also are provided for all years and both sexes combined. *n*=number of samples; SD=standard deviation.

			Standard length (cm)		Total weight (g)	
Year	Sex	*n*	Range	Mean (SD)	Range	Mean (SD)
All	All	18,207	11.8–89.2	47.1 (13.7)	22.0–9823.0	1489.9 (1016.2)
2015	All	7255	11.8–89.1	44.8 (14.7)	22.0–9823.0	1347.8 (1021.0)
	All	3322	11.9–89.1	46.7 (16.1)	25.0–9823.0	1558.4 (1228.1)
	M	3933	11.8–79.9	43.2 (13.3)	22.0–7120.0	1169.8 (761.5)
2016	All	2564	13.0–88.0	51.7 (12.3)	26.4–7420.0	1741.8 (892.9)
	F	1097	14.0–88.0	56.4 (11.3)	36.0–7420.0	2148.9 (1003.2)
	M	1467	13.0–79.0	48.3 (11.8)	26.4–4607.0	1442.5 (657.8)
2017	All	3129	14.3–89.2	48.7 (13.6)	49.0–7970.0	1547.4 (919.5)
	F	1503	17.4–89.2	51.0 (14.0)	79.0–7970.0	1742.0 (1036.8)
	M	1626	14.3–74.1	46.6 (12.9)	49.0–4685.4	1366.3 (751.2)
2018	All	3077	18.0–88.5	49.6 (12.0)	47.0–8435.0	1633.2 (1075.7)
	F	1613	18.5–88.5	52.4 (13.0)	57.0–8435.0	1931.1 (1266.4)
	M	1464	18.0–78.1	46.4 (10.0)	47.0–4805.0	1305.7 (679.6)
2019	All	2182	15.5–89.0	45.8 (12.0)	57.2–8678.0	1395.9 (1083.6)
	F	1059	16.6–89.0	48.4 (13.9)	66.0–8678.0	1691.5 (1358.1)
	M	1123	15.5–72.0	43.3 (9.60)	57.2–4288.0	1116.4 (616.9)

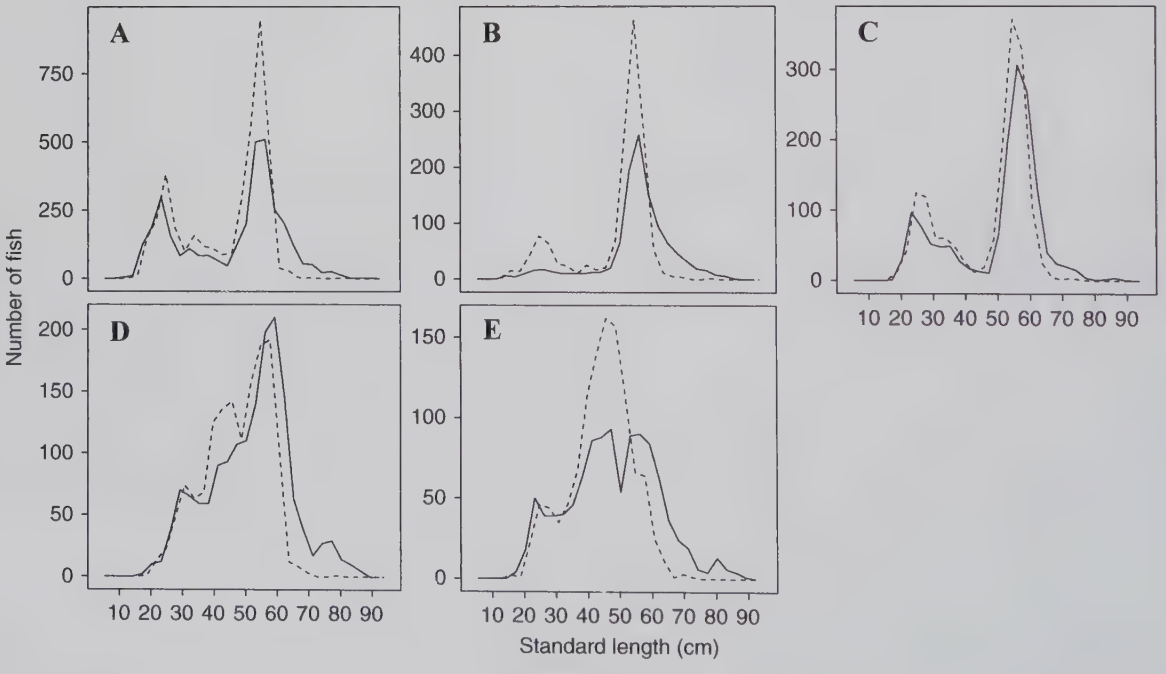

Figure 5

Distribution of standard lengths of Pacific hake (*Merluccius productus*) caught in the northern Gulf of California in Mexico, by sex, during (**A**) 2015, (**B**) 2016, (**C**) 2017, (**D**) 2018, and (**E**) 2019. The solid and dashed lines in each panel represent lengths of females and males, respectively.

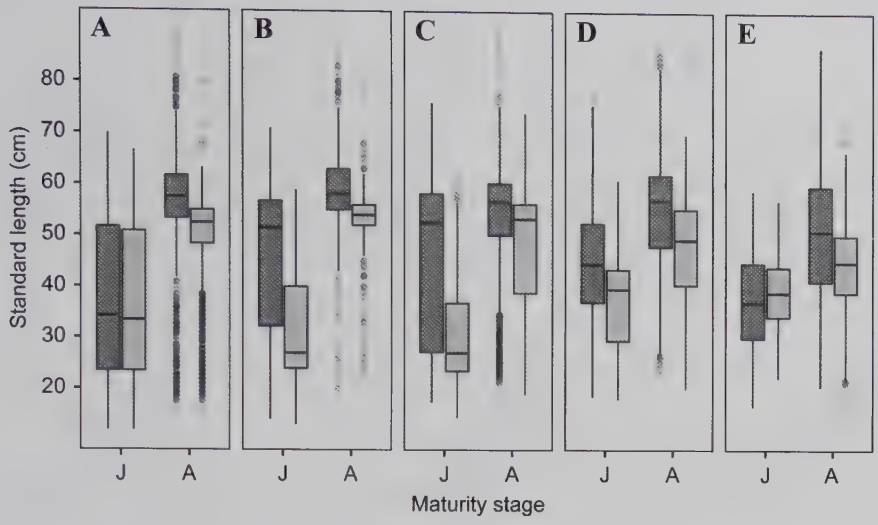

Figure 6

Box plots of standard lengths of Pacific hake (*Merluccius productus*) caught in the northern Gulf of California in Mexico, by sex and maturity stage (juvenile [J] and adult [A]), during (**A**) 2015, (**B**) 2016, (**C**) 2017, (**D**) 2018, and (**E**) 2019. Dark and light gray boxes represent lengths of females and males, respectively. The thick line within each box indicates the median, the upper and lower parts of each box represent the first and third quartiles (the 25th and 75th percentiles), and the whiskers extending above and below each box correspond to 1.5 times the interquartile range. Outliers are presented as gray dots with one-tenth transparency to improve visualization.

Table 3

Ratio of the number of males to the number of females, by maturity stage (juvenile [J] or adult [A]) and by year, for Pacific hake (*Merluccius productus*) caught in the northern Gulf of California in 2015–2019. Sex ratios also are provided for all years and both maturity stages combined. The critical value for each chi-square (χ^2) test was 3.81. Asterisks (*) indicate significant departures from the null hypothesis of an equal sex ratio (a male-to-female ratio of 1.00). M=male; F=female; and N=none.

Year	Maturity stage	Sex ratio	Observed χ^2	P	Sex bias
All	Both	1.12	57.03	<0.05*	M
All	J	1.01	0.15	0.70	N
All	A	1.16	75.09	<0.05*	M
2015	J	1.15	15.66	<0.05*	M
2016	J	1.57	28.64	<0.05*	M
2017	J	0.69	12.63	<0.05*	F
2018	J	0.36	120.37	<0.05*	F
2019	J	0.94	0.23	0.63	N
2015	A	1.22	37.36	<0.05*	M
2016	A	1.28	29.18	<0.05*	M
2017	A	1.15	13.40	<0.05*	M
2018	A	1.09	4.34	<0.05*	M
2019	A	1.08	2.72	0.09	N

general case—with all years pooled—(F=129.16, P<0.05) and consistently in every single year evaluated (Table 4; Fig. 7, A–E). Similarly, the model fits for 2015 and 2018 were close to each other (Fig. 7F); even so, statistical differences were detected (F=80.67, P<0.05). Females always had higher values of b than males. However, no significant differences were found in the LWR between juveniles and adults (F=0.72, P=0.97).

Both analyses of covariance revealed no significant effect of sex in the TL–SL (P=0.22) and FL–SL (P=0.49) relationships and a high level of correlation for both (r>0.99). The resulting estimates of the regression parameters for the TL–SL relationship were 0.89 for a and 1.21 for b, and estimates of the parameters for the FL–SL relationship were 0.51 for a and 1.10 for b.

Discussion

Reports from previous studies have highlighted that the NGC is the winter spawning ground for the Pacific hake because its larvae are dominant in larval fish assemblages (Aceves-Medina et al., 2004; Sánchez-Velasco et al., 2009; Peiro-Alcantar et al., 2013). Also, the high proportion of adults in the catch in this zone (70%) and the sudden increase of catch rates in a relatively limited area found in this study indicate that the fishery for Pacific hake

Table 4

Estimated means of the parameters a (intercept) and b (slope or allometric coefficient) from the regression power model used for analysis of the length–weight relationship of Pacific hake (*Merluccius productus*) caught in the northern Gulf of California during the fishing season in 2015–2019, by year, sex, and maturity stage (juvenile [J] or adult [A]). Estimates also are provided for all years, both sexes, and both maturity stages combined. Degrees of freedom (df), the coefficient of determination (r^2), and the standard error of the mean (SE) are provided for each estimate.

Year	Sex	Maturity stage	df	Regression parameter		
				a (SE)	b (SE)	r^2
All	All	All	18,101	0.02 (0.00)	2.89 (0.01)	0.98
All	F	All	8588	0.02 (0.00)	2.93 (0.01)	0.97
All	M	All	9511	0.05 (0.00)	2.63 (0.01)	0.97
All	All	J	5075	0.02 (0.00)	2.90 (0.01)	0.98
All	All	A	1,2941	0.02 (0.00)	2.82 (0.02)	0.98
2015	F	All	3323	0.01 (0.00)	3.06 (0.01)	0.97
2016	F	All	1100	0.03 (0.00)	2.78 (0.02)	0.98
2017	F	All	1487	0.02 (0.00)	2.86 (0.02)	0.99
2018	F	All	1613	0.02 (0.00)	2.90 (0.02)	0.99
2019	F	All	1057	0.02 (0.00)	2.90 (0.02)	0.99
2015	M	All	3923	0.01 (0.00)	3.02 (0.01)	0.97
2016	M	All	1406	0.03 (0.00)	2.74 (0.02)	0.97
2017	M	All	1595	0.03 (0.00)	2.77 (0.02)	0.98
2018	M	All	1461	0.02 (0.00)	2.87 (0.01)	0.97
2019	M	All	1118	0.02 (0.00)	2.90 (0.01)	0.98

in the NGC occurs during a transient spawning aggregation (Domeier, 2012). Additionally, spawning aggregations of Pacific hake have a male-biased sex ratio, as has been reported for the offshore population of Pacific hake (Saunders and McFarlane, 1997). Several explanations have been proposed for this phenomenon in other hake species, including early arrival and late departure of males to the spawning ground, females spawning in midwater and a consequently higher proportion of males at the bottom, and a biological strategy to ensure fecundation (Botha, 1986; Di Giácomo et al., 1993; Pájaro et al., 2005; Bustos et al., 2007; Korta et al., 2015).

It is essential to note that the sampling period (and the fishing season for Pacific hake) begins once fishermen obtain high catch rates and once Pacific hake reach commercial size (>40 cm SL). The season ends once the catch rate and mean SL diminish to unprofitable levels. Given the low ex-vessel prices of Pacific hake, with an average price of $0.61/kg (in 2019 U.S. dollars) during the study period, the profitability of the fishery for Pacific hake depends on achieving high catch rates with low fishing effort (i.e., few fishing days). In addition, the presence of other aggregated and more highly valued finfish species, such as the Gulf croaker (*Micropogonias megalops*), for which the fishing season occurs during March–August (Ramírez-Rodríguez, 2017; Arzola-Sotelo et al., 2018), could offer a concomitant explanation for the shift in the species targeted by the trawler fleet during the spring.

A pattern of catch rates of Pacific hake decreasing during January–March has been observed in other studies in the Gulf of California (Mathews et al., 1974; Grande-Vidal, 1983; Godínez-Pérez, 2016). The reduction in the catch rates in this study and in these other studies could be related to the end of the spawning aggregation of Pacific hake in the NGC. The progressive absence of large (in length and weight) adults reduces the number of individuals of Pacific hake in the fishing grounds and the mean size of the fish caught.

In the NGC, the high concentrations of larvae of Pacific hake are related to the ephemeral presence of an anticyclonic eddy during winter (Sánchez-Velasco et al., 2009). The presence of this eddy seems to influence the spawning areas of other fish species that inhabit the Gulf of California (Contreras-Catala et al., 2012). Therefore, the spawning areas of Pacific hake could be associated with the winter eddy in this zone. The influence of oceanographic structures on spawning areas has been reported for other hake species (Di Giácomo et al., 1993; Marrari et al., 2019).

Results from previous studies indicate that at depths >100 m, winter temperatures (<18°C) in the NGC remain vertically homogeneous (Lavín and Marinone, 2003). Water temperature homogeneity might partially explain the absence of a clear depth-dependent profile of catch rate or mean SL because the fleet deploys trawl nets at depths >200 m during the daytime, when fish have been

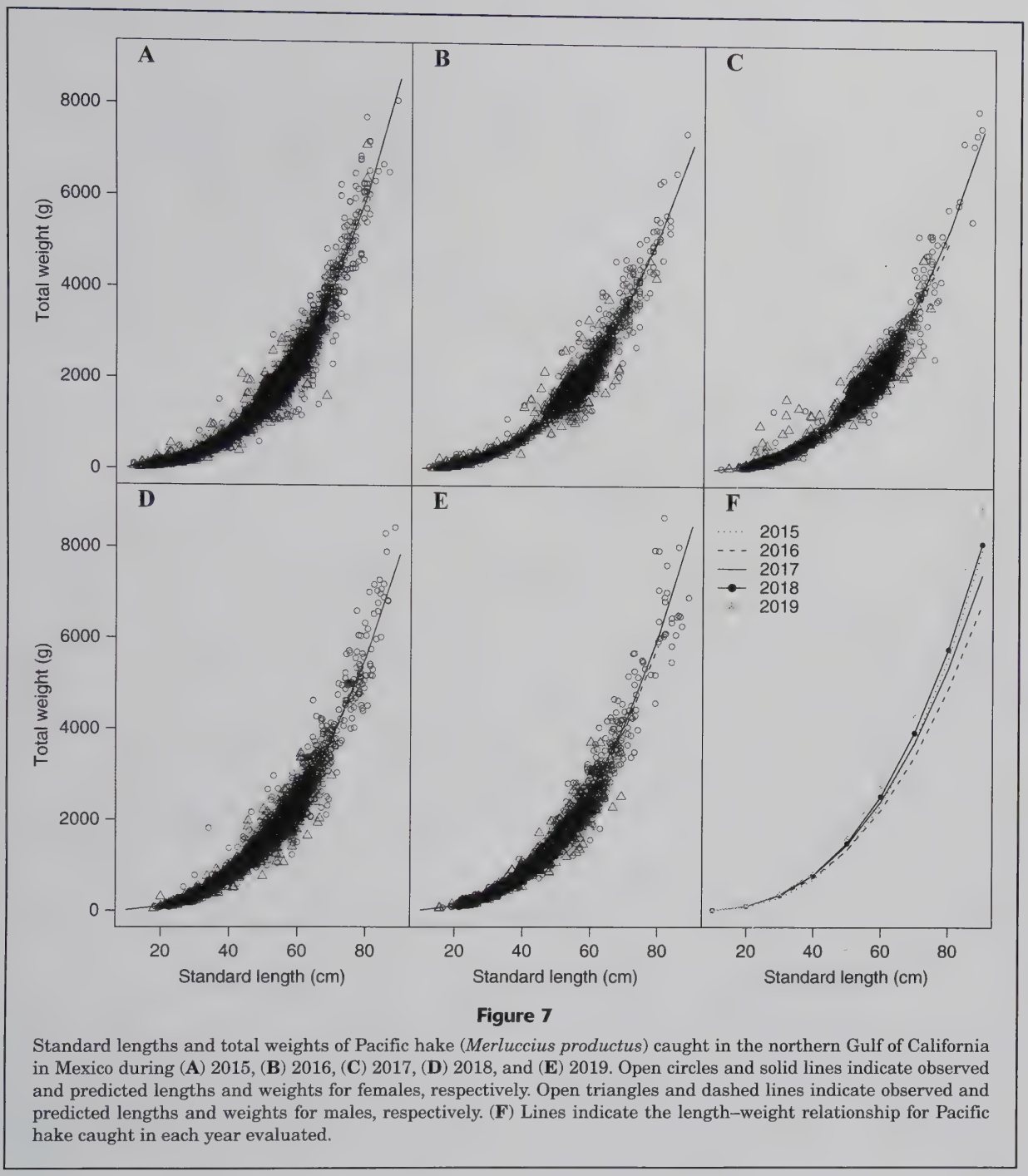

Figure 7

Standard lengths and total weights of Pacific hake (*Merluccius productus*) caught in the northern Gulf of California in Mexico during (**A**) 2015, (**B**) 2016, (**C**) 2017, (**D**) 2018, and (**E**) 2019. Open circles and solid lines indicate observed and predicted lengths and weights for females, respectively. Open triangles and dashed lines indicate observed and predicted lengths and weights for males, respectively. (**F**) Lines indicate the length–weight relationship for Pacific hake caught in each year evaluated.

observed to migrate nearer to the bottom (Godínez-Pérez, 2016). Diel vertical migration has been reported for Pacific hake in other regions (Hamel et al., 2015).

Winter spawning of Pacific hake has been reported for other populations in the eastern Pacific Ocean (Saunders and McFarlane, 1997). However, slight differences exist between the spawning time and sites of Pacific hake from the NGC and those for Pacific hake from the coastal stock and from Baja California Sur. The Pacific hake in the coastal stock spawn during January–March several kilometers offshore (Agostini et al., 2006), and Pacific hake from Baja California Sur spawn during February–May, peaking in May (Balart-Páez, 2005). Pacific hake in NGC spawn only during December–May, peaking in December–February (Denton-Castillo, 2018). The difference in spawning times and sites between these stocks could serve as a gene flow barrier that fosters the genetic isolation indicated by results of other studies (Iwamoto et al., 2015; García-De León et al., 2018).

Table 5

Transformed standard lengths (SLs) reported in the literature for Pacific hake (*Merluccius productus*), by source, sex, season, region, and original type of length measurement (total length [TL], fork length [FL], or SL). Regions used in sources include Canada (CAN), Strait of Georgia (SG), Vancouver Island (VI), Washington (WA), Oregon (OR), California (CA), Baja California Sur (BCS), and the northern, central, and southern Gulf of California (NGC, CGC, and SGC).

SL (cm)					Original length type	Source
Range	Mean	Sex	Season	Region		
≤62.3	48.2	F	All	CA	TL	Best (1963)
≤54.0	44.9	M	All	CAN, WA, OR, CA	TL	Alverson and Larkins (1969)
24.2–65.7	42.3	All				
9.5–61.3	–	All				
9.5–72.2	–	F	Spring–summer	CA, OR, WA	FL	Dark (1975)
9.5–59.5	–	M				
9.2–28.7	16.7	All	Spring	CGC–SGC	TL	Mathews (1975)
15.9–88.1	–	All	All	NGC	TL	Mathews (1985)
9.5–72.2	39.5	All	All	SG	FL	McFarlane and Beamish (1985)
37.7–63.6	42.8	All				
37.7–67.7	46.8	F	All	VI	FL	Beamish and McFarlane (1985)
37.7–59.5	49.0	M				
11.7–53.2	33.6	All	Spring	WA, OR, CA	TL	Stepanenko (1989)
–	41.2	F	Winter	WA, OR, CA	FL	Saunders and McFarlane (1997)
–	40.2	M				
7.5–33.5	17.3	All	All	BCS	SL	Balart-Páez (2005)
32.5–40.7	40.7	All	Spring	NGC	TL	Mazorra-Manzano et al. (2008)
–	34.9	F	Summer			
–	33.0	M				
–	35.0	F	Fall	CAN	FL	King et al. (2012)
–	27.4	M				
–	30.4	F	Winter			
–	25.9	M				
10.4–81.5		All	Winter	NGC	TL	Godínez-Pérez (2016)
11.9–89.2	47.4	All				
11.9–89.2	50.0	F	Winter–spring	NGC	SL	This study
11.9–79.9	45.0	M				

Our results indicate that Pacific hake in the NGC present sex dimorphism because adult females had greater maximum lengths, weights, and allometric coefficients than males. These findings are similar to those of other studies that observed differences in size at age after sexual maturity (Dark, 1975; Mathews, 1975; Francis, 1983; Balart-Páez, 2005; King et al., 2012). Additionally, the maximum size that has been reported for Pacific hake was observed in the NGC in this study (Table 5).

In all years except 2015, the allometric coefficient was lower than 3 but above the threshold of a b value of 2.5 that Pauly (1984) and Froese et al. (2011) considered an indication of negative allometric growth. Furthermore, we did not find differences in the LWR between maturity stages, indicating that length and weight increase proportionally throughout the life of Pacific hake. In this regard, the variability of the allometric coefficient could be interpreted as seasonal growth in weight, as suggested by Bailey et al. (1982). They found that Pacific hake lose 5–10% of total weight during their spawning season (because of inanition) and gain 11–30% during their feeding season. Unfortunately, because all Pacific hake were sampled during winter (spawning season) and no stomachs were collected in our study, it was not possible to provide evidence of seasonal changes in weight.

Our data indicate that there was no effect of mesh size on mean SL. Homogeneity in mean SL can be explained by smaller individuals escaping because of the mesh size of nets and then, once the net becomes clogged with large individuals, selectivity of nets remaining constant. Likewise, the low abundance of fish in the size class of 30–45 cm SL during 2015–2017 might be evidence of a size-dependent migratory pattern, ontogenetic differences in their spatial distribution, or interannual variability of abundance and distribution linked to environmental conditions (Agostini et al., 2008).

Although these results shed light on the basic biology and fishery of the Pacific hake in the NGC, future studies should address management questions to foster sustainable development. Although population characteristics, such as age structure, growth, maturity, and mortality, and fisheries ecology remain poorly understood for this

species in the NGC, data-limited stock assessments could provide temporary reference points for management.

The maximum size of Pacific hake in the NGC (108.8 cm TL) is at least 3-fold of that reported for Pacific hake in the southern Gulf of California and Baja California Sur (33.5 cm TL), and information about that stock is very limited (Mathews, 1975; Balart-Páez, 2005; Salinas-Mayoral, 2018). In the short term, focusing commercial fishing for Pacific hake on the NGC is a potential management strategy.

As a precautionary measure, the specification that only vessels licensed to take Pacific hake can take individuals of this species in the NGC could help to eliminate fishing effort over the currently allowed level that is a result of illegal, or incidental, catch by other ships that fish in the NGC. In future research, particular attention must be set on examining the possible adverse effects of fishing over a reproductive aggregation.

Acknowledgments

The generous collaboration of the fishing companies of the hake fishery made this study possible. We thank the Posgrado en Ciencias del Mar y Limnología and Consejo Nacional de Ciencia y Tecnología for financial support and the Facultad de Ciencias del Mar for logistical support. This study is based on an observer program that is funded by the Environmental Defense Fund, the David and Lucile Packard Foundation, the alliance of the World Wildlife Fund and Carlos Slim Foundation, and the Walton Family Foundation. We are grateful to the observers who worked on board vessels in the fishery for Pacific hake, especially the late E. Estrada Alemán. Comments made by the reviewers are appreciated.

Literature cited

Aceves-Medina, G., S. P. A. Jiménez-Rosenberg, A. Hinojosa-Medina, R. Funes-Rodríguez, R. J. Saldierna-Martínez, and P. E. Smith.
2004. Fish larvae assemblages in the Gulf of California. J. Fish Biol. 65:832–847.

Agostini, V. N., R. C. Francis, A. B. Hollowed, S. D. Pierce, C. Wilson, and A. N. Hendrix.
2006. The relationship between Pacific hake (*Merluccius productus*) distribution and poleward subsurface flow in the California Current System. Can. J. Fish. Aquat. Sci. 63:2648–2659.

Agostini, V. N., A. N. Hendrix, A. B. Hollowed, C. D. Wilson, S. D. Pierce, and R. C. Francis.
2008. Climate–ocean variability and Pacific hake: a geostatistical modeling approach. J. Mar. Syst. 71:237–248.

Alverson, D. L., and H. A. Larkins.
1969. Status of the knowledge of the Pacific hake resource. CalCOFI Rep. 13:24–31.

Arzola-Sotelo, E. A., J. López-Martínez, C. H. Rábago-Quiroz, J. G. Padilla-Serrato, and E. Morales-Bojórquez.
2018. Population dynamics of the bigeye croaker *Micropogonias megalops* in the northern Gulf of California. CalCOFI Rep. 59:86–101.

Bailey, K. M., R. C. Francis, and P. R. Stevens.
1982. The life history and fishery of Pacific whiting, *Merluccius productus*. CalCOFI Rep. 23:81–98.

Balart-Páez, E. F.
2005. Biología y ecología de la merluza bajacaliforniana *Merluccius angustimanus* Garman, 1899, en la costa occidental de Baja California Sur, México. Ph.D. diss., 158 p. Univ. Aut. Nuevo León, Monterrey, Mexico. [In Spanish.]

Beamish, R. J., and G. A. McFarlane.
1985. Pacific whiting, *Merluccius productus*, stocks off the west coast of Vancouver Island, Canada. Mar. Fish. Rev. 47(2):75–81.

Benson, A. J., G. A. McFarlane, S. E. Allen, and J. F. Dower.
2002. Changes in Pacific hake (*Merluccius productus*) migration patterns and juvenile growth related to the 1989 regime shift. Can. J. Fish. Aquat. Sci. 59:1969–1979.

Best, E. A.
1963. Contribution to the biology of the Pacific hake, *Merluccius productus* (Ayres). CalCOFI Rep. 9:51–56.

Botha, L.
1986. Reproduction, sex ratio and rate of natural mortality of Cape hakes *Merluccius capensis* Cast. and *M. paradoxus* Franca in the Cape of Good Hope area. S. Afr. J. Mar. Sci. 4:23–35.

Burnham, K. P., and D. R. Anderson.
2004. Multimodel inference: understanding AIC and BIC in model selection. Sociol. Methods Res. 33:261–304.

Bustos, C. A., F. Balbontín, and M. F. Landaeta.
2007. Spawning of the southern hake *Merluccius australis* (Pisces: Merlucciidae) in Chilean fjords. Fish. Res. 83:23–32.

Contreras-Catala, F., L. Sánchez-Velasco, M. F. Lavín, and V. M. Godínez.
2012. Three-dimensional distribution of larval fish assemblages in an anticyclonic eddy in a semi-enclosed sea (Gulf of California). J. Plankton Res. 34:548–562.

Dark, T. A.
1975. Age and growth of Pacific hake, *Merluccius productus*. Fish. Bull. 73:336–355.

Denton-Castillo, J.
2018. Agregaciones y aspectos reproductivos de la merluza *Merluccius productus* (Ayres, 1855) en el centro y norte del Golfo de California. M.S. thesis, 109 p. Univ. Aut. Sin. Mazatlan, Mexico. [In Spanish.]

Di Giácomo, E. E., J. Calvo, M. R. Perier, and E. Morriconi.
1993. Spawning aggregations of *Merluccius hubbsi*, in Patagonian waters: evidence for a single stock? Fish. Res. 16:9–16.

DOF (Diario Oficial de la Federación).
2018. Acuerdo por el que se da a conocer la actualización de la Carta Nacional Pesquera. Diario Oficial Fed. 777(10):1–112 (Segunda Sección). [In Spanish.] [Available from website.]

Domeier, M. L.
2012. Revisiting spawning aggregations: definitions and challenges. *In* Reef fish spawning aggregations: biology, research and management (Y. S. Mitchenson and P. L. Colin, eds.), p. 1–20. Springer Science and Business Media B. V., Dordrecht, Netherlands.

Francis, R. C.
1983. Population and trophic dynamics of Pacific hake (*Merluccius productus*). Can. J. Fish. Aquat. Sci. 40:1925–1943.

Froese, R., A. C. Tsikliras, and K. I. Stergiou.
2011. Editorial note on weight–length relations of fishes. Acta Ichthyol. Piscat. 41:261–263.

García-De León, F. J., C. Galván-Tirado, L. S. Velasco, C. A. Silva-Segundo, R. Hernández-Guzmán, I. D. L. A. Barriga-Sosa, P. D. Jaimes, M. Canino, and P. Cruz-Hernández.
2018. Role of oceanography in shaping the genetic structure in the North Pacific hake *Merluccius productus*. PLoS ONE 13(3):e0194646.

Grande-Vidal, J. M.
1983. Evaluación biotecnológica de los recursos demersales vulnerables a redes de arrastre de fondo en el golfo de California 1978–1980. Cienc. Pesq. 4:97–125. [In Spanish.]

Grandin, C. J., K. F. Johnson, A. M. Edwards, and A. M. Berger.
2020. Status of the Pacific hake (whiting) stock in U.S. and Canadian waters in 2020, 273 p. Prepared by the Joint Technical Committee of the U.S. and Canada Pacific Hake/Whiting Agreement, National Marine Fisheries Service and Fisheries and Oceans Canada. [Available from website.]

Godínez-Pérez, C. A.
2016. Identificación acústica de la merluza del Pacífico norte *Merluccius productus* en el Golfo de California. M.S. thesis, 132 p. Cent. Interdiscip. Cienc. Mar., Inst. Politéc. Nac., La Paz, Mexico. [In Spanish.]

Guisan, A., T. C. Edwards Jr., and T. Hastie.
2002. Generalized linear and generalized additive models in studies of species distributions: setting the scene. Ecol. Model. 157:89–100.

Hamel, O. S., P. H. Ressler, R. E. Thomas, D. A. Waldeck, A. C. Hicks, J. A. Holmes, and G. W. Fleischer.
2015. Biology, fisheries, assessment and management of Pacific hake (*Merluccius productus*). *In* Hakes: biology and exploitation (H. Arancibia, ed.), p. 234–262. John Wiley and Sons, West Sussex, UK.

Holden, M. J., and D. F. S. Raitt.
1975. Manual of fisheries science. Part 2: methods of resource investigations and their application. FAO Fish. Tech. Paper 115, 214 p. FAO, Rome.

Iwamoto, E. M., A. E. Elz, F. J. García-De León, C. A. Silva-Segundo, M. J. Ford, W. A. Palsson, and R. G. Gustafson.
2015. Microsatellite DNA analysis of Pacific hake *Merluccius productus* population structure in the Salish Sea. ICES J. Mar. Sci. 72:2720–2731.

King, J. R., G. A. McFarlane, S. R. M. Jones, S. R. Gilmore, and C. L. Abbott.
2012. Stock delineation of migratory and resident Pacific hake in Canadian waters. Fish. Res. 114:19–30.

Korta, M., D. García., M. Santurtún, N. Goikoetxea, E. Andonegi, H. Murua, P. Álvarez, S. Cerviño, J. Castro, and A. Murillas.
2015. European hake (*Merluccius merluccius*) in the Northeast Atlantic Ocean. *In* Hakes: biology and exploitation (H. Arancibia, ed.), p. 1–37. John Wiley and Sons, West Sussex, UK.

Lavín, M. F., and S. G. Marinone.
2003. An overview of the physical oceanography of the Gulf of California. *In* Nonlinear processes in geophysical fluid dynamics (O. U. Velasco-Fuentes, J. Sheinbaum, and J. Ochoa, eds.), p. 173–204. Springer, Drordrecht, Netherlands.

Lloris, D., J. Matallanas, and P. Oliver.
2003. Merluzas del mundo (Familia Merlucciidae). Catálogo comentado e ilustrado de las merluzas conocidas. FAO catálogo de especies para los fines de la pesca 2, 57 p. FAO, Rome. [In Spanish.]

Marín-Enríquez, E., X. G. Moreno-Sánchez., F. J. Urcádiz-Cázares., E. Morales-Bojorquez., and J. S. Ramírez-Pérez.
2020. A spatially explicit model for predicting the probability of occurrence of zero-catch quadrants in the tuna purse seine fishery of the Eastern Tropical Pacific Ocean. Cienc. Mar. 46:19–38.

Marrari, M., G. J. Macchi, B. Santos, and E. Leonarduzzi.
2019. Influence of environmental conditions on the reproductive success and recruitment of the Argentine hake *Merluccius hubbsi* (southwestern Atlantic Ocean). Fish. Oceanogr. 28:66–81.

Mathews, C. P.
1975. Some observations on the ecology and the population dynamics of *Merluccius angustimanus* in the south Gulf of California. J. Fish Biol. 7:83–94.
1985. Meristic studies of the Gulf of California species of *Merluccius*, with a description of a new species. J. Nat. Hist. 19:697–718.

Mathews, C. P., J. L. Granados, and J. Arvizu.
1974. Results of the exploratory cruises of the Alejandro de Humboldt in the Gulf of California. CalCOFI Rep. 17:101–111.

Maunder, M. N., and A. E. Punt.
2004. Standardizing catch and effort data: a review of recent approaches. Fish. Res. 70:141–159.

Mazorra-Manzano, M. A., R. Pacheco-Aguilar, J. C. Ramirez-Suarez, and G. García-Sánchez.
2008. Pacific whiting (*Merluccius productus*) underutilization in the Gulf of California: muscle autolytic activity characterization. Food Chem. 107:106–111.

McFarlane, G. A., and R. J. Beamish.
1985. Biology and fishery of Pacific whiting, *Merluccius productus*, in the Strait of Georgia. Mar. Fish. Rev. 47(2):23–34.

Padilla-García, M. A.
1981. Biomasa de sardina (*Sardinops sagax*) y merluza (*Merluccius productus*). Febrero, 1977. Cienc. Pesq. 1:35–43. [In Spanish.]

Pájaro, M., G. J. Macchi, and P. Martos.
2005. Reproductive pattern of the Patagonian stock of Argentine hake (*Merluccius hubbsi*). Fish. Res. 72:97–108.

Pauly, D.
1984. Fish population dynamics in tropical waters: a manual for use with programmable calculators. ICLARM Stud. Rev. 8, 325 p. Int. Cent. Living Aquat. Resour. Manage., Manila, Philippines.

Peiro-Alcantar, M. T., R. Funes-Rodríguez, R. González-Armas, R. Palomares-García, M. O. Nevárez-Martínez, and B. Shirasago-Germán.
2013. Influence of hydrographic conditions on larval fish assemblage structure in the northern Gulf of California. Rev. Biol. Mar. Oceanogr. 48:535–551.

R Core Team.
2019. R: a language and environment for statistical compunting. R Foundation for Statistical Computing, Vienna, Austria. [Available from website, accessed October 2019.]

Ramírez-Rodríguez, M.
2017. A profitability analysis of catch quotas for the Pacific hake fishery in the Gulf of California. North Am. J. Fish. Manage. 37:23–29.

Ressler, P. H., J. A. Holmes, G. W. Fleischer, R. E. Thomas, and K. C. Cooke.
2007. Pacific hake, *Merluccius productus*, autecology: a timely review. Mar. Fish. Rev. 69(1–4):1–24.

Ritz, C., and J. C. Streibig.
2008. Nonlinear regression with R, 144 p. Springer, New York.

Salinas-Mayoral, C. A.
2018. Dinámica poblacional de la merluza del Pacífico *Merluccius productus* (Ayres, 1855), en la costa occidental de BCS,

México. M.S. thesis, 71 p. Cent. Investig. Biol. Noroeste, La Paz, Mexico. [In Spanish.] [Available from website.]

Sánchez-Velasco, L., M. F. Lavín, M. Peguero-Icaza, C. A. León-Chávez, F. Contreras-Catala, S. G. Marinone, I. V. Gutiérrez-Palacios, and V. M. Godínez.
2009. Seasonal changes in larval fish assemblages in a semi-enclosed sea (Gulf of California). Cont. Shelf Res. 29:1697–1710.

Saunders, M. W., and G. A. McFarlane.
1997. Observations on the spawning distribution and biology of offshore Pacific hake (*Merluccius productus*). CalCOFI Rep. 38:147–157.

Silva-Segundo, C. A., M. Brito-Chavarria, E. F. Balart, I. de los A. Barriga-Sosa, R. Rojas-Esquivel, M. I. Roldán, G. Murugan, and F. J. García-De León.
2011. Clarifying the taxonomic status of *Merluccius* spp. in the northeastern Pacific: a combined morphological and molecular approach. Rev. Fish Biol. Fish. 21:259–282.

Smith, B. D., G. A. McFarlane, and M. W. Saunders.
1992. Inferring the summer distribution of migratory Pacific hake (*Merluccius productus*) from latitudinal variation in mean lengths-at-age and length frequency distributions. Can. J. Fish. Aquat. Sci. 49:708–721.

Stepanenko, M. A.
1989. Distribution, size composition, and abundance of the Pacific hake (*Merluccius productus*) along the Pacific coast of North America in 1985. *In* Effects of ocean variability on recruitment and an evaluation of parameters used in stock assessment models (R. J. Beamish and G. A. McFarlane, eds.), p. 81–86. Can. Spec. Publ. Fish. Aquat. Sci. 108. Dep. Fish. Oceans, Ottawa, Canada.

Zar, J. H.
1999. Biostatistical analysis, 4th ed., 663 p. Prentice-Hall, Upper Saddle River, NJ.

Zuur, A., E. N. Ieno., N. Walker., A. A. Saveliev, and G. M. Smith.
2009. Mixed effects models and extensions in ecology with R, 574 p. Springer-Verlag, New York.

National Marine
Fisheries Service
NOAA

Fishery Bulletin
established in 1881

Spencer F. Baird
First U.S. Commissioner
of Fisheries and founder
of *Fishery Bulletin*

Development of harvest control rules for hard-to-age crab stocks: the example of the golden king crab (*Lithodes aequispinus*) in the eastern Aleutian Islands in Alaska

Shareef M. Siddeek (contact author)[1]
Benjamin Daly[2]
André E. Punt[3]
Steve Martell[4]
Jie Zheng[1]
Mark Stichert[2]

Email address for contact author: shareef.siddeek@alaska.gov

[1] Division of Commercial Fisheries
Alaska Department of Fish and Game
P.O. Box 115526
Juneau, Alaska 99811

[2] Division of Commercial Fisheries
Alaska Department of Fish and Game
351 Research Court
Kodiak, Alaska 99615

[3] School of Aquatic and Fishery Sciences
University of Washington
P.O. Box 355020
Seattle, Washington 98105-5020

[4] Sea State Inc.
9401 NE Tidal Court
Bainbridge Island, Washington 98110

Abstract—The golden king crab (*Lithodes aequispinus*) has traditionally been managed in the Aleutian Islands by using a constant catch strategy but interest in abundance-based management has emerged with the recent adoption of a size-based stock assessment model. Management strategy evaluation (MSE) is commonly used to quantify conservation and economic trade-offs of alternative management strategies, but computational constraints can impede the representation of all sources of uncertainty. We conducted a simplified MSE for the golden king crab that focused on what we regarded as the major uncertainties, including initial stock abundance, future recruitment, estimation of mature male biomass and abundance, and catch implementation error, while capturing the existing unique federal and state cooperative management framework for crab stocks in the Bering Sea and Aleutian Islands. The simplified MSE identified recruitment variability as the most important factor in determining overall fishery performance, and conservation and economic metrics highlight benefits of a 15% over a 30% exploitation rate. We feel this simplified approach results in a robust analysis despite the reduced computational demands compared with those of a full MSE. Similar approaches can be used for other stocks, but managers must define management objectives, consider stock dynamics, and identify factors likely to have the greatest effect on expected performance.

Manuscript submitted 15 March 2020.
Manuscript accepted 7 December 2020.
Fish. Bull. 118:380–398 (2020).
Online publication date: 30 December 2020.
doi: 10.7755/FB.118.4.7

The views and opinions expressed or implied in this article are those of the author (or authors) and do not necessarily reflect the position of the National Marine Fisheries Service, NOAA.

Strategies for calculating catch limits have evolved from the use of constant catch, constant exploitation rate, and fixed escapement to a focus on threshold harvest control rules (HCRs). The latter are considered superior because they include limits and targets for sizes of the stock and modify exploitation levels to rebuild stocks to, or sustain them at, healthy levels (Quinn et al., 1990; Zheng et al., 1993; Caddy and Mahon, 1995; Restrepo and Powers, 1999; Punt et al., 2008). However, it is necessary to specify parameter values for HCR formulas (for HCRs, see Figure 1 and Supplementary Figure 1 [online only]) because each set of parameter values will lead to different outcomes. Management strategy evaluation (MSE) is becoming an increasingly common tool for quantification of trade-offs among conservation and economic goals for management strategies (Punt et al., 2016). Management strategy evaluation involves identifying management objectives, identifying the key uncertainties and representing them in a mathematical model of the system (hereafter referred to as the *operating model*), identifying the candidate management strategies (the combination of a method for estimating stock status and an HCR), projecting the population forward in the operating model for each candidate management strategy, and summarizing the results through the use of performance metrics.

Because MSE is computationally intensive, addressing all major uncertainties, including modeling, estimation, observation, process, and implementation, can be impractical. As such, if MSE is to be a practical management tool, it must accurately represent the management framework and narrow sources of uncertainty down to a key subset and represent them in the operating model. Here, we describe how to employ MSE in a simplified form in a unique federal and state cooperative management framework, using the stock of golden king crab (*Lithodes aequispinus*) in the eastern Aleutian Islands as an example. The data-poor nature and complexity of the assessment of this stock necessitated employment of a simplified MSE in which the stock assessment process is simulated stochastically rather than modeled explicitly (for a similar approach, see Punt et al., 2008).

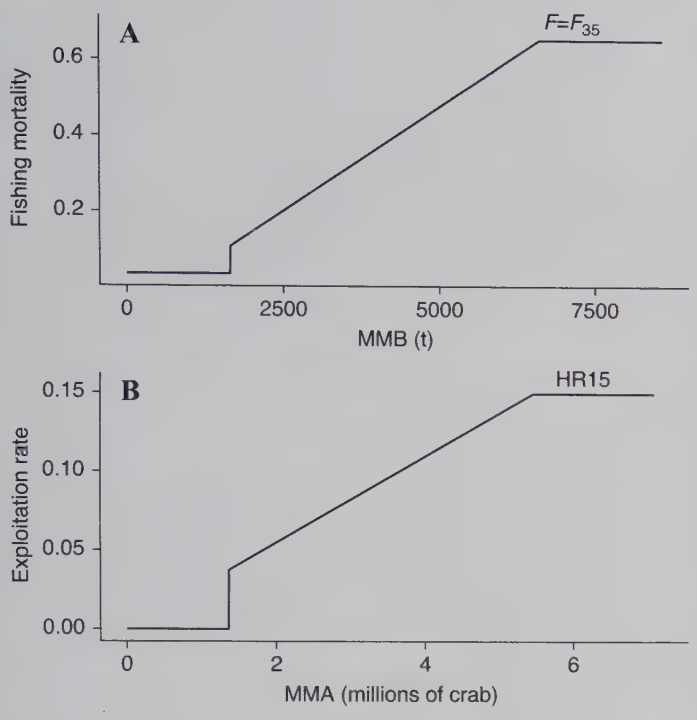

Figure 1

Graphs of the currently implemented (**A**) federal and (**B**) state harvest control rules (HCRs) for golden king crab (*Lithodes aequispinus*) in the eastern Aleutian Islands. The federal stock assessment establishes the overfishing level on the basis of an HCR that is a function of instantaneous fishing mortality (F), shown in decimal form per year, and mature male biomass (MMB), shown in metric tons (t). The state HCR (HR15) determines a discrete exploitation rate, shown in decimal form, as a function of mature male abundance (MMA). The directed pot fishery closes when MMA or MMB reaches a proportion of 0.25 of average MMA or a proportion of 0.25 of MMB_{35}, which is 35% of the unfished level of MMB (i.e., MMB given $F=F_{35}$, which is 35% of the unfished spawning biomass per recruit), indicated by the vertical drops in the lines for the HCRs. The vertical drop in panel A does not reach zero because F attributable to bycatch can still occur in the groundfish fishery when the directed fishery is closed.

The rest of this section provides a background of the stock of golden king crab in the eastern Aleutian Islands and its associated management system, which is used to determine which aspects are included in the operating model. We then outline the candidate management strategies (those currently implemented and alternative choices for HCRs), including some with lower and higher target fishing mortality rates than those previously considered appropriate, and compare them by using conservation and economic performance metrics.

Background and fishery

Golden king crab in the Aleutian Islands inhabit relatively deep water (at depths of 300–1000 m) on structurally complex habitat, such as rock and coral. They are caught by using rectangular crab pots ranging in length from 1.2 to 3.0 m. Because of deep habitats, pots are deployed with longlines, with each string having 30–40 pots, each approximately 200 m apart from the next pot. Golden king crab in the Aleutian Islands compose what is considered one stock but are managed in 2 areas: east and west of the longitude 174°W. The fishery is male-only with a minimum size limit. The fishery has been managed by using a constant catch management strategy since the 1996–1997 fishing season. Rationalization of crab stocks in the Bering Sea and Aleutian Islands in the 2005–2006 fishing season resulted in dramatic changes in fishing practices, including those for golden king crab in the Aleutian Islands: most notably, reduced fleet size and increased average pot soak time (Fina, 2005). Although the directed fishery accounts for most of the total fishery mortality, a small amount of bycatch occurs in other crab fisheries and the groundfish trawl and pot fisheries (<1% of the total number of removed animals; Leon et al., 2017). There was a belief by industry members that the stock could sustain higher levels of fishing intensity because no adverse effects to the population were detected through the use of fishery-dependent data under the constant catch management strategy (Siddeek et al., 2020).

Assessment and management system

A stock assessment provides inputs to HCRs (i.e., annual population abundance estimates and measures of productivity) and evaluates whether overfishing has occurred (i.e., whether total fishing mortality exceeds the corresponding overfishing level [OFL]) or whether the stock is in an overfished state (i.e., whether the stock size is below the minimum stock size threshold [MSST], which can be no lower than one half of the biomass [B] corresponding to maximum sustainable yield [MSY] or $0.5B_{MSY}$). The stock assessment for golden king crab in the Aleutian Islands has been based on a male-only, size-structured population dynamics model, which was adopted for management by the North Pacific Fishery Management Council in 2016. Unlike for other major crab stocks in the Bering Sea and Aleutian Islands, area-swept abundance estimates are not available for this stock because of the lack of a bottom trawl survey (NPFMC, 2018). Consequently, the assessment for the stock in the Aleutian Islands is based on fishery-dependent data (catch per unit of effort [CPUE] and catch size composition) and accounts for changes in fishing behavior due to crab fishery rationalization by fitting the operating model to separate sets of CPUE indices and by estimating fishery selectivity patterns for the pre- and post-rationalization periods (Siddeek et al., 2020).

The North Pacific Fishery Management Council fishery management plan for the king and Tanner crabs in the Bering

Sea and Aleutian Islands established a state and federal cooperative management regime that defers crab management to the state of Alaska with federal oversight (NPFMC[1]). As part of the federal process, status determination criteria, including OFLs and acceptable biological catches (ABCs), are calculated annually for crab stocks on the basis of a 5-tier system that accommodates varying levels of uncertainty, in which stocks with more biological information and greater assessment richness fall into lower tiers (NPFMC[1]). Annual catch levels (i.e., total allowable catches [TACs]) are determined by the state of Alaska according to fishery regulations established by the Alaska Board of Fisheries, but catch levels and management actions need to be consistent with the provisions of the fishery management plan of the North Pacific Fishery Management Council, the national standards of the Magnuson-Stevens Conservation and Management Act, and other applicable federal regulations (NPFMC[1]). As such, it is necessary to consider the federal and state HCRs to adequately represent the management system.

The federal stock assessment establishes the OFL on the basis of an HCR (Fig. 1A) that is a function of instantaneous fishing mortality and mature male biomass (MMB), includes a proxy for F_{MSY} (F_{35}, the fishing mortality rate corresponding to 35% of the unfished spawning biomass per recruit; Clark, 1991, 2002) and a proxy of B_{MSY} (B_{35}, the spawning biomass corresponding to F_{35}). The ABC is then computed as 75% of the OFL. The directed fishery closes when MMB is $<0.25B_{MSY}$.

The state HCR (Fig. 1B, Suppl. Fig. 1B [online only]) determines a (discrete) exploitation rate as a function of mature male abundance (MMA), involves a target level of average MMA (MMA_{ave}), a threshold for opening and closing the directed fishery ($0.25MMA_{ave}$), and a maximum exploitation rate on MMA (Daly et al., 2019). The outcomes from this HCR may be constrained by a maximum number of legal-sized males that are allowed to be removed, or they may be unconstrained.

The final TAC is the minimum of the outcomes of the state HCR (when expressed as a catch) and the ABC. We investigated only options for the state HCR in this study but simulated both federal and state HCRs because, for example, increasing the target exploitation rate in the state HCR may have no effect on stock dynamics if the resulting catch is less than the federal ABC (i.e., is a lower level to prevent catch exceeding OFL). Historically, the outcome of the state HCR has been substantially lower than that of the ABC (Suppl. Fig. 2) (online only).

Materials and methods

The recently developed stock assessment model for golden king crab in the Aleutian Islands provides the input required to support a state HCR that scales the target exploitation rate by using population abundance. However, the shift to abundance-based management needs to be evaluated by using analyses tailored to the management framework for golden king crab in the Aleutian Islands. We evaluated 5 HCRs (Table 1) for the stock of gold king crab in the eastern portion (i.e., east of 174°W) of the Aleutian Islands by projecting the population (in the operating model) forward in time with catches determined by the state HCRs (constrained by the federal ABCs). For the initial year of 2018, stock abundance by size class and operating model parameter values were estimated by using an integrated size-structured assessment model based on data for 1981–2018 (Siddeek et al., 2020; Suppl. Materials [online only]). The 30-year projections were replicated 1000 times. The fishing mortality rate for the groundfish fishery was set to the average during 1999–2018. We chose a 30-year period for the projections because survival for animals in the population in 2018 would be <1% by 30 years, assuming an instantaneous natural mortality rate of 0.21/year. The trajectories of selected performance metrics appear to stabilize within ~20 years (for example, for trends in MMB and MMA, see Figure 2).

Selection of uncertainties

It is computationally impossible to consider all possible sources of uncertainty associated with a stock and fishery. Rather, the sources of uncertainty considered in analyses were selected because they were thought to be those most likely to substantially affect performance of management strategies (following table 3 in Punt et al., 2016):

- Uncertainty in stock productivity and recruitment variability: captured with alternative values for the steepness (h) of the stock–recruitment relationship in the Ricker model (Ricker, 1954) and with the extent of variation and autocorrelation in recruitment in the stock–recruitment relationship;
- Estimation uncertainty: captured with the extent of variation and autocorrelation in estimates of biomass and abundance and with linear and nonlinear relationships between CPUE and stock abundance;
- Initial stock size uncertainty: captured with alternative specifications for initial stock abundance by size class and with the extent of variation and correlations in initial stock abundance among size classes; and
- Implementation uncertainty: accounted for with the extent of variation in realized catch with regard to TAC.

There are many other possible uncertainties that could have been but were not included in the simplified MSE, owing to a lack of evidence for such factors based on historical data and a lack of data with which to parameterize them in the operating model:

- Process error: depensation in the stock–recruitment relationship and occasional catastrophic mortality or recruitment events;

[1] NPFMC (North Pacific Fishery Management Council). 2008. Final environmental assessment for Amendment 24 to the fishery management plan for Bering Sea/Aleutian Islands king and Tanner crabs to revise overfishing definitions, 177 p. [Available from website.]

Table 1

Summary of the 5 harvest control rules (HCRs) of the U.S. government and state of Alaska evaluated for golden king crab (*Lithodes aequispinus*) in the eastern portion of the Aleutian Islands. The management strategy with zero exploitation rate (HR0) is the reference HCR; HR10 has a maximum 10% exploitation rate with a 0.25 catch proportion cap on legal-sized male abundance, HR15 has a maximum 15% exploitation rate with a 0.25 catch proportion cap on legal-sized male abundance, HR15U has a maximum 15% exploitation rate without a cap on the proportion of legal-sized male abundance that can be caught, and HR30 has a maximum 30% exploitation rate with a 0.25 catch proportion cap on legal-sized male abundance. Average mature male abundance (MMA_{ave}) was estimated for the period from the 1985–1986 fishing season through the 2018–2019 fishing season. The HCR currently implemented by the state of Alaska for golden king crab in the eastern portion of the Aleutian Islands is HR15. F=fishing mortality rate; MMB=mature male biomass; OFL=overfishing level; and ABC=allowable biological catch.

Government	Harvest control rule	Maximum F	Minimum MMB for a fishery to take	ABC	Minimum MMA for a fishery to take	Maximum exploitation rate	Catch limit	Catch proportion cap on legal-sized male abundance
Federal		F_{35}	$0.25MMB_{35}$	$0.75OFL$				
State	HR0				$0.25MMA_{ave}$	0.00		0.25
	HR10				$0.25MMA_{ave}$	0.10		0.25
	HR15				$0.25MMA_{ave}$	0.15	≤ABC	0.25
	HR15U				$0.25MMA_{ave}$	0.15	≤ABC	None
	HR30				$0.25MMA_{ave}$	0.30	≤ABC	0.25

- Non-stationarity: changes over time in the form and parameters of the stock–recruitment relationship and time-varying natural mortality, growth, and selectivity; and
- Other factors: spatial and stock structure and time-varying movement.

Key features of the operating model

The basic dynamics are governed by this equation:

$$N_{t+1,j} = \sum_{i=1}^{j}\left[N_{t,i}e^{-M} - (\widehat{C}_{t,i} + \widehat{D}_{t,i} + \widehat{Tr}_{t,i})e^{(y_t-1)M}\right]X_{i,j} + R_{t+1,j} \quad (2018 \le t \le 2047), \quad (1)$$

where $N_{t+1,j}$ = the number of male golden king crab in size class j at the start (1 July, the start of fishing year) of year t+1;

$\widehat{C}_{t,i}$ = the number of individuals retained in catch of the directed pot fishery for size class i during year t;

$\widehat{D}_{t,i}$ = the number of individuals discarded or dead in the pot fishery catch for size class i during year t;

$\widehat{Tr}_{t,i}$ = the number of individuals discarded or dead in the groundfish fishery catch for size class i during year t;

$X_{i,j}$ = the probability of animals in size class i growing into size class j during the year;

y_t = the time from 1 July to the midpoint of the fishery period during year t;

M = the instantaneous rate of natural mortality (assumed to be 0.21/year for all size classes and over time; Siddeek et al., 2020); and

$R_{t+1,j}$ = the recruitment to size class j during year t+1.

The equations used to compute future retained and discarded catches are provided in Equations A1–A4 in Supplementary Materials (online only).

Future recruitment is an essential part of the operating model. However, fitted stock–recruitment models often fail to show the link between spawning individuals and recruits for many species (Subbey et al., 2014), including for most commercially important crab stocks in the Bering Sea and Aleutian Islands. Biomass of mature females is a general choice for an index of egg production for finfish species (e.g., Martell et al., 2008; Punt et al., 2008; Subbey et al., 2014). However, MMB has been adopted as a proxy for reproductive output for stocks of golden king crab in the Aleutian Islands, largely as a result of uncertainties related to identifying the component of the mature population that participates in mating and to defining optimal sex ratios and because fisheries have a male-only retention requirement (NPFMC[1]). The MMB is computed by using this equation:

$$MMB_t = \sum_{j=m}^{n}\left\{N_{t,j}e^{-y'M} - (\widehat{C}_{t,j} + \widehat{D}_{t,j} + \widehat{Tr}_{t,j})e^{(y_t-y')M}\right\}w_j, \quad (2)$$

where y' = the time from 1 July to 15 February in the following year (NPFMC[1]);

w_j = the weight for size class j (Siddeek et al., 2020);

m = the lowest size class with mature animals (i.e., maturity is assumed to be a knife-edged function of size at the carapace length [CL] of 111 mm; Daly et al., 2019); and

n = number of size classes.

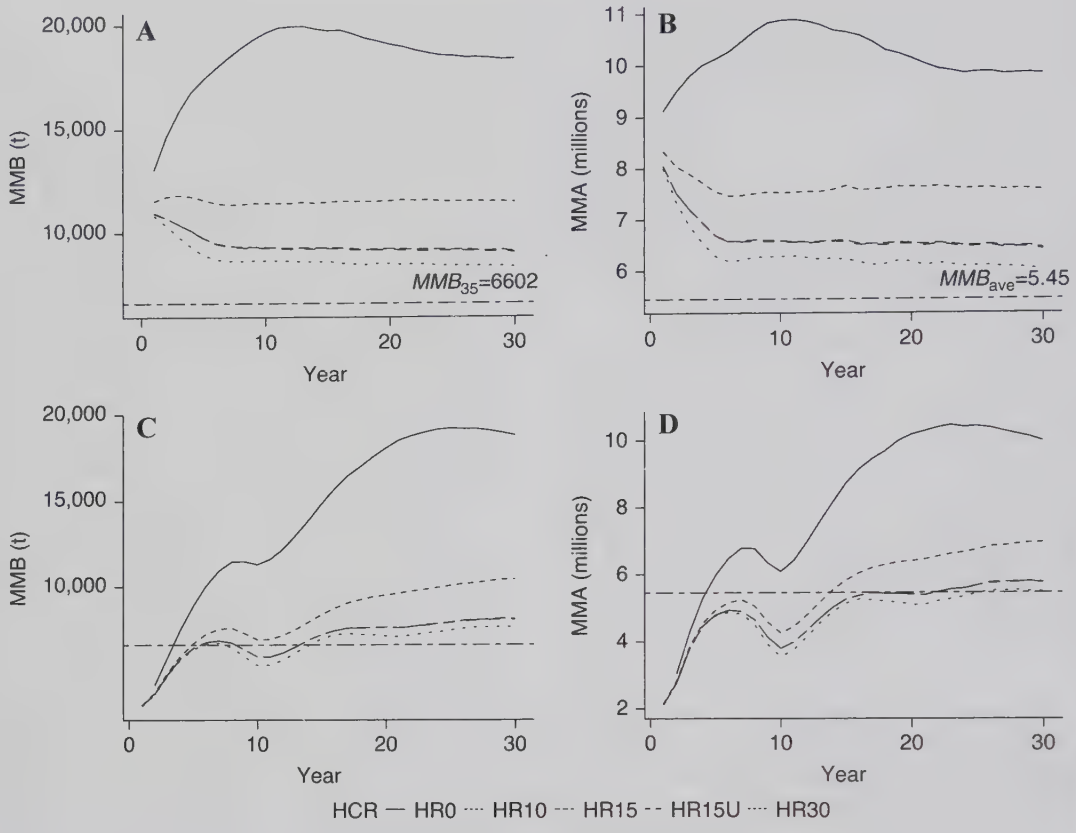

Figure 2

Median mature male biomass (MMB) and median mature male abundance (MMA) of golden king crab (*Lithodes aequispinus*) in the Aleutian Islands under 5 harvest control rules (HCRs), with the initial state of the stock set at (**A** and **B**) healthy or (**C** and **D**) overfished, for scenario 1 of the operating model in which a linear relationship between catch per unit of effort and selected abundance is assumed. Metric tons (t) is the unit for MMB, and number of crab is the unit for MMA. Values are based on a 30-year projection period that begins with 2018. The stock is projected from 2 initial levels of abundance: a healthy state (i.e., MMB_{2018}/MMB_{35}=1.55, where MMB_{2018} is MMB in 2018 and MMB_{35} is 35% of the unfished level of MMB) and an overfished state (i.e., MMB_{2018}/MMB_{35}=0.50). Horizontal dashed lines indicate the MMB_{35} and average MMA (MMA_{ave}) thresholds. The HCRs include HR0, the reference HCR with a zero exploitation rate; HR10, with a maximum 10% exploitation rate and a 0.25 catch proportion cap on legal-sized male abundance; HR15, with a maximum 15% exploitation rate and a 0.25 catch proportion cap on legal-sized male abundance; HR15U, with a maximum 15% exploitation rate and no cap on the proportion of legal-sized male abundance that can be caught; and HR30, with a maximum 30% exploitation rate and a 0.25 catch proportion cap on legal-sized male abundance. Data used in the model are for golden king crab in 1981–2018.

Mature male abundance is determined from Equation 2 without w_j.

Parameterization of the operating model

The population dynamics model has seventeen 5-mm size classes over the size range of 101–185 mm CL. The last size class (181–185 mm CL) is a plus group that includes all golden king crab larger than 185 mm CL. The values for the parameters of the model were estimated on the basis of fitting the model to available data (Siddeek et al., 2020; for some of the estimated parameters, see Supplementary Figure 3 [online only]). Although Bayesian or Monte Carlo methods could have been used to estimate distributions for the parameters of the operating model, these methods were not pursued because they were found to be computationally infeasible. The parameters of the operating model differed depending on whether CPUE was assumed to be proportional to selected abundance or the square root of selected abundance because the operating model was fitted to the available monitoring data for golden king crab in the Aleutian Islands (for the results for linear relationship [hereafter referred to as the *linear choice*], see Tables 2 and 3 and Supplementary Tables 1 and 2 [online only]; for the results for the nonlinear relationship [hereafter referred to as the *nonlinear choice*], see Supplementary Tables 3–6 [online only]). Tables and figures for the linear choice are provided (selected tables and figures for the nonlinear choice are given in Supplementary Materials [online only]).

The value of h was determined through the use of a 2-step procedure. The first step was to calculate F_{35} by using an analysis of spawning biomass per recruit (for a plot of spawning potential ratio [SPR] versus fishing mortality [F], where the SPR for a given level of fishing mortality is the ratio of the spawning biomass per recruit at that level of fishing mortality to the spawning biomass per recruit in an unfished state, see Supplementary Figure 4A [online only]). The value of F is related to the total fishing mortality for the directed pot fishery when computing SPR, with fishing mortality attributable to bycatch in the groundfish fishery set to the estimated average during 1999–2018 (although this source of mortality is negligible). The second step was to calculate MMB for various h values by projecting the population model forward deterministically given $F=F_{35}$ and to find h such that $MMB=0.35\times MMB_0$ (where MMB_0 is the virgin mature male biomass; Suppl. Fig. 4B [online only]).

The selected value of h ensures that fishing at F_{35} produces MMB_{35}, which is equivalent to $0.35\times MMB_0$ (a proxy for B_{MSY}), and a proxy MSY (see Supplementary Figure 5 [online only]). Figure 3 shows the fitted (deterministic) Ricker stock–recruitment relationship when h was set by using this procedure (h=0.729, R_0=2.528 million crab, MMB_0=18,862 metric tons) along with the MMB_{t-8} (MMB estimated 8 years prior to year t) and recruit (R_t) pairs of data points from the stock assessment model. Figure 4 depicts the estimated number of recruits from the model, along with a 95% confidence interval, indicating that uncertainty in these estimates increased over time.

Table 2

The factors considered during the evaluation of the performance of harvest control rules for golden king crab (*Lithodes aequispinus*) in the eastern portion of the Aleutian Islands. The 3 values are lower limits; the model estimates for 2018, indicated with asterisks (*); and upper limits considered in the evaluation of the performance of harvest control rules. The values are based on the operating model in which a linear relationship between catch per unit of effort and selected abundance is assumed. Data used in the model are for golden king crab in 1981–2018. MMB=mature male biomass; MMA=mature male abundance.

Factors	Values
Steepness (h)	0.600, 0.729*, 1.200
Recruitment variation (σ_R)	0.100, 0.274*, 0.800
Autocorrelation in recruitment (ρ_R)	0.000, 0.455*, 0.900
Extent of annual catch implementation error (σ_C)	0.000, 0.039*, 0.100
Extent of MMB estimation error (σ_B)	0.000, 0.214*, 0.300
Autocorrelation in MMB estimation error (ρ_B)	0.000, 0.700, 0.900
Extent of MMA estimation error (σ_N)	0.000, 0.216*, 0.300
Autocorrelation in MMA estimation error (ρ_N)	0.000, 0.700, 0.900

Harvest control rules

Federal harvest control rule The federal HCR is based on MMB and is needed to determine the OFL and the ABC for each year of the projection period. The OFL fishing mortality (F_{OFL}) is determined by using this equation (NPFMC[1]):

$$F_{OFL,t}=\begin{cases} F_{35} & \text{if } MMB_t>MMB_{35}, \\ F_{35}\left(\dfrac{\frac{MMB_t}{MMB_{35}}-\alpha}{1-\alpha}\right) & \text{if } 0.25MMB_{35}<MMB_t\ll MMB_{35}, \text{ and} \\ 0 & \text{if } MMB_t\ll 0.25MMB_{35}, \end{cases} \quad (3)$$

where α = 0.1 (a preset value).

The OFL of total catch is calculated by applying $F_{OFL,t}$ to male stock abundance through the use of Equations A1–A3 in Supplementary Materials (online only) and by summing

Table 3

The reference points used in the evaluation of candidate harvest control rules for golden king crab (*Lithodes aequispinus*) from the eastern portion of the Aleutian Islands: a proxy for biomass corresponding to maximum sustainable yield (35% of the unfished level of mature male biomass [MMB_{35}]), the fishing mortality rate corresponding to 35% of the unfished spawning biomass per recruit (F_{35}), mean catch, average mature male abundance (MMA_{ave}), and mean catch per unit of effort (CPUE). The estimates are based on the operating model in which a linear relationship between CPUE and selected abundance is assumed. Data used in the model are for golden king crab in 1981–2018.

Reference point	Estimate	Basis of estimation
MMB_{35}	6601.61 t	Assessment model
F_{35}	0.656/year	Assessment model
Mean catch	1492.82 t	Period from the 2005–2006 fishing season through the 2018–2019 fishing season (post-rationalization period)
MMA_{ave}	5.45 million crab	Period from the 1985–1986 fishing season through the 2018–2019 fishing season (estimation period)
Mean CPUE	31.70 crab/pot lift	Period from the 2005–2006 fishing season through the 2018–2019 fishing season (post-rationalization period)

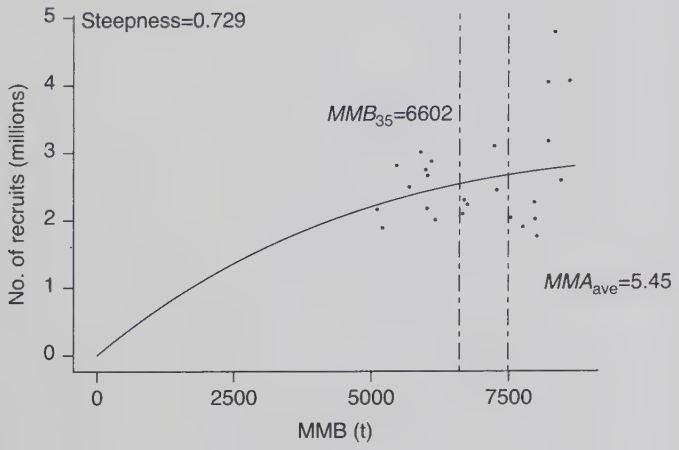

Figure 3

The stock–recruitment relationship from the Ricker model fitted to the stock and recruitment data for golden king crab (*Lithodes aequispinus*) in the eastern Aleutian Islands during 1981–2018. The vertical dashed lines indicate the respective reference points: 35% of the unfished level of mature male biomass (MMB_{35}), which is a proxy for biomass corresponding to maximum sustainable yield, and average mature male abundance (MMA_{ave}). The steepness value is the estimate for 2018. In the operating model used in this analysis, catch per unit of effort is assumed to be proportional to selected abundance. t=metric tons.

over the predicted catches in weight by source of mortality, in other words, by using this equation:

$$OFL_t = \sum_{j=1}^{n}\left(\widehat{C'}_{t,j}w_j + \widehat{D'}_{t,j}w_j + \widehat{Tr'}_{t,j}w_j\right), \quad (4)$$

where the prime symbols indicate that the catch and bycatch are calculated by using $F=F_{OFL,t}$. The ABC (which applies to all sources of fishery-related mortality) is calculated (NPFMC, 2018) with this equation:

$$ABC_t = 0.75 \times OFL_t. \quad (5)$$

State harvest control rule options We compared 5 candidate state HCRs, with the aim to maintain consistency with state of Alaska commercial fishery regulations, the Alaska Board of Fisheries policy on king and Tanner crab resource management (ABF[2]), the North Pacific Fishery Management Council fishery management plan (NPFMC[1]), and National Standards 1 and 2 of the Magnuson-Stevens Fishery Conservation and Management Act (NPFMC[1]). The candidate HCRs were informed by catch policies for other stocks of king crab species in the Bering Sea and Aleutian Islands, historical exploitation rate estimates for the fishery for golden king crab in the Aleutian Islands, and stakeholder input.

[2] ABF (Alaska Board of Fisheries). 1990. Policy on king and Tanner crab resource management. Policy no. 90-04-FB. [Available from website.]

The currently adopted state HCR is HR15, with a maximum exploitation rate of 15% and a 0.25 catch proportion cap on abundance (number) of legal-sized males. An alternative HCR is HR10, with a maximum exploitation rate of 10% and a 0.25 catch proportion cap on legal-sized male abundance; HR15U is an alternative HCR with a maximum exploitation rate of 15% without any cap on the proportion of legal-sized male abundance that can be caught, HR30 is an alternative HCR with a maximum exploitation rate of 30% and a 0.25 catch proportion cap on legal-sized male abundance, and HR0 is a reference HCR with no directed fishery (i.e., zero exploitation rate) (Table 1, Fig. 1, Suppl. Fig. 1 [online only]). The state HCR is based on MMA and computes the catch proportion for year t, HR_t, as follows:

$$HR_t = \begin{cases} x & \text{if } MMA_t > MMA_{ave}, \\ x\left(\dfrac{MMA_t}{MMA_{ave}}\right) & \text{if } 0.25MMA_{ave} < MMA_t \ll MMA_{ave}, \text{ and} \\ 0 & \text{if } MMA_t \ll 0.25MMA_{ave}, \end{cases} \quad (6)$$

where x = the maximum exploitation rate; and MMA_{ave} = the average MMA during 1985–2018.

The exploitation rate from Equation 6 is converted into an instantaneous fishing mortality rate (F_t in year t) by solving this equation:

$$HR_t = \frac{F_t \times S^T}{Z_t}\left(1.0 - e^{-Z_t}\right), \quad (7)$$

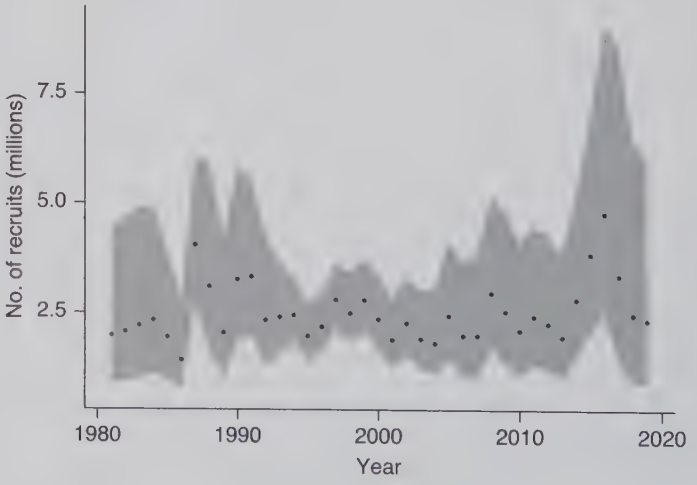

Figure 4

The number of recruits of golden king crab (*Lithodes aequispinus*) in the eastern Aleutian Islands for 1981–2019 estimated with the stock assessment model. The gray shaded area indicates the 95% confidence interval. In the operating model used in this analysis, catch per unit of effort is assumed to be proportional to selected abundance.

where S^T = the total selectivity (a curve for selection of all susceptible sizes of retained and discarded crab to pot gear, fixed at the assessment model estimates); and

Z^T = the instantaneous total mortality during year t (including components for the directed pot fishery and bycatch in the groundfish fishery).

A cap on the proportion of legal-sized male abundance that can be caught is included in the state HCRs for several Alaska crab stocks, such as the stock of red king crab (*Paralithodes camtschaticus*) in Bristol Bay (Zheng et al., 1995). The HR_t may therefore be further modified for conservation purposes by constraining the predicted catch (in numbers) by the directed pot fishery to not exceed 25% of the legal-sized male abundance (crab size ≥136 mm CL; Siddeek et al., 2020), in other words,

$$\sum_{j=L}^{n} \widehat{C}_{t,j} \le 0.25 \sum_{j=L}^{n} N_{t,j},$$

where L = the legal minimum size of golden king crab in the Aleutian Islands.

The predicted catch (in weight) by the directed pot fishery cannot exceed the retained component of the ABC (currently adopted precautionary state management policy is to avoid exceeding the federal fishery management limit, the OFL), in other words,

$$\sum_{j=1}^{n} \widehat{C}_{t,j} w_j \le 0.75 \times \sum_{j=1}^{n} \widehat{C'}_{t,j} w_j.$$

Representing uncertainties

Uncertainty about future recruitment Many types of stock–recruitment relationships can be fitted to the results from an assessment, but the Ricker model (Ricker, 1954) was chosen for this study given its previous use for king crab species (*Lithodidae* spp.) (e.g., Zheng et al., 1995; Bechtol and Kruse, 2009). Future recruitment is generated with variation and temporal autocorrelation, with this equation:

$$R_{t+1,j} = R_0 \frac{MMB_{t-k}}{MMB_0} e^{-1.25\ln(5h)\left[\frac{MMB_{t-k}}{MMB_0}-1\right]} e^{\varepsilon_t - \frac{\sigma_R^2}{2}} \Omega_j, \quad (8)$$

$$\varepsilon_t = \rho_R \varepsilon_{t-1} + \sqrt{1-\rho_R^2}\, e_t, \text{ and}$$

$$e_t \sim N\left(0, \sigma_R^2\right),$$

where R_0 = the number of recruits at unfished equilibrium;

MMB_{t-k} = the MMB (in metric tons) in year $t-k$ given a k-year lag between spawning and recruits entering the model (k=8; Daly et al., 2019);

MMB_0 = the unfished MMB;

h = the steepness parameter;

ρ_R = the extent of autocorrelation in the recruitment deviations;

σ_R = the standard deviation of recruitment; and

Ω_j = a normalized gamma function that determines the distribution of recruits to each size class:

$$\Omega_j = \frac{\int_{l_j-2.5}^{l_j+2.5} gamma(x|\alpha_r, \beta_r)dx}{\sum_{j=1}^{n}\int_{l_j-2.5}^{l_j+2.5} gamma(x|\alpha_r, \beta_r)dx} \text{ and} \quad (9)$$

$$gamma\left(x|\alpha_r, \beta_r\right) = \frac{x^{\alpha_r - 1} e^{\frac{x}{\beta_r}}}{\beta_r^{\alpha_r}\Gamma_{(\alpha_r)}},$$

where α_r = a parameter of the gamma distribution;

β_r = a parameter of the gamma distribution;

l_j = the midpoint of size class j; and

n = the number of recruiting size classes, fixed to 5.

Uncertainty about the state of the stock in 2018 For simplicity, most parameter values were fixed at their best estimates. However, uncertainty was introduced to the size composition for the first projection year (2018), according to the following equation:

$$N_{2018,j} = \widehat{N}_{2018,j} e^{\vartheta_{i,j} - \frac{\sigma_{2018,j}^2}{2}}, \quad (10)$$

$$\vartheta_{i,j} \sim MN\left(\underline{0}, V\right),$$

where $\widehat{N}_{2018,j}$ = the estimate of the number of males in size class j at the start of 2018;

$\sigma_{2018,j}$ = the standard error of the logarithm of the estimate of $\widehat{N}_{2018,j}$; and

V = the variance–covariance matrix for the numbers by size class at the start of 2018.

Estimates of $\widehat{N}_{2018,j}$ and V were obtained from the assessment model. Stock status in each projection was determined by using the best estimates from the assessment model rather than by sampling parameter vectors from a posterior or a bootstrap distribution, as would commonly be done in a full MSE.

Uncertainty when applying the federal and state harvest control rules Uncertainty in the estimates of MMB and MMA are accounted for by replacing MMB and MMA in Equations 3 and 6 as follows:

$$MMB_t^{estimated} = MMB_t e^{\delta_t - \frac{\sigma_B^2}{2}}, \quad (11)$$

$$\delta_t = \rho_B \delta_{t-1} + \sqrt{1-\rho_B^2}\,\varphi_t, \text{ and}$$

$$\varphi_t \sim N\left(0, \sigma_B^2\right); \text{ and}$$

$$MMA_t^{estimated} = MMA_t e^{\omega_t - \frac{\sigma_N^2}{2}}, \quad (12)$$

$$\omega_t = \rho_N \omega_{t-1} + \sqrt{1-\rho_N^2}\,\varnothing_t, \text{ and}$$

$$\varnothing_t \sim N\left(0, \sigma_N^2\right),$$

where $MMB_t^{estimated}$ = the estimate of MMB for year t;

$MMA_t^{estimated}$ = the estimate of MMA for year t;
MMB_t and MMA_t = the true MMB and MMA during year t in the operating model;
ρ_B and ρ_N = the extents of autocorrelation in stock status estimation error; and
σ_B and σ_N = the extents of estimation error.

The values for σ_B and σ_N are set to the standard deviations of the logarithms of the estimates of MMB and MMA for 2018 rather than those of MMB/MMB_{35} and MMA/MMA_{ave} because the estimates of average MMB and MMA are precise. The autocorrelation in estimation error cannot be obtained from the assessment model; therefore, a range of plausible values are considered in the analyses.

Implementation error

The fishery does not catch the TAC exactly; therefore, implementation error is introduced as follows:

$$C_{t,j}^{actual} = \hat{C}_{t,j} + \tau_{t,j} \text{ and} \quad (13)$$

$$\tau_{t,j} \sim N\left(0, \sigma_{C,t,j}^2\right),$$

where $C_{t,j}^{actual}$ = the true catch for animals in size class j during year t;
$\hat{C}_{t,j}$ = the expected catch of animals in size class j during year t based on the simulated fishing mortality from the HCR; and
$\sigma_{C,t,j}$ = the standard deviation of the differences between TACs and actual catches for size class j based on the standard deviation of the differences between the TAC and total landed catches, σ_C, in other words,

$$\sigma_{C,t,j} = \frac{\sigma_{Cj}}{\sum_{j=1}^{n} \hat{C}_{t,j}}, \quad (14)$$

where $\sum_{j=1}^{n} \hat{C}_{t,j}$ = the sum of the expected retained catches of all size classes during year t.

Simulation design

The design of the simplified MSE involved combining levels for each of the uncertainties. In total, 53 scenarios based on the selected uncertainties were considered for each relationship between CPUE and selected abundance (Table 2; Suppl. Tables 1–5 [online only]).

Scenario 1 was based on the best estimates of the parameters, and the specifications of this scenario are indicated by asterisks in Table 2 and Supplementary Table 5 (online only). Scenario 1 was also based on the middle level of autocorrelation in error when MMB and MMA were estimated (for the full list of scenarios and specifications, see Supplementary Tables 1 and 2 [linear choice] [online only] and Supplementary Tables 3 and 4 [nonlinear choice] [online only]). Scenarios 2–17 involved changing the value of one of the parameters of scenario 1, and scenarios 18–53 changed the value of more than one parameter. The scenarios did not explore all possible combinations of parameters owing to computational and presentational limitations.

Two options (applied separately for each of the linear and nonlinear choices) were considered for the size structure at the start of the projection period (1 July 2018): 1) estimate in the assessment model (i.e., MMB/MMB_{35}=1.55; Siddeek et al., 2020) and 2) the MSST ($0.5MMB_{35}$). The second option was implemented by increasing the fishing mortality rate on the size structure for 2018 such that MMB approached $0.5MMB_{35}$. Performances of candidate HCRs were evaluated by projecting the stock from the initial abundance levels from these 2 options, in other words, a healthy state ($MMB>MMB_{35}$) and an overfished state ($MMB=0.5MMB_{35}$).

Performance metrics

We considered conservation and economic criteria when evaluating the candidate HCRs. The conservation criteria were 1) the probability (across simulations and the entire 30-year period) of the stock being below MSST (i.e., a threshold for being overfished), 2) the probability of total catch being greater than OFL (i.e., a threshold for overfishing occurring), 3) the probability of total catch being greater than ABC, and 4) the probability that MMB is less than MMB_{35}. The economic criteria were 1) the probability of fishery closure, 2) the average annual catch (across simulations) for the directed fishery, 3) the annual variability of catch in the directed fishery, 4) the probability of retained catch being less than mean retained catch during 2005–2018 (post-rationalization period), 5) the average CPUE, 6) the probability of CPUE being less than mean CPUE for the period 2005–2018, 7) fishing effort (number of pot lifts, as approximated by using $Catch/[CPUE \times 0.00195]$, where mean crab weight is assumed to be 0.00195 metric tons on the basis of unpublished data [Ben[3]] on the retained catch in 2018), and 8) the probability of MMA being less than MMA_{ave} (an average value for the period 1985–2018), an indication of whether the exploitation rate for a given management strategy reaches the maximum allowable exploitation rate in expectation. The reference points for comparison with simulation results are listed in Table 3 (linear choice) and Supplementary Table 6 (nonlinear choice) (online only).

In addition, the time series of MMB, MMA, catch, effort, and catch variation were summarized as follows:

- Time trends in median (over simulations) MMB, MMA, catch, and effort over the projection period;
- Rebuilding time from the overfished level ($0.5MMB_{35}$) to MMB_{35} and the rebuilding time from the corresponding MMA to MMA_{ave}; and
- Median (over simulations) annual catch variability (AAR) computed with this equation:

$$AAR = \frac{\sum_t |C_t - C_{t-1}|}{\sum_t C_t}. \quad (15)$$

[3] Ben, D. 2018. Unpubl. data. Div. Commer. Fish., Alaska Dep. Fish Game, 351 Research Ct., Kodiak, AK 99615.

The 5 HCRs were ranked within each conservation and economic performance criteria leading to a risk matrix that involved grouping these performance metrics into 3 categories: conservation, catch, and catch stability. Overall ranks within each category were based on average ranks across all criteria.

Results

Performance of harvest control rules (scenario 1)

The time trajectories of MMB and MMA for scenario 1 (i.e., the best estimates of the parameters when CPUE was assumed to be linearly proportional to selected abundance; Suppl. Table 1 [online only]) stabilized toward the end of the 30-year projection period in median terms for the 5 HCRs. As expected, HR10, HR15, HR15U, and HR30 led to much lower MMB and MMA than HR0. The alternative policy of HR30 resulted in slightly lower MMB (Fig. 2, A and C) and MMA (Fig. 2, B and D) than HR10, HR15, and HR15U, with the latter 2 HCRs having very similar trajectories of MMB and MMA. The MMB and MMA trajectories remained above MMB_{35} and MMA_{ave}, respectively, throughout the projection period when the simulation started above MMB_{35} and reached the respective reference points toward the end of the projection period when the simulation started in an overfished state (Fig. 2). The estimates of MMB and MMA are qualitatively similar, a result that was expected given MMB is MMA multiplied by average weight, which did not change much over time. The results are similar for scenario 1 when CPUE was assumed to be proportional to the square root of abundance (Suppl. Tables 7–9) (online only).

Catch and effort stabilized (in median terms) toward the end of the 30-year projection period for HR10, HR15, HR15U, and HR30. However, the time trajectories of catch and effort differed depending on the initial state. The median catch declined over time when MMB_{2018} was greater than MMB_{35} (Fig. 5A) but increased over time for when MMB_{2018} was equal to $0.5MMB_{35}$ (Fig. 5C). Effort was almost constant over the projection period when

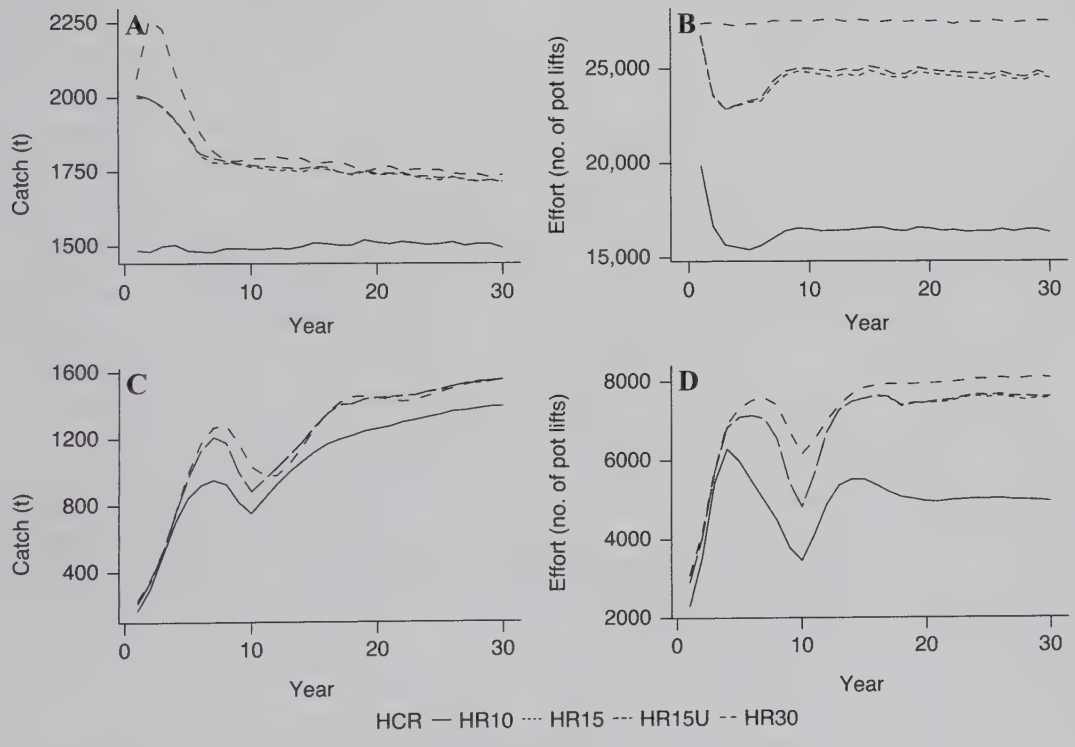

Figure 5

Median catch and median effort of the directed pot fishery for golden king crab (*Lithodes aequispinus*) in the eastern Aleutian Islands under 4 harvest control rules (HR10, HR15, HR15U, and HR30), with the initial state of the stock set at (**A** and **B**) healthy or (**C** and **D**) overfished, for scenario 1 of the operating model in which a linear relationship between catch per unit of effort and selected abundance is assumed. Values are based on a 30-year projection period that begins with 2018. The stock is projected from 2 initial levels of abundance, measured in mature male biomass (MMB): a healthy state (i.e., MMB_{2018}/MMB_{35}=1.55, where MMB_{2018} is MMB in 2018 and MMB_{35} is 35% of the unfished level of MMB) and an overfished state (i.e., MMB_{2018}/MMB_{35}=0.50). Data used in the model are for golden king crab in 1981–2018. For details about the harvest control rules, see Table 1. t=metric tons.

MMB_{2018} was greater than MMB_{35} (Fig. 5B) but increased over time when MMB_{2018} was equal to $0.5MMB_{35}$ (Fig. 5D). The alternative of HR30 led to slightly higher catches but substantially higher effort when MMB_{2018} was greater than MMB_{35}. The alternative of HR10 led to lower catches than HR15, HR15U, and HR30. The alternative of HR15U led to negligibly higher catches than HR15 (Fig. 5A). Results were similar for scenario 1 when CPUE was assumed to be proportional to the square root of abundance (Suppl. Table 8) (online only).

The probabilities of the stock of golden king crab in the Aleutian Islands being overfished ($MMB<MSST$) and severely overfished ($MMB<0.5MSST$) and of overfishing occurring (i.e., catch exceeding OFL) were zero, and the probability of this stock being below MMB_{35} was <0.02 for all policies when MMB_{2018} was greater than MMB_{35} when CPUE was assumed to be linearly proportional to abundance (Table 4). The probability of this stock of golden crab being below MMB_{35} was higher for HR15, HR15U, and HR30 when CPUE was proportional to the square root of selected abundance, but the trends were similar to those with the linear relationship of CPUE to abundance (Suppl. Table 7) (online only). The fact that the probability of overfishing occurring was zero across policies was expected, given the constraint that the predicted catch (in weight) in the directed fishery could not exceed the retained catch component of the ABC. Interestingly, the probabilities of the stock of golden king crab in the Aleutian Islands being severely overfished and of overfishing occurring were also zero when the stock was initially overfished. Probabilities of this stock being below MMB_{35} were greater for all policies when it was initially in an overfished state, yet probabilities of this stock staying overfished during the projection period were <0.031 for all policies, indicating a resiliency of this population in the simulations.

Results from consideration of economic criteria for HR0 were largely moot; therefore, only HR10, HR15, HR15U, and HR30 were ranked for these metrics. The alternative of HR10 resulted in lower catch in comparison with that of the rest of the HCRs but led to improved performance for other economic metrics, such as reduced effort (i.e., fewer pot lifts needed to achieve a low TAC; see Tables 4 and 5 for the linear choice and Supplementary Tables 7 and 8 [online only] for the nonlinear choice). Most economic criteria were similar between HR15 and HR15U for both initial conditions, indicating that the catch limit on legal-sized male abundance had little overall effect (see Table 5 for the linear choice and Supplementary Table 8 [online only] for the nonlinear choice).

Table 4

Conservation performance metrics for golden king crab (*Lithodes aequispinus*) in the Aleutian Islands, with the initial state of the stock set at healthy or overfished, for scenario 1 (based on best parameter estimates) of the operating model in which a linear relationship between catch per unit of effort and selected abundance is assumed. Values for the 5 harvest control rules (HCRs) evaluated by conservation criteria, HR0, HR10, HR15, HR15U, and HR30, are probabilities that the estimated quantity, such as mature male biomass (MMB) or total catch, is above or below the associated reference point, such as minimum stock size threshold (MSST), overfishing level (OFL), allowable biological catch (ABC), or 35% of the unfished level of MMB (MMB_{35}), calculated for the last 10 years of the 30-year projection period, which begins with 2018. For example, values for $MMB<MSST$ are the probabilities that MMB is below MSST. Harvest control rules were ranked among each other for each performance metric (ranks are given in parentheses; ranks are the same for HCRs if probabilities are the same for those HCRs). Total catch is the catch retained in the directed pot fishery plus the discard mortality in the directed fishery and the bycatch mortality in the groundfish fishery. The stock is projected from 2 initial levels of abundance, measured in MMB: a healthy state (i.e., MMB_{2018}/MMB_{35}=1.55, where MMB_{2018} is MMB in 2018) and an overfished state (i.e., MMB_{2018}/MMB_{35}=0.50). For details about the HCRs, see Table 1. B_{MSY}=the biomass corresponding to maximum sustainable yield.

Metric	Description	HR0	HR10	HR15	HR15U	HR30
Healthy						
Overfished	$MMB<MSST$	0.000 (1)	0.000 (1)	0.000 (1)	0.000 (1)	0.000 (1)
Severely overfished	$MMB<0.5MSST$	0.000 (1)	0.000 (1)	0.000 (1)	0.000 (1)	0.000 (1)
Overfishing (OFL)	Total catch>OFL	0.000 (1)	0.000 (1)	0.000 (1)	0.000 (1)	0.000 (1)
Overfishing (ABC)	Total catch>ABC	0.000 (1)	0.000 (1)	0.000 (1)	0.000 (1)	0.000 (1)
Below B_{MSY}	$MMB<MMB_{35}$	0.000 (1)	0.000 (1)	0.001 (3)	0.001 (3)	0.016 (5)
Overfished						
Overfished	$MMB<MSST$	0.000 (1)	0.000 (1)	0.000 (1)	0.000 (1)	0.000 (1)
Severely overfished	$MMB<0.5MSST$	0.000 (1)	0.000 (1)	0.000 (1)	0.000 (1)	0.000 (1)
Overfishing (OFL)	Total catch>OFL	0.000 (1)	0.000 (1)	0.000 (1)	0.000 (1)	0.000 (1)
Overfishing (ABC)	Total catch>ABC	0.000 (1)	0.000 (1)	0.000 (1)	0.000 (1)	0.000 (1)
Below B_{MSY}	$MMB<MMB_{35}$	0.000 (1)	0.000 (1)	0.063 (3)	0.063 (4)	0.141 (5)

Table 5

Economic performance metrics for golden king crab (*Lithodes aequispinus*) in the Aleutian Islands, with the initial state of the stock set at healthy or overfished, for scenario 1 (based on best parameter estimates) of the operating model in which a linear relationship between catch per unit of effort and selected abundance is assumed. Values for the 4 harvest control rules (HCRs) evaluated by economic criteria, HR10, HR15, HR15U, and HR30, are probabilities that the estimated quantity is above or below the associated reference point (e.g., $MMA<0.25MMA_{ave}$ indicates the probability that mature male abundance [MMA] is below 25% of average MMA [MMA_{ave}]), calculated for the last 10 years of the 30-year projection period, which begins with 2018. The exceptions are for values of catch (mean in metric tons), $CPUE_1$ (given as the number of crab per pot lift), and effort (given as the number of pot lifts). Harvest control rules were ranked among each other for each performance metric (ranks are given in parentheses; ranks are the same for HCRs if probabilities are the same for those HCRs). Catch is the catch retained in the directed pot fishery. The stock is projected from 2 initial levels of abundance, measured in mature male biomass (MMB): a healthy state (i.e., $MMB_{2018}/MMB_{35}=1.55$, where MMB_{2018} is MMB in 2018 and MMB_{35} is 35% of the unfished level of MMB) and an overfished state (i.e., $MMB_{2018}/MMB_{35}=0.50$). For details about the HCRs, see Table 1. $Catch_{AveHist}$=historical average catch; $CPUE_{AveHist}$=historical average CPUE; and $MMA_{AveHist}$=historical average MMA.

Metric	Description or unit	HR10	HR15	HR15U	HR30
Healthy					
Fishery closure	$MMA<0.25MMA_{ave}$	0.000 (1)	0.000 (1)	0.000 (1)	0.000 (1)
Catch	Mean	1508 (4)	1732 (3)	1735 (2)	1770 (1)
Catch variability	Annual proportional change in catch	0.049 (1)	0.052 (3)	0.055 (4)	0.052 (2)
Relative catch	$Catch<Catch_{AveHist}$	0.468 (4)	0.140 (2)	0.141 (3)	0.101 (1)
$CPUE_1$	Mean number	47.4 (1)	36.7 (2)	36.4 (3)	33.0 (4)
$CPUE_2$	$CPUE<CPUE_{AveHist}$	0.000 (1)	0.153 (2)	0.174 (3)	0.408 (4)
Effort	Number of pot lifts	16,315 (1)	24,202 (2)	24,444 (3)	27,506 (4)
Stock status	$MMA<MMA_{AveHist}$	0.002 (1)	0.075 (2)	0.078 (3)	0.196 (4)
Overfished					
Fishery closure	$MMA<0.25MMA_{ave}$	0.000 (1)	0.000 (1)	0.000 (1)	0.000 (1)
Catch	Mean	1354 (4)	1510 (2)	1512 (1)	1508 (3)
Catch variability	Annual proportional change in catch	0.048 (1)	0.050 (3)	0.052 (4)	0.049 (2)
Relative catch	$Catch<Catch_{AveHist}$	0.807 (4)	0.477 (2)	0.475 (1)	0.503 (3)
$CPUE_1$	Mean number	139.6 (1)	103.8 (2)	103.5 (3)	96.7 (4)
$CPUE_2$	$CPUE<CPUE_{AveHist}$	0.000 (1)	0.000 (1)	0.000 (1)	0.000 (1)
Effort	Number of pot lifts	4974 (1)	7460 (2)	7492 (3)	7997 (4)
Stock status	$MMA<MMA_{AveHist}$	0.037 (1)	0.396 (2)	0.398 (3)	0.535 (4)

The alternative of HR30 was the most aggressive policy, but with only marginally higher catches than HR15 and HR15U, and HR15U had the most variable catches (see Table 5 for the linear choice and Supplementary Table 8 [online only] for the nonlinear choice).

Performance of harvest control rules (all scenarios)

Catch variability was high for the highest value of σ_R (scenarios 3, 20–21, and 27–29) and very high when σ_R and ρ_R were at their maxima (scenarios 35–37 and 52–53 in Figure 6). In contrast, catch variability was insensitive to the other factors considered and to the choice of management strategy (Fig. 6). The probabilities of catch being less than mean catch and CPUE being less than mean CPUE were very high when σ_R and ρ_R were at their maxima (scenarios 35–37 and 52–53) (see Figure 7 for the linear choice and Supplementary Figure 6 [online only] for the nonlinear choice). The probability of not achieving mean CPUE was higher for HR30 (Fig. 7H, Suppl. Fig. 6H [online only]) than for HR10, HR15, and HR15U for all scenarios, with probability levels lower for the nonlinear choice than for the linear choice.

Figure 8 and Supplementary Figure 7 (online only) show the probabilities of MMA being less than MMA_{ave} and of MMB being less than MMB_{35} for the linear and nonlinear choices, respectively, when MMB_{2018} was greater than MMB_{35} for the 5 HCRs. Spawning biomass and abundance declined even under HR0 (i.e., $F=0$) for scenarios 35–37 and 52–53 because of high recruitment variability for the base level of the steepness parameter (Fig. 8, A and F; Suppl. Fig. 7, A and F [online only]). The probabilities of MMB being less than MSST and of MMA being less than $0.25MMA_{ave}$ were closer to zero for all scenarios and HCRs across simulations and for the entire projection period (results not shown).

The median rebuilding time for all HCRs under the linear choice increased for scenarios 35–37 and 52–53 because of high recruitment variability (Fig. 9). As expected, HR0 had the shortest rebuilding time. The

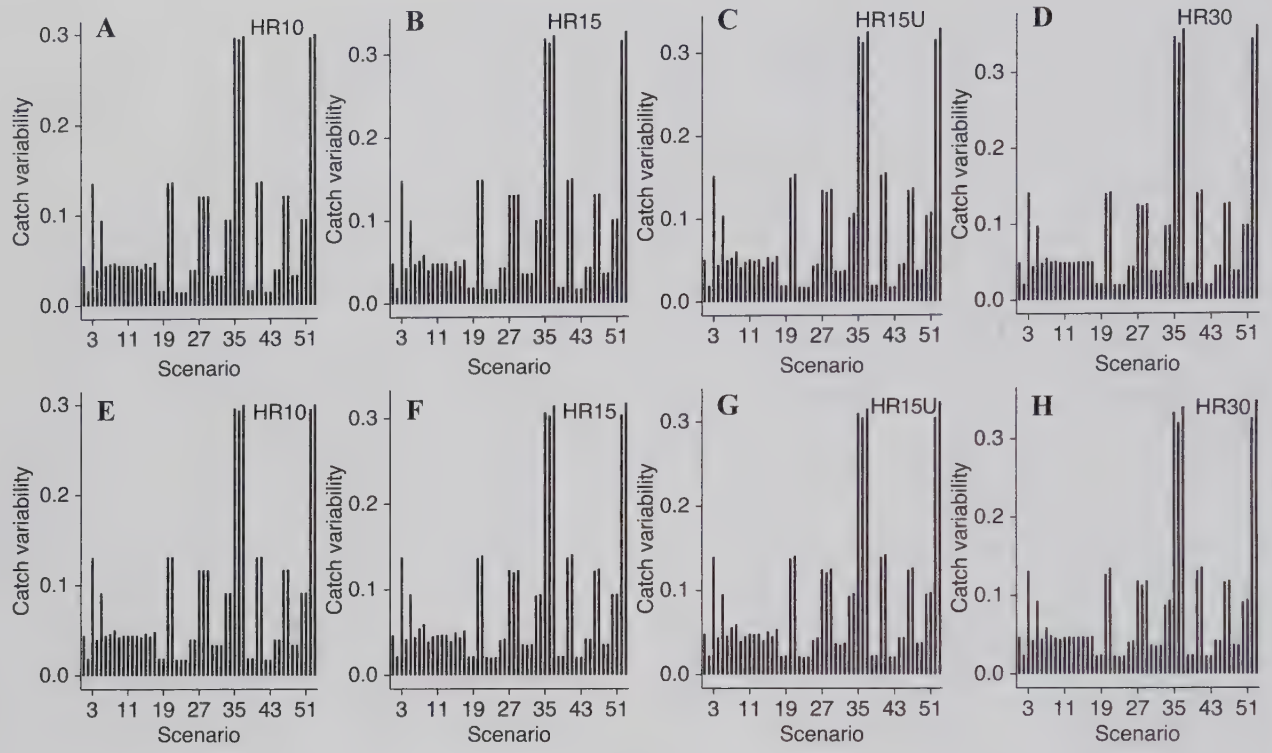

Figure 6

Median catch variability in the directed pot fishery for golden king crab (*Lithodes aequispinus*) in the Aleutian Islands during the last 10 years of a 30-year projection period, which begins in 2018, for 53 scenarios of an operating model used to evaluate harvest control rules (HCRs). The stock is projected from 2 initial levels of abundance, measured in mature male biomass (MMB). Values are given in numbers without a unit for HCRs (**A**) HR10, (**B**) HR15, (**C**) HR15U, and (**D**) HR30, with the stock set initially at a healthy state (i.e., MMB_{2018}/MMB_{35}=1.55, where MMB_{2018} is MMB in 2018 and MMB_{35} is 35% of the unfished level of MMB), and for HCRs (**E**) HR10, (**F**) HR15, (**G**) HR15U, and (**H**) HR30, with the stock set initially at an overfished state (i.e., MMB_{2018}/MMB_{35}=0.50). In the model used in this analysis, a linear relationship between catch per unit of effort and selected abundance is assumed. Data used in the model are for golden king crab in 1981–2018. For details about the HCRs, see Table 1.

rebuilding time is short when values for steepness are higher (e.g., scenario 9) and is longer for HR30 than for HR10, HR15, and HR15U for most scenarios. The rebuilding times necessary to achieve MMA_{ave} are longer than those necessary to achieve MMB_{35} for all non-zero exploitation rates. The results for the nonlinear choice are similar (results not shown).

The MMA and CPUE distributions for scenario 1 (with parameters estimated through the use of the assessment model) indicate that HR10, HR15, and HR15U performed better than HR30. Fewer instances of MMA being lower than MMA_{ave} and more frequent values of higher CPUE were observed for HR10, HR15, and HR15U than for HR30 (Fig. 10). Catch distributions were similar for HR15 and HR30 and for the equilibrium state; size compositions of crab in total catch as well as in retained catch did not differ significantly from those for HR15 and those for HR30 (Suppl. Fig. 8) (online only). This result occurred because the stock was projected from a healthy state ($MMB>MMB_{35}$) and because the effective F under both HR15 and HR30 was dampened because of reduction in abundance over the years.

The results for the conservation and economic performance criteria of HR15 and HR15U for the last 10 years of the 30-year projection period were very similar for the linear and the nonlinear relationships of CPUE to abundance (Tables 4–6, Suppl. Tables 7–9 [online only]). When compared with HR10 and HR30, HR15 may optimize the balance between conservation and economic criteria (Tables 4–6). Conservation metrics were similar among all HCRs except for HR30 (nonlinear choice; Suppl. Table 7 [online only]). Probabilities of fishery closures were zero, and catch variability was similar for all HCRs, yet relative stock status was lower under HR30. Relative to HR15, HR10 required substantially lower effort (~48% lower) to achieve the TAC, yet the TAC itself was lower (~15% lower); in contrast, HR30 required higher effort (~14% higher) to achieve only a marginally higher (~2% higher) TAC (Table 5).

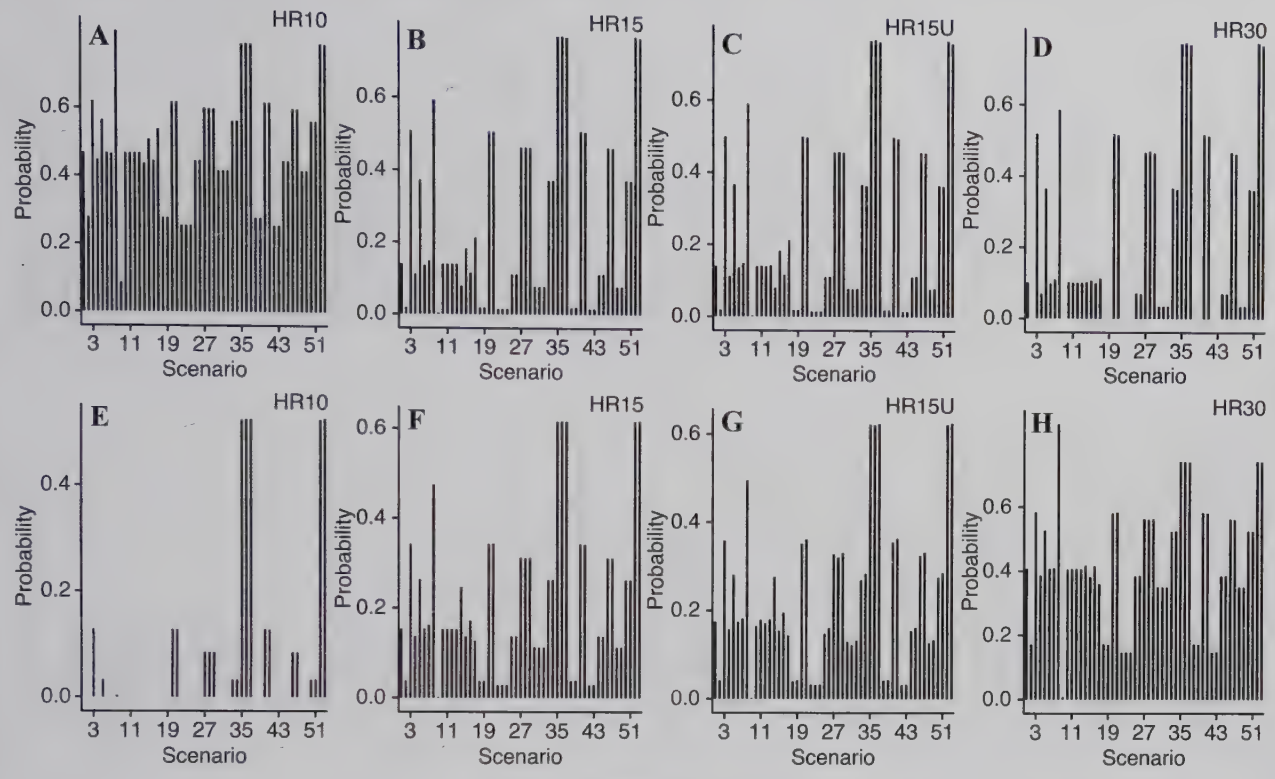

Figure 7

The probability of (**A–D**) catch and (**E–H**) catch per unit of effort (CPUE) being below their mean values for the period after crab stocks were rationalized, from the 2005–2006 fishing season through the 2018–2019 fishing season, in the directed pot fishery for golden king crab (*Lithodes aequispinus*) in the Aleutian Islands, by model scenario, under harvest control rules (HCRs) HR10, HR15, HR15U, and HR30. Estimates are based on the last 10 years of a 30-year projection period for 53 scenarios of an operating model used to evaluate HCRs. The stock is projected from an initial level of abundance, measured in mature male biomass (MMB): $1.55MMB_{35}$, where MMB_{35} is 35% of the unfished level of MMB. In the model used in this analysis, a linear relationship between CPUE and selected abundance is assumed. For details about the HCRs, see Table 1.

Discussion

We have demonstrated the utility of the simplified MSE for evaluating HCRs through consideration of conservation and economic trade-offs. Our results indicate that HR15 and HR15U are preferable to HR10 and HR30, given the desire to balance the trade-off between sustainability and economic viability, and this notion was supported under both the linear and nonlinear assumptions about the relationship between CPUE and selected abundance. Although HR30 yielded the highest catch, it performed poorest in terms of other economic and conservation criteria. Specifically, HR30 had the highest relative probabilities of MMB being below MMB_{35} and of MMA being below the historical average MMA, had the lowest CPUE, and required substantially more effort to realize marginally higher (~2% higher) catches compared with HR10, HR15, and HR15U. Relative to HR10, HR30 required 69% more effort to achieve 17% more catch (Table 5). Therefore, criteria beyond projected average TAC are important from an economic viewpoint because costs required to make excessive numbers of fishing trips when fishing effort is high may outweigh modest increases in TAC.

Although we suggest that HR15 is the optimal HCR, given the trade-offs between conservation, catch, and catch stability, we acknowledge that the preferred HCR may differ depending on management and stakeholder priorities. Although HR10 yielded improved performance in terms of some conservation and economic criteria (e.g., higher CPUE, MMA, MMB, and reduced effort), it yielded lower catch compared with that from HR15, HR15U, and HR30. Our analysis is meant to provide managers and stakeholders with a tool to evaluate the trade-offs between various fishery management criteria relative to risk.

The conservation and economic criteria were very similar for HR15 and HR15U. Although the catch limit on legal-sized male abundance did not meaningfully affect the performance of the management strategy, it is likely

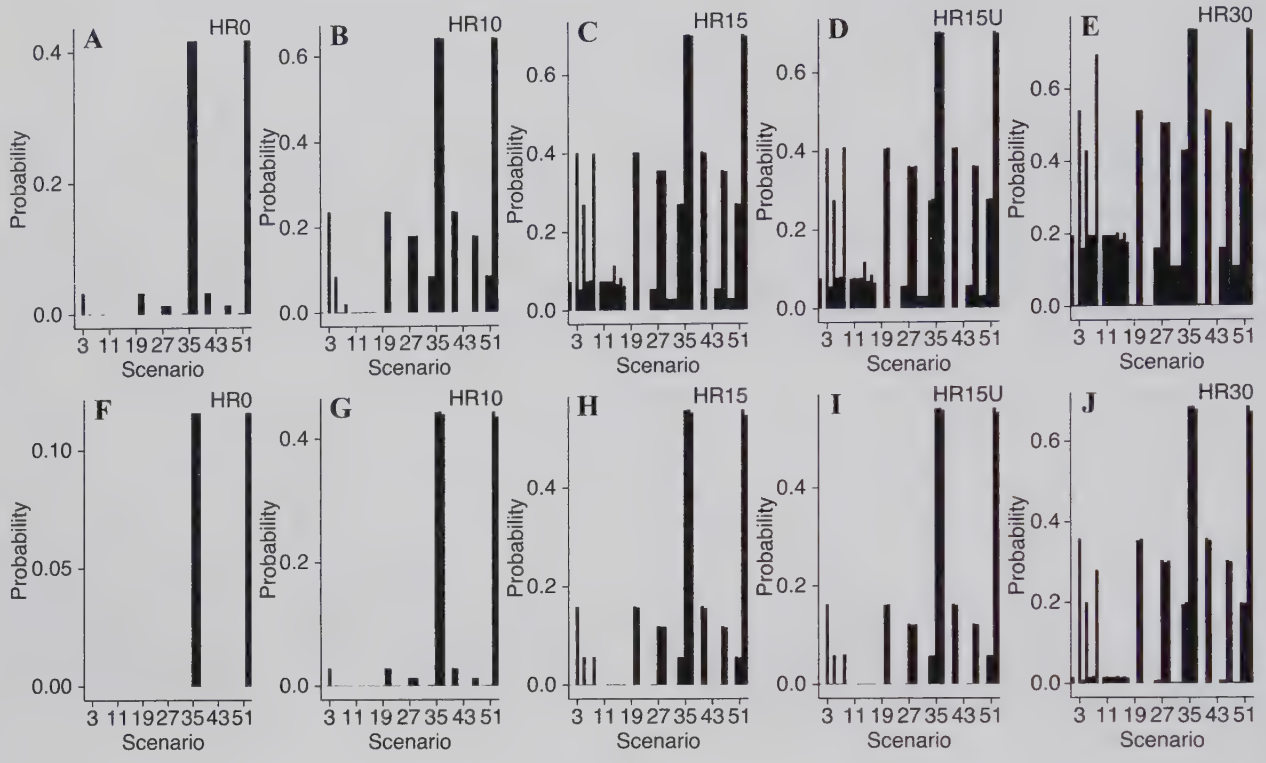

Figure 8

The probability (**A**–**E**) of mature male abundance (MMA) being less than average MMA (MMA_{ave}) and (**F**–**J**) of mature male biomass (MMB) being less than 35% of the unfished level of MMB (MMB_{35}) for golden king crab (*Lithodes aequispinus*) in the Aleutian Islands during the period from the 1985–1986 fishing season through the 2018–2019 fishing season, by model scenario, under harvest control rules (HCRs) HR0, HR10, HR15, HR15U, and HR30. Estimates are based on the last 10 years of a 30-year projection period for 53 scenarios of an operating model used to evaluate HCRs. The stock is projected from an initial level of abundance: $1.55MMB_{35}$. In the model used in this analysis, a linear relationship between CPUE and selected abundance is assumed. For details about the HCRs, see Table 1.

an important conservation component of the management strategy given the desire to ensure future recruitment. Realized exploitation rates on abundance of legal-sized male golden king crab is expected to be higher when population abundance is on an increasing trend (i.e., when mature male recruits have yet to reach the legal size) because the exploitation rate is scaled to MMA. The maximum exploitation rate on legal-sized male abundance provides an additional level of protection against overfishing of legal-sized males in years when legal-sized male abundance is low relative to the abundance for the entire size range of mature males and is a commonly adopted step in the HCRs for other crab stocks in the Bering Sea and Aleutian Islands (e.g., red king crab in Bristol Bay; Pengilly and Schmidt[4]; Zheng et al., 1997).

It is important to note that our simulations limited the catch in the directed fishery by the retained catch component of the ABC. As such, the more aggressive HCRs likely performed more conservatively (i.e., there was zero probability of exceeding OFL and ABC) than any of the HCRs that did not constrain the directed fishery catch below the retained catch component of the ABC. However, our simulations best approximate how management for crab stocks occurs in the North Pacific Ocean because TACs would not be set above estimated ABCs in practice.

Incorporating uncertainty is a fundamental challenge in MSE. Parameters, such as natural mortality, catchability, growth, maturity, selectivity, and the stock–recruitment relationship are assumed to be correct and time invariant, and the projections ignore spatial and environmental variability (Somerton and Otto, 1986; Hollowed et al., 2001; Clark and Hare, 2002). However, the ability to use MSE to help achieve management goals depends on how well uncertainty in the system is represented in simulations (Punt et al., 2016). Because it is

[4] Pengilly, D., and D. Schmidt. 1995. Harvest strategy for Kodiak and Bristol Bay red king crab and St. Matthew Island and Pribilof blue king crab. Alaska Dep. Fish Game, Spec. Publ. 7, 10 p. [Available from website.]

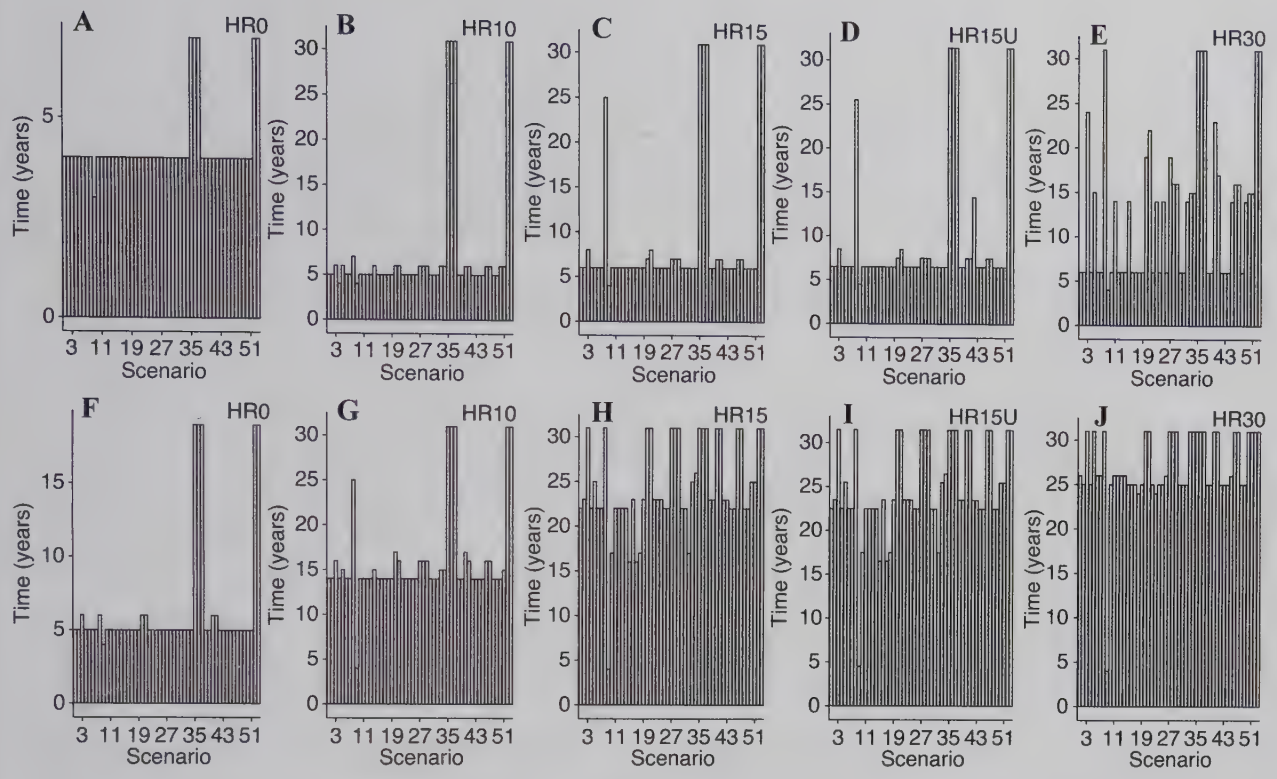

Figure 9

Median time, in years, for a stock of golden king crab (*Lithodes aequispinus*) in the Aleutian Islands (**A**–**E**) to rebuild from an initial overfished state of $0.5MMB_{35}$, where MMB_{35} is 35% of the unfished level of mature male biomass, to a full MMB_{35} and (**F**–**J**) to rebuild from the corresponding mature male abundance to average mature male abundance under harvest control rules (HCRs) HR0, HR10, HR15, HR15U, and HR30, for the 53 scenarios of the operating model in which a linear relationship between catch per unit of effort and selected abundance is assumed. Data used in the model are for golden king crab in 1981–2018. For details about the HCRs, see Table 1.

computationally prohibitive to address all uncertainties by using a projection model, we considered a small set of scenarios focused on those uncertainties most likely to affect the performance of HCRs under the linear and nonlinear choices.

Our findings indicate how projection results respond to changes in steepness, variation, and autocorrelation of the stock–recruitment relationship, error in estimating MMB and MMA, and catch implementation error (Table 2, Suppl. Tables 1–5 [online only]). Although the values of the performance metrics differ between the linear and nonlinear choices, trends in HCR ranks were largely unchanged between these choices, indicating that our analysis for these choices is robust for evaluating policy trade-offs. The results presented here are based on approximate closed-loop simulations because, although errors in estimating MMB and MMA are considered, the full stock assessment is not simulated because of computational limitations, and our analysis is not a full MSE. Comparison of the full suite of scenarios (i.e., a range of contrasting parameter values) reveals the level of risk related to each source of uncertainty when relying on best estimates of parameters for decision-making.

The projections in our study identify recruitment variability as the most important factor determining the performances of the HCRs, yet understanding causes of recruitment fluctuations is a fundamental challenge in modeling crab population dynamics. The results of our simulations may underestimate recruitment variability or fail to capture the non-stationarity of the nature of recruitment, and such underestimation or failure may bias estimates of HCR performance. Well-defined stock–recruitment relationships are rare for crab and lobster species because the underlying physical and biological processes that influence larval survival to the juvenile stages are difficult to define (Wahle, 2003). For red king crab in Bristol Bay, recruitment trends are consistent with decadal climate shifts (Zheng and Kruse, 2003), indicating the importance of environmental factors (Zheng and Kruse, 2006). Nevertheless, because of uncertainties in the stock–recruitment relationship (or lack thereof) for golden king crab in the Aleutian Islands,

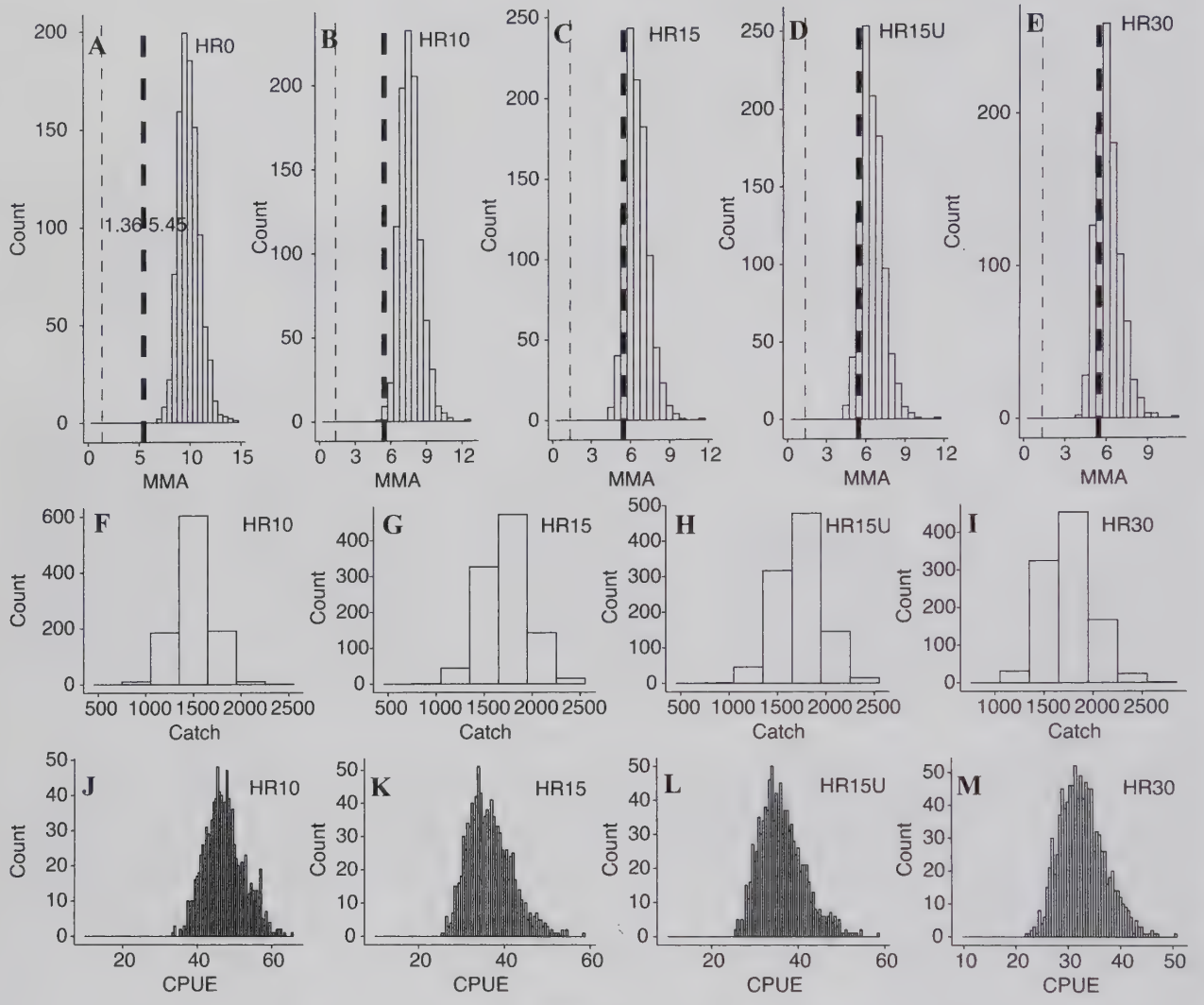

Figure 10

Distributions of (**A**–**E**) mature male abundance (MMA), (**F**–**I**) retained catch, and (**J**–**M**) catch per unit of effort (CPUE), all given in frequency counts, of golden king crab (*Lithodes aequispinus*) in the Aleutian Islands under harvest control rules (HCRs) HR0, HR10, HR15, HR15U, and HR30. Distributions are from 1000 simulations for scenario 1 of the operating model in which a linear relationship between CPUE and selected abundance is assumed. The stock is projected from an initial level of abundance, measured in mature male biomass (MMB): a healthy state (i.e., MMB_{2018}/MMB_{35}=1.55, where MMB_{2018} is MMB in 2018 and MMB_{35} is 35% of the unfished level of MMB). The vertical thick dashed lines in the top row of panels indicate average mature male abundance (MMA_{ave}), and the vertical thin dashed lines indicate $0.25MMA_{ave}$. Data used in the model are for golden king crab in 1981–2018. For details about the HCRs, see Table 1.

understanding the sensitivity of the performance of candidate HCRs to changes in recruitment parameters will assist managers in decision-making.

We feel that the approach of using a simplified MSE presented here is a fair balance between a robust analysis with reduced computational demands and a full MSE that can be applied to any stock that is hard to age and for which there are several candidate HCRs. Although we highlight the importance of recruitment variability, managers of other stocks should consider their management goals, dynamics of the stock that they manage, uncertainties, and candidate catch policies. The ability to objectively evaluate conservation and economic tradeoffs leads to a level of transparency between managers and fishermen that allows productive dialogue regarding emerging HCRs.

Acknowledgments

We thank members of the Crab Plan Team of the North Pacific Fishery Management Council for technical

Table 6

Decision matrix based on average policy ranks within each metric used to evaluate harvest control rules (HR0, HR10, HR15, HR15U, and HR30) for golden king crab (*Lithodes aequispinus*) in the Aleutian Islands, when a linear relationship between catch per unit of effort and selected abundance is assumed in the operating model. Values are based on the last 10 years of the 30-year projection period, which begins with 2018. The stock is projected from 2 initial levels of abundance, measured in mature male biomass (MMB): a healthy state (i.e., MMB_{2018}/MMB_{35}=1.55, where MMB_{2018} is MMB in 2018 and MMB_{35} is 35% of the unfished level of MMB) and an overfished state (i.e., MMB_{2018}/MMB_{35}=0.50). Values are average ranks within each metric, with ranks of the average metric ranks given in parentheses. The ranks of the catch metric correspond only to the long-term averages of retained catch; therefore, no average ranks were computed. For details about the harvest control rules, see Table 1.

Metric	Conservation	Catch	Catch stability
Healthy			
HR0	1.00 (1)		
HR10	1.00 (1)	4	1.43 (1)
HR15	1.40 (3)	3	2.00 (2)
HR15U	1.40 (3)	2	2.86 (3)
HR30	1.80 (5)	1	2.86 (3)
Overfished			
HR0	1.00 (1)		
HR10	1.00 (1)	4	1.43 (1)
HR15	1.50 (3)	2	1.86 (2)
HR15U	1.75 (4)	1	2.29 (3)
HR30	2.00 (5)	3	2.71 (4)

suggestions on the projection simulations and stakeholders of the fishery for golden king crab in the Aleutian Islands for suggestions on management strategy scenarios. This manuscript is contribution PP–285 of the Commercial Fisheries Division of the Alaska Department of Fish and Game, Juneau, Alaska.

Literature cited

Bechtol, W. R., and G. H. Kruse.
2009. Analysis of stock–recruit relationship for red king crab off Kodiak Island, Alaska. Mar. Coast. Fish. 1:29–44.

Caddy, J. F., and R. Mahon.
1995. Reference points for fisheries management. FAO Fish. Tech. Pap. 347, 83 p. FAO, Rome. [Available from website.]

Clark, W. G.
1991. Groundfish exploitation rates based on life history parameters. Can. J. Fish. Aquat. Sci. 48:734–750.
2002. $F_{35\%}$ revisited ten years later. North Am. J. Fish. Manage. 22:251–257.

Clark, W. G., and S. R. Hare.
2002. Effects of climate and stock size in on recruitment and growth of Pacific halibut. North Am. J. Fish. Manage. 22:852–862.

Daly, B., M. S. M. Siddeek, M. Stichert, S. Martell, and J. Zheng.
2019. Recommended harvest strategy for Aleutian Islands golden king crab. Alaska Dep. Fish Game, Fish. Manuscr. Ser. 19-03, 50 p. [Available from website.]

Fina, M.
2005. Rationalization of the Bering Sea and Aleutian Islands crab fisheries. Mar. Policy 29:311–322.

Hollowed, A. B., S. R. Hare, and W. S. Wooster.
2001. Pacific Basin climate variability and patterns of Northeast Pacific marine fish production. Prog. Oceanogr. 49:257–282.

Leon, J. M., J. Shaishnikoff, E. Nichols, and M. Westphal.
2017. Annual management report for shellfish fisheries of the Bering Sea–Aleutian Islands management area, 2015/16. Alaska Dep. Fish Game, Fish. Manage. Rep. 17-10, 188 p. [Available from website.]

Martell, S. J. D., W. E. Pine, and C. J. Walters.
2008. Parameterizing age-structured models from a fisheries management perspective. Can. J. Fish. Aquat. Sci. 65:1586–1600.

NPFMC (North Pacific Fishery Management Council).
2018. Stock assessment and fishery evaluation report for the king and Tanner crab fisheries of the Bering Sea and Aleutian Islands regions: 2018 final crab SAFE, 1462 p. NPFMC, Anchorage, AK. [Available from website.]

Punt, A. E., M. W. Dorn, and M. A. Haltuch.
2008. Evaluation of threshold management strategies for groundfish off the U.S. West Coast. Fish. Res. 94:251–266.

Punt, A. E., D. S. Butterworth, C. L. de Moor, J. A. A. De Oliveira, and M. Haddon.
2016. Management strategy evaluation: best practices. Fish Fish. 17:303–334.

Quinn, T. J., II, R. Fagen, and J. Zheng.
1990. Threshold management policies for exploited populations. Can. J. Fish. Aquat. Sci. 47:2016–2029.

Restrepo, V. R., and J. E. Powers.
1999. Precautionary control rules in US fisheries management: specification and performance. ICES J. Mar. Sci. 56:846–852.

Ricker, W. E.
1954. Stock and recruitment. J. Fish. Res. Board Can. 11:559–623.

Siddeek, M. S. M., J. Zheng, C. Siddon, B. Daly, M. J. Westphal, and L. Hulbert.
2020. Aleutian Islands golden king crab stock assessment. *In* Stock assessment and fishery evaluation report for the king and Tanner crab fisheries of the Bering Sea and Aleutian Islands regions, p. 8-1–8-129. North Pac. Fish. Manage. Counc., Anchorage, AK. [Available from website].

Somerton, D. A., and R. S. Otto.
1986. Distribution and reproductive biology of the golden king crab, *Lithodes aequispina*, in the eastern Bering Sea. Fish. Bull. 84:571–584.

Subbey, S., J. A. Devine, U. Schaarschmidt, and R. D. M. Nash.
2014. Modelling and forecasting stock–recruitment: current and future perspectives. ICES J. Mar. Sci. 71:2307–2322.

Wahle, R. A.
2003. Revealing stock–recruitment relationships in lobsters and crabs: is experimental ecology the key? Fish. Res. 65:3–32.

Zheng, J., and G. H. Kruse.
2003. Stock–recruitment relationships for three major Alaskan crab stocks. Fish. Res. 65:103–121.

2006. Recruitment variation of eastern Bering Sea crabs: climate-forcing or top-down effects? Prog. Oceanogr. 68:184–204.

Zheng, J., T. J. Quinn II, and G. H. Kruse.
1993. Comparison and evaluation of threshold estimation methods for exploited fish populations. *In* Proceedings of the international symposium on management strategies for exploited fish populations; Anchorage, AK, 21–24 October 1992. Alaska Sea Grant Rep. 93-02 (G. Kruse, D. M. Eggers, R. J. Marasco, C. Pautzke, and T. J. Quinn II, eds.), p. 267–289. Alaska Sea Grant Coll. Program, Univ. Alaska, Fairbanks, AK.

Zheng, J., M. C. Murphy, and G. H. Kruse.
1995. A length-based population model and stock–recruitment relationships for red king crab, *Paralithodes camtschaticus*, in Bristol Bay, Alaska. Can. J. Fish. Aquat. Sci. 52:1229–1246.
1997. Analysis of harvest strategies for red king crab, *Paralithodes camtschaticus*, in Bristol Bay, Alaska. Can. J. Fish. Aquat. Sci. 54:1121–1134.

National Marine Fisheries Service
NOAA

Fishery Bulletin
established in 1881

Spencer F. Baird
First U.S. Commissioner of Fisheries and founder of *Fishery Bulletin*

Seasonal distribution and habitat use of the common thresher shark (*Alopias vulpinus*) in the western North Atlantic Ocean inferred from fishery-dependent data

Jeff Kneebone (contact author)[1]
Heather Bowlby[2]
Joseph J. Mello[3]
Camilla T. McCandless[4]
Lisa J. Natanson[4]
Brian Gervelis[5]
Gregory B. Skomal[6]
Nancy Kohler[4]
Diego Bernal[7]

Email address for contact author: jkneebone@neaq.org

[1] Anderson Cabot Center for Ocean Life
New England Aquarium
1 Central Wharf
Boston, Massachusetts 02110

[2] Bedford Institute of Oceanography
Fisheries and Oceans Canada
1 Challenger Drive
P.O. Box 1006
Dartmouth, Nova Scotia B2Y 4A2, Canada

[3] Northeast Fisheries Science Center
National Marine Fisheries Service, NOAA
166 Water Street
Woods Hole, Massachusetts 02543

[4] Northeast Fisheries Science Center
National Marine Fisheries Service, NOAA
28 Tarzwell Drive
Narragansett, Rhode Island 02882

[5] Integrated Statistics for Northeast Fisheries Science Center
National Marine Fisheries Service, NOAA
16 Sumner Street
Woods Hole, Massachusetts 02543

[6] New Bedford Office
Massachusetts Division of Marine Fisheries
836 South Rodney French Boulevard
New Bedford, Massachusetts 02744

[7] University of Massachusetts Dartmouth
285 Old Westport Road
Dartmouth, Massachusetts 02747

Abstract—Improved understanding of the seasonal distribution, habitat use, and fishery interactions of the common thresher shark (*Alopias vulpinus*) in the western North Atlantic Ocean (WNA) is required for future management. We compiled and analyzed 3478 fishery-dependent capture records in the WNA between 1964 and 2019 to examine dynamics by sex and life stage (i.e., young of the year, juvenile, and adult). Sharks were captured over a broad geographic range from the Gulf of Mexico to the Grand Banks, primarily in continental shelf waters shallower than 200 m. Seasonal north–south movements along the east coasts of the United States and Canada were observed for all life stages and both sexes, with individuals generally occurring at more northerly latitudes in the summer and more southerly latitudes in the winter. Distinct areas of more frequent capture in fisheries were identified for all life stages throughout their range. Common thresher sharks were observed in waters with sea-surface temperatures of 4–31°C, most commonly of 12–18°C. The results of this study will help to identify essential fish habitat for each life stage of common thresher sharks along the U.S east coast and to develop management measures for the WNA population.

Manuscript submitted 22 June 2020.
Manuscript accepted 15 December 2020.
Fish. Bull. 118:399–412 (2020).
Online publication date: 31 December 2020.
doi: 10.7755/FB.118.4.8

The views and opinions expressed or implied in this article are those of the author (or authors) and do not necessarily reflect the position of the National Marine Fisheries Service, NOAA.

The common thresher shark (*Alopias vulpinus*) is one of 2 species in the family Alopiidae that occurs in temperate and subtropical regions of the North Atlantic Ocean (Compagno, 2001). In the western North Atlantic Ocean (WNA), common thresher sharks are thought to represent a discrete population (Castro, 2011; Rigby et al., 2019) and occur from Cuba to Newfoundland, Canada (Compagno, 2001). There is currently no large-scale, directed commercial fishery for this species in the WNA, but common thresher sharks are often caught incidentally in pelagic longline and demersal gill-net fisheries and occasionally are retained for sale in the United States (NMFS, 2019a). The common thresher shark is also the target of an extensive recreational shark fishery from Virginia to Maine with the majority of sharks landed (NMFS, 2019a) because their flesh is considered excellent (Compagno, 2001).

There is limited and conflicting information on the status of the population of common thresher sharks in the WNA. Results of studies examining pelagic longline logbook data collected since the late 1980s for *thresher sharks* (i.e., the common thresher shark and the bigeye thresher, *A. superciliosus*, combined) indicate that their relative abundance has declined by 63–80%

over the time series (Baum et al., 2003; Cortés et al., 2007). In contrast, pelagic longline fisheries observer data indicate that relative abundance had either stabilized at low levels (Baum and Blanchard, 2010) or increased (Cortés et al., 2007) during the 1990s into the early 2000s. Results of recent analyses of pelagic longline logbook and observer data for common thresher sharks from the period 1992–2013 also indicate a stabilized trend in relative abundance at low levels (Young et al., 2016) to an overall increasing trend when temperature profiles are incorporated into the analyses (Lynch et al., 2018). Relative abundance indices derived from data from 5 long-term recreational sportfishing tournaments based out of New York and New Jersey also indicate an overall increasing trend but with high annual variability (Young et al., 2016).

Although recent analyses provide an optimistic outlook, the true extent to which these trends are representative of the population of common thresher sharks in the WNA remains unknown. For example, although observer data are often considered more reliable than fishery logbook data, especially for bycatch species, the sample size for observer data is much smaller and interactions of individuals with the pelagic longline fishery are likely limited by the coastal and temperate distribution of this species (Young et al., 2016). Nonetheless, this species is currently listed as vulnerable by the International Union for Conservation of Nature (IUCN) in the IUCN Red List of Threatened Species, with a decreasing population trend assumed throughout its global range (Rigby et al., 2019). There are also no formal stock assessments, international management measures, or species-specific quotas for common thresher sharks in the WNA, and there are only limited biological and ecological data for the development of domestic and international management policies.

Detailed information on seasonal distribution, habitat use, migration patterns, and population structure of common thresher sharks in the WNA is limited. Although records from fishery-dependent catch data support a north–south movement pattern along the U.S. east coast (e.g., Castro, 2011; Natanson and Gervelis, 2013), published movement data are limited to fishery-dependent data from the recapture of 2 individuals from the 230 common thresher sharks tagged by the National Marine Fisheries Service (NMFS) Cooperative Shark Tagging Program from 1962 through 2018 (tag return rate: ~0.9%). Both recaptured sharks had a north–south movement pattern along the northeastern coast of the United States (Kohler and Turner, 2019). However, the records of these recaptures provide minimal insight into the spatial and temporal extent of the annual movements of this species, given the extended times at liberty (1533 and 2934 d) and the fact that both recapture events occurred in June. Migratory routes are also poorly known (Castro, 2011), and only general descriptions of distribution and habitat use by sex or life stage have been presented from historical catch data.

Given the uncertainty over the status of the population of common thresher sharks in the WNA, there is a need to improve our understanding of this species' life history and general susceptibility to capture in commercial and recreational fisheries. Improved knowledge is needed considering that their life history parameters (i.e., relatively slow growth, late age to maturity, and low fecundity; Gervelis and Natanson, 2013; Natanson and Gervelis, 2013) increase their susceptibility to population decline (Smith et al., 1998) and that ecological data on their temperature and habitat preferences are few. Accordingly, we compiled and summarized fishery-dependent data on catch of common thresher sharks throughout the WNA 1) to document their seasonal distribution and habitat use by sex and life stage, 2) to better understand fishery interactions, and 3) to provide information that facilitates the identification of essential fish habitat (EFH) by life stage in U.S. waters.

Materials and methods

At-sea observer and other catch data on common thresher sharks originated mainly from the NMFS, specifically from the Northeast Fisheries Observer Program, Pelagic Longline Observer Program of the Southeast Fisheries Science Center, Shark Bottom Longline Observer Program, Cooperative Shark Tagging Program of the Apex Predators Program, Cooperative Tagging Center of the Southeast Fisheries Science Center, and Large Pelagics Survey. Additional records were obtained from the Industry Surveys Database of Fisheries and Oceans Canada (H. Bowlby, personal commun.), which is used to archive at-sea observer information from commercial fisheries. Data from each source were subjected to editing and quality control a priori by the provider and represent all records of common thresher sharks available in their respective databases through 2019. Data requested from each source include the date of capture, location of capture (i.e., latitude and longitude), shark sex, shark length (i.e., fork length [FL] and total length [TL]) and nature (i.e., measured or estimated) of the length, shark weight (i.e., whole [or round] and dressed) and nature (i.e., measured or estimated) of the weight, gear type used for capture, and the observed sea-surface temperature (SST, in degrees Celsius) at the time and location of capture.

Prior to analysis, records with no geographical information were removed, and a series of steps were taken to standardize and validate length and weight data among the various sources. All capture records for which a measured FL was provided were considered reliable and retained. Records with a measured or estimated TL or whole weight were converted to an estimated FL by using the appropriate conversion equation (TL to FL: coefficient of multiple determination [R^2]=0.83; whole weight [in kilograms] to FL: R^2=0.93; NMFS[1]). Reported weights were also used to

[1] NMFS (National Marine Fisheries Service). 2020. Unpubl. data. Apex Predators Program, Northeast Fish. Sci. Cent., Natl. Mar. Fish. Serv., NOAA, 28 Tarzwell Dr., Narragansett, RI 02882.

reconcile any lengths that appeared to have been inaccurately labeled (e.g., labeled as TL when the weight was more consistent with a fish near the same FL). Length data for any record that had a measured or estimated FL below the published size of near-term embryos (50 cm FL; Gervelis and Natanson, 2013) or markedly above the estimated maximum length (350 cm FL; Cailliet et al., 1983) were considered unreliable and excluded from ontogenetic analyses. Lastly, all common thresher sharks with a measured or estimated FL were assigned to 1 of 3 life stages, on the basis of published estimates of length at age (Gervelis and Natanson, 2013) and length at 50% maturity (Natanson and Gervelis, 2013) for individuals from the WNA: young of the year (YOY), if ≤100 cm FL; juvenile, for males 101–187 cm FL and for females 101–215 cm FL; and adult, for males ≥188 cm FL and for females and sharks of unknown sex ≥216 cm FL.

Distribution analysis

Spatial and temporal patterns in presence and fishery interactions of common thresher sharks by sex, life stage, and season were qualitatively analyzed following the general approach of Curtis et al. (2014). All analyses were performed in R (vers. 4.0.3; R Core Team, 2020). Maps and figures were created by using the tidyverse collection of packages (vers. 1.3.0; Wickham et al., 2019) and the sf package (vers. 0.9.6; Pebesma, 2018) in R. Seasons were classified as winter (January–March), spring (April–June), summer (July–September), or fall (October–December).

Because of the limitations of using presence-only data when detectability is unknown, location data over the full time series (1964–2019) were plotted by season, both in aggregate and by sex and life stage, to assess distribution patterns. To meet confidentiality requirements for commercially derived data, latitudes and longitudes (under the World Geodetic System 1984) were aggregated in a raster grid (0.5° × 0.5°) spanning the WNA, including the Gulf of Mexico. Grid cell counts (number of captures) were natural log transformed for plotting to increase contrast among small values.

Habitat use

Fishery-dependent records with a recorded SST were aggregated by month and summarized by using box plots to examine monthly and seasonal trends. To visually examine distribution of common thresher sharks in relation to typical seasonal SST conditions in the WNA, grid cells were plotted over NMFS Southwest Fisheries Science Center monthly composite climatologies (data set ID: erdAGsstamday_LonPM180; available from the ERDDAP server at website) averaged over the most recent years for which data were available (2009–2016); 62% of all capture events occurred over this period. The SST data were downloaded by using the rerddap package (vers. 0.6.5; Chamberlain, 2019) in R. To explore any association with bathymetry, the local depth was assigned to each record by using data from the NOAA ETOPO1 1 Arc-Minute Ocean Relief Model (NOAA National Geophysical Data Center, model available from website, accessed June 2019; Amante and Eakins, 2009) in the R package marmap (vers. 1.0.5; Pante and Simon-Bouhet, 2013). Histograms were used to examine SST and depth occupancy by life stage.

Results

A total of 3478 fishery-dependent records of the capture of common thresher sharks were compiled between 1964 and 2019, representing 1035 males, 1039 females, and 1404 sharks of unknown sex (Tables 1 and 2). The number of

Table 1

Source, number, and time period for fishery-dependent capture records compiled to examine spatial distribution and habitat use of common thresher sharks (*Alopias vulpinus*) in the western North Atlantic Ocean between 1964 and 2019. DFO=Department of Fisheries and Oceans; NMFS=National Marine Fisheries Service; SEFSC=Southeast Fisheries Science Center.

Data source	Number of records	Time period
DFO Canada: Industry Surveys Database	299	1982–2019
NMFS Cooperative Shark Tagging Program	235	1964–2019
NMFS Large Pelagics Survey	198	2002–2018
NMFS Shark Bottom Longline Observer Program	39	1996–2019
NOAA Northeast Fisheries Observer Program	2165	1990–2019
NOAA Southeast Pelagic Observer Program	526	1992–2017
NOAA SEFSC Cooperative Tagging Program	16	1978–1996
Total	3478	1964–2019

Table 2

Summary of fishery-dependent data by life stage and sex as well as the range of associated sea-surface temperatures (SST) and depths from capture records for common thresher sharks (*Alopias vulpinus*) in the western North Atlantic Ocean between 1964 and 2019. Ranges and means, with standard deviations in parentheses, are presented for SST and depth. YOY=young of the year; unknown=unknown life stage or sex.

	Number of records				SST (°C)		Depth (m)	
Life stage	Total	Male	Female	Unknown	Range	Mean	Range	Mean
YOY	1136	425	432	279	6–26	16 (3)	1–2077	21 (86)
Juvenile	1083	338	376	369	6–31	17 (4)	1–4535	262 (556)
Adult	423	182	83	158	5–30	18 (4)	1–5401	414 (902)
Unknown	836	90	148	598	4–30	18 (4)	1–5427	1197 (1581)
Overall	3478	1035	1039	1404	4–31	17 (4)	1–5427	434 (1039)

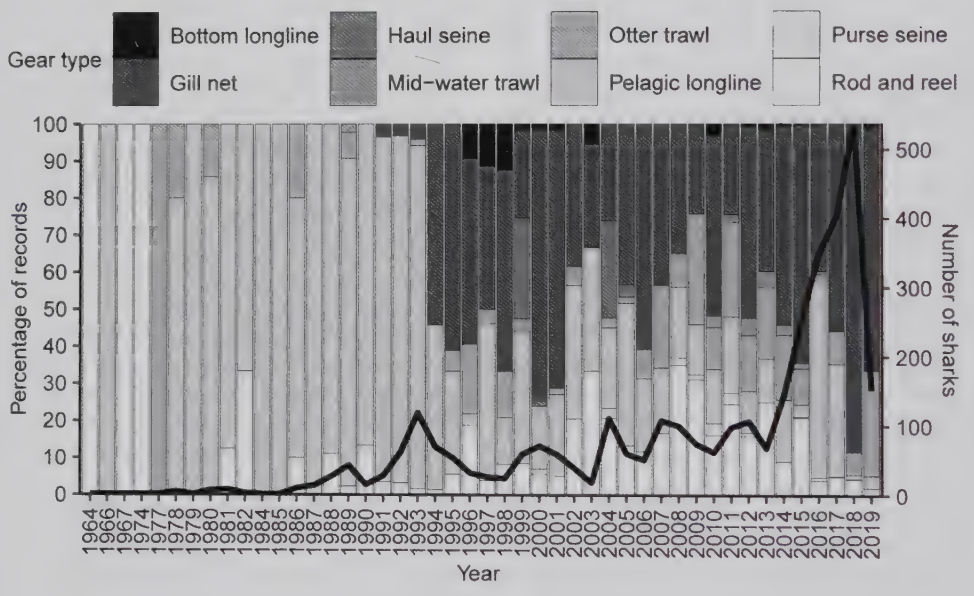

Figure 1

Percentage of the total number of capture records from fishery-dependent data, by gear type, and the total number of records, by year, for common thresher sharks (*Alopias vulpinus*) in the western North Atlantic Ocean from 1964 through 2019. The shade or pattern of each bar indicates gear type, and the solid line indicates number of records.

records obtained per year ranged from 1 to 538 (mean: 76 [standard deviation (SD) 109]) with 48.7% of all records occurring between 2015 and 2019 (Fig. 1). Lengths were available for 3072 (88.3%) individuals, including 1720 (49.4%) sharks that were measured and 1352 (38.9%) sharks whose lengths were estimated either at the time of capture or by a length conversion. Measured FLs ranged from 59 to 320 cm (mean: 125 cm [SD 48]), and estimated FLs ranged from 60 to 330 cm (mean: 160 cm [SD 56]) (Fig. 2). Five length records were eliminated because of biologically implausible length estimates or measurements. Life stage was assigned to 2642 (76.0%) sharks of which 1136 (32.7%) were YOY, 1083 (31.1%) were juvenile, and 423 (16.0%) were adult (Table 2, Fig. 2). Sex was noted for only 21 of the sharks captured in Canada; therefore, any comparisons among sexes and juvenile and adult life

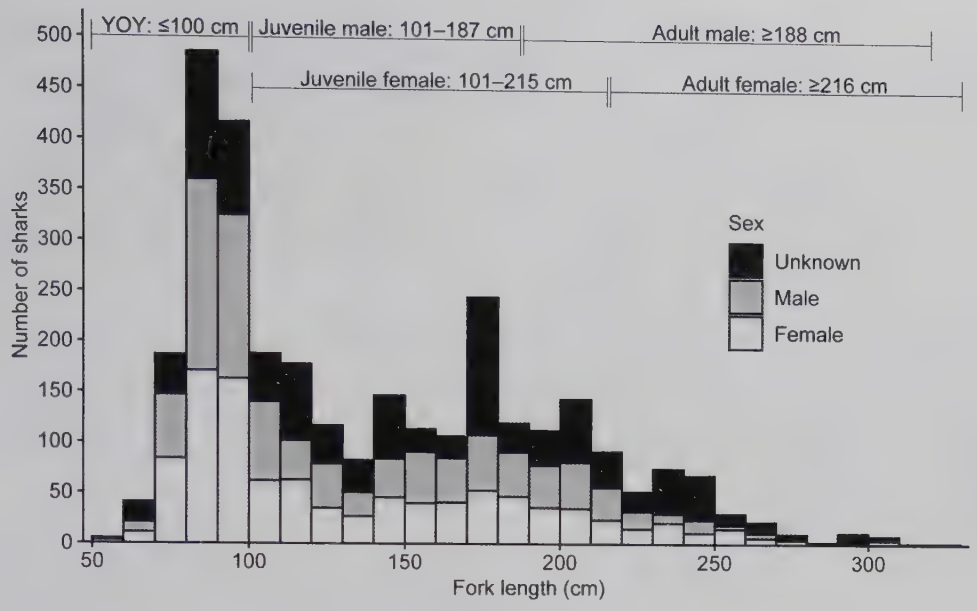

Figure 2

Length-frequency histogram for 3072 common thresher sharks (*Alopias vulpinus*), representing males, females, and those with unknown sex for which a measured or estimated length was available, captured from 1964 through 2019 in the western North Atlantic Ocean. The classification of life stages, based on sizes at 50% maturity from Natanson and Gervelis (2013), is provided at the top of the figure for males and females. YOY=young of the year.

stages almost exclusively represent sharks captured in U.S. waters.

Gear interactions

Common thresher sharks were captured with a wide range of gear types, including commercial bottom longline, pelagic longline, gill net (sink and floating), haul (beach) seine, purse seine, (bottom) otter trawl, mid-water trawl, and recreational rod and reel (Fig. 1). Of these gears, gill nets (50.0%; primarily sink gill nets) and pelagic longlines (27.1%) accounted for the majority of capture records, followed by rod and reel (10.4%) and otter trawl (9.2%). All other gears accounted for no more than 1.4% of the total number of records. The most common life stage of sharks captured by gill nets was YOY (88.4%), but YOY sharks were also caught by otter trawls, haul seines, and rod and reel (Fig. 3). Juveniles were captured by all gear types but were most commonly taken in gill nets (43.1%) and pelagic longlines (33.3%). Adults were captured by every gear type except haul seine, but they most commonly were taken by pelagic longline (39.2%) and rod and reel (26.7%).

Seasonal distribution

Common thresher sharks were captured over a broad geographic range extending from 23.9°N to 46.3°N and from 42.8°W to 95.1°W (Fig. 4). The majority of records (number of sharks [*n*]=2751; 79.1%) were from continental shelf waters shallower than 200 m; however, numerous individuals (*n*=727; 20.9%) were encountered in deeper (>200 m) offshore waters of the WNA. Records were available from all months and seasons with the greatest number of them from the winter (Table 2). The increase in capture records during winter was partially due to a large number of YOY and juveniles being taken in 2018 by gill-net fisheries off North Carolina.

Throughout the year, north–south changes in distribution along the east coasts of the United States and Canada were noted for common thresher sharks over all life stages. In general, individuals occurred at more northerly latitudes in the summer and more southerly latitudes in the winter (Fig. 4). During the winter, sharks were primarily encountered off the coast of North Carolina, both in the vicinity of Cape Hatteras and in waters near the edge of the continental shelf. A considerable number of specimens were also caught in continental shelf waters off the east coast of Florida during the winter. Sharks were distributed over the broadest area during the spring, with the center of distribution from North Carolina to Long Island, New York. During the summer, sharks were captured most commonly in continental shelf waters off the mid-Atlantic states, southern New England, and the Gulf of Maine, and sharks were rarely encountered south of Maryland. In the

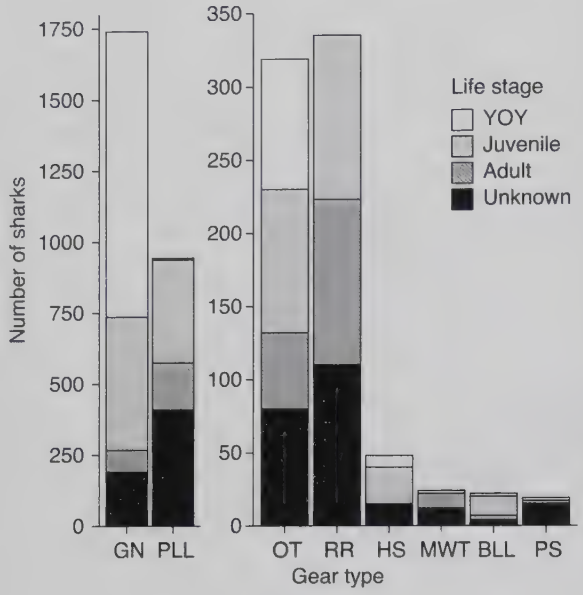

Figure 3

Number of common thresher sharks (*Alopias vulpinus*) caught in the western North Atlantic Ocean, based on compiled fishery-dependent data from 1964 through 2019. Sharks were captured with the following gear types: gill net (GN), pelagic longline (PLL), otter trawl (OT), rod and reel (RR), haul (beach) seine (HS), mid-water trawl (MWT), bottom longline (BLL), and purse seine (PS). Note the difference in scale between the y-axes. YOY=young of the year.

fall, 2 centers of distribution were evident: one from North Carolina to New Jersey and another off the Scotian Shelf in Canada.

Young of the year Common thresher sharks classified as YOY were distributed almost exclusively (99.1%) in continental shelf waters north of 33.5°N (Fig. 5). Only 6 individuals were captured south of 33.5°N, including a single record from the Gulf of Mexico (27.8°N, 88.6°W), which may have been a misidentification. Sharks of this life stage migrated along the coast in a north–south pattern, with overwintering grounds off Cape Hatteras. During the summer, sharks were most commonly taken off New Jersey and Long Island, New York, but their distribution ranged as far north as Cape Cod, Massachusetts. During the spring and fall, their distribution spanned between these summer and overwintering grounds.

Juveniles and adults Because of the inability to assign a life stage to all recorded common thresher sharks and the limited data from adults (Table 2), composite distribution maps were made for the juvenile and adult life stages (Fig. 6). The lack of sex data for sharks captured in Canada also precluded a thorough assessment of juvenile and adult distribution in waters of Canada, particularly along the Scotian Shelf. The winter distribution of these life stages occurred off the coast of North Carolina and the center of summer distribution extended from the mid-Atlantic states north to the Gulf of Maine. The distribution patterns of both juvenile and adult sharks are consistent with a seasonal, north–south distribution pattern along the east coasts of the United States and Canada, with extensive movements between the winter and summer habitat areas.

Males and females In general, the overall and seasonal distributions of male and female common thresher sharks were similar and followed the patterns previously described for this species and for each life stage (Fig. 7).

Habitat use

Sea-surface temperature at the time and location of capture was recorded for 2764 common thresher sharks and ranged from 4°C to 31°C (mean: 17°C [SD 4]) (Table 2); 78.2% of all records were for sharks captured in waters with temperatures of 10–22°C (Fig. 8). Young-of-the-year sharks were associated with the narrowest temperature range (6–26°C); however, each life stage and both sexes were generally associated with a similar range of SSTs (males: 5–30°C [mean: 17°C (SD 4)]; females: 6–30°C [mean: 17°C (SD 4)]). Monthly and seasonal fluctuations in SST at capture were evident for all life stages (Fig. 9). Sharks were taken in areas with depths ranging from 1 to 5427 m (mean: 433 m [SD 1032]), with 43.7% of all records from waters 10–25 m deep (Table 2, Fig. 8). In particular, 98.4% of YOY were caught in depths from 1 to 50 m, and 61.7% of juveniles were caught in depths from 10 to 100 m. Males and females were taken in areas with depths from 1 to 5427 m (mean: 165 m [SD 533]) and from 1 to 5401 m (mean: 146 m [SD 497]), respectively.

Discussion

The results of our analysis of over 50 years of fishery-dependent data advance the scientific understanding of the distribution and habitat use of common thresher sharks in the WNA and will improve our ability to assess and sustainably manage the population of this species nationally and internationally. Although trends of relative abundance for common thresher sharks in the WNA appear to have stabilized or slightly increased in recent years, current levels are still well below historic values of abundance (Young et al., 2016; Lynch et al., 2018) and fishery interactions are increasing across some gear types (Fig. 1) (Gervelis and Natanson, 2013; NMFS, 2019a). New insights into habitat use by sex and life stage will also promote the identification of EFH in U.S. waters. Accurate EFH designations allow potential effects on species in areas of proposed development or other activities to be considered before approval and provide a basis for

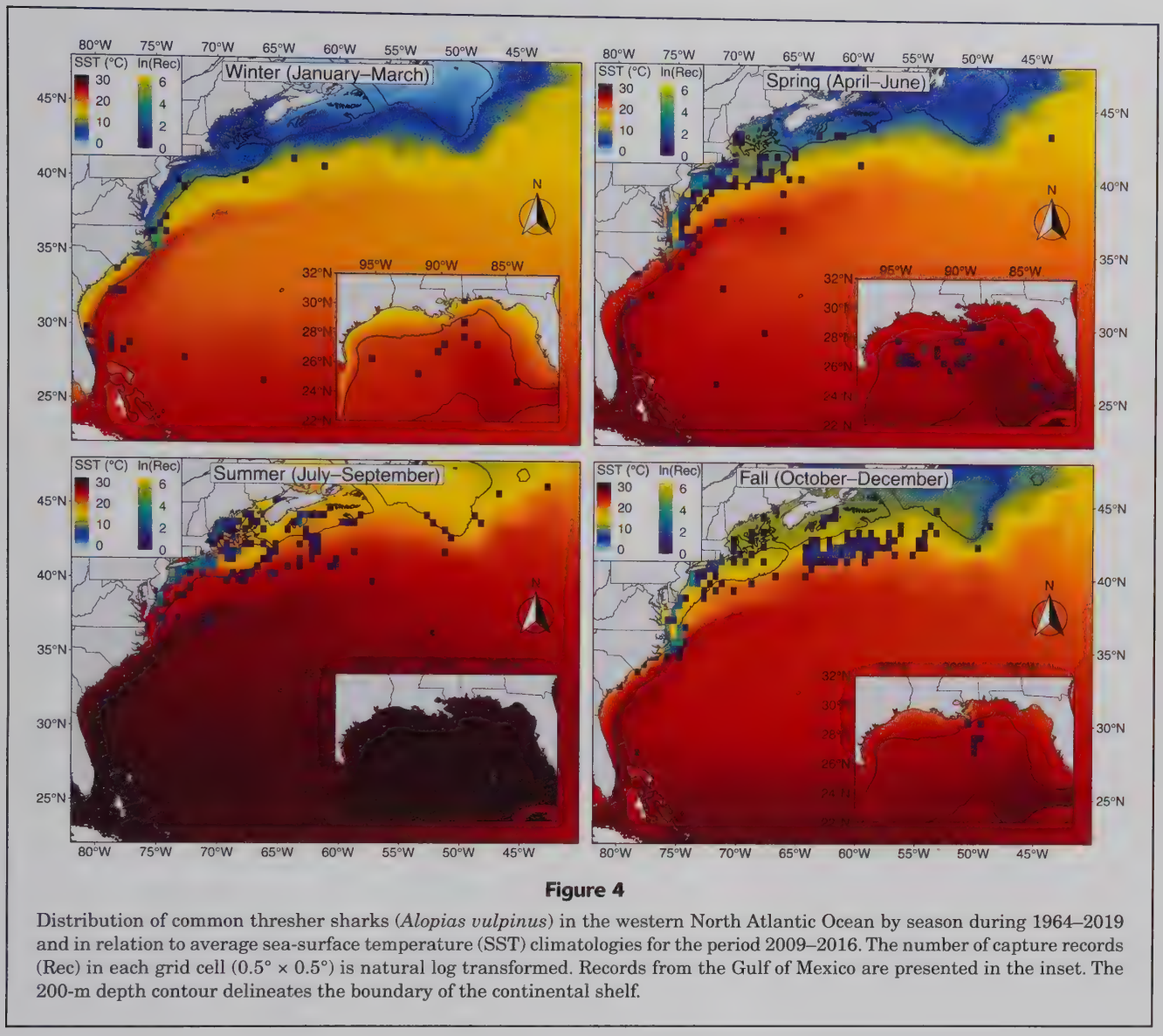

Figure 4

Distribution of common thresher sharks (*Alopias vulpinus*) in the western North Atlantic Ocean by season during 1964–2019 and in relation to average sea-surface temperature (SST) climatologies for the period 2009–2016. The number of capture records (Rec) in each grid cell (0.5° × 0.5°) is natural log transformed. Records from the Gulf of Mexico are presented in the inset. The 200-m depth contour delineates the boundary of the continental shelf.

evaluating time or area closures to assist in the recovery of overfished populations.

Analyses of presence-only data are a useful and cost-effective way to understand the distribution and habitat use of wide-ranging species for which limited species-specific survey data exist (Elith and Leathwick, 2009; Curtis et al., 2014). Their main limitation is the potential for bias due to spatial and temporal variability in fishing effort or in catchability by both gear type and life stage (Pearce and Boyce, 2006; Curtis et al., 2014). For example, common thresher sharks are the target of a relatively large, seasonal recreational shark fishery that operates from Virginia to Maine (Gervelis and Natanson, 2013), and >99% of the observed rod-and-reel capture events occurred over this geographic area. However, commercial fisheries data would be expected to be less biased, given that common thresher sharks are caught almost exclusively as bycatch in the WNA (Castro, 2011; Young et al., 2016) and that effort in trawl, gill-net, and pelagic longline fisheries is relatively consistent, widespread, and year-round along the U.S. east coast (Beerkircher et al., 2004; Guiet et al., 2019). Because 94.9% of records originated from a variety of commercial fisheries that operate throughout the range of this species, the overall and seasonal trends we report herein may largely reflect animal distribution. Nonetheless, spatial and temporal concentration in fishing effort may have influenced the number of captured sharks by season; for example, the large number of YOY observed off North Carolina during the winter and spring.

Seasonal distribution and habitat use

Our results are consistent with those of previous reports that indicate that the common thresher shark is primarily

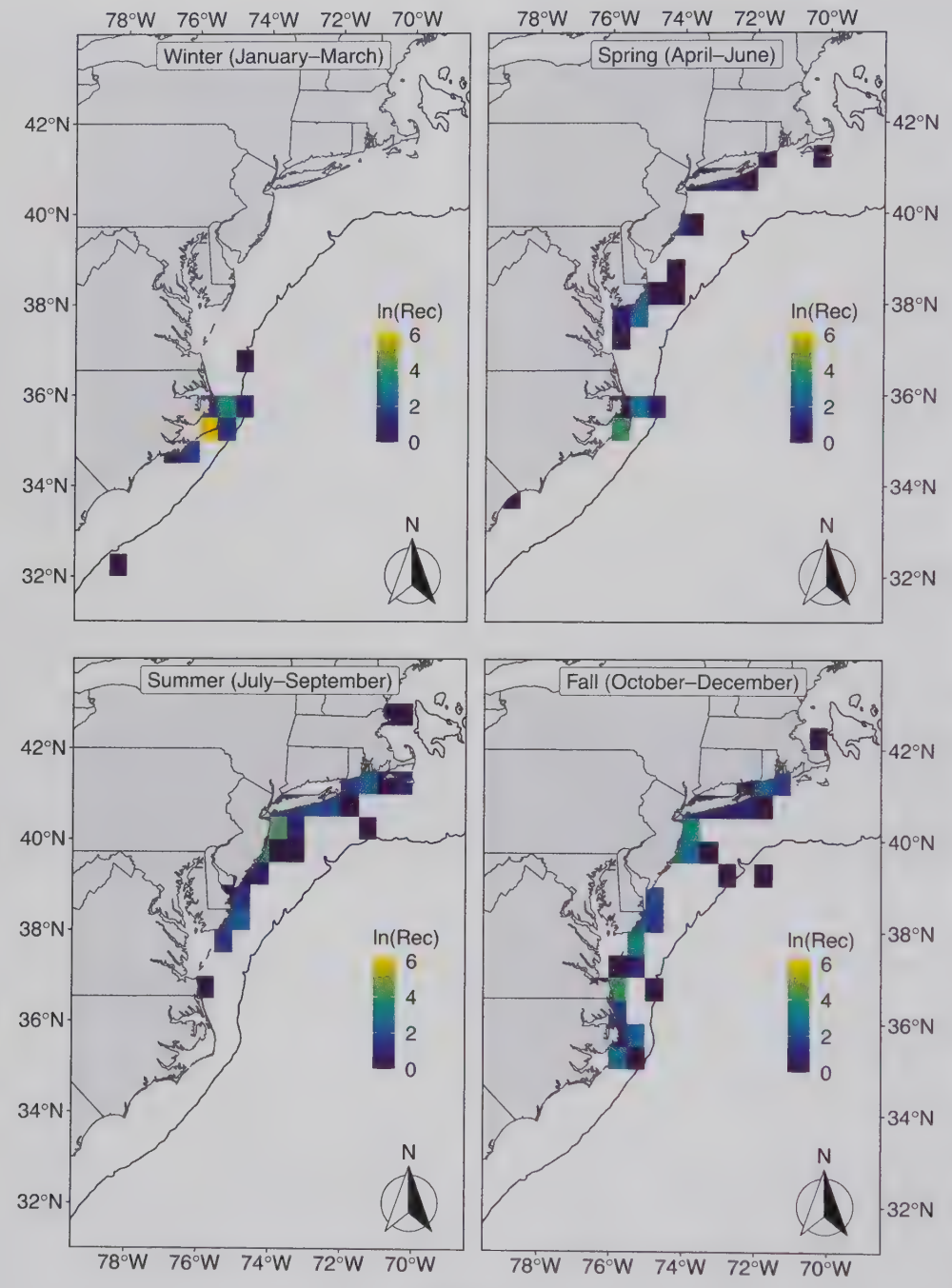

Figure 5

Distribution of young-of-the-year common thresher sharks (*Alopias vulpinus*) by season in the western North Atlantic Ocean between 1964 and 2019. The number of capture records (Rec) in each grid cell (0.5° × 0.5°) is natural log transformed. One record of a capture in the Gulf of Mexico is not presented because it may have been a misidentification. The 200-m depth contour delineates the boundary of the continental shelf.

distributed at depths <200 m in the continental shelf waters in the WNA but that its range seasonally extends farther offshore, closer to the northern edge of the Gulf Stream along the Scotian Shelf and Grand Banks (Fig. 4) (Castro, 2011). Although higher rates of observer coverage in coastal fisheries (NMFS, 2019b) would contribute to more frequent capture of common thresher sharks in continental shelf waters, their limited occurrence in the extensive and fairly well-monitored pelagic longline fisheries in offshore waters of the United States and Canada

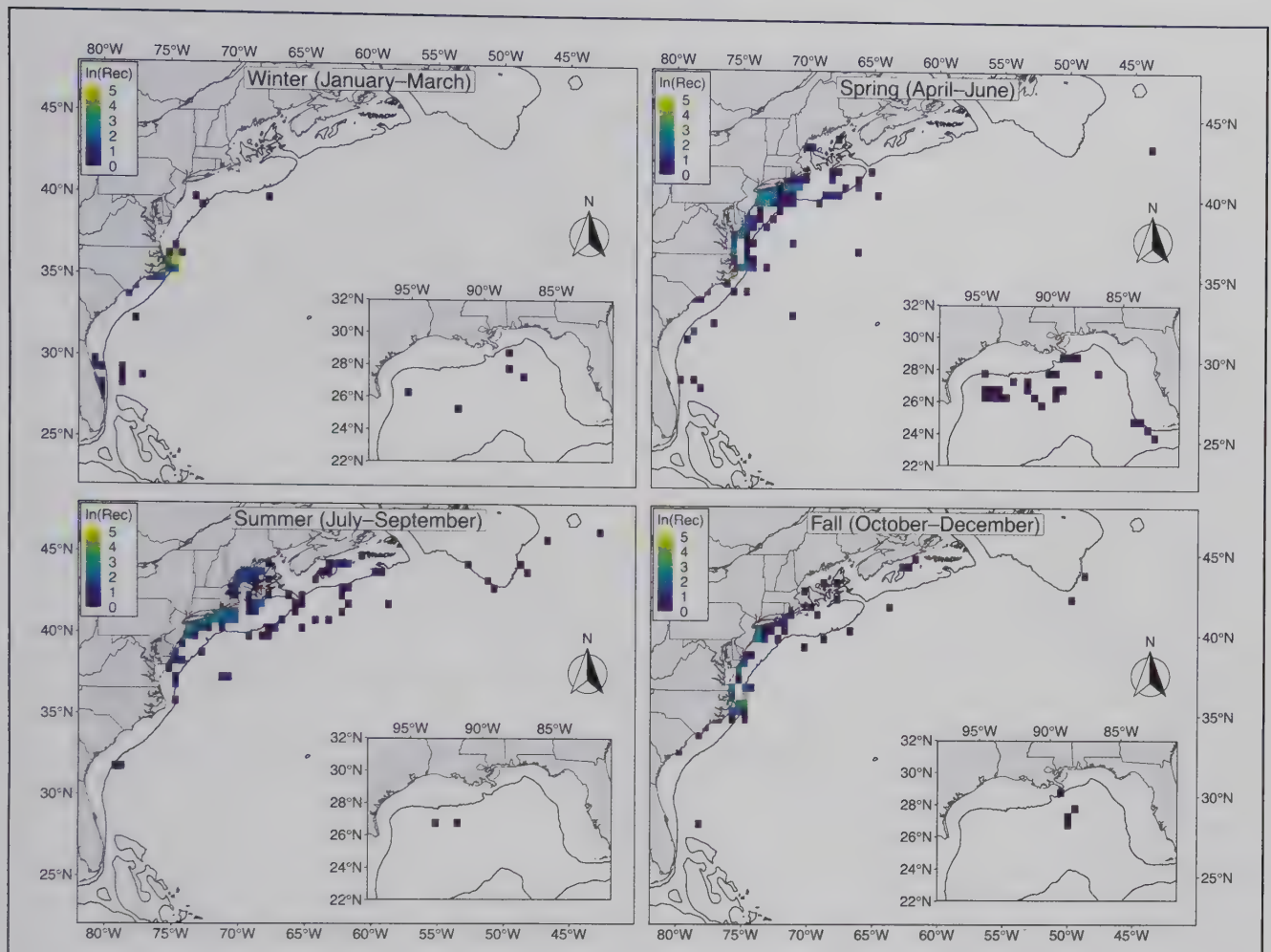

Figure 6

Distribution of juvenile and adult common thresher sharks (*Alopias vulpinus*) by season in the western North Atlantic Ocean between 1964 and 2019. The number of capture records (Rec) in each grid cell (0.5° × 0.5°) is natural log transformed. The lack of records in the maps for waters of Canada is a result of missing data on sex of sharks and the subsequent inability to assign a life stage to sharks captured in Canada. Records from the Gulf of Mexico are presented in the inset. The 200-m depth contour delineates the boundary of the continental shelf.

(Beerkircher et al., 2004; Hanke et al.[2]) indicates that this species does not occur as frequently in deep, offshore waters. Capture of common thresher sharks has been recorded sporadically throughout tropical offshore waters, including in the Gulf of Mexico. However, species identification could not be verified, and it is possible that some capture records represent misidentifications of bigeye thresher, the only other alopiid that occurs in the WNA (Compagno, 2001). Of note, misidentification would be most likely in the pelagic longline records from offshore areas in the Gulf of Mexico, where the distribution of bigeye threshers is well-documented (Fernandez-Carvalho et al., 2015) and the species tends to be encountered 4 times more frequently than the common thresher shark (Young et al., 2016).

Trends in distribution are consistent with a seasonal, north–south movement pattern in the WNA, with distribution focused shoreward of the continental shelf edge in depths <200 m along the east coasts of the United States and Canada. This distribution and movement pattern is similar to those of many other highly migratory species that inhabit the temperate WNA, such as the shortfin mako (*Isurus oxyrinchus*) (Vaudo et al., 2017) and bluefin tuna (*Thunnus thynnus*) (Galuardi et al., 2010), except with no evidence of frequent movements to the tropical Atlantic Ocean. It also aligns with the seasonal distribution and movements of common thresher sharks in the eastern Pacific Ocean, where northward (spring and summer) and southward (fall) movements occur between Baja

[2] Hanke, A. R., I. Andrushchenko, and G. Croft. 2012. Observer coverage of the Atlantic Canadian swordfish and other tuna longline fishery: an assessment of current practices and alternative methods. DFO Can. Sci. Advis. Secr. Res. Doc. 2012/049, 84 p. [Available from website.]

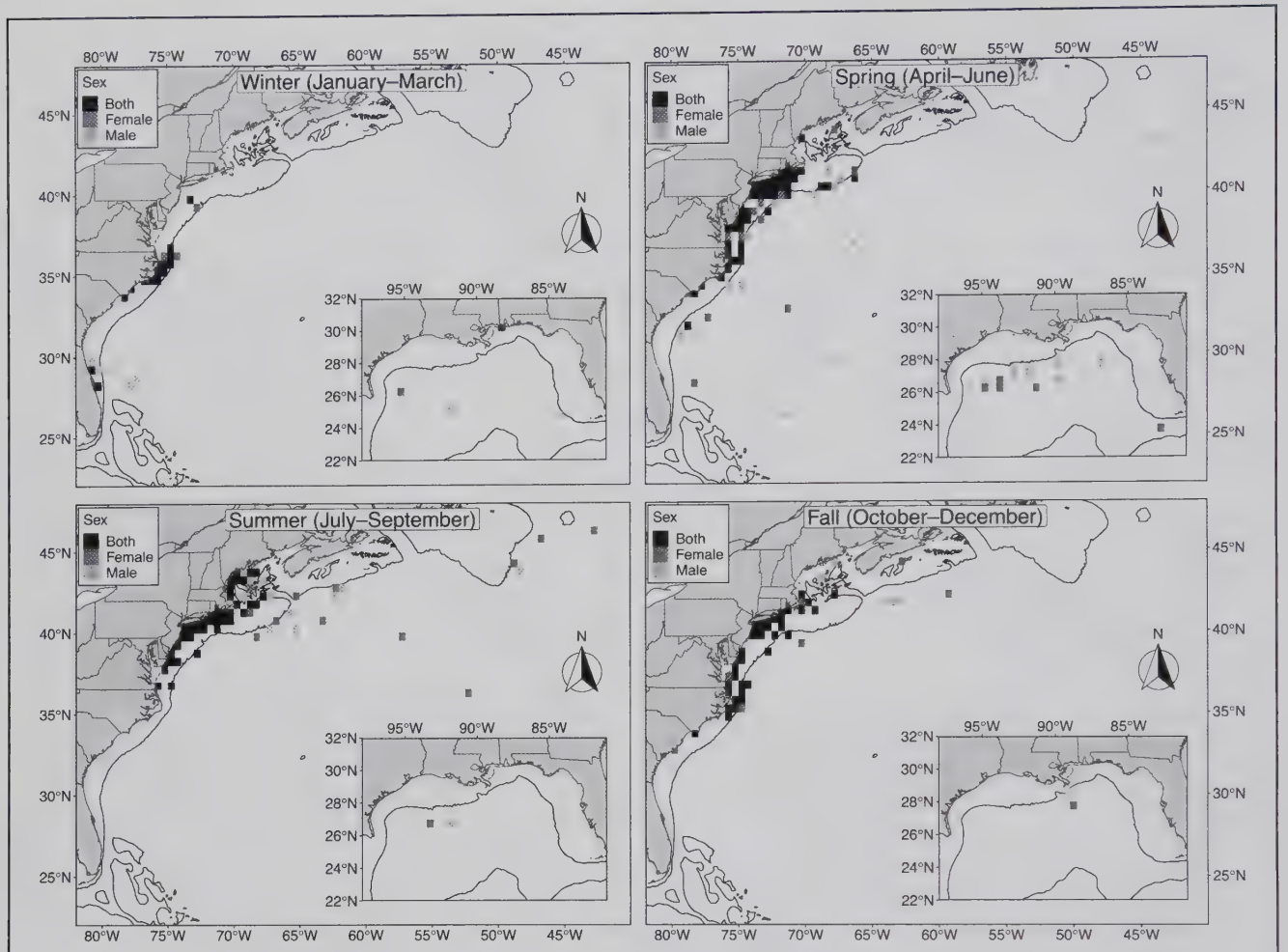

Figure 7

Distribution of male and female common thresher sharks (*Alopias vulpinus*) and of both sexes combined in the western North Atlantic Ocean between 1964 and 2019, by season and aggregated in grid cells (0.5° × 0.5°). The lack of capture records in maps for waters of Canada is a result of missing data on sex of sharks. Records from the Gulf of Mexico are presented in the inset. The 200-m depth contour delineates the boundary of the continental shelf.

California, Mexico, to as far north as British Columbia, Canada (Hanan et al., 1993; Cartamil et al., 2016; Kinney et al., 2020). The distribution of common thresher sharks in the WNA was more contracted during the winter than in any other season, with individuals being most commonly taken in relatively small areas off the coast from Virginia to North Carolina (outside of the barrier islands) and off the east coast of Florida.

The seasonal distribution of common thresher sharks changes markedly over ontogeny. Parturition for this species occurs from May through August in the mid-Atlantic states and in southern New England (Natanson and Gervelis, 2013; Young et al., 2016), consistent with the elevated occurrence of YOY throughout these areas during the summer months (Fig. 5). In the winter, YOY were taken almost exclusively in depths <50 m off the coast of North Carolina from Oregon Inlet to Cape Lookout. These results align with previous hypotheses that inshore waters from North Carolina to Massachusetts support nursery habitat for YOY and juvenile common thresher sharks (Natanson and Gervelis, 2013) and indicate that specific areas off New York, New Jersey, and Cape Hatteras (Fig. 5) may be of particular importance to individuals in these life stages. Investigation into why YOY occur more frequently in these areas than in others was beyond the scope of this study; however, their presence may be related to environmental preferences (see subsequent paragraphs) or prey distribution.

The distribution of common thresher sharks expands and individuals move into deeper waters of the WNA as they grow to maturity. A similar range expansion has been documented for juveniles and adults of this species off the U.S. west coast (Smith et al., 2008; Kinney et al., 2020) and may be related to changes in diet or physiological limitations imposed by environmental variation (Knip et al., 2010). Note that the inability to assign a life stage to

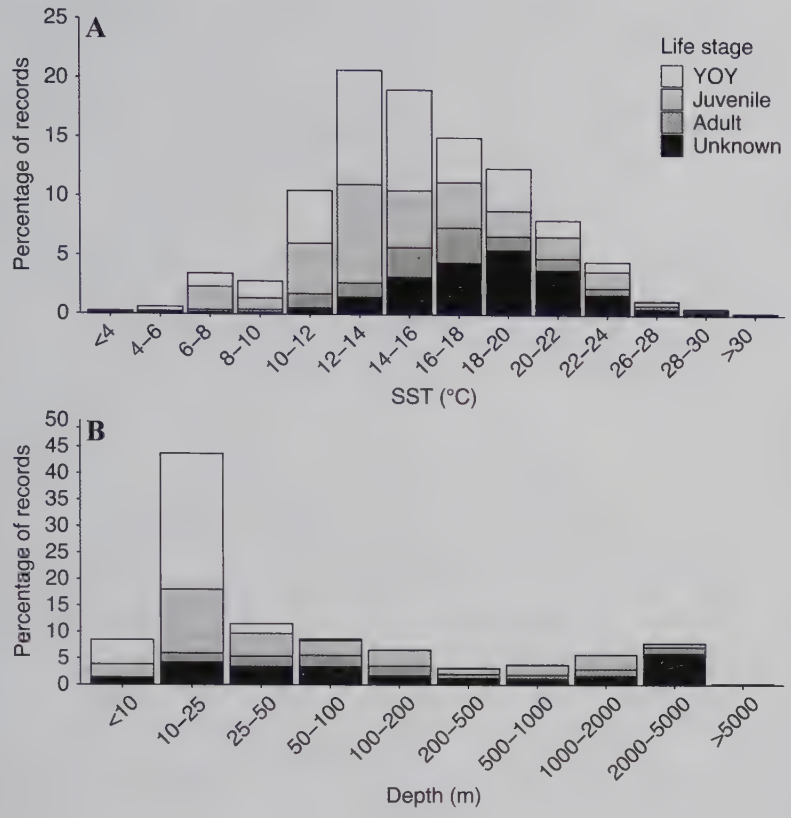

Figure 8

Percentage of the total number of capture records from fishery-dependent data of common thresher sharks (*Alopias vulpinus*) in the western North Atlantic Ocean between 1964 and 2019 by (**A**) sea-surface temperature (SST) and (**B**) depth for each life stage: young of the year (YOY), juvenile, adult, and unknown.

24.0% of the captured sharks and the low number of adults (i.e., 423 sharks) hindered our ability to describe the distribution and habitat use of sharks in these life stages, particularly in Canada. However, the clear association of YOY with shallow waters (depths <50 m) indicates that records from deep, offshore waters of Canada were of juveniles and adults. Difficulties measuring or estimating the total length of common thresher sharks and variability in size at maturity (Natanson and Gervelis, 2013) may have also led to the misclassification of life stage for some individuals and confounded our descriptions of distribution for each life stage.

Contrary to research in other regions (Moreno et al., 1989; Smith et al., 2008; Kinney et al., 2020), our results indicate that there is no strong evidence of sex-specific spatial or depth segregation of the population in the WNA. Segregation by sex tends to be most apparent in the adult life stage (Speed et al., 2010), and it is possible that we did not have sufficient information on this life stage for trends to be apparent. There is some evidence of sexual segregation of common thresher sharks in southern New England based on observations of large aggregations of predominantly female sharks in late summer (senior author and D. Bernal, unpubl. data).

Sea-surface temperatures recorded at the time of capture indicate that the common thresher shark occurs over a wide range of temperatures but is most commonly associated with temperatures from 10°C to 22°C. Previously, this species has been observed in SSTs ranging from 16.5°C to 19.8°C off the east coast of Florida (Castro, 2011), from 8°C to 28°C near the Republic of the Marshall Islands (Cao et al., 2011), and from 9°C to 21°C off the U.S. west coast (Cartamil et al., 2016). Preferred temperatures have been reported as 18–20°C (Cao et al., 2011) and 14–17°C (Cartamil et al., 2016), which are relatively similar to the temperature range over which the greatest number of capture events were recorded during this study (i.e., 12–18°C; Fig. 8). The overall range and mean SST at capture was also similar for all life stages (Table 2); however, YOY were observed over the narrowest temperature range. This result may be due to the lower capacity for metabolic heat retention in small individuals, which have a higher surface-to-volume ratio and therefore a decreased capacity to retain heat through regional endothermy (Bernal and Sepulveda, 2005).

The monthly and seasonal patterns in SST at capture indicate that temperature may be one of the key determinants of distribution and migration of common thresher sharks in the WNA. In general, captured sharks rarely occurred north of ~37°N in the winter and south of ~37°N in the summer (Fig. 4), the seasons during which the lowest and highest mean SSTs were observed, respectively (Fig. 9). This pattern is typical of migratory species that inhabit coastal waters of the WNA. By contrast, temperature was not one of the main factors driving movements and distribution off the U.S. west coast, with more broad-scale extrinsic seasonal factors (e.g., North Pacific Gyre Oscillation) being more influential (Kinney et al., 2020). Of note, the trends reported herein solely represent SST at the time and location of capture and do not necessary represent the temperatures that sharks experience at depth, which are likely the main drivers of movement and distribution. This is supported by Lynch et al. (2018), who demonstrated that water temperature profiles influenced catch rates for common thresher sharks in the pelagic longline fishery that operates off the Atlantic coast of the United States.

Fishery interactions and management implications

Capture records were available for common thresher sharks of all life stages; however, YOY was the most

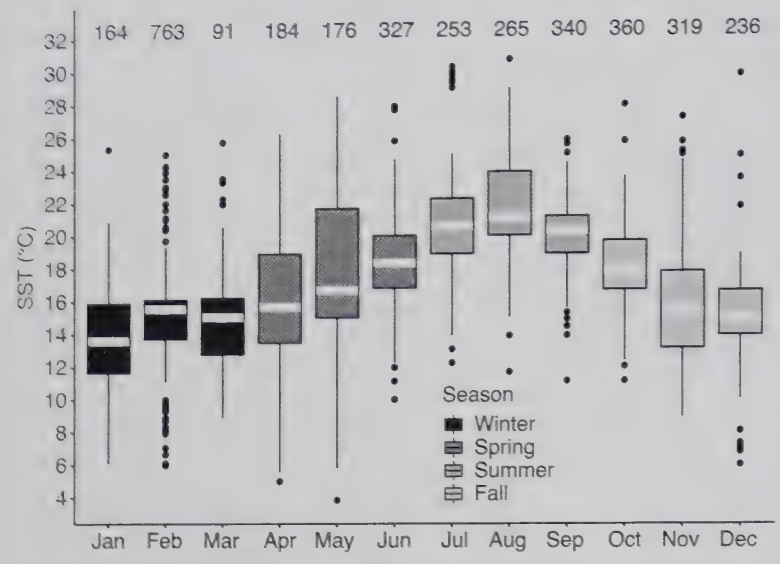

Figure 9

Box plot of sea-surface temperatures (SST) recorded, by month and season, as part of capture records from fishery-dependent data of common thresher sharks (*Alopias vulpinus*) in the western North Atlantic Ocean between 1964 and 2019. The numerals above the boxes indicate the number of records for each month. The upper and lower parts of each box represent the first and third quartiles (the 25th and 75th percentiles), and the horizontal white line is the median. The whiskers that extend above and below the box correspond to 1.5 times the interquartile range, and the black circles represent values outside this range.

commonly observed life stage, possibly because the restricted distribution of YOY in depths <50 m. There are no minimum commercial size limits for this species in the U.S. waters of the Atlantic Ocean and a review of the data provided by the Northeast Fisheries Observer Program indicate that many YOY are retained for sale. For example, between January and April 2018, at least 367 YOY were captured by gill nets during observed trips in the vicinity of Cape Hatteras. Assuming an average brood size of 3.7 young (Natanson and Gervelis, 2013), these captured sharks represent the reproductive output of approximately 100 adult females. Given the bi- or triennial reproductive cycle of this species in the WNA (Natanson and Gervelis, 2013) and the fact that the total number of YOY removed in the fishery may be many times greater than what was observed, such removals may represent a significant loss in recruitment in the WNA. However, because of their small size, landed weight of YOY common thresher sharks may not constitute a large percentage of the total quota for pelagic sharks in the Atlantic Ocean (i.e., 488.0 metric tons in dressed weight; NMFS, 2006).

Our results provide new insight into the environmental conditions and habitats used by common thresher sharks for each life stage and will assist managers in the designation of EFH by life stage off the U.S. east coast, as required under the Magnuson-Stevens Fishery Conservation and Management Act. Because of insufficient data on individual life stages, all life stages currently share a single EFH that spans continental shelf waters from Cape Lookout to Georges Bank and from Cape Ann, Massachusetts, to Bar Harbor, Maine (NMFS, 2017). However, our results provide information that should be sufficient to differentiate EFH for YOY. Although the extent of fishery-dependent data compiled for YOY common thresher sharks ranges from the Gulf of Maine to off South Carolina (consistent with Natanson and Gervelis, 2013), our analyses clearly identify areas of high levels of interaction off New York and New Jersey during the summer and off Cape Hatteras during the winter. Additional, direct information on the residency and movements of YOY common thresher sharks in these areas, however, is needed to confirm whether they warrant designation as nursery areas (Heupel et al., 2007). Additional fishery-independent (e.g., tagging and survey) data are also needed to better define juvenile and adult EFH and to confirm the broader conclusions regarding distribution and habitat use of common thresher sharks presented herein.

Acknowledgments

This study would not have been possible if not for the extensive efforts of those who worked to collect, edit, and compile the fishery-dependent data used herein. We thank L. Beerkircher, S. Cushner, J. Carlson, A. Mathers, E. Orbesen, and D. Snodgrass of the Southeast Fisheries Science Center for providing data. This work was supported by award NA16NMF4270231 from the NOAA Saltonstall-Kennedy Grant Program. This article is Massachusetts Division of Marine Fisheries contribution number 117.

Literature cited

Amante, C., and B. W. Eakins.
2009. ETOPO1 1 Arc-Minute Global Relief Model: procedures, data sources and analysis. NOAA Tech. Memo. NESDIS NGDC-24, 19 p.

Baum, J. K., and W. Blanchard.
2010. Inferring shark population trends from generalized linear mixed models of pelagic longline catch and effort data. Fish. Res. 102:229–239.

Baum, J. K., R. A. Myers, D. G. Kehler, B. Worm, S. J. Harley, and P. A. Doherty.
2003. Collapse and conservation of shark populations in the Northwest Atlantic. Science 299:389–329.

Beerkircher, L. R., C. J. Brown, D. L. Abercrombie, and D. W. Lee.
2004. SEFSC pelagic observer program data summary for 1992–2002. NOAA Tech. Memo. NMFS-SEFSC-522, 25 p.

Bernal, D., and C. A. Sepulveda.
2005. Evidence for temperature elevation in the aerobic swimming musculature of the common thresher shark, *Alopias vulpinus*. Copeia 2005:146–151.

Cailliet, G. M., L. K. Martin, J. T. Harvey, D. Kusher, and B. A. Welden.
1983. Preliminary studies on the age and growth of blue, *Prionace glauca*, common thresher, *Alopias vulpinus*, and shortfin mako, *Isurus oxyrinchus*, sharks from California waters. *In* Proceedings of the international workshop on age determination of oceanic pelagic fishes: tunas, billfishes, sharks (E. D. Prince and L. M. Pulos, eds.), p. 179–188. NOAA Tech. Rep. NMFS 8.

Cao, D.-M., L.-M. Song, Y. Zhang, K.-K. Lv, and Z.-X. Hu.
2011. Environmental preferences of *Alopias superciliosus* and *Alopias vulpinus* in waters near Marshall Islands. N.Z. J. Mar. Freshw. Res. 45:103–119.

Cartamil, D., J. Wraith, N. C. Wegner, D. Kacev, C. H. Lam, O. Santana-Morales, O. Sosa-Nishizaki, M. Escobedo-Olvera, S. Kohin, J. B. Graham, and P. Hastings.
2016. Movements and distribution of juvenile common thresher shark *Alopias vulpinus* in Pacific coast waters of the USA and Mexico. Mar. Ecol. Prog. Ser. 548:153–163.

Castro, J. I.
2011. The sharks of North America, 640 p. Oxford Univ. Press, New York.

Chamberlain, S.
2019. rerddap: general purpose client for 'ERDDAP' servers. R package, vers. 0.6.5. [Available from website, accessed June 2019.]

Compagno, L. J. V.
2001. Sharks of the world. An annotated and illustrated catalogue of shark species known to date. Vol. 2. Bullhead, mackerel and carpet sharks (Heterodontiformes, Lamniformes and Orectolobiformes). FAO species catalogue for fishery purposes 1, 269 p. FAO, Rome.

Cortés, E., C. A. Brown, and L. R. Beerkircher.
2007. Relative abundance of pelagic sharks in the western North Atlantic Ocean, including the Gulf of Mexico and Caribbean Sea. Gulf Caribb. Res. 19(2):37–52.

Curtis, T. H., C. T. McCandless, J. K. Carlson, G. B. Skomal, N. E. Kohler, L. J. Natanson, G. H. Burgess, J. J. Hoey, and H. L. Pratt Jr.
2014. Seasonal distribution and historic trends in abundance of white sharks, *Carcharodon carcharias*, in the western North Atlantic Ocean. PLoS ONE 9(6):e99240.

Elith, J., and J. R. Leathwick.
2009. Species distribution models: ecological explanation and prediction across space and time. Annu. Rev. Ecol. Evol. Syst. 40:677–697.

Fernandez-Carvalho, J., R. Coelho, J. Mejuto, E. Cortés, A. Domingo, K. Yokawa, K.-M. Liu, B. García-Cortés, R. Forselledo, S. Ohshimo, et al.
2015. Pan-Atlantic distribution patterns and reproductive biology of the bigeye thresher, *Alopias superciliosus*. Rev. Fish Biol. Fish. 25:551–568.

Galuardi, B., F. Royer, W. Golet, J. Logan, J. Neilson, and M. Lutcavage.
2010. Complex migration routes of Atlantic bluefin tuna (*Thunnus thynnus*) question current population structure paradigm. Can. J. Fish. Aquat. Sci. 67:966–976.

Gervelis, B. J., and L. J. Natanson.
2013. Age and growth of the common thresher shark in the western North Atlantic Ocean. Trans. Am. Fish. Soc. 142:1535–1545.

Guiet, J., E. Galbraith, D. Kroodsma, and B. Worm.
2019. Seasonal variability in global industrial fishing effort. PLoS ONE 14(5):e0216819.

Hanan, D. A., D. B. Holts, and A. L. Coan Jr.
1993. The California drift gill net fishery for sharks and swordfish, 1981–82 through 1990–91. Calif. Dep. Fish Game, Fish Bull. 175, 90 p.

Heupel, M. R., J. K. Carlson, and C. A. Simpfendorfer.
2007. Shark nursery areas: concepts, definition, characterization and assumptions. Mar. Ecol. Prog. Ser. 337:287–297.

Kinney, M. J., D. Kacev, T. Sippel, H. Dewar, and T. Eguchi.
2020. Common thresher shark *Alopias vulpinus* movement: Bayesian inference on a data-limited species. Mar. Ecol. Prog. Ser. 639:155–167.

Knip, D. M., M. R. Heupel, and C. A. Simpfendorfer.
2010. Sharks in nearshore environments: models, importance, and consequences. Mar. Ecol. Prog. Ser. 402:1–11.

Kohler, N. E., and P. A. Turner.
2019. Distributions and movements of Atlantic shark species: a 52-year retrospective analysis of mark and recapture data. Mar. Fish. Rev. 81(2):1–93.

Lynch, P. D., K. W. Shertzer, E. Cortés, and R. J. Latour.
2018. Abundance trends of highly migratory species in the Atlantic Ocean: accounting for water temperature profiles. ICES J. Mar. Sci. 75:1427–1438.

Moreno, J. A., J. I. Parajúa, and J. M. Ayala.
1989. Biología reproductiva y fenología de *Alopias vulpinus* (Bonnaterre, 1788) (Squaliformes: Alopiidae) en el Atlántico nor-oriental y Mediterráneo occidental. Sci. Mar. 53:37–46. [In Spanish.]

Natanson, L. J., and B. J. Gervelis.
2013. The reproductive biology of the common thresher shark in the western North Atlantic Ocean. Trans. Am. Fish. Soc. 142:1546–1562.

NMFS (National Marine Fisheries Service).
2006. Final consolidated Atlantic highly migratory species fishery management plan, 1600 p. Highly Migratory Species Manage. Div., Off. Sustainable Fish., Natl. Mar. Fish. Serv., Silver Spring, MD. [Available from website.]
2017. Final amendment 10 to the 2006 consolidated Atlantic highly migratory species management plan: essential fish habitat and environmental assessment, 289 p. Highly Migratory Species Manage. Div., Off. Sustainable Fish., Natl. Mar. Fish. Serv., Silver Spring, MD. [Available from website.]
2019a. 2018 stock assessment and fishery evaluation (SAFE) report for Atlantic highly migratory species, 234 p. Highly Migratory Species Manage. Div., Natl. Mar. Fish. Serv., Silver Spring, MD. [Available from website.]
2019b. National observer program FY 2017 annual report. NOAA Tech. Memo. NMFS-F/SPO-200, 28 p.

Pante, E., and B. Simon-Bouhet.
2013. marmap: a package for importing, plotting and analyzing bathymetric and topographic data in R. PLoS ONE 8(9):e73051.

Pearce, J. L. and M. S. Boyce.
2006. Modelling distribution and abundance with presence-only data. J. Appl. Ecol. 43:405–412.

Pebesma, E.
2018. Simple features for R: standardized support for spatial vector data. R J. 10(1):439–446.

R Core Team.
2020. R: a language and environment for statistical computing. R Foundation for Statistical Computing, Vienna, Austria. [Available from website, accessed December 2020.]

Rigby, C. L., R. Barreto, D. Fernando, J. Carlson, S. Fordham, M. P. Francis, K. Herman, R. W. Jabado, K. M. Liu, A. Marshall et al.
2019. *Alopias vulpinus*. The IUCN Red List of Threatened Species 2019:e.T39339A2900765. [Available from website, accessed May 2020.]

Smith, S. E., D. W. Au, and C. Show.
1998. Intrinsic rebound potentials of 26 species of Pacific sharks. Mar. Freshw. Res. 49:663–678.

Smith, S. E., R. C. Rasmussen, D. A. Ramon, and G. M. Cailliet.
2008. The biology and ecology of thresher sharks (Alopiidae). *In* Sharks of the open ocean: biology, fisheries and conservation (M. D. Camhi, E. K. Pikitch, and E. A. Babcock, eds.), p. 60–68. Blackwell Publishing, Oxford, UK.

Speed, C. W., I. C. Field, M. G. Meekan, and C. J. A. Bradshaw.
2010. Complexities of coastal shark movements and their implications for management. Mar. Ecol. Prog. Ser. 408:275–293.

Vaudo, J. J., M. E. Byrne, B. M. Wetherbee, G. M. Harvey, and M. S. Shivji.
2017. Long-term satellite tracking reveals region-specific movements of a large pelagic predator, the shortfin mako shark, in the western North Atlantic Ocean. J. Appl. Ecol. 54:1765–1775.

Wickham, H., M. Averick, J. Bryan, W. Chang, L. D'Agostino McGowan, R. François, G. Grolemund, A. Hayes, L. Henry, J. Hester, et al.
2019. Welcome to the tidyverse. J. Open Source Softw. 4(43):1686.

Young, C. N., J. K. Carlson, M. Hutchinson, D. R. Kobayashi, C. T. McCandless, M. H. Miller, S. Teo, and T. Warren.
2016. Status review report: common thresher shark (*Alopias vulpinus*) and bigeye thresher (*Alopias superciliosus*) sharks, 199 p. Final report to National Marine Fisheries Service, Office of Protected Resources. [Available from website.]

Acknowledgment of reviewers

The editorial staff of *Fishery Bulletin* would like to acknowledge the scientists who reviewed manuscripts in 2019–2020. Their contributions have helped ensure the publication of quality science.

Scott Akenhead
Allen Andrews
Peter Armstrong

Henry Bart Jr.
Carolina Bastidas
Richard Beamish
William Bemis
Hugues Benoît
Katelyn Bosley
Beth Bowers
Keith Brander
David Bryan
Jeffrey Buckel

David Cairns
Matthew Campbell
Daniel Cartamil
Martin Castonguay
Shannon Cass-Calay

Martin Dorn
William Driggers III
J. Marcus Drymon

Kevin Feldheim
Clive Fox
Kenneth Frank
James Franks
Bryan Frazier

John Galbraith
James Gelsleichter
R. Grant Gilmore Jr.
Gretchen Grammer
John Green

Owen Hamel
Jill Hendon
Frank Hernandez Jr.
Alistair Hobday
Eric Hoffmayer

Albert Imsland

Kelsey James
Nina Jonsson
Warren Joyce

Stephen Kajiura
Matthew Kendall
James Kennedy
Raouf Kilada
Olav Kjesbu

Mario La Mesa
Richard Langton
Robert Leaf
Yu-Jia Lin
Kwang-Ming Liu
Carlos Lozano

Charles Manire
Katey Marancik
Richard McBride
Howard McElderry
W. David McElroy
Kevin McNeel
Richard Merrick
Richard Methot
A. Whitman Miller

Lisa Natanson
Stephen Newman
Gabriel Ng

Martin O'Connell
Matthew Ogburn
M. Pilar Olivar
Joseph O'Malley
Guðmundur Óskarsson

Juan Pérez Jiménez
Frank Parrish
Michelle Passerotti
Torstein Pedersen
Cassidy Peterson
Mark Peterson
Graham Pierce

Kyle Piller
Jennifer Potts
Gregg Poulakis
Craig Proctor
André Punt

Joseph Quattro

Pedro Range
Andrew Read
Jim Reynolds
Jason Romine
Christopher Rooper

Skyler Sagarese
Bianca Santos
Chiyuki Sassa
William Satterthwaite
Steven Schroder
Burton Shank
Jonathan Shenker
David Smith
Stephen Smith
Dave Somerton
Philip Stevens
James Sulikowski

Jim Treasurer
Mark Tupper

Douglas Vaughan
Francisco Velasco

Terence Walker
John Walter III
William Watson
Frederick Wenzel
Bruce Wright
Krystan Wilkinson

Fishery Bulletin

Guidelines for authors

Contributions published in *Fishery Bulletin* describe original research in marine fishery science, fishery engineering and economics, and marine environmental and ecological sciences (including modeling). Preference will be given to manuscripts that examine processes and underlying patterns. Descriptive reports, surveys, and observational papers may occasionally be published but should appeal to an audience outside the locale in which the study was conducted.

Although all contributions are subject to peer review, responsibility for the contents of papers rests upon the authors and not on the editor or publisher. *Submission of an article implies that the article is original and is not being considered for publication elsewhere.*

All submissions are subject to a double-blind review to remove the identity of author and reviewer during the review process.

Plagiarism and double publication are considered serious breaches of publication ethics. To verify the originality of the research in papers and to identify possible previous publication, manuscripts may be screened with plagiarism-detection software.

Manuscripts must be written in English; authors whose native language is not English are strongly advised to have their manuscripts checked by English-speaking colleagues before submission.

Once a paper has been accepted for publication, online publication takes approximately 2 weeks.

There is no cost for publication in *Fishery Bulletin*.

Types of manuscripts accepted by the journal

Articles generally range from 20 to 30 double-spaced typed pages (12-point font) and describe an original contribution to fisheries science, engineering, or economics. Tables and figures are not included in this page count, but the number of figures should not exceed 1 figure for every 4 pages of text. Articles contain the following divisions: abstract, introduction, methods, results, discussion, and conclusions.

Notes are generally less than 10 double-spaced typed pages (12-point font), including the Literature cited section. Like articles, notes describe an original contribution to fisheries science. They follow a format similar to that for articles: abstract, introduction, methods, results, and discussion, but the results and discussion sections may be combined and a conclusions section should not be included. They should include no more than 2 figures or tables (2 of each would be too many). They are distinguished from full articles in that they report a noteworthy new observation or discovery—such as the first report of a new species, a unique finding, condition, or event that expands our knowledge of fisheries science, engineering, or economics—and do not require a lengthy discussion. Manuscripts on range extensions will not be considered.

Companion articles should be submitted together and are published together as a scientific contribution. Both articles should address a closely related topic and may be articles that result from a workshop or conference.

Review articles of exceptional quality may be considered occasionally for publication on a case-by-case basis. They address a timely topic that is relevant to aspects of fisheries science. They should include an abstract, but the format of the article, per se, will be up to the author. Please contact the Scientific Editor to discuss your ideas regarding a potential review article before embarking on such a project.

Preparation of manuscript

Title page should include authors' full names, mailing addresses, and the senior author's email address.

Abstract should be limited to 200 words (one-half typed page), state the main scope of the research, and emphasize the authors' conclusions and relevant findings. Do not review the methods of the study or list the contents of the paper. Because abstracts are circulated by abstracting agencies, it is important that they represent the research clearly and concisely.

General text must be typed in 12-point Times New Roman font throughout. A brief introduction should convey the broad significance of the paper; the remainder of the paper should be divided into the following sections: Materials and methods, Results, Discussion, and Acknowledgments. Headings within each section must be short, reflect a logical sequence, and follow the rules of subdivision (i.e., there can be no subdivision without at least 2 subheadings). The entire text should be intelligible to interdisciplinary readers; therefore, all acronyms, abbreviations, and technical terms should be written out in full and defined the first time they are mentioned. Abbreviations should be used sparingly because they are not carried over to indexing databases and slow readability for those readers outside a discipline. They should never be used for the main subject (species, method) of a paper.

For general style, follow the U.S. Government Publishing Office *Style Manual* (2016, available at website) and *Scientific Style and Format: the CSE Manual for Authors, Editors, and Publishers* (2014, 8th ed.) published by the Council of Science Editors. For scientific nomenclature, use the current edition of the American Fisheries Society's *Common and Scientific Names of Fishes from the United States, Canada, and Mexico* and its companion volumes

(*Crustaceans, Mollusks, Cnidaria and Ctenophora*, and *World Fishes Important to North Americans*). For species not found in the above mentioned AFS publications and for more recent changes in nomenclature, use the Integrated Taxonomic Information System (ITIS, available at website), or, secondarily, the California Academy of Sciences *Catalog of Fishes* (available at website) for species names not included in ITIS. Common (vernacular) names of species should be lowercase. Citations must be given for the identification of specimens. For example, "Fish species were identified according to Collette and Klein-MacPhee (2002); sponges were identified according to Stone et al. (2011)."

Dates should be written as follows: 11 November 2018. Measurements should be expressed in metric units, for example, "58 metric tons (t);" if other units of measurement are used, please make this fact explicit to the reader. Use numerals, not words, to express whole and decimal numbers in the general text, tables, and figure captions (except at the beginning of a sentence). For example, "We considered 3 hypotheses. We collected 7 samples in this location." Use American spelling. Refrain from using the shorthand slash (/), an ambiguous symbol, in the general text.

Cite all software, special equipment, and chemical solutions used in the study within parentheses in the general text, for example, "SAS, vers. 6.03 (SAS Institute Inc., Cary, NC)."

Word usage and grammar that may be useful are the following:

- *Aging*
  For our journal, the word *aging* is used to mean both age determination and the aging process (senescence). Authors should make clear which meaning is intended where ambiguity may arise.

- *Fish and fishes*
  The plural of the word fish (a collective noun that implies individuals without regard to species) is *fish*.
  Example: The *fish* were collected by trawl net.
  Example: The numbers of *fish* collected that season were less than the numbers from previous years.

  The plural for *fish species* is *fishes* (a contrived plural used by taxonomists to mean several or more *fish species*) or one can use *fish species* (which is preferred in this journal for clarity across disciplines).
  Example: The *fishes* of Puget Sound [biodiversity is implied] or
  Example: The *fish species* of Puget Sound [preferred plural for clarity across disciplines].

- *Crab and crabs, squid and squids, etc.*
  The plural of the word *crab* (i.e., many individuals without regard to species) is *crab*.
  Example: The crab were sorted by weight.
  Example: Many red king *crab* were dying [Many individuals of one species of crab.]

  The plural of *crab species* is *crabs* (a word used by taxonomists) or *crab species* (the latter is preferred in this journal for clarity).
  Example: These *crabs* were selected for treatment. [Different crab species are implied.]
  Example: These *crab species* were selected for treatment. [Preferred word choice for clarity of meaning.]
  Example: Snow *crabs* are found throughout the North Pacific Ocean and Bering Sea. [There are 2 species of snow crab and therefore the word *crabs* can be used here.]
  Example: *Two species* of snow *crab* are found throughout the North Pacific Ocean and Bering Sea. [Preferred usage for clarity.]
  Example: Three crabs were selected for treatment. [3 species of crab are implied.]
  Example: Three crab species were selected for treatment. [Preferred word choice for clarity.]

- *Fisherman and fisher*
  We use *fisherman* and *fishermen* in this journal not *fisher* and *fishers*. One can always use crew member, vessel operator, and angler (the latter for recreational fishing.

- *The definite article with common names of species*
  When the singular common name of a species represents the entire class or group to which it belongs, use the definite article.
  Example: Only one species of the genus *Salmo* is found in the Atlantic Ocean—*the* Atlantic salmon (*Salmo salar*).
  Example: The sonic emissions of *the* bottlenose dolphin are complex.

  For plural common names, this rule does not apply.
  Example: Chinook salmon are found throughout the Pacific Ocean.
  Example: Bottlenose dolphins are found in temperate and tropical waters.

- *Sex*
  For the meaning of male and female, use the word *sex*, not *gender*. Do not write "fish were sexed." Write, "sex was determined."

- *Participles*
  As adjectives, participles must modify a specific noun or pronoun.
  Example: Using mark-recapture methods, these scientists determined the size of the population. [Correct. The participle *using* modifies the word *scientists*.]
  Example: These scientists, based on the collected data, concluded that the mortality rate of these fish had increased. [Incorrect. The scientists were not based on the collected data.]
  Example: These scientists concluded, on the basis of collected data, that the mortality rate of these fish had increased. [Correct. The offending participle has been eliminated and an adverbial phrase modifies the verb *concluded*.]

Equations and mathematical symbols should be set from a standard mathematical program (MathType or Equation Editor). Equations formatted in LaTex are not acceptable. For mathematical symbols in the general text (α, χ^2, π, $\pm$, etc.), use the symbols provided by the MS Word program and italicize all variables, except those variables represented by Greek letters and the superscript and subscript parts of variables and expressions. Do not use photo mode when creating these symbols in the general text, and do not cut and paste equations, letters, or symbols from a different software program.

Number equations (if there are more than one) for future reference by scientists; place the number within parentheses at the end of the first line of the equation.

Literature cited section comprises published works and those accepted for publication (in press) in peer-reviewed journals. Follow the name and year system for citation format in this section (i.e., citations should be listed alphabetically by the authors' last names, and then by year if there is more than one citation by the same author. A list of abbreviations for citing journal titles can be found on our website.

Authors are responsible for the accuracy and completeness of all citations. Avoid the use of multiple citations when a single citation sufficiently supports a statement; cite the work that first reported the information that supports a statement, not all of the subsequent works. Literature citation format: Authors (last name, followed by initials for first name and, if given, middle name of first author; then list names of additional authors with initials before last names). Year. Title of article. Abbreviated title of the journal in which it was published. Always include either the range of page numbers (for a journal article) or a total number of pages (for a book or other type of publication). List a sequence of citations in the general text chronologically, for example, "(Smith, 1932: Green. 1947; Smith and Jones, 1985)."

Acknowledgments should be no more than 6 lines of text. Only those who have contributed in an outstanding way should be acknowledged by name. For recognition of other persons or groups, use a general term, such as *crew*, *observers*, or *research coordinators*, and do not include names with these terms.

Digital object identifier (doi) code ensures that a publication has a permanent location online. A doi link (which may include a doi code) should be included at the end of citations of published literature. Authors are responsible for submitting accurate doi links. Faulty links will be deleted at the page-proof stage.

Footnotes are used for all documents that have not been formally peer reviewed and for observations and personal communications, but these types of references should be cited sparingly in manuscripts submitted to the journal.

All reference documents, administrative reports, internal reports, progress reports, project reports, contract reports, personal observations, personal communications, unpublished data, manuscripts in review, and council meeting notes are footnoted in 10-point font and placed at the bottom of the page on which they are first cited. Footnote format is the same as that for formal literature citations. A link to the online source (e.g., [Available from http://www..., accessed July 2017.]), or the mailing address of the agency or department holding the document, should be provided so that readers may obtain a copy of the document.

Tables are often overused in scientific papers; it is seldom necessary to present all the data associated with a study. Tables should not be excessive in size and must be cited in numerical order in the text. Headings should be short but ample enough to allow the table to be intelligible on its own.

All abbreviations and unusual symbols must be explained in the table legend. Other incidental comments may be footnoted with numeral footnote markers. Use asterisks only to indicate significance in statistical data. Do not put a table legend on a page separate from the table; place the legend above the table. *Do not submit tables in photo mode.*

- Note probability with a capital, italic *P*.
- Provide a zero before all decimal points for values less than one (e.g., 0.07).
- Round all values to 2 decimal points.
- Use a comma in numbers of 5 digits or more (e.g., 13,000 but 3000).

Figures must be cited in numerical order in the text. Graphics should aid in the comprehension of the text, but they should be limited to presenting patterns rather than raw data. The number of figures should not exceed 1 figure for every 4 pages of text.

Figure legends should explain all symbols and abbreviations seen in the figure and should be double spaced on a separate page at the end of the manuscript.

Line art and halftone figures should be saved at resolutions >600 dots per inch (dpi) and >300 dpi, respectively. Color is allowed in figures to show morphological differences among species (for species identification), to show stain reactions, to show gradations (such as those of temperature and salinity within maps), and to distinguish between numerous lines and symbols in graphs. Figures approved for color should be saved in CMYK format.

All figures must be submitted as PDF, TIFF, or EPS files.

- Capitalize only the first letter of the first word and proper nouns in all labels within figures.
- Do not use overly large font sizes for labels in maps and for axis labels in graphs.

- Use the same point size for all labels, except for panel labels (e.g., **A**), which should be slightly larger than other labels (e.g., 11 point versus 8 point).
- Use a sans serif font for all labels. Panel labels (e.g., **A**), however, should be in Times New Roman font.
- Do not use bold fonts or bold lines in figures. Do not use italic fonts. Exceptions include use of italic fonts for labels of bodies of water in maps and a bold font for panel labels (e.g., **A**).
- Do not place outline rules around graphs.
- Do not include vertical and horizontal lines in the background of graphs. Ticks for values on the x-axis and y-axis will suffice.
- Place a north arrow and label degrees latitude and longitude (e.g., 170°E) in all maps. If scale of map requires more than degrees, use degrees minutes, not decimal degrees.
- Place panel labels (e.g., **A**, **B**, **C**) within the upper-left area of each graph or photo in a multi-panel figure, from left to right, then top to bottom. If the letter is not visible against a dark background, put a white box behind it. Do not use white labels.
- Avoid placing labels vertically or diagonally. Y-axis labels can be vertical. Words in horizontal labels can be stacked vertically to fit.
- Use symbols, shadings, or patterns (not clip art) in maps and graphs.
- For scale bars in maps, use kilometers. Use the label *km* or *kilometers* (lowercased).

Supplementary materials that are considered essential, but are too large or impractical for inclusion in a paper (e.g., metadata, figures, tables, videos, and websites), may be provided at the end of an article. These materials are subject to the editorial standards of the journal. A URL to the supplementary material and a brief explanation for including such material should be sent at the time of initial submission of the paper to the journal.

- **Metadata, figures, and tables** should be submitted in standard digital format (MS Word or PDF file) and should be cited in the general text, for example, as "... was determined (Suppl. Table 3, Suppl. Fig. 1)."
- **Websites** should be cited with a URL in the general text.
- **Videos** must not be larger than 30 MB to allow a swift technical response for viewing the video. Authors should consider whether a short video uniquely captures what text alone cannot capture for the understanding of a process or behavior under examination in the article. Supply an online link to the location of the video.

Copyright law does not apply to *Fishery Bulletin*, which falls within the public domain. However, if an author reproduces any part of an article from *Fishery Bulletin*, reference to source is considered correct form (e.g., Source: Fish. Bull. 97:105).

Failure to follow these guidelines and failure to correspond with editors in a timely manner will delay publication of a manuscript.

Submission of manuscript

Submit a manuscript online at the ScholarOne Manuscripts website for *Fishery Bulletin*. Commerce Department authors must provide proof of internal clearance of their manuscripts with either a completed and signed NOAA Form 25-700 or a copy of the clearance email from the Research Publication Tracking System. For further details on electronic submission, please contact the associate editor, Cara Mayo, at

cara.mayo@noaa.gov.

When requested, the text and tables should be submitted in MS Word format. Each figure should be sent as a separate PDF, TIFF, or EPS file. Send a copy of a figure in the original software if conversion to any of these formats yields a degraded version of the figure.

Questions? If you have questions regarding these guidelines, please contact the managing editor, Kathryn Dennis, at

kathryn.dennis@noaa.gov.

Questions regarding manuscripts under review should be addressed to Associate Editor Cara Mayo.

Fishery Bulletin

Subscription form

Superintendent of Documents **Publications** Order Form

*5178

☐ YES, please send me the following publications:

____ Subscriptions to *Fishery Bulletin*
for $32.00 per year ($44.80 foreign)

The total cost of my order is $ _____ . Prices include regular domestic postage and handling and are subject to change.

_____
(Company or Personal Name) (Please type or print)

_____
(Additional address/attention line)

_____
(Street address)

_____
(City, State, ZIP Code)

_____
(Daytime phone including area code)

_____
(Purchase Order No.)

Charge your order. IT'S EASY!

VISA

MasterCard

Please Choose Method of Payment:

☐ Check payable to the Superintendent of Documents
☐ GPO Deposit Account ☐☐☐☐☐☐☐–☐
☐ VISA or MasterCard Account
☐☐☐☐☐☐☐☐☐☐☐☐☐☐☐☐
☐☐☐☐ (Credit card expiration date)

To fax your orders (202) 512-2104

_____
(Authorizing Signature)

Mail to: Superintendent of Documents
P.O. Box 979050, St. Louis, Missouri 63197
Tel. no. (U.S. callers): 866-512-1800
Tel. no. (International callers): 1-202-512-1800

Thank you for your order!

Also available online at
https://bookstore.gpo.gov/products/fishery-bulletin
email: ContactCenter@gpo.gov